THERMOPHYSICAL PROPERTIES OF NANOFLUIDS AND EMPIRICAL CORRELATIONS

by
Katia Haviters

Submitted to Graduate School of Natural and Applied Sciences
in Partial Fulfillment of the Requirements
for the Degree of Master of Science in
Chemical Engineering

Yeditepe University
2021

THERMOPHYSICAL PROPERTIES OF NANOFLUIDS AND EMPIRICAL CORRELATIONS

APPROVED BY:

Assist. Prof. Cem Levent Altan ……
(Thesis Supervisor)
(Yeditepe University)

Assoc. Prof. Tuğba Davran Candan ……
(Yeditepe University)

Assist. Prof. Murat Oluş Özbek ……
(Gebze Technical University)

DATE OF APPROVAL: …./…./2021

I hereby declare that this thesis is my own work and that all information in this thesis has been obtained and presented in accordance with academic rules and ethical conduct. I have fully cited and referenced all material and results as required by these rules and conduct, and this thesis study does not contain any plagiarism. If any material used in the thesis requires copyright, the necessary permissions have been obtained. No material from this thesis has been used for the award of another degree.

I accept all kinds of legal liability that may arise in case contrary to these situations.

Name, Last name ……. Katia Haviters……

Signature …..…….……..

ACKNOWLEDGEMENTS

First and foremost, I would like to express my special gratitude to my supervisor Assist. Prof. Dr. Cem Levent Altan, for his enormous knowledge, motivation, effort, and guidance throughout my thesis. I could not imagine a better mentor that could raise me into the person that I am today. He did not only guide me through my academic path with his marvelous mind and ideas but despite his busyness, he has always been there for me, taught me about life, was patient about my infinite number of questions, opened my mind, and guided me in the best way possible. I can never find the exact words to describe the gratitude that I have, but I feel extremely lucky for having the chance to work with him. Without him, this dream of mine could have not been possible. I would additionally like to thank him for being such a great professor and a wonderful person at the same time. He has always been motivating and enthusiastic, which encouraged me enormously during my hard times. I believe all the efforts he puts and the young souls that he guides will change the world someday, just like he changes them in the best way.

Furthermore, I would like to thank to all my professors in the Chemical Engineering Department, who have taken a significant part in my education. Among all, I would like to offer my special thanks to my committee members Assoc Prof. Tuğba Davran Candan and Assist. Prof. Murat Oluş Özbek who, by sharing their brilliant comments and suggestions, made my defense more pleasurable. I would additionally like to thank them for being such great persons as well as great professors and making each subject much more enjoyable. Moreover, I would like to offer my special thanks to Dr. Melis Çağdaş who has always been there for me from the first day I met her. She has been a special role model for me and kept opening my mind through each conversation we had, throughout my masters. I'm so grateful for her guidance, support and all the things she taught me. I also feel extremely lucky to have the chance to be her assistant during Chem 113 laboratories, which was a unique and mind opening experience which has leveled me up in many ways.

I would also like to thank Sibel Özbal for her invaluable helps during the hard times I had opposed by the technical problems encountered with the Flucon Lambda. I feel so lucky to know her. Without her, a part of the thesis would literally not be possible.

I am grateful to all my friends who have cheered me up during my stressful times, have always supported me mentally and physically, have made me laugh even if it was not possible and have proven me billion times that I am extremely lucky to be surrounded by so many wonderful souls. There are so many of them that I cannot state but I thank them all, with all my heart. Among all, I would like to offer my special thanks to Beyza Abişoğlu, Ezgi Uslu and Kemal Düzkar who have witnessed every phase of my thesis, supported me with their helps in the laboratory and surrounded me with a unique atmosphere during the majority of my masters. This journey would have been less amusing without their presence.

Lastly, I would like to thank with all my heart, my unique family members, my mom, dad and brother, for their trust in me. I feel extremely lucky for feeling their presence and support throughout my masters. They are the heroes that have saved me from my darkest times, encouraged me to do better, helped me fulfill my dreams, filled me with unconditional love and positive energy. It would be extremely hard to complete my study without their tremendous understanding and encouragement in the past few years. I thank them furthermore, for being the best souls in the whole universe and for always supporting me follow my dreams. There are no words that could serve to express my gratitude and love towards them. Moreover, I would also like to offer my special thanks to the rest of my family members who have always checked up on me and empowered me with lots of love, kindness, and support.

ABSTRACT

THERMOPHYSICAL PROPERTIES OF NANOFLUIDS AND EMPIRICAL CORRELATIONS

Nanofluids are two phased systems and colloidal suspensions of nanoparticles in convenient carrier fluids and used in a wide variety of applications from medicine to engineering. Among these potential applications, nanofluids in heat transfer devices has been comprehensively studied in recent years as it was shown that the thermophysical properties of base fluids are highly affected by the addition of nanoparticles. By considering the significant role of the thermophysical properties of materials in heat transfer applications, the investigation of these features of nanofluids such as density, viscosity, and thermal conductivity is crucial in order to use them efficiently in practical applications. In addition, it is known that nanofluids are not conventional suspensions thus, their thermophysical properties are not described by classical theories. Although models that are capable of predicting the aforementioned properties for particular nanoparticle-base fluid systems were presented in the literature, correlations that can be used for a more extensive class of nanofluids are limited. Therefore, it is necessary to formulate empirical correlations to estimate thermophysical properties of nanofluids where direct measurement is not applicable. Current study focuses on the investigation of the thermophysical properties such as density, viscosity, and thermal conductivity of conventional heat transfer fluids consisting of magnetite, copper oxide and silver nanoparticles. Furthermore, it is intended to generate empirical correlations that serve to predict the thermophysical properties of nanofluids as a function of particle loading and temperature by using the measured data. The results indicate that the viscosity and thermal conductivity of base fluids are highly affected by the addition of nanoparticles as compared to density for which the corresponding base fluid values may be considered for applications. In addition, the empirical models which were formulated by using the measured data demonstrated the possibility of estimating system specific thermophysical properties and inability of forming generalized correlations.

ÖZET

NANOAKIŞKANLARIN TERMOFİZİKSEL ÖZELLİKLERİ VE AMPİRİK KORELASYONLARI

Nanoakışkanlar, uygun taşıyıcı sıvıların içerisinde askıda kalmış nanoparçacıkların bulunduğu iki bileşenli koloidal süspansiyonlardır ve tıptan mühendisliğe kadar çok çeşitli uygulamalarda kullanılabilmektedirler. Geleneksel olarak kullanılan ısı transferi akışkanlarına ait termofiziksel özelliklerin, nanoparçacıkların eklenmesi ile önemli derecede değişime uğraması sebebiyle tüm bu potansiyel uygulamalar arasında nanoakışkanların ısı transferi uygulamaları da kapsamlı olarak incelenmiştir. Nanoakışkanların, yoğunluk, viskozite ve termal iletkenlik gibi termofiziksel özelliklerinin, ısı transferi uygulamalarındaki önemli rolleri sebebiyle detaylı bir şekilde incelenmesi de son derece önemlidir. Ancak, nanoakışkanlar geleneksel süspansiyonlara benzerlik göstermedikleri için termofiziksel özellikleri klasik teoriler ile tanımlanamamaktadır. Her ne kadar bahsi geçen özelliklerin spesifik nanoparçacık ve taşıyıcı sıvı sistemler için tahmin edilmesine imkan sağlayan modeller bulunsa da daha geniş ve farklı bir çok nanoakışkanı kapsayan korelasyonların sayısı sınırlıdır. Bu sebeple, termofiziksel özelliklerin ölçümünün mümkün ve uygulanabilir olmadığı durumlarda hesaplanabilmeleri için deneysel korelasyonlara ihtiyaç vardır. Bu çalışma, geleneksel ısı transferi sıvılarına ait yoğunluk, viskozite ve termal iletkenlik gibi termofiziksel özelliklerin, magnetit, bakır oksit ve gümüş nanoparçacıklarının eklenmesi sonucunda değişimlerinin incelenmesini ve elde edilen veriler kullanılarak nanoakışkanlara ait belirtilen özelliklerin, parçacık konsantrasyonu ve sıcaklığa bağlı olarak tahmin edilmesine olanak sağlayan modellerin oluşturulmasını hedeflemektedir. Elde edilen sonuçlar, taşıyıcı sıvıya ait viskozite ve termal iletkenliğin, yoğunluğa kıyasla nanoparçacıkların eklenmesi ile beraber önemli derecede değişime uğradığını ve yoğunluk için uygulamalarda gerektiğinde baz akışkanın değerlerinin kullanılabileceğini göstermiştir. Ek olarak, ölçüm verileri kullanılarak formüle edilen deneysel korelasyonlar, sadece tekil sistemlerin termofiziksel özelliklerine yönelik tahminin mümkün olduğunu buna karşın genelleştirilmiş korelasyonların formüle edilmesinin de mümkün olmadığını göstermiştir.

TABLE OF CONTENTS

LIST OF FIGURES

LIST OF TABLES

LIST OF SYMBOLS/ABBREVIATIONS

Abs	Absorbance
Ag	Silver
Au	Gold
Al_2O_3	Aluminium oxide
$CoFe_2O_4$	Cobalt ferrite
COP	Co-precipitation
C_p	Specific heat
Cp	Centipoise
Cu	Copper
CuO	Copper oxide
D	Characteristic length
DIW	Deionized water
DM	Density model
EG	Ethylene glycol
Fe	Iron
Fe_3O_4	Magnetite
F-GNP	Functionalized graphene nanoplatelets
g	Grams
k	Thermal conductivity
k_{bf}	Thermal conductivity of the base fluid
k_{nf}	Thermal conductivity of the nanofluid
kDa	Kilodalton
M	Molarity
ml	Milliliter
MWCNT	Functionalized multiwalled carbon nanotubes
mW/m.K	Milli watts per meter-kelvin
Nm	Nanometer

Np	Nanoparticle
Obs	Observation
PAA	Polyacrylic acid
PEG	Polyethylene glycol
PG	Propylene glycol
POX	Partial oxidation
Pred	Prediction
RPM	Revolutions per minute
RSM	Response surface methodology
SiO_2	Silicon dioxide
T	Temperature
TEM	Transmission electron microscopy
TiO_2	Titanium dioxide
TM	Thermal conductivity model
UV-Vis	Ultraviolet-Visible
VM	Viscosity model
Vol	Volume
ZnO	Zinc oxide
W	Water
Wt	Weight
℃	Degrees centigrade
μ	Viscosity
μ_{bf}	Viscosity of the base fluid
μ_{nf}	Viscosity of the nanofluid
ρ	Density
ρ_{bf}	Density of the base fluid
ρ_{nf}	Density of the nanofluid
$\emptyset_v$	Volumetric concentration

1. INTRODUCTION

Heat transfer fluids such as water and ethylene glycol are extensively employed in various applications involving heat transfer. Nonetheless, these conventional fluids have relatively ineffectual heat transfer abilities when compared with the majority solids and this causes limitations in related applications. As a result, many researchers have oriented towards the development of new types of heat transfer fluids to enhance the heat transfer performance. Since most solids (especially metals) have comparably greater thermal conductivity values than that of conventional heat transfer fluids [1], the idea of suspending solid particles in suitable base fluids was suggested in order to enhance the corresponding thermophysical properties. Several studies investigated the feasibility of such suspensions of milli or micrometer sized solid particles, yet some drawbacks were observed such as the rapid settlement of the particles and clogging of the flow channels [2]. Thus, the idea of suspending solid particles in a liquid was acknowledged yet was renounced for heat transfer applications. The concept of nanofluids which are two phased colloidal systems consisting of a base fluid and nanometer-sized fine particles and the idea of their great potential in heat transfer applications were first introduced by Choi [3]. These innovative heat transfer fluids were expected to exhibit superior heat transfer capabilities relative to that of traditional dispersions by virtue of their nano sized particles and larger surface areas. In addition to advantages such as long-term stability, minimal-clogging in flow passages and homogeneity [4][5], nanofluids have been found to possess enhanced thermophysical properties i.e. thermal conductivities than that of common heat transfer fluids [5–11]. This enhancement was attributed to several mechanisms such as the formation of a fluid layer of increased thermal conductivity around the nanoparticles [12–14], Brownian motion of nanoparticles at the nano-scale level [14–17], and the nanoparticle clustering [14–16]. Previous studies had put forward that Brownian motion induced convection and conduction through the agglomerates might be the most significant factor causing the radical enhancement of the thermal conductivity of base fluids [18–21]. However, the subject remains a discussion and the key mechanisms governing the thermal behavior of nanofluids are still under extensive examination.

Thermophysical properties are significant parameters that affect the heat transfer characteristics and play an important role in energy efficiency. They are, by definition, material properties that affect heat transfer and storage. Moreover, thermophysical properties of the fluids are prerequisites for the calculation of dimensionless numbers commonly used in heat transfer such as Reynolds, Nusselt and Prendtl numbers, as well as the heat transfer coefficient. Considering all these, the investigation of thermophysical properties such as density, viscosity, thermal conductivity and specific heat of nanofluids as a function of temperature and volume fraction of nanoparticles is essential in order to use them efficiently in heat transfer applications [21,22]. Relevant experimental and theoretical studies revealed that the alterations in the thermophysical properties of nanofluids further depend on other effects such as the type and the size of nanoparticles, type of the surfactant that is used to stabilize the nanoparticles and the type of base fluid.

Nanofluids are now being considered as next generation heat transfer fluids however their usage in practical heat transfer applications requires the evaluation of their thermophysical properties with respect to variable nanoparticle concentration and working temperature. The measurement of thermophysical properties in order to investigate their effect over the heat transfer applications of nanofluids is generally impractical due to lack of relevant equipment. Instead, correlations that serve to estimate the nanofluid thermophysical properties may regarded as a more practical solution. Although historical background on the subject includes well-known theoretical models for the estimation of the thermophysical properties of solid-liquid suspensions, those are found to result in inaccurate estimations when nanofluids are being considered. Hence, studies are directed towards the formation of empirical correlations that can estimate corresponding thermophysical properties as a function of variables that strongly affect their characteristics. Extensive studies published in the literature on the investigation of the thermophysical properties of various types of nanofluids has however unveiled that the results are disputable, and the behavior of nanofluids are not analogous but different for each nanoparticle-base fluid system. Thereof, many attempts have oriented towards the design of system-specific models that can estimate the thermophysical properties of specific type of nanofluids.

Present study involves the synthesis of various types of nanofluids, the measurement of corresponding thermophysical properties (i.e. density, viscosity, thermal conductivity) and the formation of empirical correlations in order to estimate nanofluid' thermophysical properties. The diverse types of nanofluids that were studied throughout the present study accounted for the effects of nanoparticle concentration, working temperature, nanoparticle type and size, type of the surfactant and type of the base fluid. Although several studies presented system (nanoparticle – base fluid) specific models for the estimation of thermophysical properties, correlations that are capable of predicting the properties for an extended group of several nanofluids are limited. Therefore, the objective of this study is to investigate the density, viscosity and thermal conductivity of various types of nanofluids and examine the possibility of forming generalized empirical correlations that can estimate the thermophysical properties of divergent nanofluids as a whole.

This thesis starts with a theoretical background which presents information about nanofluids, their applications, experimental studies on their thermophysical properties and previously proposed correlations for the estimation of thermophysical properties. Theoretical background is then followed by materials section in which materials used during the experimental studies are demonstrated. In the methods section, essential details about the measurement of thermophysical properties (density, viscosity and thermal conductivity) are described. In the succeeding experimental procedure section, the synthesis methods are explained. In the results and discussion part, the results obtained during the study are presented and discussed in detail. Finally, the gathered results are summarized, and the outcomes of the study are explained in the conclusion part.

2.THEORETICAL BACKGROUND

2.1. NANOFLUIDS

Nanofluids are two phased colloidal systems consisting of nanometer-sized (1-100nm) fine particles called nanoparticles and base fluids. Nanoparticles have been found to possess extraordinary properties by virtue of their extremely small sizes. When these nano sized particles with superior characteristics are uniformly and stably distributed in convenient base fluids, the distinct properties of the nanoparticles are transferred into these fluids, making nanofluids innovative fluids with enhanced characteristics and thus, widening the doors of scientific research.

2.1.1. Nanoparticles

Nanoparticles are ultrafine particles whose size ranges between 1 to 100 nm. Apart from their presence in nature, they can also be synthesized in laboratories via numerous chemical routes. These nano sized particles may basically be metals such as Cu, Ni, Al, Au, Ag etc., oxides such as CuO, Al_2O_3, TiO_2, SiO_2, Fe_2O_3, Fe_3O_4, etc., carbon in various forms such as carbon nanotubes, graphene etc. or several other compounds [23].

The properties of the nano sized particles often differ significantly from those of larger sized particles of the same material as their size approaches to the atomic scale. As the particle size is decreased, the surface area is increased compared to the bulk material and this leads to a greater surface area to volume ratio of the same material, resulting in the material's surface atoms dominating the material's performance. Thus, the submicroscopic size of nanoparticles provides them unique material characteristics and they exhibit markedly different physical, chemical, mechanical, optical and electrical properties compared to their bulk phases. [24–27]. Accordingly, all these discoveries have elicited intensive scientific attention towards them.

Although the main mechanism governing the behavior of nanoparticles and the main cause leading to these extraordinary property enhancements remains a discussion, the mostly declared explanation is their nano size induced enormous surface areas. As well as the high surface to volume ratio, quantum size effect is declared to be another reason behind this feature of nanoparticles [28–30]. The emerge of unusual properties by extremely small crystals due to their confinement of electrons is called quantum size effect. Decreasing the dimension of the materials to nanoscale enables them to easily confine their electrons and gives birth to the quantum size effect which significantly changes their electronic, photonic and optoelectronic performances when compared to their bulk forms [31,32].

There are several examples related with these unexpected properties due to the change in the size of materials. For instance, the ductility of copper drastically differs as size drops below 50 nm. While bulk copper is considered as a soft material which can bend, copper nanoparticles that are smaller than 50 nm are considered extremely hard materials [24]. This change in ductility is also observed for gold which is significantly harder than its bulk form [33]. Furthermore, it is observed that physical properties such as melting are also affected when the corresponding size of the material reach nanoscale. While the melting temperature of bulk gold is 1064 °C, it was shown that gold nanoparticles with a size of 2.5 nm melt at a much lower temperature around 300 °C [34].

Ever since the enhanced properties of these nano sized particles were revealed, they have been considered as one of the most fascinating functional materials and hence, researchers from many fields were encouraged to use them in diverse applications. Yet, studies have shown that the existence of solid nanoparticles alone is not generally enough, but they rather need to be dispersed in convenient base fluids.

2.1.2. Base Fluids

It is well known that water, ethylene glycol and mineral oil are the mostly preferred and used conventional fluids in many applications including heating and cooling processes, chemical

operations, electronics and transportation. Considering their significance in vast majority of fields and applications, their implementation in nanotechnology was also inevitable.

A fluid that is used to transport materials is called a carrier (base) fluid. As nanofluids are defined as colloidal suspensions of nanometer sized particles in convenient carrier fluids, the carrier fluids take an essential role for the production of nanofluids. In nanotechnology, a base fluid is referred as the fluid in which nanoparticles are suspended and thus transported if required. The choice of a carrier (base) fluid mainly depends on the purpose of the application itself.

Like in many other fields, water is one of the most common base fluid that is applied in nanotechnology as a consequence of its abundance and properties. Its favorable pH, solubility, biocompatibility and neutrality in many ways make water one of the mostly preferred base fluid for the preparation of nanofluids. Ethylene glycol, on the other hand, is the most important glycol which is commercially available and is produced on a large scale around the globe. It is the most common antifreeze fluid for heating and cooling applications. Moreover, it is used as a working fluid for convective heat transfer in thermal engineering practices including heat pumps, condensers, liquid-cooled computers and air conditioning systems [35].

Besides from water and ethylene glycol, many other carrier fluids may also be used for the preparation of nanofluids. These fluids may be oil originated fluids such as propylene glycol, engine oil and mineral oil, or organic solvents such as hexane and heptane. Nonetheless, whatever the chosen fluid is, the direct mixing of the nanoparticles with these base fluids are generally not enough to ensure stability, but they rather require the aid of a surface-active agent.

2.1.3. Surfactants

Surfactants used in nanofluids, which are also referred as dispersants, play a tremendously important role in the creation of nanofluids. Stability may be regarded as one of the most important requirements for nanofluids in practical applications. In most cases, nanoparticles tend to aggregate because of their exceptionally large surface area to volume ratios and this

results in the formation of unstable nanofluids. The high surface energy due to their large surface-to volume ratios make nanoparticles highly unstable when compared to corresponding macro level structures. Moreover, nanoparticles exhibit a tendency to diminish their surface energy by coagulation which adversely affect their stability. It is therefore crucial to develop strategies to colloidally stabilize the nanoparticles against aggregation during, or after the synthesis [36].

In order to enhance the stability of nanoparticles in convenient base fluids, the usage of surface-active agents (coating agents or dispersants) is a necessity. They are widely used as auxiliaries to obtain evenly distributed and long-term stabilized colloidal suspensions. In order to prevent precipitation of nanoparticles, in other words, to enhance the colloidal stability and overcome the van der Waals forces, various polymer and surfactants which poses anionic, cationic or non-ionic functional groups can be applied during the preparation of nanofluids. The choice of a coating agent is a notable issue and it must be done according to the type of the base fluid preferred or the essence of the application. A water-soluble surfactant must be chosen when the base fluid is a polar solvent and an oil-soluble one must be preferred when the base fluid is non-polar [37].

It is noteworthy that these additives not only enhance stability, but they also enhance biocompatibility and provide surface functionality for additional attachments in particular areas. For example, functionalization of the nanoparticles with proper surfactants plays a crucial role in the field of biomedicine in which the nanoparticles can be targeted by specific biomolecules via functional groups on their surface which broadens the range of their applications [38].

2.2. STABILITY

Nanofluids are prepared by dispersing the synthesized nanoparticles in convenient base fluids. However, as previously mentioned, direct mixing of these components generally results in poor colloidal stability, thus nanoparticles tend to agglomerate and settle down after preparation due to interparticle interactions and gravitational force, as illustrated in Figure 2.1.

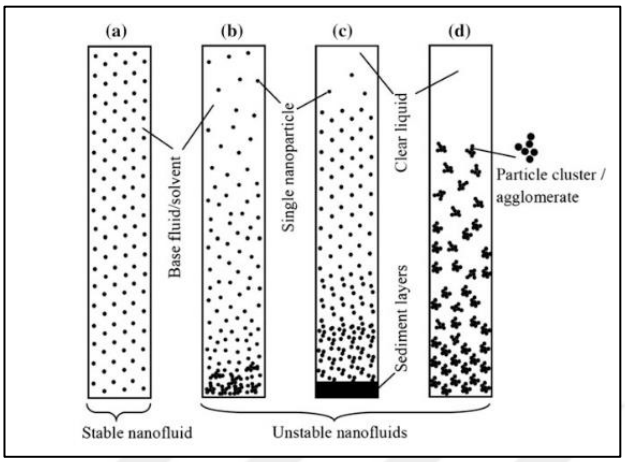

Figure 2.1. Stable and unstable nanofluids [39]

The larger surface area to volume ratios and higher surface energies of the nanoparticles are considered the reasons behind this rapid settlement. High surface energies and subsequent interactions of nanoparticles cause agglomeration and formation of clusters which results in rapid sedimentation of nanoparticles [40]. Therefore, it is initially essential to prepare colloidally stable nanofluids for their efficient implementation in applications. Sustaining the enhanced properties of the nanofluids can only be possible by preparing stable and durable nanofluids. Even though the contributions of surfactants are undeniably significant, the achievement of stable nanofluids is not always straightforward, but rather requires different approaches during the formation of nanofluids.

2.2.1. Preparation Methods of Nanofluids

The preparation of a stable nanofluid still remains as a great challenge for complicated nanoparticle, base fluid and surface-active agent complexes. There are mainly two preparation methods that can be preferred in order to ensure better stability and provide proper dispersion of nanoparticles. These methods are referred as two-step and one-step methods.

2.2.1.1. Two-Step Method

The two-step method basically consists of two consequent steps. In the first step, dry nanoparticle powders are produced first by various physical and chemical methods. In the second step, these dry nanoparticles are dispersed in convenient base fluids via various means such as magnetic or ultrasonic agitation.

It is the most extensively preferred method for the preparation of nanofluids because of its advantages such as higher production capacity and lower cost. As it is the most cost-effective method to yield nanofluids in large scale, two-step nano powder synthesis has already been scaled up to industrial production levels. However, nanofluids prepared by this method tend to aggregate over time and therefore are not colloidally stable for long term [37,40].

2.2.1.2. One-Step Method

One-step method, also referred as single-step method, involves the simultaneous synthesis and dispersion of nanoparticles in base fluids. With this method, the agglomeration of nanoparticles is minimized since extra steps like drying, storage, transportation and dispersion are eliminated. Hence, nanoparticles synthesized by this method are generally dispersed uniformly in base fluids and the colloidal stability of nanofluid is enhanced. However, one-step method has a relatively higher production cost as compared to two-step method and therefore its large scale application is relatively expensive [37,40].

2.2.2. Ultrasonication

The formation of clusters and the size of aggregates in nanofluids can significantly affect their properties. Ultrasonication is a commonly used physical treatment method to break up agglomerates and enhance dispersion of nanoparticles in base fluids. During this method, the high amount of ultrasonic energy that is applied to nanofluids serves to form a well dispersed colloidal suspension, by breaking the nanoparticle clusters. In order to break clusters of

nanoparticles and to disperse them in the base fluid, a sound energy at an ultrasonication level of at least 20 kHz is applied for a predetermined period of time [41].

Previous research has also focused on the effect of different power and frequency levels of sonication on nanofluid stability for different time intervals. The results illustrated that the optimum sonication condition of a nanofluid system is affected by various parameters such as the concentration, type and size of the particles and the type of the base fluid [40].

2.2.3. pH Control

The stability of nanofluids is directly related with their electro kinetic properties, which can be altered by regulating the pH of the system. An adjustment of the pH of the medium which leads to the modification of the charges on the surface of the particles, may enhance the stability of nanofluids by affecting the interaction between them. Acidic or basic treatment is a chemical method that can be used in order to obtain more stable nanofluids. By adding a suitable acid or alkali to the base fluid, the pH value of the base fluid can be modified and a stable nanofluid with uniform particle dispersion can be obtained as the charges of the functional groups that exist on the surface of the nanoparticles and belong to the surface-active agents are regulated. However, the usage of acid or alkali treated nanofluids are limited as it can cause some complications in some applications like corrosion. Therefore, the most suitable approach is to keep the pH of the suspension around neutral if possible [40,42].

2.3. SYNTHESIS OF NANOPARTICLES

The synthesis of nanoparticles can be achieved through numerous methods which may be classified as top-down and bottom-up approaches (Figure 2.2). The top-down method involves breaking down materials from their bulk forms while the bottom-up method relies on building nanostructures from atomic or molecular precursors, through controlled precipitation [36]. The essential synthesis pathways that proceeds via these methods for the production of nanoparticles are thermal decomposition, mechanical grinding, hydrothermal synthesis, microemulsion and co-precipitation.

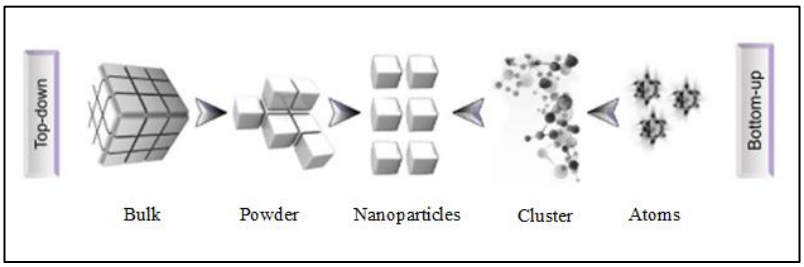

Figure 2.2. Schematic visualization of top-down and bottom-up approaches [36]

2.3.1. Thermal Decomposition

Among diverse techniques for the synthesis of nanoparticles, thermal decomposition may be referred as one of the most frequently used methods to produce stable, monodisperse nanofluids. It is an endothermic process in which chemical decomposition is accomplished through heat that breaks the chemical bonds in the precursor [43]. The decomposition temperature depends on the compound, and it is the specific temperature at which a compound is chemically decomposed. Briefly, the process includes a nucleation phase which occurs when the metal precursor is added into the heated solution in the presence of surfactant(s) and then this process is followed by the growth which takes place at elevated temperatures [44]. Nanoparticles are therefore produced as a consequence of chemical decomposition of the metal at the specific temperature [45,46]. Thermal decomposition method is capable of producing well defined smaller particles (Figure 2.3), however it is also possible to synthesize larger particles via this technique by using the smaller particles as seeds and perform growth by applying the same procedure.

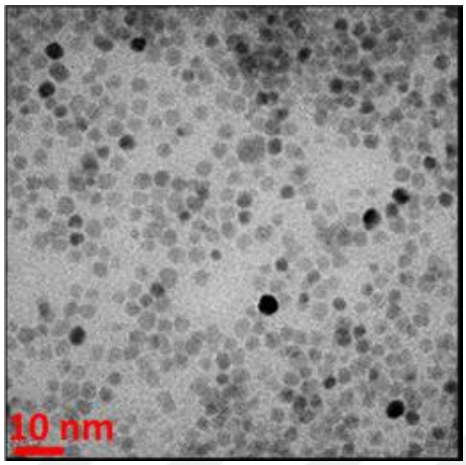

Figure 2.3. TEM image of Fe_3O_4 nanoparticles synthesized by thermal decomposition method [47]

2.3.2. Mechanical Grinding

Mechanical grinding which is also called as mechanical milling or ball-milling is a top-down method in which nanoparticles are produced from bulk material. It is an inexpensive and one of the most extensively used method to produce various nanoparticles by virtue of its simplicity. In this method different elements are grinded in an inert atmosphere to produce nanoparticles [45,46].

2.3.3. Hydrothermal Synthesis

The hydrothermal synthesis is performed via a heterogeneous reaction at high temperatures and pressures mainly within an autoclave for the production of nanocrystals for which the precursor is insoluble at ambient conditions [48]. During the synthesis, the reactants are supplied to the autoclave along with water and consequently the nanoparticle growth is carried out. Hydrothermal synthesis is typically performed at temperatures lower than 300°C, and the process necessitates the constant conservation of a temperature difference between the opposing ends of the crystallizing compartment. One of the greatest favors of this method is the

production of larger-sized and high-quality nanoparticles (Figure 2.4) that can also be tailored by changing the reaction conditions [49][50].

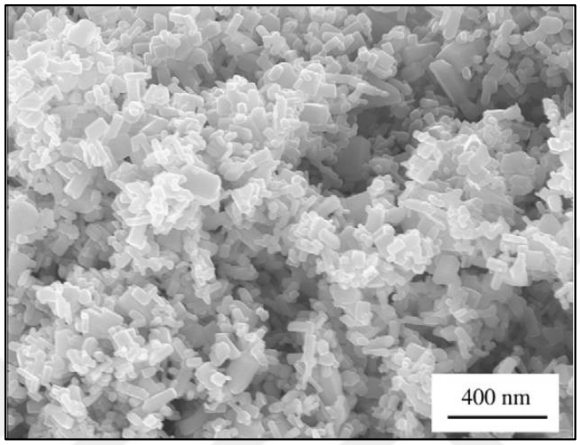

Figure 2.4. TEM image of hydrothermally synthesized ZnO nanoparticles [48]

2.3.4. Microemulsion

Microemulsion which is a thermodynamically stable isotropic dispersion of two immiscible liquids such as oil and water, is another method to synthesize nanoparticles. A microemulsion is a colloidal system of micron sized droplets of one immiscible liquid dispersed in another, in the presence of a suitable surfactant and a co-surfactant [51]. Both types of microemulsions which are direct (oil dispersed in water) and reverse (water dispersed in oil) can be used for the production of nanoparticles. In this method, the nanoparticles are spontaneously formed within the micron sized droplets which serve as a micro-reactor through vigorous stirring or sonication. During the process the aqueous phase is dispersed in the oil (water dispersed in oil) as microdroplets, and they are surrounded by a layer of surfactant molecules. The surfactant molecules also act as protective agents to prevent the nanoparticles from clustering. Briefly, the synthesis begins with the formation of nanoparticles through microemulsions and then it is followed by a reduction step in which a solvent such as acetone is added to the microemulsions and finally the precipitate can be isolated by filtering or centrifuging [49,52].

2.3.5. Co-Precipitation

Co-precipitation is one of the most basic and most common methods for the synthesis of nanoparticles. It is mainly used for the synthesis of metal oxides and magnetic nanoparticles such as Fe_3O_4 (Figure 2.5). One of the greatest benefits of this technique is the large-scale production of nanoparticles at a comparably smaller time scale [53]. Briefly the synthesis involves the mixing of metal salts in aqueous medium which are then reacted to form intermediate phases. This intermediate phase is then precipitated by changing the pH of the medium. The main disadvantage of this method is the sudden nucleation of particles due to high supersaturation values which leads to a limited growth phase that prevents control over nanoparticle properties such as average size and morphology [54]. One of the main steps of the synthesis which is the addition of a base solution such as sodium hydroxide, results in the precipitation of nanoparticles. Experimental parameters that alter the synthesis may be listed as; the nature of precursor salt used (i.e. sulfates, chlorides, nitrates), concentration of the reactants and ions, the pH, the reaction temperature and ionic strength of the media, and many other parameters that affect the reaction like the stirring rate or the rate of addition of alkali solution [36,55,56].

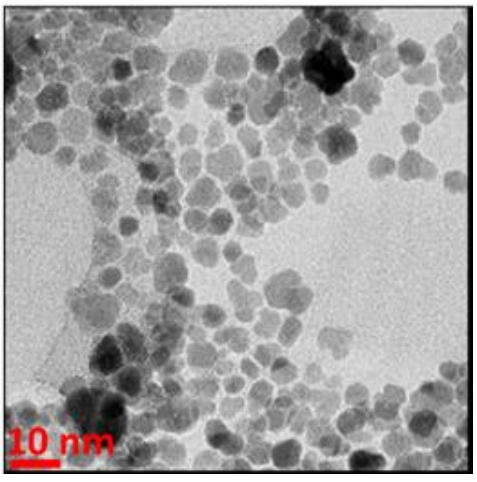

Figure 2.5. TEM image of Fe_3O_4 nanoparticles synthesized by co-precipitation method [47]

Table 2.1. Summary comparison of different synthesis methods [52,57]

Method	Synthesis	Reaction Temp (°C)	Duration	Size Distribution	Control	Yield
Thermal Decomposition	Complicated, inert atmosphere	100-320	Hours - days	Very narrow	Very good	High
Hydrothermal Synthesis	Simple, high pressure	220	Hours	Very narrow	Very good	Medium
Microemulsion	Complicated, ambient conditions	20-50	Hours	Relatively narrow	Good	Low
Co-precipitation	Very simple, ambient conditions	20-90	Hours	Relatively narrow	Poor	High
Partial Oxidation	Simple, ambient conditions	20-90	Hours	Relatively narrow	Good	High

2.4. APPLICATIONS OF NANOFLUIDS

The rewarding and significant properties of nanoparticles and nanofluids have led to a great interest towards the implementation in many fields such as in cooling and heating of various devices as well as several industrial applications [15], power generation, chemical processes, transportation, microelectronics, other micro-sized applications [7], electronics, automotive and nuclear systems where enhanced heat transfer and efficient heat dissipation is required [5], industrial heating and cooling applications, transportation industry, biomedical applications (drug delivery, cancer therapeutics, cryopreservation) [58], space and defense [37], solar energy and thermal storage materials [8], biotechnology/ biomedicine applications, magnetic resonance imaging and targeted drug delivery (Figure 2.6) [52,59].

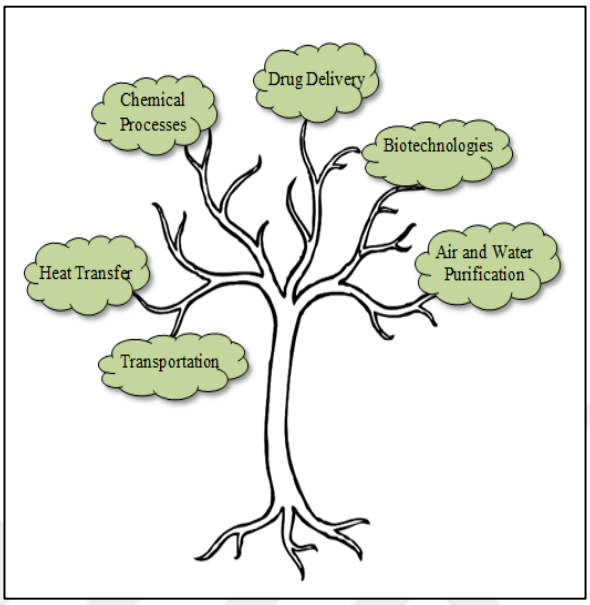

Figure 2.6. Different branches of nanotechnology

2.5. HEAT TRANSFER APPLICATIONS OF NANOFLUIDS

Improving the heat transfer efficiency is of great importance for many industrial applications. As heating and cooling fluids play a major role in applications, heat transfer performance of nanofluids has become one of the most thoroughly investigated research topics in the last two decades. As mentioned in section 2.1.2, mostly employed conventional fluids for applications involving heat transfer are water, ethylene glycol and mineral oil. However, these conventional fluids possess poor heat transfer abilities when compared with the majority of solids. The ineffectual heat transfer capabilities of these fluids are a limitation for efficiency and compactness of the heat exchangers. Accordingly, many researchers have been trying to develop new types of heat transfer fluids to enhance the heat transfer performance of these conventional heat transfer fluids [2,60–62]. Nanotechnology has opened up many opportunities on the way of overcoming the obstacles limiting the heat transfer performance of current fluids by the implementation of nanoparticles to traditional base fluids [36]. It is well known that crystalline solids possess intrinsically larger thermal conductivities than those of fluids by 1-3 orders of magnitude (Table 2.2). Furthermore, the thermal conductivity of fluids plays a critical

role for the energy efficiency improvement of heat transfer equipment [1,3,63]. Consequently, it was propounded to suspend nanosized solid, preferably metal, particles in a base fluid to increase its thermal properties. These newly engineered suspensions of solid particles were reasonably expected to present enhanced thermal conductivities relative to those of pure conventional fluids [7][63].

Table 2.2. Thermal conductivity of various materials

Material	**Thermal Conductivity (W/m.K)**
Aluminum	235
Copper	401
Engine Oil	0.15
Gold	314
Iron	67
Silver	428
Water	0.58

The concept of dispersing small solid particles in fluids can be tracked back to Maxwell's pioneering study in 1873 in which he demonstrated the possibility of increasing the thermal conductivity of a fluid upon the addition of solid particles [64][65]. On the basis of this historical background, several researchers investigated the feasibility of such suspensions with milli or micrometer sized solid particles, yet they observed some drawbacks. The rapid settlement of particles and formation of a layer on the surface were some of the problems encountered when using milli or micrometer sized particles. Moreover, the pressure drop of the fluid was increased considerably and particles tended to clog the flow channels due to rapid settlement originated from their comparably larger size, particularly if the cooling channels were narrow [2,66]. Thus, the idea of suspending particles in a liquid was well known but not realized for heat transfer operations.

Fortunately, by the development of modern materials technology, it is possible to yield nanometer-sized particles with quite different mechanical, thermal, electrical and optical properties. The implementation of nanofluids' great potential in heat transfer applications was first introduced by Choi et. al in 1995 [3]. In his work, Choi observed that the dispersion of a small number of nanoparticles altered the thermal conductivity of the base fluid remarkably. Owing to their nanosized particles and extremely large surface area to volume ratios, these innovative fluids were expected to be the next generation heat transfer fluids, exhibiting superior heat transfer properties relative to that of traditional dispersions [67][68].

All related studies have shown that nanofluids were capable of overcoming the obstacles encountered when using milli or micrometer sized particles. Due to their extremely small sizes and larger surface areas, nanoparticles have been found to satisfy the required essentials such as minimal clogging in flow channels, long-lasting stability and homogeneity [5,58]. Furthermore, in addition to all these advantages of nanofluids, they have been found to display enhanced thermophysical properties (i.e. thermal conductivities), compared to those of base fluids such as water and ethylene glycol [6,7,11,66].

As a wide variety of industrial processes involve heat transfer, the improvement of thermophysical properties of the working fluid may lead to energy saving, reduced process time and extended physical life of the equipment. Therefore, enhanced thermal conductivity means improved energy efficiency, exceptional performance, and reduced operating expenses which is a cutting-edge for applications involving heat transfer [4,69].

The two types of convective heat transfer are referred as forced and natural (free) convection. The transfer of heat via the movement of a fluid is referred to as convective heat transfer. The application is called as forced convection when the fluid is forced to flow by external means such as fans, pumps or by stirring, and as natural (free) convection when the fluid motion is triggered by variations in density, emerging from variations of temperature within the fluid [70]. The convective heat transfer coefficient, which is also a function of the thermophysical properties of the heat transfer fluid describes the efficiency of heat transfer. Taking all these into consideration, there is a decent amount of research that has been carried out on the

convective heat transfer performance of various nanofluids exhibiting unusual thermophysical properties under different flow conditions.

2.5.1. Forced Convection

The analysis of forced convection requires the calculation of dimensionless numbers such as Reynolds, Prandtl, Nusselt and Peclet numbers which are all functions of thermophysical properties of corresponding heat transfer fluid. There are several studies related with the convective heat transfer characteristics of nanofluids regardless of analyzing the thermophysical properties.

Maïga et. al. [71] investigated the laminar flow, forced convection heat transfer behavior of γ-Al_2O_3/Water and γ-Al_2O_3/EG mixtures for two distinct geometrical configurations and reported that the addition of nanoparticles leads to a significant enhancement of heat transfer coefficient. They also observed a further enhancement by the increase in nanoparticle concentration.

Xuan and Li [72], conducted experiments to investigate the convective heat transfer and flow characteristics of aqueous copper nanofluids at different concentrations by measuring the heat transfer coefficient and friction factor for both flow regimes, within a tube. Their experimental results indicated an increase in the convective heat transfer coefficient which is directly proportional with the particle loading. They reported a 60 percent increase in the convective heat transfer coefficient at 2 vol. percent, relative to that of the base fluid, at the same Reynolds number. Furthermore, they proposed a novel correlation for the nanofluid convective heat transfer.

Duangthongsuk and Wongwises [73], performed an experimental investigation on the friction factor and heat transfer performance of aqueous nanofluids containing TiO_2 nanoparticles flowing inside a heat exchanger, under turbulent flow conditions. Their results showed a 26 percent enhancement of the heat transfer coefficient with 1 vol. percent nanoparticle concentration when compared to water. In addition, they proposed a novel correlation for the prediction of Nusselt number for TiO_2/Water nanofluids.

2.5.2. Natural Convection

In contrast to forced convection, natural convection, also referred as free convection, does not require any external means. The heat transport is triggered by the density differences occurring due to temperature gradients throughout the fluid. Natural convection is an important phenomenon which is employed in different engineering applications such as geophysics, cooling of electronics, solar energy, nuclear energy and many other industrial applications [74]. Consequently, studies were performed to analyze the performance of nanofluids in natural convection applications.

Li and Peterson [75], conducted experiments on the natural convection heat transfer characteristics of aqueous Al_2O_3 nanoparticles with volume fractions ranging from 0.5 to 6 percent and they observed a deterioration of the natural convective heat transfer coefficient with increasing volume fraction of nanoparticles.

Ho et. al. [76], also investigated aqueous suspensions of Al_2O_3 nanoparticles with volume fractions ranging from 0.1 to 4 percent, experimentally. They reported a systematic deterioration in heat transfer when considering nanofluids with volume fractions greater than 2 percent and an enhancement of 18 percent as compared to the corresponding base fluid, when considering volume fractions lower than 0.1 percent.

The review of relevant literature exposes that the outcomes of studies related with the heat transfer via nanofluids is controversial. Even though most of the theoretical studies suggest a significant enhancement in the heat transfer performance of conventional fluids [77,78], some experimental results, on the contrary, display a consistent deterioration [75,79]. The uncertainty and discrepancy might be attributed to the lack of extensive studies on the subject. It should be emphasized that each nanoparticle-base fluid system exhibits different characteristics and so far there are limited data on the thermophysical properties of several nanofluid systems. Therefore, in the quest of understanding nanofluids' thermal performance, extensive experimental and theoretical studies on thermophysical properties is a necessity in order to overcome similar conflictions.

2.6. THERMOPHYSICAL PROPERTIES OF NANOFLUIDS

Material properties that alter with temperature, without changing the substance's chemical identity are defined as thermophysical properties. They can also be generalized as all material properties that influence the transfer and storage of heat and that vary with state variables such as temperature and composition, without changing the substance's chemical identity. Over the years, researchers who have committed to the investigation of the properties of nanofluids, revealed novel information about these materials. Based on extensive studies, it was established that the poor thermal conductivities of conventional fluids, which was a limitation in heat transfer applications, may be increased substantially upon the addition of nanoparticles. The discovery of the alteration in the thermal conductivity and the associated possible enhancement in the energy exchange capabilities made nanofluids potential candidates for heat and mass transfer applications. The increasing number of similar results have motivated both the industry and the science community to investigate the thermophysical properties of nanofluids [80]. The ongoing research in this regard has also showed that the addition of nanoparticles affects not solely the thermal conductivity, but also other thermophysical properties such as density and viscosity of base fluids.

The investigation of thermophysical properties such as density, viscosity, thermal conductivity and specific heat of nanofluids is essential in order to use them in practical applications involving heat transfer [6]. All these properties not solely play an important role in energy efficiency, but they are also prerequisites for the calculation of heat transfer coefficient and dimensionless numbers commonly used in heat transfer such as Reynolds number, Nusselt number and Prandtl number. Moreover, the required pumping power and the pressure loss also depends on dimensionless numbers. Density possesses a critical role in the calculation of Reynolds number while viscosity affects the Reynolds and Prandtl numbers. As for the Nusselt number, it expresses the relationship in between the heat transfer coefficient and the thermal conductivity of flowing fluid. The aforementioned dimensionless numbers that are all functions of the thermophysical properties are expressed as follows;

$$Re = \frac{\rho v D}{\mu} \tag{2.1}$$

$$Nu = \frac{hD}{k} \tag{2.2}$$

$$Pr = \frac{\mu C_p}{k} \tag{2.3}$$

In which ρ is the density of the fluid, v is the velocity of the flow, D is the characteristic length, μ is the fluid's dynamic viscosity, h is the heat transfer coefficient, C_p is the specific heat and k is the thermal conductivity of the fluid.

All in all, nanofluids are now being considered as new generation fluids for heat transport in diverse applications and their heat transfer capabilities are being studied along with their thermophysical properties. Relevant research has also shown that the alterations in the thermophysical properties of nanofluids are distinct for each nanoparticle-base fluid system and furthermore, they are affected by many variables including the size, morphology and type of nanoparticles, their concentration and temperature [7][81][82]. As a consequence, extensive studies on the thermophysical properties of diverse nanofluids with respect to altering temperature and concentration of nanoparticles are indispensable and must be proceeded, before using them in practical applications.

The evaluation of the heat transfer performance of a system requires the computation of the already existing models which are all functions of dimensionless numbers such as Reynolds (equation 2.1), Nusselt (equation 2.2) and Prandtl (equation 2.3) numbers. The heat transfer calculations involving traditional fluids such as water and ethylene glycol can comfortably be computed as all their thermophysical properties at any temperature are available in the literature. As for the case of mixtures of these fluids, mixture rules can be applied for the calculation of their thermophysical properties at any temperature. However, calculations for evaluating the heat transfer performance gets complicated when using distinct nanofluids for heat transfer purposes. Hence, the scarceness of available data of the thermophysical properties

of nanofluids has oriented the studies of researchers towards their measurement as a function of many variables, among which solid volume fraction and temperature are the most significant.

2.6.1. Measurement of Thermophysical Properties of Nanofluids

One of the routes that could be chosen when evaluating the heat transfer performance of nanofluids is obviously the direct measuring of their thermophysical properties. Accordingly, many researchers have measured the thermophysical properties such as density, viscosity and thermal conductivity of various kinds of nanoparticle-base fluid systems in order to see the effect of nanoparticle loading over the thermophysical properties and reported the results of their measurements.

2.6.1.1. Density

Density, which is among the fundamental thermophysical properties of a substance, is by definition, a measure of the mass of a substance per unit volume. Even though experimental investigations on the density of nanofluids in the literature are limited as compared to other properties such as viscosity and thermal conductivity, density has a significant role when studying the heat transfer performance of a nanofluid [83]. Studies have shown that distinct nanoparticle-base fluid systems ended up with similar results and agreed on the enhancement of base fluid densities upon the addition of nanoparticles. Moreover, those who have studied the effect of temperature reported a slight decrease in the densities of nanofluids with increasing temperature as expected.

Vajjha et. al. [80] performed density measurements of nano sized aluminum oxide, antimony-tin oxide, and zinc oxide suspensions in a 60:40 EG/water mixture, over a temperature range from 0ºC to 50ºC, for several solid volume fractions. Their results have shown that the density is increased with increasing volume fraction of nanoparticles.

Pastoriza-Gallego et. al. [9] conducted an experiment that aimed to determine the density of nanofluids composed of alumina (Al_2O_3) nanoparticles dispersed in water. They carried out

experimental density measurements for three distinct samples, at weight fractions ranging from 0.5 to 7 percent and a pressure range from atmospheric pressure to 25 MPa, at three different temperatures. Results illustrated that the effect of particle size over the density of nanofluid is not critical but also not negligible and smaller nanoparticles lead to higher nanofluid densities. Moreover, it was also shown that density is enhanced with increasing particle concentrations.

O. Mahian, A. Kianifar and S. Wongwises [8] studied the densities of ZnO nanoparticles in an ethylene glycol-water mixture (40:60). In their study, the densities of ZnO nanofluids with distinct volume fractions (from 0.25 to 4 percent) were measured at a temperature range of 25-40ºC. Their experimental results have similarly revealed that the density of the base fluid increases considerably with increasing particle loading. They additionally reported a slight decrease in the densities of nanofluids with increasing temperature (Figure 2.7).

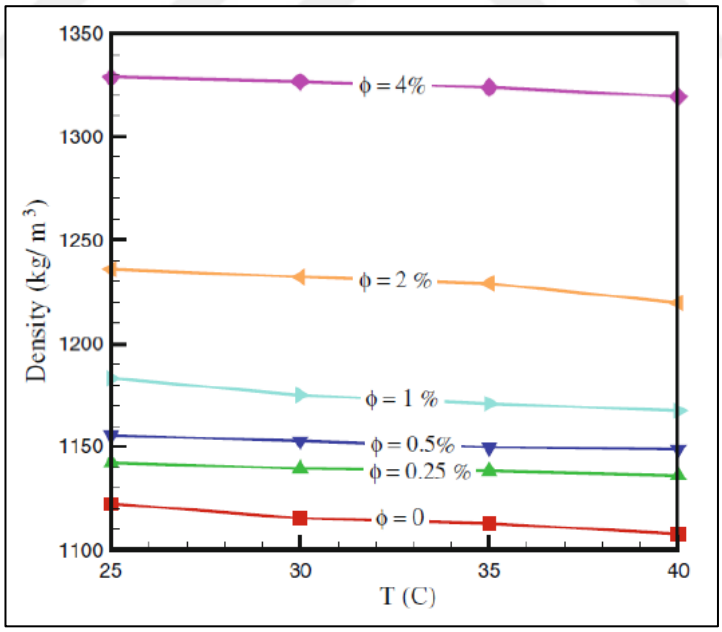

Figure 2.7. Density variation of ZnO/EG:Water nanofluid with respect to temperature and concentration [8]

Naddaf et. al. [84] investigated the effects of temperature and mass concentration on the densities of various kinds of carbon suspensions in diesel oil. The concentrations of nanofluids

were varied from 0.05 to 0.5 percent by mass and the measurements were conducted in the range from 5 to 100℃. They reported a decrease in the densities of all nanofluids with increasing temperature as well as an increase that is directly proportional to particle concentration at constant temperature.

2.6.1.2. Viscosity

Viscosity basically is a measure of a substance's resistance to flow, and it mainly depends on the friction between the molecules in a fluid. It is one of the essential transport properties for all applications involving fluids. It is tremendously important when establishing accurate heat transfer coefficient as well as the required pumping power of the fluid. Moreover, the pressure drop is directly proportional to the viscosity of the fluid and Prandtl and Reynolds numbers are both functions of it. Hence, viscosity is a property that is as crucial as thermal conductivity in engineering systems involving fluid flow and it is essential to understand the rheological properties of nanofluids for practical uses [23,85,86]. However, limited studies have been devoted to the viscous properties of nanofluids whereas an enormous effort was dedicated to their thermal conductivity investigations [65]. Recent reports on the rheological behavior of nanofluids indicated that the viscosity of base fluids generally enhances considerably with increasing loading of nanoparticles and deteriorates upon increasing temperature [87].

Pak and Cho [88] conducted experiments on aqueous nanofluids containing γ-Al_2O_3 and TiO_2 nanoparticles with mean diameters of 13 and 27 nm, respectively. Conducting viscosity measurements up to 10 vol. percent, they reported that the viscosity of nanofluids increased remarkably with an increase in particle concentration.

Toghraie et. al. [89] measured the viscosities of magnetite (Fe_3O_4/Water) nanofluids between temperature range from 20°C to 55°C for various particle volume fractions ranging from 0.1, to 3 percent. Their measurements indicated a remarkable augmentation in the viscosity of the base fluid with increasing nanoparticle volume fraction, which was even more apparent at higher volume fractions. They reported a maximum viscosity enhancement of 129.7 percent for 3.0 vol. percent and at a temperature of 55℃. Moreover, they reported that the dynamic

viscosity of the nanofluids decrease dramatically with an increase in temperature and a similar path was followed by all nanofluids.

W. Duangthongsuk and S. Wongwises [7] have measured the viscosity of TiO_2/Water nanofluids with volume fractions of 0.2 – 2 vol. percent between a temperature range from 15ºC to 35ºC. It was similarly shown that the viscosity of the base fluid was enhanced upon the addition of nanoparticles. Furthermore, they also reported that the enhancement in viscosity increases with increasing particle concentration and deteriorates with increasing temperature (Figure 2.8).

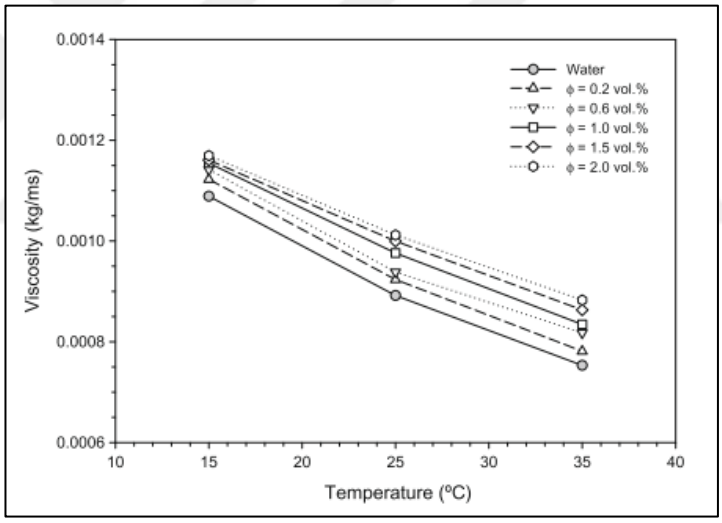

Figure 2.8. Influence of particle loading and temperature on the viscosity of TiO_2/Water nanofluids [7]

Li et. al. [90] conducted experiments to measure the viscosities of CuO/Water nanofluids at different temperatures and mass fractions of nanoparticles and indicated that the viscosity of the base fluid enhances upon particle loading and deteriorates with increasing temperature by following the trend of the corresponding base fluid.

Sundar et. al. [91] made experimental investigations on the viscosity of magnetic nanofluid consists of Fe_3O_4 nanoparticles synthesized via coprecipitation method. The viscosity of

magnetic nanofluids up to 2 vol. percent of nanoparticles for a temperature range from 20 ℃ to 60 ℃ was measured and the results illustrated that the viscosity of the base fluid was enhanced upon increasing particle volume fraction and deteriorated with an increasing temperature (Figure 2.9). The highest viscosity enhancement was observed for 2 vol. percent and at 60℃ which was almost 3 times higher than that of the base fluid.

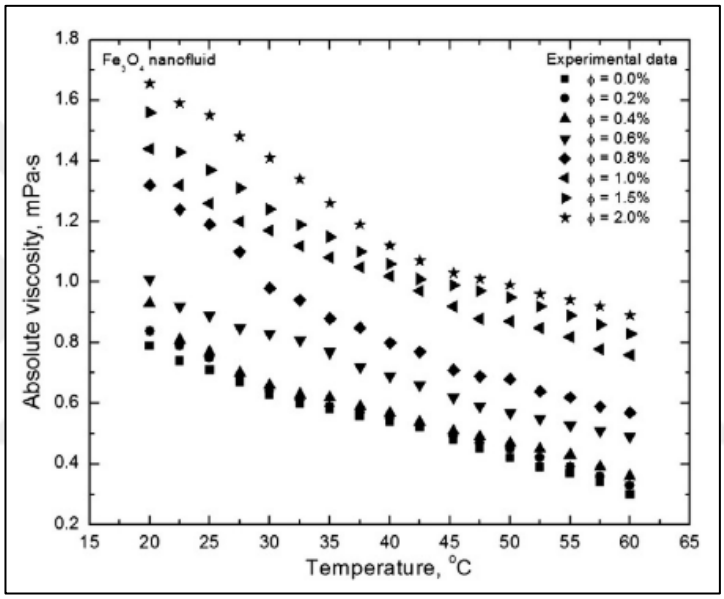

Figure 2.9. Viscosity of Fe_3O_4/Water nanofluid with the effects of volume concentration and temperature [91]

Nyugen et. al. [92] investigated the influence of particle size over the viscosities of Al_2O_3 and CuO containing aqueous nanofluids. For this purpose, 36 nm and 47 nm of Al_2O_3 along with 29 nm of CuO nanoparticles were analyzed. The results indicated that the effect of particle size is negligible for particle volume fractions lower than 4 percent, whereas nanofluids with bigger sized nanoparticles exhibit higher viscosities at higher volume fractions.

He et. al. [93] similarly examined the effect of particle size over the rheological behavior of TiO_2 nanofluids containing different sized nanoparticles and reported that the viscosity of the nanofluids is proportional with average particle size. On the other hand, Namburu et. al. [86] measured the viscosities of various SiO_2 nanofluids consist of particles having different average

particle sizes (20, 50 and 100 nm) suspended in a mixture of ethylene glycol and water (60:40 by weight) and reported that the viscosity of nanofluids were decreased with an increase in average particle size. Similar outcomes were also shown by Chevalier et. al. [94] for SiO_2 nanoparticles dispersed in ethanol.

The viscosity of nanofluids which is composed of CuO nanoparticles dispersed in a mixture of base fluids was also investigated by Naik et. al. [82]. The experimental study pointed out that the viscosity of CuO nanoparticles suspended in a Propylene Glycol-Water mixture decreases exponentially with an augmentation in temperature while the highest enhancements were found for the highest particle loading (Figure 2.10).

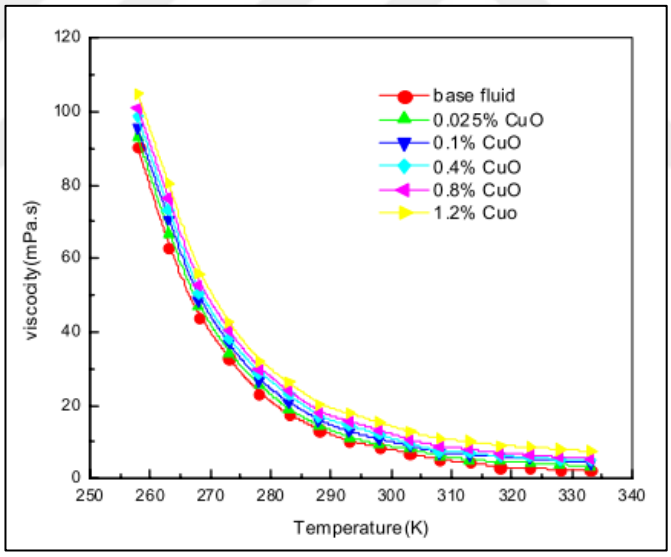

Figure 2.10. Viscosity of CuO/PG:Water nanofluids with the effects of volume concentration and temperature [82]

A summary of studies related with the dynamic viscosity of various nanoparticle-base fluid systems is presented in Table 2.3.

Table 2.3. Summary of literature survey on the viscosity enhancements of various nanofluids [23,95]

Researcher	**Base fluid**	**Particle name**	**Particle size (nm)**	**Volume fraction (%)**	**Viscosity enhancement (%)**
Anoop et. al.	Water	Al_2O_3	45	2-8	1-6
Anoop et. al.	Water	Al_2O_3	150	2-8	1-3
Anoop et. al.	Water	Al_2O_3	95	0.5-6	3-77
Chen et. al.	EG	TiO_2	25	0.1-1.86	0.5-23
Chevalier et. al.	Ethanol	SiO_2	35	1.2-5	15-95
Chevalier et. al.	Ethanol	SiO_2	94	1.4-7	12-85
Duangthongsuk and Wongwises	Water	TiO_2	21	0.2-2	4-15
Masuda et. al.	Water	TiO_2	27	1-4.3	11-60
Mojarrad et. al.	Water	Al_2O_3	20-30	0.25-0.7	30
Murshed et. al.	DIW	TiO_2	15	1-5	4-86
Nyugen et. al.	Water	Al_2O_3	36	2.1-13	10-210
Nyugen et. al.	Water	Al_2O_3	47	1-13	12-430
Nyugen et. al.	Water	CuO	29	0.15-13	1811
Pastoriza-Gallego et. al.	Water	CuO	11	1-10	2.5-73
Prasher et. al.	PG	Al_2O_3	27	0.5-3	7-29
Prasher et. al.	PG	Al_2O_3	40	0.5-3	6-36
Sekhar et. al.	Water	Al_2O_3	47	0.01-1	28
Silambarasan et. al.	Water	TiO_2	100-344	0.27-1.39	10
Sundar et. al.	Water	Fe_3O_4	13	0.2-2	6-109
Toghraie et. al.	Water	Fe_3O_4	25	3	129.7
Wang et. al.	EG	Al_2O_3	28	1.-3.5	7-39

2.6.1.3. Thermal Conductivity

Thermal conductivity, which is used to describe the thermal behavior of materials is another essential property of crucial importance when dealing with thermal applications involving fluids. It is defined as the ability of a material to conduct heat and used frequently for the process calculations. Thus, it is one of the most significant thermophysical properties of a substance.

As the thermal conductivity of traditional heat transfer fluids such as water and ethylene glycol are relatively poor as compared to that of solids, the suspensions of solids in convenient fluids were expected to display enhanced thermal conductivities. Therefore, several studies were performed and focused on the investigation of thermal conductivities of various types of nanofluids. The majority of these studies have shown an enhancement in the thermal conductivity of base fluids upon the addition of nanoparticles [74]. However, contradictory results have also been illustrated.

W. Duangthongsuk and S. Wongwises [7] conducted experimental investigations on the thermal conductivities of TiO_2/Water nanofluids, along with their viscosities. Data was collected for a volume fraction range of 0.2 – 2 vol. percent and between a temperature range from 15ºC to 35ºC. The results indicated that the thermal conductivities of the nanofluids were higher than that of the base fluid and further enhanced with increasing nanoparticle concentration as well as increasing temperature (Figure 2.11).

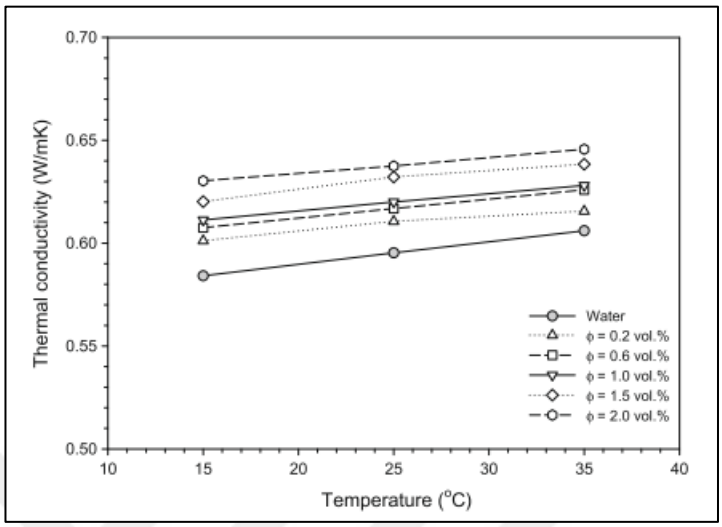

Figure 2.11. Influence of particle loading and temperature on the thermal conductivity of TiO_2/Water nanofluids [7]

Sundar et. al. [91] similarly investigated the viscosities and thermal conductivities of magnetic Fe_3O_4/Water nanofluids containing particles synthesized by coprecipitation method with an average size of 13 nm. The measurements that were performed for concentrations up to 2 vol. percent and 60 ^oC indicated that the thermal conductivity of water enhances with increasing volume fraction of magnetic nanoparticles and temperature (Figure 2.12). They reported a maximum thermal conductivity enhancement of 4 percent for a volume fraction of 2 percent at 60°C.

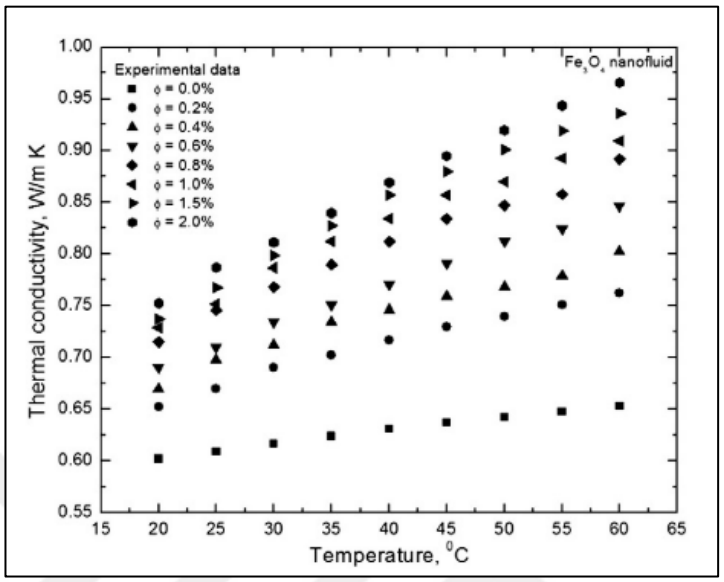

Figure 2.12. Influence of particle loading and temperature on the thermal conductivity of Fe_3O_4 /Water nanofluids [91]

Das et. al. [96] experimentally studied the effect of temperature and concentration over the thermal conductivity of aqueous Al_2O_3 and CuO nanofluids. The measurements were conducted at different temperatures and illustrated a considerable enhancement of thermal conductivity from 2 to 10.8 percent as the temperature augmented from 21℃ to 51℃, respectively. The enhancement was even greater for nanofluids containing higher concentrations of nanoparticles. The maximum enhancement of 24.3 percent was obtained for nanofluids having a concentration of 4 vol. percent at 51°C.

Kwak and Kim [97] investigated the thermal conductivities of various concentrations of 12 nm CuO nanoparticles suspended in ethylene glycol at 298 K. They reported that the thermal conductivity enhancement is only attainable when the particle concentration is below the dilute limit.

Philip et. al. [19] analyzed a kerosene based magnetic (Fe_3O_4) nanofluid and observed a thermal conductivity enhancement of 300 percent with a nanoparticle loading of 6.3 vol. percent for a particle size of 6.7 nm under the effect of an applied magnetic field. Parekh and Lee [98]

similarly studied Fe_3O_4 nanoparticles dispersed in kerosene, under transverse magnetic field and observed an 30 percent enhancement in the thermal conductivity, for 4.7 vol. percent.

Gavali et. al. [99] investigated experimentally the thermal conductivity of water based ferrofluids containing Fe_3O_4 nanoparticles having an average particle size of 10 nm, under the presence of an external magnetic field. They reported a 200 percent enhancement in the thermal conductivity at 5.0 percent volume fraction.

Karimi et. al. [100] performed experimental investigations on the thermal conductivity of aqueous suspensions of magnetic Fe_3O_4 and $CoFe_2O_4$ nanoparticles in the absence and presence of a uniform magnetic field for a maximum volume fraction of 4.8 percent. Results indicated that the thermal conductivity of magnetic nanofluids increases with increasing nanoparticle concentration and magnetic field intensity before attaining saturation. They reported a maximum enhancement of 196 and 148 percent, for Fe_3O_4 and $CoFe_2O_4$ nanofluids, respectively.

Yu et. al. [101] studied the thermal conductivity of oleic acid coated magnetic Fe_3O_4 nanoparticles having a relatively larger average particle size of 155 nm suspended in kerosene. They found a 34 percent enhancement in the thermal conductivity of the base fluid at a considerably dilute concentration. Similarly, Eastman et. al. [63] measured the thermal conductivity of Cu nanoparticles having a mean diameter smaller than 10 nm that are suspended in ethylene glycol. They reported an enhancement up to 40 percent in the effective thermal conductivity of ethylene glycol for 0.3 vol. percent of Cu nanoparticles.

Altan et. al. [102] studied the variations in thermal conductivities of fluids upon addition of magnetic (Fe_3O_4) nanoparticles synthesized by various synthesis methods and suspended in diverse base fluids. Based on their experiments they reported an enhancement up to 28 percent for 2.5 wt. percent of magnetic nanoparticles in hexane. The results also illustrated that the enhancement in thermal conductivity was found to be dependent on the concentration of the nanoparticles, the method of preparation and the base fluid.

Altan et. al. [103] also investigated the thermal conductivity of both aqueous and heptane based Fe_3O_4 nanofluids in the presence of an external magnetic field. The thermal conductivities of water and heptane based nanofluids with concentrations below 2 percent were enhanced up to 5.2 and 2.8 percent, respectively, in the presence of external magnetic field.

A summary of studies related with the thermal conductivities of various types of nanofluids is presented in Table 2.4.

Table 2.4. Summary of literature survey on the thermal conductivity enhancements of various nanofluids [66]

Rescherear	**Base fluid**	**Particle name**	**Particle size (nm)**	**Maximum Concentration (%)**	**Maximum Enhancement in k (%)**
Altan et. al.	Hexane	Fe_3O_4	6	2.5	28
Eastman et. al.	Water	Al_2O_3	33	5	29
Eastman et. al.	Water	CuO	36	5	60
Eastman et. al.	EG	Cu	<10	0.3	40
Hong et. al.	EG	Fe	10	0.55	18
Hwang et. al.	EG	CuO	35.4	1	9
Kumar et. al.	Water	Au	4	0.00013	20
Kwak and Kim	EG	CuO	12	1	6
Lee et. al.	EG	Al_2O_3	38	5	18
Lee et. al.	EG	CuO	23.6	4	22
Liu et. al.	EG	CuO	29	5	23

Table 2.4. Summary of literature survey on the thermal conductivity enhancements of various nanofluids (Continued) [66]

Rescherear	**Base fluid**	**Particle name**	**Particle size (nm)**	**Maximum Concentration (%)**	**Maximum Enhancement in k (%)**
Murshed et. al.	DIW	TiO_2	15	5	30
Murshed et. al.	DIW	Al_2O_3	80	5	24
Murshed et. al.	EG	TiO_2	15	5	18
Murshed et. al.	EG	Al	80	5	45
Wang et. al.	Water	Al_2O_3	28	3	12
Wang et. al.	EG	Al_2O_3	28	5	26
Wang et. al.	EG	Al_2O_3	29	4	18
Wang et. al.	EG	TiO_2	40	5	13
Wang et. al.	DIW	CuO	50	0.4	17
Wen and Ding	Water	TiO_2	34	0.66	6
Xie et. al.	EG	Al_2O_3	60.4	5	30
Xuan and Li	Water	Cu	100	5	54
Xuan et. al.	Water	Cu	35.4	2	24
Zhu et. al.	Water	Fe_3O_4	10	4	38

Although, the vast majority of studies agreed on enhancement of thermal conductivity upon addition of nanoparticles in appropriate base fluids, the results are contradictory. Whereas some studies reported a dramatic increase of thermal conductivity even for relatively low volume fractions, other showed moderate increases for concentrated nanofluids. Moreover, some

studies revealed a possible decrease in the thermal conductivity of the corresponding base fluid, especially for water, upon the addition of nanoparticles. For instance, Altan et. al. [104] who investigated experimentally the effect of silver nanoparticles over the thermal conductivity of several base fluids reported a nearly 10 percent deterioration in the effective thermal conductivity of water with 1 wt. percent of silver nanoparticles. Consequently, the main mechanism governing the heat conduction of nanoparticles is still not fully understood.

2.6.2. Empirical and Theoretical Models for The Estimation of Thermophysical Properties of Nanofluids

Based on several experimental studies it is evident that nanofluids mostly exhibit substantially higher thermophysical properties than those of conventional heat transfer fluids. Ever since the enhancement in the thermophysical properties of base fluids by the addition of nanoparticles was discovered, many researchers have concentrated on mechanisms governing these variations. The enhancement in the thermophysical properties of nanofluids is generally attributed to several mechanisms such as formation of a fluid layer around nanoparticles, Brownian motion of nanoparticles and nanoparticle clustering. Some studies had put forward that Brownian motion induced convection and conduction through the agglomerates might be the most significant factor causing the radical enhancement of thermal conductivity [12,13,105]. Although the alterations of the thermophysical properties of nanofluids have been interpreted by several mechanisms and models, no agreement has been reached and the key mechanism governing the thermal behavior of nanofluids is unfortunately still not known. Their unpredictable behavior may be attributed to the fact that thermophysical properties of nanofluids depend on various factors such as the size and type of the nanoparticles, type of the base fluid, the solution pH and even the solution-ageing [7].

It is well known that all of these properties of nanofluids are affected by the size, type and volume fraction of nanoparticles and temperature. Considering all these variables, measurement of necessary thermophysical properties is time consuming and not a practical solution for heat transfer applications. Thus, it is necessary to formulate new correlations in order to predict the thermophysical properties of nanofluids at different concentrations and temperatures. The usage

of novel and convenient correlations for nanofluids would surely be more practical than the measurement of these properties which are dependent on numerous variables.

The most well-known theoretical models to predict the thermophysical properties of solid-liquid suspensions available in the literature are; the Einstein model [82] for the viscosity and the Maxwell model [64] for the thermal conductivity. However, neither of these models is developed for nanoparticles and their effective usage is limited by some constraints. The applicability of Einstein's model is limited to low volumetric fraction of particles (<1 percent) and is valid only for spherical particles [65][92]. In addition, related studies have reported that it underestimates the viscosity of nanofluids because it assumes no interaction between the particles. As for the Maxwell model for the prediction of the thermal conductivity of solid-liquid suspensions, it is applicable to homogeneous and dilute liquid–solid suspensions with randomly dispersed, uniformly sized and non-interacting spherical particles. Later on, Hamilton and Crosser [64] generalized the Maxwell model for the case of non- spherical particles. Yet, many researchers who have investigated the reliability of the previously existing models have reported discrepancies. Moreover, there were several studies which reported that these models are not appropriate to give adequate estimations and consequently, underestimate the enhancements in the thermophysical properties of nanofluids [7].

By considering the extensive amount of experimental studies which have been devoted to the measurement of thermophysical properties of various nanofluids, a remarkable distribution of data and discrepancies between outcomes are observed. Although, a considerable amount of data have been collected over the years, investigations have not yet led to a complete understanding of the role of nanoparticles in the enhancement of thermophysical properties. The lack of reliable experimental data may be regarded as one of the essential reasons behind the absence of a universal theoretical or empirical model. Meanwhile, the lack of molecular level understanding of nanosized particles is a hindrance for determining exact mechanisms responsible for the unusual behaviors of nanofluids. The uncertainty dominating the field may be arising from many factors. The lack of reproducible and reliable data may be attributed to many factors such as variations in preparing and characterizing the samples, particle clustering and aggregation, measuring techniques, and versatile amounts of variables affecting the

thermophysical properties such as particle size, morphology etc. In spite of these, it is evident that nanofluids exhibit substantially higher thermophysical properties than those of conventional base fluids and at least empirical models are needed in order to predict the thermophysical properties rather than making measurements for all nanoparticle-base fluid systems which is practically time consuming [9][92][102][106].

As a consequence, it was concluded that nanofluids are not conventional suspensions and their thermophysical properties cannot be described by classical theories [62,107]. Hence, the understanding of their heat transfer capabilities and improvement of new models explaining their mechanism holds a great importance, yet still remains as a great challenge. Therefore, many researchers have focused on constructing new empirical models to predict the nanofluid thermophysical properties at different conditions.

2.6.2.1. Density

Pak and Cho [88], considering solely the concentration effect of nanoparticles, proposed a pioneering equation in the following form, to calculate the densities of nanofluids at constant temperature (298K).

$$\rho = (1 - \emptyset_v)\rho_w + \emptyset_v\rho_p \tag{2.4}$$

Where $\emptyset_v$ is the volume fraction of nanoparticles, ρ_w and ρ_p are the densities of water and metal oxide particles, respectively.

Using the experimental data of Ho. Et. al., Khanafer and Vafai [69] proposed a correlation for the density of Al_2O_3/Water nanofluids considering the effects of both concentration and temperature. However, the proposed correlation is only valid for Al_2O_3/Water nanofluids with volume fractions lower than 0.04 and temperatures lower than 40°C. The developed correlation was expressed as;

$$\rho = 1001.064 + 2738.6191\emptyset_p - 0.2095T \quad (2.5)$$

Where $\emptyset_p$ and T represent volume fraction of nanoparticles and temperature, respectively. Mahian et. al. [8], conducting density measurements of ZnO nanoparticles in an ethylene glycol and water mixture (60:40), proposed the following correlation;

$$\rho_{nf} = 1146.948 + 51.123\emptyset - 0.743T \quad (2.6)$$

in which $\emptyset$ and T are volume fraction of nanoparticles and temperature, respectively. The proposed correlation is valid for ZnO/EG-Water nanofluids with volume fractions lower than 4 percent and for temperature range from 25 to 40°C.

Sharipfur et. al. [108] measured the densities of various nanofluids (SiO_2/Water, Glycerol based MgO and CuO, SiO_x/EG/Water) for a volume fraction range of 1 to 6 percent and a temperature range from 10 to 40°C. According to the measurements, a model is proposed for the density of nanofluids which takes into account the equivalent void thickness of the nanolayer as well as the densities of nanoparticles and base fluid, average nanoparticle size and volume fraction.

$$\rho_{nf} = \frac{\rho_{nf}}{(1-\emptyset) + \emptyset(r_p + t_v)^3/r_p^3} \quad (2.7)$$

In Equation 2.4, the terms $\emptyset, \rho_{nf}, r_p, t_v$ indicate particle volume fraction, density of the nanofluid, nanoparticle radius and equivalent void thickness, respectively.

Montazer et. al. [109] proposed a model to evaluate the densities of carbon based MWCNT–COOH and F-GNP nanofluids with changing nanoparticle mass fraction and temperature by using response surface methodogoly (RSM). RSM was successfully applied for predicting the densities of carbon based nanofluids and the predicted values showed good agreement with the experimental data. The density equations for MWCNT–COOH and F-GNP nanofluids are

given in Equations 2.5 and 2.6 where ∅ is the nanoparticle weight fraction and *T* is the temperature.

$$\rho_{(MWCNT-COOH)} = -0.00443T^2 + 0.096\emptyset T - 0.02468T + 18.40\emptyset + 1000.15 \quad (2.8)$$

$$\rho_{(F-GNP)} = -0.00518T^2 + 25.6\emptyset^2 - 0.0184\emptyset T + 0.01741T + 2.456\emptyset + 999.8 \quad (2.9)$$

2.6.2.2. Viscosity

Duangthongsuk and Wongwises [7] experimentally measured the effective viscosities of TiO_2/Water nanofluids with volumetric fractions from 0.2 to 2 percent, between a temperature range from 15 to 35°C. In addition, they proposed a correlation for the prediction of the viscosities of TiO_2/Water nanofluids that is only valid between the considered concentration and temperature ranges.

$$\frac{\mu_{nf}}{\mu_w} = a + b\emptyset + c\emptyset^2 \quad (2.10)$$

Where *a*, *b* and *c* are constant values listed in the following table:

Table 2.5. Correlation constants a, b and c [7]

Temperature (°C)	**A**	**B**	**C**
15	1.0226	0.0477	-0.0112
25	1.013	0.092	-0.015
35	1.018	0.112	-0.0177

Toghraie et. Al. [89] investigated experimentally the viscosities of magnetic Fe_3O_4/Water nanofluids with various volume fractions up to 3 percent and between a temperature range from 20 °C to 55°C. By computing the obtained experimental data, they suggested a novel model for

the determination of the dynamic viscosity of water-based magnetite nanofluids, in the following form:

$$\frac{\mu_{nf}}{\mu_{bf}} = 1.01 + (0.007165T^{1.171}\emptyset^{1.509}) x\ exp(-0.00719T\emptyset) \tag{2.11}$$

Where T is the temperature in ℃ and $\emptyset$ is the solid volume fraction in percent.

Nguyen et. Al. [92], investigated the effect of nanoparticle volume fraction, temperature and particle size of Al_2O_3 (36 nm and 47 nm) and a CuO (29 nm) suspensions in water and proposed several correlations for both nanofluids. While some of the correlations related the viscosity of nanofluids solely to the volume fraction, the others additionally takes into consideration the effect of temperature. The proposed correlations for Al_2O_3/Water nanofluids containing particles that have average sizes of 47 nm and 36 nm are as follows, respectively:

$$\frac{\mu_{nf}}{\mu_{bf}} = 0.904e^{0.148\emptyset} \tag{2.12}$$

$$\frac{\mu_{nf}}{\mu_{bf}} = 1 + 0.025\emptyset + 0.015\emptyset^2 \tag{2.13}$$

Whereas the correlation proposed for CuO/Water nanofluids is;

$$\frac{\mu_{nf}}{\mu_{bf}} = 1.475 - 0.319\emptyset + 0.051\emptyset^2 + 0.009\emptyset^3 \tag{2.14}$$

Kulkarni et. Al. [110] studied the rheological behavior of CuO nanoparticles of 29 nm diameter that are dispersed in water for various volume fractions from 5 to 15 percent, up to 50℃. Moreover, they proposed a novel correlation relating the viscosity of copper oxide nanoparticles to both temperature and volumetric concentration of the nanoparticles.

$$ln\mu = A\left(\frac{1}{T}\right) - B \tag{2.15}$$

Where *T* is the temperature in Kelvin and A and B are the following polynomials which are functions of volume fractions ∅ (ranging from 0.05 to 0.15);

$$A = 20587\emptyset^2 + 15857\emptyset + 1078.3 \quad (2.16)$$

$$B = -107.12\emptyset^2 + 53.548\emptyset + 2.8715 \quad (2.17)$$

Namburu et. Al. [86] carried out experimental investigations on the viscosity of silicon dioxide nanoparticles with diverse diameters (20, 50 and 100 nm) suspended in an ethylene glycol-water mixture. Nanofluids with distinct volume fractions from 0 to 10 percent were prepared and their viscosities were measured at a temperature range from -35 to 50°C. By using the experimental data, a new correlation for the viscosity of these nanofluids was developed. A statistical analysis of their experimental data yielded an empirical correlation in the form;

$$\log(\mu_s) = Ae^{-BT} \quad (2.18)$$

where μ_s is the viscosity of silicon dioxide nanofluid in cP, *T* is the temperature and *A* and *B* are the functions of volumetric particle concentration expressed as follows;

$$A = 0.1193\emptyset^3 - 1.9289\emptyset^2 - 2.245\emptyset + 167.17 \quad (2.19)$$

$$B = -7x10^{-6}\emptyset^2 - 0.0004\emptyset + 0.0192 \quad (2.20)$$

In which ∅ ranges from 2 to 10 vol. percent.

Hemmat Esfe et. Al. [87] studied the dynamic viscosity of ZnO nanoparticles with an average particle size of 18 nm that are suspended in ethylene glycol. The viscosities of nanofluids with nanoparticle volume fractions from 0.25 to 5 percent were measured with varying temperature up to 50°C. Furthermore, they proposed an empirical correlation for the viscosity of nanofluids which included the effects of both nanoparticle volume fraction and temperature.

$$\frac{\mu_{nf}}{\mu_{bf}} = 0.9118\exp(5.49\emptyset - 0.00001359T^2) + 0.0303\ln(T) \quad (2.21)$$

In another study, Hemmat Esfe et. Al. [111], prepared Al_2O_3 suspensions in engine oil with numerous solid volume fractions ranging from 0.25 to 2 percent and measured their viscosities up to 65℃ (Figure 2.13). Studying the effects of working temperature and concentration of nanoparticles on the dynamic viscosity of nanofluids, they further proposed several correlations to predict the viscosities of nanofluids at specific temperatures and different volume fractions.

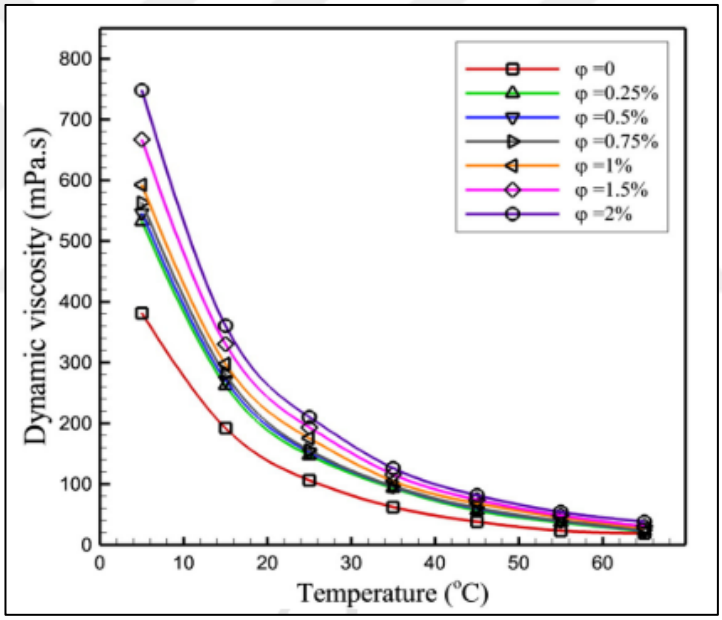

Figure 2.13. Influence of particle loading and temperature on the viscosity of Al2O3/Engine oil nanofluids [111]

Masoumi et. Al. [65], analyzed Al_2O_3 nanofluids consisting of 13 nm and 28 nm particles that are suspended in water and expressed a new theoretical correlation for calculating the nanofluid viscosity considering the effect of Brownian motion of nanoparticles. The suggested equation calculates viscosity of nanofluids accounting for the effects such as mean diameter of nanoparticles, solid volume fraction, temperature, nanoparticle density and physical properties

of the base fluid. They reported that the proposed model shows good agreement with their experimental results.

Akbari et. Al. [35] conducted dynamic viscosity measurements of SiO_2/EG nanofluids for various volume fractions up to 3 percent, in between 30°C to 50°C (Figure 2.14). By using the empirical data, a new correlation in the form of equation 2.22 is proposed to predict the dynamic viscosity of Silica/ethylene glycol nanofluids as a function of both temperature and volume fraction.

$$\frac{\mu_{nf}}{\mu_{bf}} = -24.81 + 3.23T^{0.08014}\exp(1.838\emptyset^{0.002334}) - 0.0006779T^2 + 0.024\emptyset^3 \quad (2.22)$$

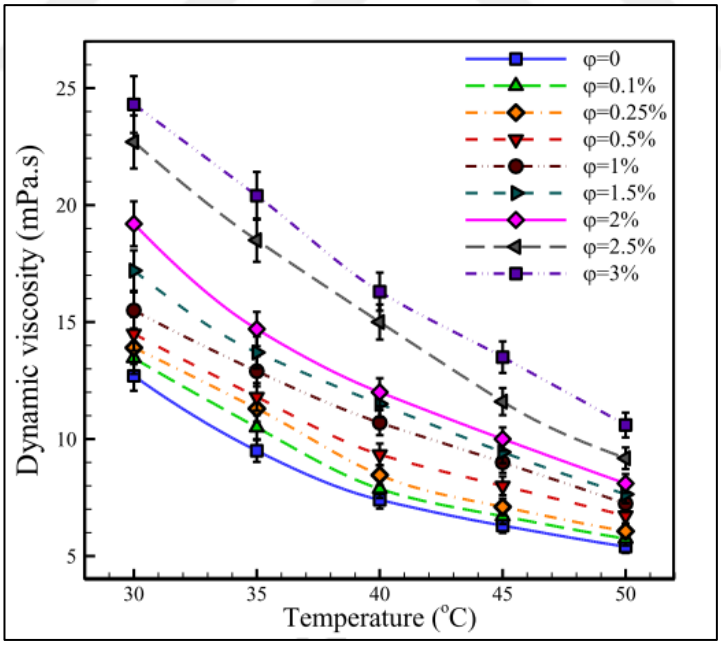

Figure 2.14. Dynamic viscosity variations of SiO_2/EG nanofluids with temperature at different nanoparticle volume fractions [35]

Table 2.6. Summary of theoretical and experimental correlations developed for the viscosity of various nanofluids

Researcher	Proposed Correlation	Remarks
Duangthongsuk and Wongwises [7]	$\frac{\mu_{nf}}{\mu_w} = 1.0226 + 0.0477\emptyset - 0.0112\emptyset^2$ $\frac{\mu_{nf}}{\mu_w} = 1.013 + 0.092\emptyset - 0.015\emptyset^2$ $\frac{\mu_{nf}}{\mu_w} = 1.018 + 0.112\emptyset - 0.0177\emptyset^2$	-Constructed for 15, 25 and 35℃, respectively -Valid for TiO_2/Water nanofluids with volumetric fractions from 0.2 to 2%
Asadi et. Al. [10]	$\frac{\mu_{nf}}{\mu_{bf}} = 6.8376 + 15.2522w(wt\%) + 0.038779w(wt\%).T(℃) - 2.63029(w(wt\%)^2$	-Valid for silicon dioxide nanoparticle suspensions in an oleic acid/liquid paraffin mixture
Akbari et. Al. [35]	$\frac{\mu_{nf}}{\mu_{bf}} = -24.81 + 3.23T^{0.08014}\exp(1.838\emptyset^{0.002334}) - 0.0006779T^2 + 0.024\emptyset^3$	-Valid for ethylene glycol based silicon dioxide nanofluids
Einstein [112]	$\mu_{nf} = \mu_{bf}(1 + 2.5\emptyset)$	-Valid for relatively low volume fractions of spherical particles, <0.02
Brinkman et. Al. [113]	$\frac{\mu_{nf}}{\mu_{bf}} = \frac{1}{(1-\emptyset)^{2.5}}$	-Valid for high moderate particle concentrations
Drew and Passman [114]	$\mu_{nf} = (1 + 2.5\emptyset)\mu_w$	-Valid for spherical particles with concentrations less than 5.0 vol%

Table 2.6. Summary of theoretical and experimental correlations developed for the viscosity of various nanofluids (Continued)

Researcher	Proposed Correlation	Remarks
Batchelor et. Al. [115]	$\mu_{nf} = (1 + 2.5\emptyset + 6.5)/\mu_w$	-Valid for rigid and spherical nanoparticles
Wang et. Al. [116]	$\mu_{nf} = (1 + 7.3\emptyset + 123\emptyset^2)/\mu_w$	- For nanoparticle suspensions
Frankel and Acrivos [117]	$\frac{\mu_{nf}}{\mu_{bf}} = \frac{9}{8}.\left[\frac{\left(\frac{\emptyset}{\emptyset_m}\right)^{\frac{1}{3}}}{1-\left(\frac{\emptyset}{\emptyset_m}\right)^{\frac{1}{3}}}\right]$	-Valid for uniform spherical particles -$\emptyset_m$is the maximum particle volume fraction determined experimentally
Tseng and Lin [118]	$\frac{\mu_{nf}}{\mu_{bf}} = 13.47e^{35.98\emptyset}$	-Valid for TiO_2/Water nanofluids
Chen et. Al. [119]	$\frac{\mu_{nf}}{\mu_{bf}} = 1 + 10.6\emptyset + (10.6\emptyset)^2$	-Valid for ethylene glycol based titania nanofluids
Namburu et. Al. [86]	$\log(\mu_s) = Ae^{-BT}$ $A = 0.1193\emptyset^3 - 1.9289\emptyset^2 - 2.245\emptyset + 167.17$ $B = -7x10^{-6}\emptyset^2 - 0.0004\emptyset + 0.0192$	-Valid for ethylene glycol based silicon dioxide nanofluids with volume fractions between 2 and 10%, and a temperature up to 50℃
Hemmat Esfe et. Al. [87]	$\frac{\mu_{nf}}{\mu_{bf}} = 0.9118\exp(5.49\emptyset - 0.00001359T^2) + 0.0303\ln(T)$	-Valid for ethylene glycol based zinc oxide nanofluids

Table 2.6. Summary of theoretical and experimental correlations developed for the viscosity of various nanofluids (Continued)

Researcher	Proposed Correlation	Remarks
Toghraie et. Al. [89]	$\frac{\mu_{nf}}{\mu_{bf}} = 1.01 + (0.007165T^{1.171}\emptyset^{1.509})x\ exp(-0.00719$	-Valid for Fe_3O_4/Water nanofluids with volume fractions up to 3% and between a temperature range from 20 ℃ to 55℃
Nguyen et. Al. [92]	$\frac{\mu_{nf}}{\mu_{bf}} = 0.904e^{0.148\emptyset}$	-Vaid for Al_2O_3/Water nanofluids with average particle sizes of 47 nm
Nguyen et. Al. [92]	$\frac{\mu_{nf}}{\mu_{bf}} = 1 + 0.025\emptyset + 0.015\emptyset^2$	-Vaid for Al_2O_3/Water nanofluids with average particle sizes of 36 nm
Nguyen et. Al. [92]	$\frac{\mu_{nf}}{\mu_{bf}} = 1.475 - 0.319\emptyset + 0.051\emptyset^2 + 0.009\emptyset^3$	-Valid for CuO/Water nanofluids with 29nm particle size
Kulkarni et. Al. [110]	$ln\mu = A\left(\frac{1}{T}\right) - B$ $A = 20587\emptyset^2 + 15857\emptyset + 1078.3$ $B = -107.12\emptyset^2 + 53.548\emptyset + 2.8715$	-Valid for CuO/Water nanofluids with particle sizes of 29 nm -Valid for volume fractions ranging from 0.05 to 0.15 and a temperature up to 50℃

2.6.2.3. Thermal Conductivity

Toghraie et. Al. [120], measured experimentally the thermal conductivities of water-based hybrid nanofluids composed of multiwalled carbon nanotubes and CuO nanoparticles. The measurements of nanofluids having solid volume fractions from 0.05 to 0.6 percent were conducted between a temperature range from 25℃ to 50℃ (Figure 2.15). Their experimental results revealed an enhancement in the thermal conductivity of water with increasing solid volume fraction as well as increasing temperature. Furthermore, they proposed a correlation to predict the thermal conductivity of the hybrid nanofluid at various particle volume fractions and temperatures. The proposed correlation is expressed in the following form (equation 2.23) and is only valid for the volume fraction and temperature range that was considered during the study.

$$\frac{k_{nf}}{k_{bf}} = 0.907\exp\left(0.36\emptyset^{0.3111} + 0.000956T\right) \tag{2.23}$$

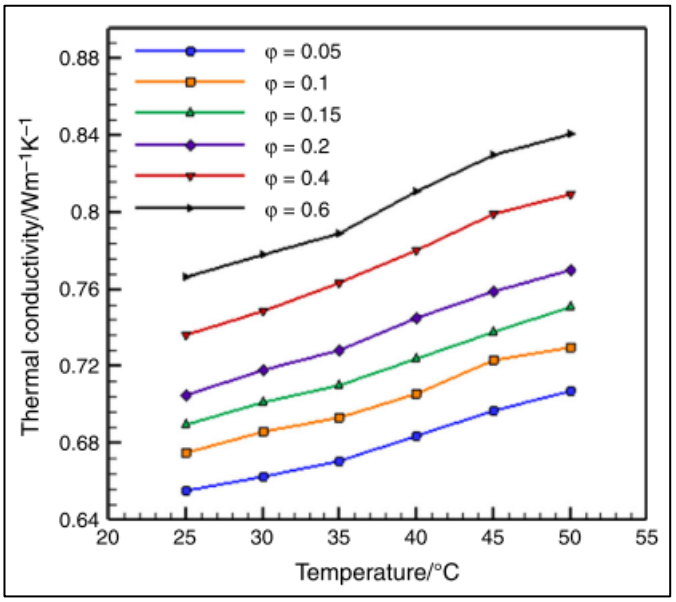

Figure 2.15. Thermal conductivity of MWCN-CuO/Water hybrid nanofluids versus temperature at different concentrations

[120]

Li et. Al. [10] measured the thermal conductivities of SiO_2-oleic acid nanoparticles suspended in liquid paraffin from 25 to 70℃. The proposed empirical model for the prediction of the nanofluid thermal conductivity with respect to both altering mass concentration and temperature is given in Equation 2.24.

$$\frac{k_{nf}}{k_{bf}} = 0.756951 + 0.0735396w(wt\%) - 8.26715x10^{-5}(T(℃))^2 + 0.0123973T(℃) \quad (2.24)$$

Hemmat Esfe et. Al. [121] examined the thermal conductivity of Al_2O_3/EG nanofluids with respect to variable volume fraction up to 5 percent, at different temperatures ranging from 24 to 50℃. According to the data, two different correlations were formed that relate the thermal conductivity of nanofluids by taking into consideration the effects of both temperature and volume fraction. Moreover, they presented several additional correlations for estimating the thermal conductivity of nanofluids at specific temperatures in order to increase the accuracy of the models.

$$\frac{k_{nf}}{k_{bf}} = 1.04 + 5.91x10^{-5}T + 0.00154T\emptyset + 0.0195\emptyset^2 - 0.014\emptyset - 0.00253\emptyset^3 - 0.000104T\emptyset^2 - 0.0357\, x \sin(1.72 + 0.407\emptyset^2 - 1.67\emptyset) \quad (2.25)$$

$$\frac{k_{nf}}{k_{bf}} = 0.999 + 9.58x10^{-5}T + 0.00142T\emptyset + 0.0519\emptyset^2 + 0.00208\emptyset^2 + 0.00208\emptyset^4 - 0.00719\emptyset - 0.0193\emptyset^3 - 8.21x10^{-5}T\emptyset^2 \quad (2.26)$$

Duangthongsuk and Wongwises [7] conducted experimental investigations on the effective thermal conductivity of TiO_2/Water nanofluids as well as their effective viscosities. Based on their empirical data they proposed an equation relating the thermal conductivity of nanofluids to both volume fraction and temperature which is given in Equation 2.27. The proposed equation is only valid for the temperature and volume fraction ranges which were considered during the study.

$$\frac{k_{nf}}{k_w} = a + b\emptyset \tag{2.27}$$

where *a* and *b* are constant values listed in Table 2.5:

Table 2.7. Correlation constants a and b [7]

Temperature (℃)	**A**	**B**
15	1.0225	0.0272
25	1.0204	0.0249
35	1.0139	0.0250

.

Karimi et. Al. [100] investigated the thermal conductivity of two aqueous magnetic nanofluids namely, Fe_3O_4 and $CoFe_2O_4$ in the absence and presence of a magnetic field. Thermal conductivities of the magnetic nanofluids having volume fractions up to 4.8 percent were measured in the presence of a magnetic field intensity up to 500G. Using their experimental results, they proposed new correlations for the prediction of thermal conductivities of magnetic nanofluids both in the absence and the presence of an externally applied magnetic field. The proposed correlation for the thermal conductivity of magnetic nanofluids in the absence of magnetic field is as follows;

$$k_{nf} = (1 + a\emptyset(\frac{T}{T_{max}}))^b k_{bf} \tag{2.28}$$

where ∅ is the particle volume fraction ($0 < \emptyset < 4.8$ percent), *T* is the temperature of nanofluid ($20 < T < 60$℃). The thermal conductivity of the base fluid (k_{bf}) is calculated by Equation 2.29;

$$k_{bf} = -6.58x10^{-6}T^2 + 0.0018T + 0.5694 \tag{2.29}$$

Table 2.8. Summary of theoretical and experimental correlations developed for the thermal conductivity of various nanofluids

Researcher	Proposed Correlation	Remarks
Duangthongsuk and Wongwises [7]	$\frac{k_{nf}}{k_w} = 1.0225 + 0.0272\emptyset$ $\frac{k_{nf}}{k_w} = 1.0204 + 0.0249\emptyset$ $\frac{k_{nf}}{k_w} = 1.0139 + 0.0250\emptyset$	-Constructed for 15, 25 and 35℃, respectively -Valid for TiO_2/Water nanofluids with volumetric fractions from 0.2 to 2%
Maxwell [64]	$k_{nf} = k_{bf}\left(\frac{k_p + 2k_{bf} + 2(k_p - k_{bf})\emptyset}{k_p + 2k_{bf} - (k_p - k_{bf})\emptyset}\right)$	-Valid for low volume concentration of spherical nanoparticles
Karimi et. Al. [100]	$k_{nf} = (1 + a\emptyset(\frac{T}{T_{max}}))^b k_{bf}$	-Valid for water based magnetic Fe_3O_4 and $CoFe_2O_4$ in the absence of magnetic field and volume fractions up to 4.8%, for a temperature range between 20 and 60℃

Table 2.8. Summary of theoretical and experimental correlations developed for the thermal conductivity of various nanofluids (Continued)

Hemmat Esfe et. Al. [121]	$\frac{k_{nf}}{k_{bf}} = 1.04 + 5.91x10^{-5}T + 0.00154T\emptyset + 0.0195\emptyset^2 - 0.014\emptyset - 0.00253\emptyset^3 - 0.000104T\emptyset^2 - 0.0357\ x \sin(1.72 + 0.407\emptyset^2 - 1.67\emptyset)$ $\frac{k_{nf}}{k_{bf}} = 0.999 + 9.58x10^{-5}T + 0.00142T\emptyset + 0.0519\emptyset^2 + 0.00208\emptyset^2 + 0.00208\emptyset^4 - 0.00719\emptyset - 0.0193\emptyset^3 - 8.21x10^{-5}T\emptyset^2$	-Valid for Al_2O_3/EG nanofluids with volume fractions up to 5% and a temperature range from 24 to 50°C.
Hamilton-Crosser [122]	$k_{nf} = \left[\frac{k_p + (n-1)k_{bf} - (n-1)\emptyset(k_{bf} - k_p)}{k_p + (n-1)k_{bf} + \emptyset(k_{bf} - k_p)}\right]k_{bf}$	-$n = 3/\Psi$ -n is the empirical shape factor and Ψ is the sphericity which is the ratio of the sphere's surface area to the particle's surface area -sphericity is 1 for spherical and 0.5 for cylindrical shapes
Wasp [123]	$k_{nf} = k_{bf}\left[\frac{k_p + 2k_{bf} - 2(k_{bf} - k_p)\emptyset}{k_p + 2k_{bf} + (k_{bf} - k_p)\emptyset}\right]$	-Valid for spherical particles

Table 2.8. Summary of theoretical and experimental correlations developed for the thermal conductivity of various nanofluids (Continued)

Yu and Choi [124]	$k_{nf} = \left[\frac{k_p + 2k_w + 2(k_p - k_w)(1+\beta)^3\emptyset}{k_p + 2k_w - (k_p - k_w)(1+\beta)^3\emptyset}\right] k_w$	-β is the ratio of the nanolayer thickness to the main particle radius -β= 0.1 is used to calculate the thermal conductivity of nanofluids
Timofeeva [125]	$k_{nf} = k_{bf}(1 + 3\emptyset)$	-Valid for alumina nanofluids
Rohini Priya et. Al. [126]	$\frac{k_{nf}}{k_{bf}} = 1 + 5.224\emptyset + 2.6456T^{1.713}\emptyset$	-Valid for copper oxide/water nanofluids -Encompasses the relative thermal conductivity range from 1.03 to 1.35 -Nanoparticle concentration range between 0.004 and 0.016 vol% -Temperature range from 28 to 55 °C.

Table 2.8. Summary of theoretical and experimental correlations developed for the thermal conductivity of various nanofluids (Continued)

Li et. Al. [10]	$\frac{k_{nf}}{k_{bf}} = 0.756951 + 0.0735396w(wt\%) - 8.26715x10^{-5}(T(℃))^2 + 0.0123973(T(℃))$	-Valid for silicon dioxide nanoparticle suspensions in an oleic acid/liquid paraffin mixture -SiO_2 nanoparticle concentration range from 0.005 to 5.0 wt% -Temperature range from 25 to 70 °C.
Toghraie et. al. [120]	$\frac{k_{nf}}{k_{bf}} = 0.907\exp(0.36\emptyset^{0.3111} + 0.000956T)$	-Valid for hybrid MWCN-CuO nanofluids -Nanoparticle concentration range from 0.05 to 0.6 vol% -Temperature range from 25 to 50 °C.
Sundar et. al. [91]	$k_{nf} = k_{bf}(1 + 10.5\emptyset)^{0.1051}$	-Valid for magnetite nanofluids within a concentration range from 0.0 to 2.0 vol% and a temperature range from 20 to 60 °C.

As a consequence of all the studies and data presented in the literature, it is evident that the results are not consistent even when the same nanoparticle-base fluid system is considered. One of the main reasons behind this contradiction may be attributed to the effect of different experimental equipment used for measurements. For instance, while some of the researchers use handmade equipment based on hot-wire method for the thermal conductivity measurements while the rest uses more advanced devices manufactured for this purpose. Additionally, the method of preparation chosen for the synthesis of same nanoparticles are also varied which results in particles having different average sizes and morphologies and these variables are not essentially taken into consideration while constructing a model for the prediction of thermophysical properties of nanofluids. Moreover, it is clearly seen from literature survey that each researcher focuses on a different type of nanoparticle-base fluid system which has distinct characteristics. The latter strongly restricts the applicability of the derived models while bringing forward many limitations associated with the usability of the proposed correlations in general. It is evidently observed that most of the correlations are convenient for a specific type of nanofluid only, over a specific volume fraction and temperature ranges. Nonetheless there is an infinite amount of nanoparticle-base fluid combinations whereas these might also include nanoparticles with distinct types, shapes and sizes which also affect the properties of the nanofluid. Considering all these, the objective of this study is to synthesize several nanofluids that consist of different size and type of nanoparticles suspended in different carrier fluids by using various surfactants and to measure their thermophysical properties with respect to varying concentration and temperature, in order to analyze the possibility of forming generalized empirical models that can estimate the thermophysical properties of the majority of nanoparticle-carrier fluid systems.

3. MATERIALS

3.1. CHEMICALS

The materials used during the experiments were of analytical grade and are in Table 3.1.

Table 3.1. Chemical formula and structures of chemicals

Chemical name	Chemical formula	Chemical structure	Supplier
Acetic Acid	CH_3COOH	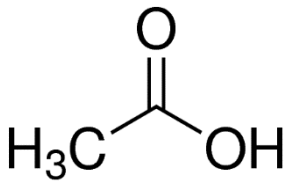	Sigma-Aldrich
Citric Acid	$C_6H_8O_7$	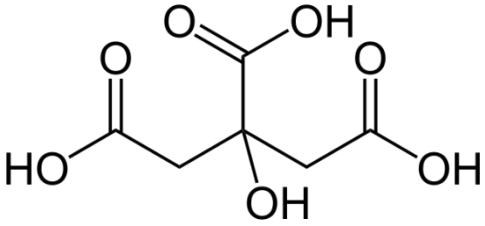	Sigma-Aldrich
Copper (II) Acetate Monohydrate	$Cu(CH_3COO)_2.H_2O$	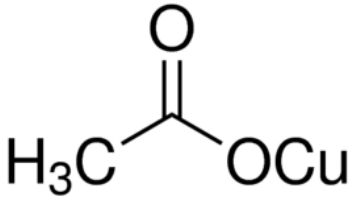	Emplura
Ethylene Glycol	$C_2H_6O_2$	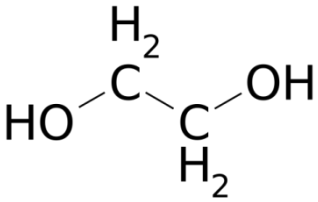	Aksem Kimya

Table 3.1. Chemical formula and structures of chemicals (Continued)

Chemical name	Chemical formula	Chemical structure	Supplier
Hydrochloric Acid (37%)	HCl	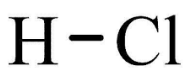	Sigma-Aldrich
Iron (III) Chloride	$FeCl_3$	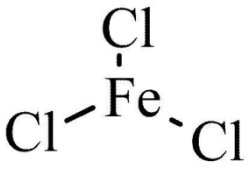	Merck Millipore
Iron (II) Sulfate Heptahydrate	$FeSO_4.7H_2O$	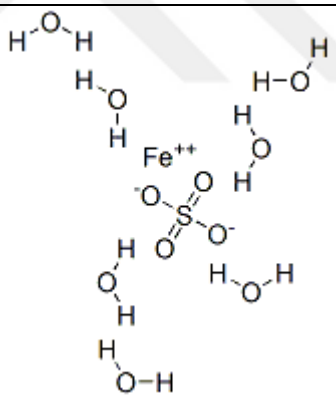	Sigma-Aldrich
Polyacrylic Acid (250kDa)	$(C_3H_4O_2)_n$	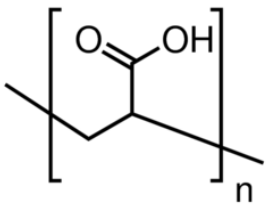	Aldrich
Polyacrylic Acid (450kDa)	$(C_3H_4O_2)_n$	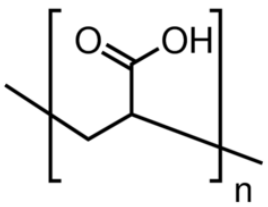	Sigma-Aldrich

Table 3.1. Chemical formula and structures of chemicals (Continued)

Chemical name	Chemical formula	Chemical structure	Supplier
Potassium Hydroxide	KOH	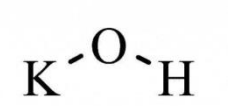	Emsure
Potassium Nitrate	KNO_3	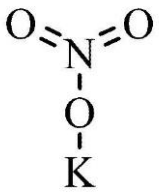	Sigma-Aldrich
Sodium Hydroxide	NaOH	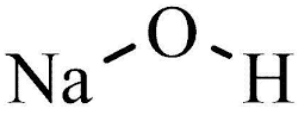	Riedel-de Haën
Tiron	$C_6H_4Na_2O_8S_2$	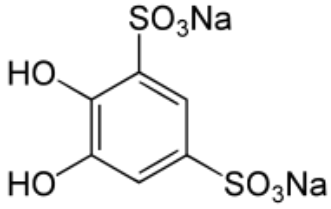	Fluka

4. METHODS

4.1. DENSITY METER

Density measurements of nanofluids were performed with Anton Paar DMA 4100 density meter throughout this study. Anton Paar DMA 4100 density meter can measure the densities of samples with 4-digit accuracy, at a desired temperature. In order to perform a density measurement, 2 ml of a sample is injected into the U-shaped borosilicate glass tube with the help of a syringe and then the desired temperature is set. After the sample injection, the system determines the period of oscillation of the U-tube through excitation of the sensors and reception of signals. Since the tube volume is known, the computing device calculates the density of the liquid sample filled into the U-tube based on its resonant frequency. Finally, the calculated density value (in g/cm^3) is displayed on the device screen.

The densities of nanofluid samples were measured at a temperature range from 20 to 60°C and each sample was measured in triplicates.

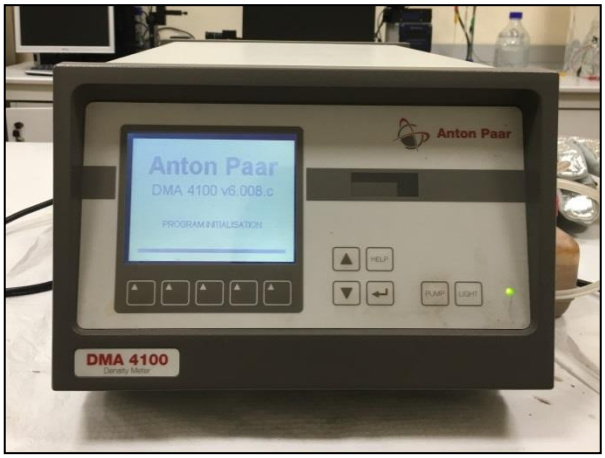

Figure 4.1. Anton Paar DMA 4100

4.2. VISCOSITY METER

In this study, the viscosity measurements were performed via a Brookfield DV-III Ultra Programmable Rheometer. The Brookfield Viscometer measures the viscosity of a fluid at a given shear rate. The viscometer motor rotates the spindle at a defined speed (measured in rpm) or shear rate and measures the torque necessary to overcome the viscous resistance to the induced force, then reports a viscosity value in cP.

In order to measure the viscosity of nanofluids at desired temperatures a water bath was connected to the sample reservoir. After setting the water bath to the desired temperature, 0.6 ml of sample was placed at the center of the sample holder. When the desired temperature was reached, the rotational speed was entered, and the measurement was commenced. After computing the measurement, the viscosity value is displayed on the rheometer screen.

The viscosities of nanofluids were measured between a temperature range from 20 to 60℃ and each sample was measured in triplicates.

Figure 4.2. Brookfield Rheometer DV-III Ultra

4.3. THERMAL CONDUCTIVITY METER

The thermal conductivity measurements of samples were performed via Flucon LAMBDA 01/L which measures the thermal conductivity of samples by means of the hot-wire method. The instrument is a custom designed device for measuring the thermal conductivities of nanofluids, along with many other fluids. The hot wire in the LAMBDA sample reservoir serves as both the heat source and the temperature sensor. The hot wire is subjected to a constant current to generate a temperature rise and as the surrounding medium warms up, the resistance of the hot wire changes according to the surrounding medium. Therefore, the change of voltage in the hot wire designates the change of temperature taking place in the surrounding medium. Finally, the thermal conductivity value at the set temperature is displayed on the device screen in mW/mK. In order to measure the thermal conductivity of the nanofluid, nearly 40ml of sample was transferred into the sample holder and in order to compute the measurement at desired temperatures, the sample holder was placed inside a controllable oil bath. When the desired temperature was reached, the data displayed on the device screen were recorded over a period of around 10 minutes. The thermal conductivities of nanofluids were measured between a temperature range from 20 to 60℃ and each sample was measured in triplicates.

Figure 4.3. Flucon LAMBDA 01/L

4.4.UV-VIS SPECTROPHOTOMETER

In order to determine the concentrations of synthesized magnetic nanofluids, the samples were subjected to Tiron chelation test for which the absorbance values were needed at 480 nm. For this purpose, the absorbances of the samples were measured with Thermo Scientific Evolution 201 UV-Visible Spectrophotomer. A UV-Vis Spectrophotometer is a device that measures the decrease in the intensity of a light beam after it passes through a sample or is reflected from a sample surface. UV-Vis spectrophotometry uses light from the ultraviolet and visible regions of the electromagnetic spectrum. Light that belongs to this wavelength can excite electrons in the ground state to higher energy levels, resulting in absorbance at wavelengths specific to each molecule. When a light beam passes through a material or a solution, some of the light is absorbed and the remnant is transmitted through the sample. A spectrophotometer records the degree of absorption by a sample at diverse wavelengths, thus the concentration of an analyte can be calculated at a certain wavelength.

Figure 4.4. Thermo Scientific Evolution 201 UV-Visible Spectrophotometer

4.5. XLSTAT

XLSTAT is an add on software to perform statistical analysis in Excel. In this study, XLSTAT was used to perform non-linear regression on the measured data in order construct the empirical models for thermal conductivity, density and viscosity as a function of temperature and volume fraction of nanoparticles. The output of regression process yields the constants related with the chosen model as well as statistical summary, goodness of fit statistics, predictions, residuals and data plots.

5. EXPERIMENTAL PROCEDURE

5.1. SYNTHESIS OF MAGNETITE NANOFLUIDS

In this study, two different synthesis methods namely, partial oxidation and co-precipitation methods, were used for the synthesis of magnetic nanofluids containing magnetite nanoparticles. The diverse kind of synthesis routes bear magnetite nanoparticles with distinct magnetic properties associated with their different sizes. Magnetic nanoparticles may have superparamagnetic or ferrimagnetic properties depending on particle size. Superparamagnetic nanoparticles possess magnetic behavior and align themselves in the presence of an externally applied magnetic field while in the absence they do not have any remaining magnetization. In contrast to superparamagnetic nanoparticles, ferrimagnetic magnetite nanoparticles have higher saturation magnetizations and hold their magnetization even when the applied magnetic field is removed [57]. The mainly employed conventional co-precipitation method yields nanoparticles with relatively smaller average sizes (<20nm) which exhibit superparamagnetic properties, while partial oxidation method produces particles that have higher saturation magnetizations, ferrimagnetic properties and relatively larger sizes (>20nm) due to slower reaction kinetics.

5.1.1. Co-Precipitation Method

Co-precipitation method was used in order to synthesize superparamagnetic magnetite nanoparticles with relatively smaller sizes. To prevent aggregation of nanoparticles and achieve colloidal stabilization, surfactants and polymers such as citric acid and polyacrylic acid (250 kDa and 450 kDa) were introduced to the medium by adjusting the ratio of iron content to functional groups of the polymer to 1:1.

In this method, briefly the required amount of polymer was weighed and dissolved in a 50 ml of distilled water by using a magnetic stirrer. Subsequently, the 50 ml of polymer solution along with a 30 ml of additional water was transferred into a jacketed reactor which was connected to

a water bath previously set to 60℃ and de-aerated by using nitrogen flow at a constant stirring rate of 450 RPM by using a mechanical stirrer for 30 minutes. Then, 0.242g of $FeSO_4.7H_2O$ and 0.282g of $FeCl_3$ were weighed and transferred into the reactor while the de-aeration process was being continued. After 15 minutes, 0.514g of NaOH was dissolved in 20 ml of water and the prepared base solution was added to the reactor. Upon the addition of base solution, the color of the mixture turned from orange to black instantly, indicating the formation of magnetite nanoparticles (Figure 5.1). Then the mixture was left for aging at 60 ℃ for 30 minutes. At the end of the synthesis, the nanofluid was centrifuged at 6000 RPM for 15 minutes and washed with distilled water to eliminate the excess reagents and decrease the pH.

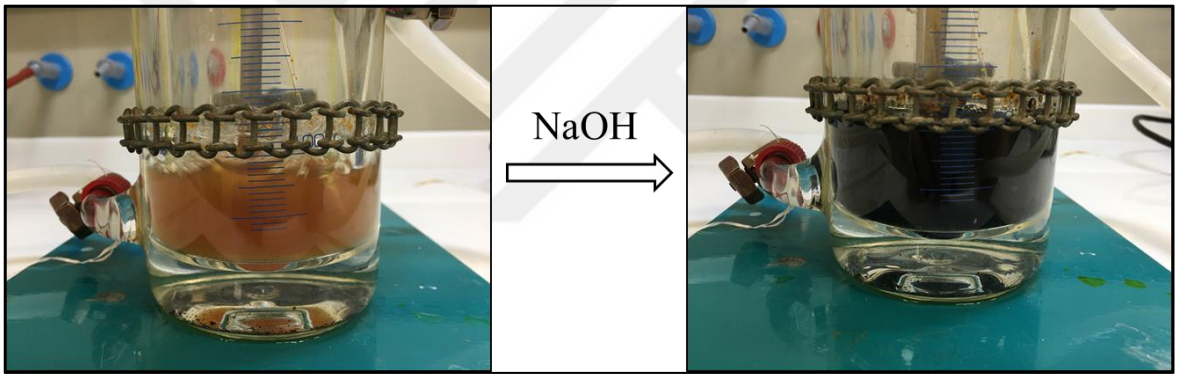

Figure 5.1. Formation of magnetite nanoparticles upon the addition of base solution

5.1.2. By Partial Oxidation Method

In order to synthesize ferrimagnetic magnetite nanoparticles, partial oxidation method was used. Briefly, the appropriate amounts of hydrophilic polymers were dissolved in 50ml of distilled water. Meanwhile, 2.525g of KNO_3 was dissolved in water in a 50 ml volumetric flask and furthermore, 0.974g of KOH was dissolved in 10 ml of water. All the prepared solutions and an additional 5 ml of water were subsequently transferred into a three necked round bottom flask. Additionally, 10 ml of water was put in a separate vial. Then both the water and the mixture in the round bottom flask were sealed and de-aerated for one hour. The deaeration process was

carried out by passing nitrogen gas through both the reaction medium and the water. At the end of one-hour deaeration process, the reactor was replaced in a preheated ethylene glycol bath (at a constant temperature of 90ºC). Afterwards, 0.8685g of $FeSO_4.7H_2O$ was dissolved in the separately de-aerated water and then this iron salt solution was injected into the reactor. After one minute, the nitrogen gas flow was turned off and the mixture was left for aging at 90ºC for four hours. At the end of the synthesis, the nanofluid was centrifuged at 6000 RPM for 15 minutes and then washed with distilled water to remove excess reagents and decrease the pH.

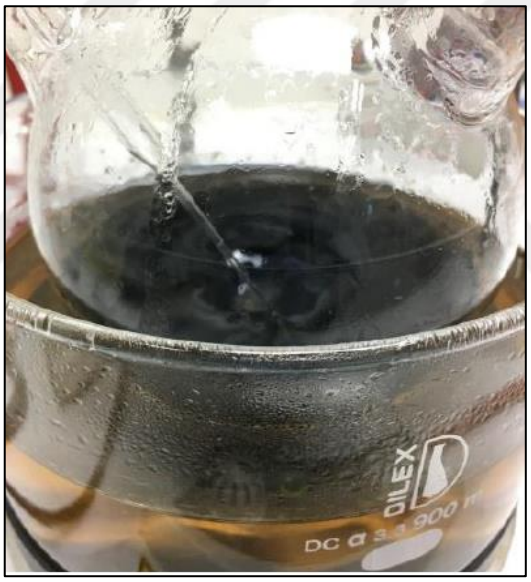

Figure 5.2. Magnetic nanofluid prepared via partial oxidation method after the synthesis

5.1.3. Tiron Test for Determining the Concentration of Magnetite Nanofluids

Tiron chelation test is used for determining the iron concentration of magnetic nanofluid samples with unknown concentrations. Tiron is a chemical compound used for its ability to form strong complexes with titanium and iron. In Tiron test, firstly ferrous and ferric ions are liberated by the addition of concentrated hydrochloric acid solution. The addition of acid also serves for removing the surface coating around the particles. Then, Tiron forms a complex with iron at a ratio of three Tiron molecules to each iron ion. For samples having a pH greater than 9, this

complex exposes a strong absorbance at 480 nm. Thus, a sodium hydroxide solution is added in the subsequent step. The instantaneous color change from yellow to red indicates the chelation of liberated iron ions with the Tiron molecules [127]. Then, the absorbance of the final solution is measured with a spectrophotometer at 480 nm. Finally, using the obtained absorbance value, the unknown concentration of the magnetite sample can be calculated by using equation 5.1 in which DF is the dilution factor.

$$Concentration\ \left(\frac{g}{mL}\right) = \frac{(ABS@480\ nm) \times (DF) \times 231.52 \times 25}{39986 \times 162.15 \times 3 \times 0.1} \qquad (5.1)$$

Throughout the experimental studies, Tiron test was carried out to calculate the concentrations of magnetite nanofluids synthesized by both co-precipitation and partial oxidation methods. During the test, an exceedingly small amount of magnetic fluid sample (0.1ml) was put into a 25 ml volumetric flask and mixed with 0.4 ml of concentrated HCl solution in order to liberate ferrous and ferric ions. The resulting solution was then heated with a heat gun for a few seconds until the color change to yellow. The heated solution was then allowed to cool down to room temperature and subsequently, 0.6 ml of Tiron solution (0.083g/ml) was added into the mixture. Later on, 3 ml of 4M NaOH solution was added. During this step a color change from yellow to red was observed (Figure 5.3).

Figure 5.3. Change of color from yellow to red

Finally, the volume of the solution was made up to 25 ml by adding distilled water and the absorbance of the solution was measured at λ=480 nm, by using a UV-Vis Spectrophotometer. By substituting the obtained absorbance value into Equation 5.1, the concentrations of magnetite nanofluids were calculated. Some of the highly concentrated magnetic nanofluids were diluted by a factor of 4 or 8 in order to obtain reasonable absorbance values. The formulation of Tiron Test is presented in Table 5.1.

Table 5.1. Formulation of Tiron Test

Ingredients	**Amounts**
Magnetic Nanofluid	0.1 ml
Hydrochloric Acid (37%)	0.4 ml
Tiron Solution	0.083 g/ml
Sodium Hydroxide Solution (4M)	3 ml

5.2. PREPARATION OF COPPER OXIDE NANOFLUIDS

Unlike magnetite nanofluids, copper oxide nanofluids were synthesized by a two-step method. A wet chemical method which was adapted from a work of Zhu et. al. [128] was used for the synthesis of copper oxide nanoparticles. For the synthesis, a 200ml of 0.2M copper acetate solution and a 10ml of 8M NaOH solution were prepared. The reaction was carried out in a 500 ml round bottom flask under a reflux system. At the beginning of the synthesis 200 ml of copper acetate solution was transferred into the round bottom flask along with 600µl of glacial acetic acid. The round bottom flask was then placed into an oil bath previously set to 110℃. Subsequently, the mixture was let to reach thermal equilibrium under magnetic stirring. When the mixture temperature reached around 100℃, 10 ml of 8M NaOH solution was added into the round bottom flask. By the addition of the alkali solution the color of the mixture turned from blue to black immediately, and a black suspension was formed simultaneously. The reaction was then carried out under magnetic stirring and at boiling for an additional two hours. At the

end, the reaction mixture was cooled down to room temperature and centrifuged at 6000rpm for 10 minutes. After centrifugation the supernatant was separated, and the wet precipitates were dried in a vacuum oven at 60℃.

When preparing nanofluids via two-step method, the treatment of the suspension by a mechanical method is an important step to reduce aggregation of the nanoparticles. Ultrasonication is undoubtedly the most widely preferred and most effective mechanical method for this purpose. Thus, CuO nanofluids with different volume fractions were obtained by re-dispersing different amounts of the dried nanoparticle powders in appropriate base fluids through ultrasonication. However, the sonication process also generates heat through vibration and this causes a rise in the nanofluid temperature, especially in continuous mode which was used during this study. Therefore, the water in the ultrasonic bath was changed every 15 minutes in order to maintain the temperature of the nanofluid around 20℃ and to prevent evaporation of the sample. The ultrasonication process was continued for 9 hours. Following the same procedure, dried CuO nanoparticles were suspended in two distinct base fluids; water and ethylene glycol.

6. RESULTS AND DISCUSSION

The aim of the study is to develop generalized empirical correlations for thermophysical properties of nanofluids that accounts for the effects of temperature and concentration of nanoparticles. For this purpose, different types of nanoparticle-base fluid systems were prepared and their corresponding thermophysical properties were measured. The type of nanoparticles and base fluids, the size effect, temperature and volume fraction of nanoparticles were considered in order to evaluate their effects over the corresponding thermophysical properties. The effect of nanoparticle type was compared by synthesizing both magnetite and copper oxide nanoparticles and then dispersing them in aqueous medium. For the size effect, magnetite nanoparticles were synthesized via co-precipitation and partial oxidation methods which are capable of producing particles exhibiting different average sizes and magnetic properties. For the comparison of base fluids, copper oxide nanoparticles were dispersed in both water and ethylene glycol and finally, the effect of surfactant type was analyzed by coating magnetite nanoparticles with citric acid and polyacrylic acid (250 kDa and 450 kDa). As a consequence, diverse nanoparticle-base fluid systems were prepared and their thermophysical properties such as density, viscosity and thermal conductivity were measured with respect to changing temperature and volume fraction of nanoparticles. Ultimately, empirical models were constructed by using the collected data and evaluated by considering their accuracies in order to be appreciated as generalized forms for all nanofluids.

6.1. DENSITY OF NANOFLUIDS

According to the studies presented in the literature, it was revealed that the density of base fluids increases upon the addition of nanoparticles and decreases slightly with an increase in temperature. In this study, the densities of nanofluids consisting of polyacrylic acid (250 kDa and 450kDa) coated ferrimagnetic and citric acid coated superparamagnetic magnetite

nanoparticles, as well as water and ethylene glycol-based suspensions of copper oxide nanoparticles were investigated.

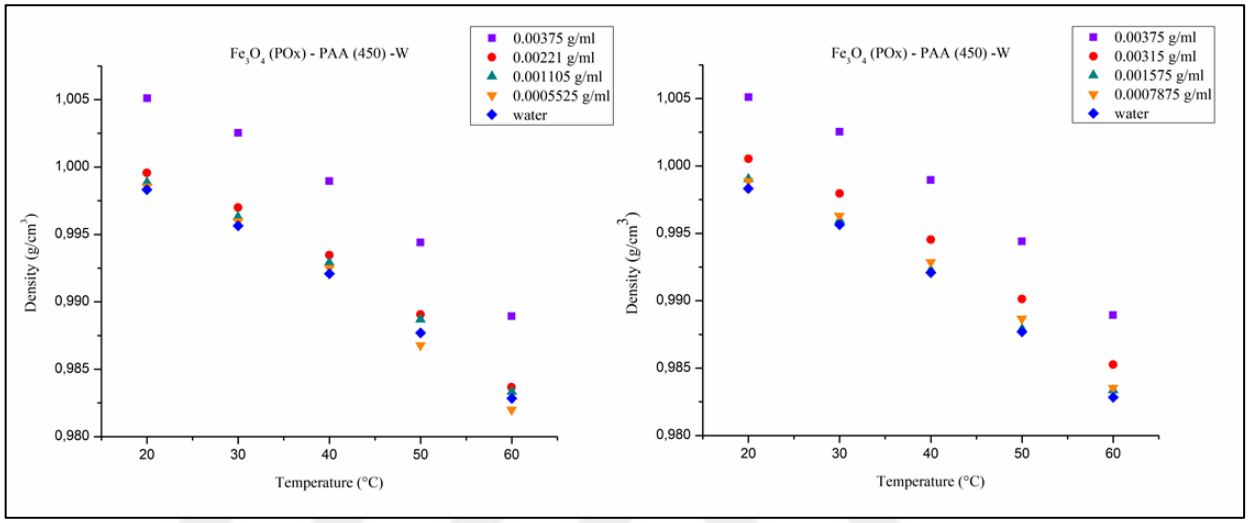

Figure 6.1. Influence of particle loading and temperature on the density of 450kDa PAA coated ferrimagnetic magnetite/water nanofluids

In Figure 6.1, the densities of nanofluids containing 450kDa polyacrylic acid coated ferrimagnetic magnetite nanoparticles at different concentrations are plotted with respect to varying temperature. These particles were synthesized via partial oxidation method and expected to exhibit ferrimagnetic properties. The results indicate that the density of the base fluid (water) is enhanced upon the addition of nanoparticles and is slightly decreased with increasing temperature, as expected. The highest density enhancement of 0.68 percent was obtained for nanofluid that contains nanoparticles at the highest concentration (0.00375g/ml) at 20°C. Moreover, it is observed that the nanofluid with the highest concentration (0.00375g/ml) exhibits the highest density at all temperatures, whereas the density of the nanofluid approaches to that of the base fluid as its concentration is decreased indicating that there is almost no change at low concentrations. Hence, it can be said that the enhancement in the density of the base fluid is not notable at low concentrations, yet it gets clearer as the particle loading is increased.

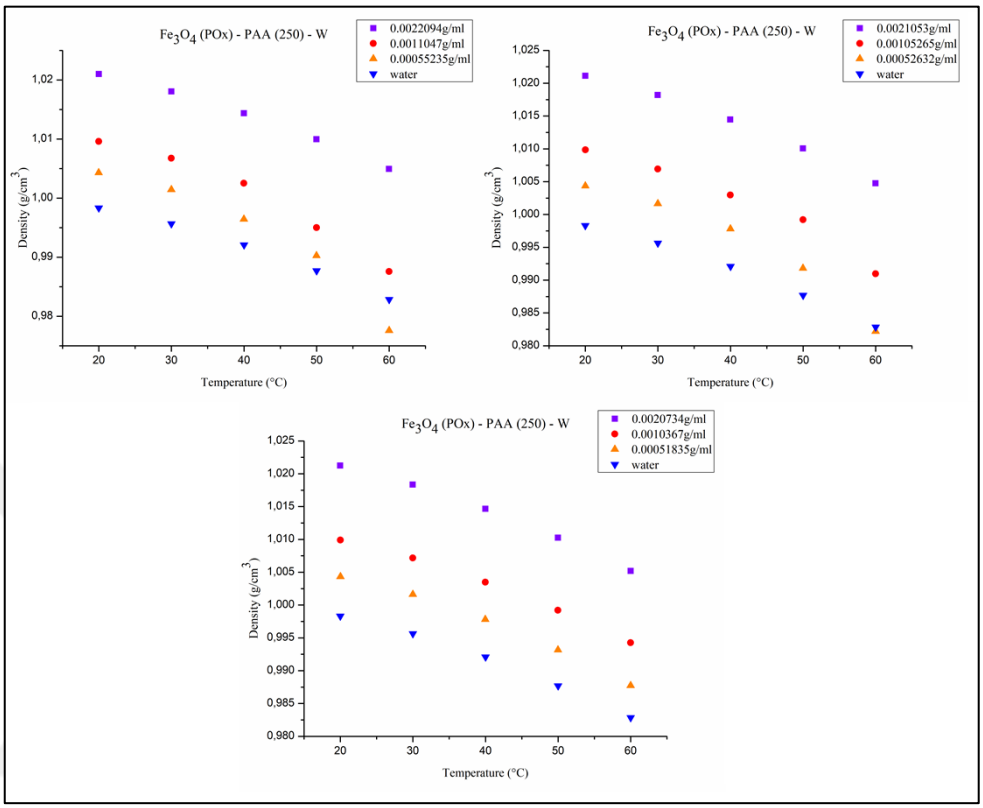

Figure 6.2. Influence of particle loading and temperature on the density of 250kDa PAA coated ferrimagnetic magnetite/water nanofluids

In Figure 6.2, the densities of magnetic nanofluids containing 250kDa polyacrylic acid coated magnetite nanoparticles with different concentrations are plotted with respect to varying temperature. As shown for the previous case, the densities of nanofluids having the highest concentrations, exhibited the highest densities (~2.3 percent for 0.002073 g/ml) and for all concentrations, the densities of all nanofluids decrease with an increase in temperature. In addition, the density of nanofluids containing particles that are coated with 250 kDa polyacrylic acid exhibited higher values than the ones containing similar particles but coated with 450 kDa polyacrylic acid at comparable concentrations. This outcome points out the importance of surfactant types when evaluating the thermophysical properties.

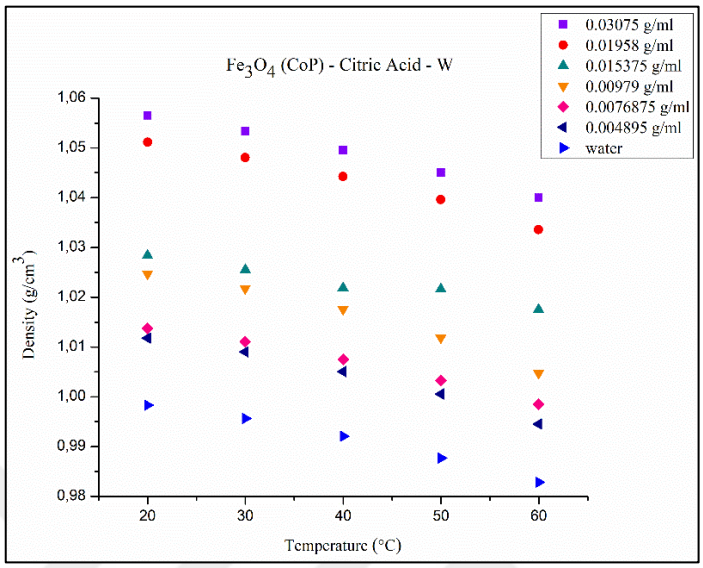

Figure 6.3. Influence of particle loading and temperature on the density of citric acid coated superparamagnetic magnetite/water nanofluids

In Figure 6.3, the densities of nanofluids containing citric acid coated superparamagnetic magnetite nanoparticles having considerably smaller average sizes were plotted with respect to varying temperature. These particles were synthesized via co-precipitation method and expected to exhibit superparamagnetic properties. It should also be noted that it was possible to attain higher concentrations via this method as compared to partial oxidation due to the nature of the reaction kinetics. As shown in Figure 6.3, the results indicate that the density of the base fluid clearly increases with increasing particle concentration and the highest enhancement was 5.8 percent for the nanofluid exhibiting the highest concentration (0.03075 g/ml). Similar to all previous results, an increase in the particle concentration leads to further enhancements and for dilute suspensions the density of nanofluids approaches to that of the base fluid (water).

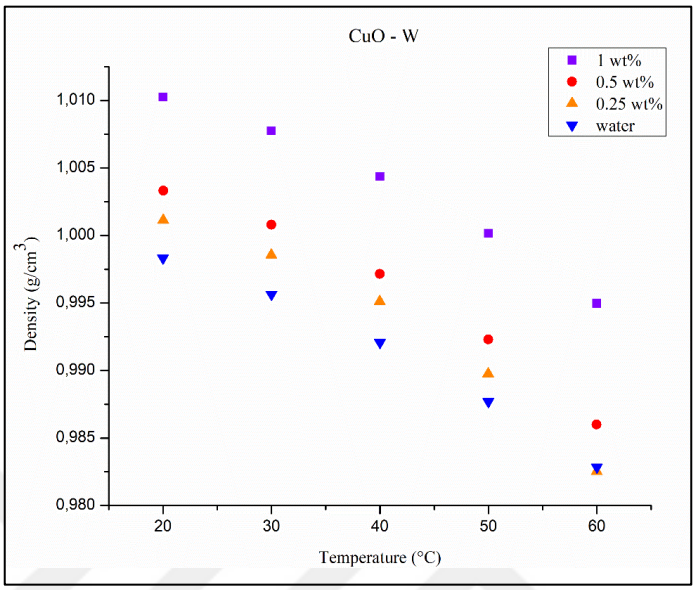

Figure 6.4. Influence of particle loading and temperature on the density of copper oxide/water nanofluids

In Figure 6.4, the densities of aqueous copper oxide nanofluids at different concentrations are plotted with varying temperature. The results similarly showed that the density of CuO based nanofluids increases upon increasing particle loading and decreases with increasing temperature at all concentrations as in the case of magnetite base nanofluids. Accordingly, the highest density enhancement relative to that of water was found to be 1.2 percent and was observed for the most concentrated (1 wt. percent) copper oxide nanofluid, at 20°C. When comparing magnetite and copper oxide nanoparticles with similar mass fractions it is observed that 0.96 percent by mass (0.00979g/ml) of magnetite nanoparticles coated with citric acid have led to a 2.64 percent increase, whereas 1.00 percent by mass of copper oxide nanoparticles has led to a 1.2 percent increase when compared to that of water, which means that citric acid coated nanoparticles exhibited a higher density at the same temperature and comparable mass fraction. This can be attributed to the effect of polymer that was used to coat magnetite nanoparticles in order to provide stability as copper oxide nanoparticles did not require one.

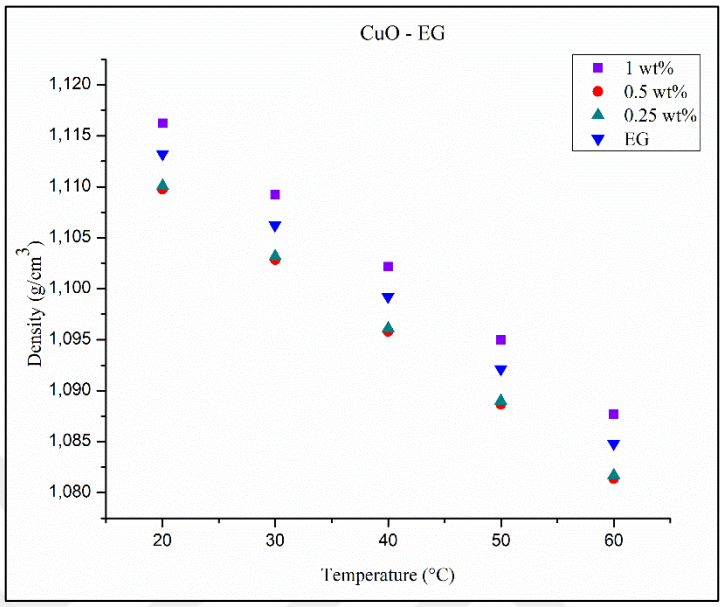

Figure 6.5. Influence of particle loading and temperature on the density of copper oxide/ ethylene glycol nanofluids

Figure 6.5 demonstrates the effect of concentration and temperature over the density of ethylene glycol-based copper oxide nanofluids. It is observed again that the density of nanofluids decrease upon increasing temperature, following the same trend as ethylene glycol. However, the effect of concentration over the density of ethylene glycol based nanofluids is insignificant and it can be concluded that the pure base fluid thermophysical properties can be used for this system especially at low volume fraction of nanoparticles.

As a consequence of all density measurements performed for different nanoparticles coated with different surface-active agents and dispersed in different base fluids, it can be said that the density of all nanofluids increases with increasing particle concentration and decreases with temperature regardless of the nanoparticle – base fluid system, as expected. It is necessary to remind at this point that nanofluids are promising candidates for their potential use in heat transfer applications and the motivation behind this study was to investigate the corresponding thermophysical properties. Considering all the measurements performed, the obtained results

illustrate that the density of the base fluid is not altered significantly at low concentrations upon the addition of nanoparticles and therefore the density of the base fluid can directly be used for necessary heat transfer calculations since the effect of nanoparticles are negligible in dilute cases.

The scope of the present study also focuses on analyzing the possibility of forming a generalized empirical model that can estimate the thermophysical properties of various types of nanoparticle-carrier fluid systems. For this purpose, the empirical data were used as input for the formation of empirical correlations which are based on models published previously for specific types of nanofluids (Table 6.1);

Table 6. 1. Models bases for the density of nanofluids

Model number	**Correlation form**
DM 1	$\rho_{nf} = A + B\emptyset + CT$
DM 2	$\rho_{nf} = A\emptyset + B(1 - \emptyset)$
DM 3	$\rho_{nf} = A + BT + CT^2 + D\emptyset + E\emptyset^2 + FT\emptyset$
DM 4	$\frac{\rho_{nf}}{\rho_{bf}} = A + B\emptyset + CT$
DM 5	$\frac{\rho_{nf}}{\rho_{bf}} = A\emptyset + B(1 - \emptyset)$
DM 6	$\frac{\rho_{nf}}{\rho_{bf}} = A + BT + CT^2 + D\emptyset + E\emptyset^2 + FT\emptyset$

The model bases for empirical correlations essentially contains temperature (T) in degrees Celsius (℃) and mass percent ($\emptyset$) of nanoparticles in percent (%) except for models 2 and 5 where the mass fraction is used as it is. It is noteworthy to emphasize that models 2 and 5 serve to predict the density of nanofluids at a desired concentration and at a constant temperature of 20℃, whereas the rest of the models are functions of both nanoparticle concentration and temperature.

In order to construct the desired models, XLSTAT add on was used. The density values of the nanofluids which were measured as a function of both concentration and temperature were used as input to the software along with the base of the desired correlation. Through non-linear regression the selected data were computed, and the equation parameters were estimated and presented by the software. For example, in order to construct a model of type 1 (DM1) that can estimate the density of citric acid coated magnetite/water nanofluids as a function of concentration and temperature, the relevant data were introduced to XLSTAT along with the general form of Model 1. After computation of the data through non-linear regression, the model parameters were found as 1.012, 0.0198 and $-4x10^{-4}$, respectively, leading to an equation in the following form;

$$\rho_{nf} = 1.012 + 0.0198\emptyset - 4x10^{-4}T \quad (6.1)$$

Equation 6.1, which is obtained through non-linear regression of the empirical data, relates the densities of nanofluids to both mass fraction (%) of nanoparticles and temperature. The model is valid only for small mass fractions of citric acid coated magnetite/water nanofluids synthesized via co-precipitation method and for a temperature range from 20℃ to 60℃ since the relevant 30 observations were used for its construction.

The average percent errors of the models were calculated based on the absolute values of predictions and the empirical data. Accordingly, the average error of Equation 6.1 was found to be 0.4 percent, meaning that the model is well able to estimate the density of a citric acid coated Fe_3O_4/water nanofluid at specific mass fraction (%) and temperature ranges. Along with the computed model parameters, XLSTAT also displays two statistical analysis graphs that aid to evaluate the accuracy of the constructed model.

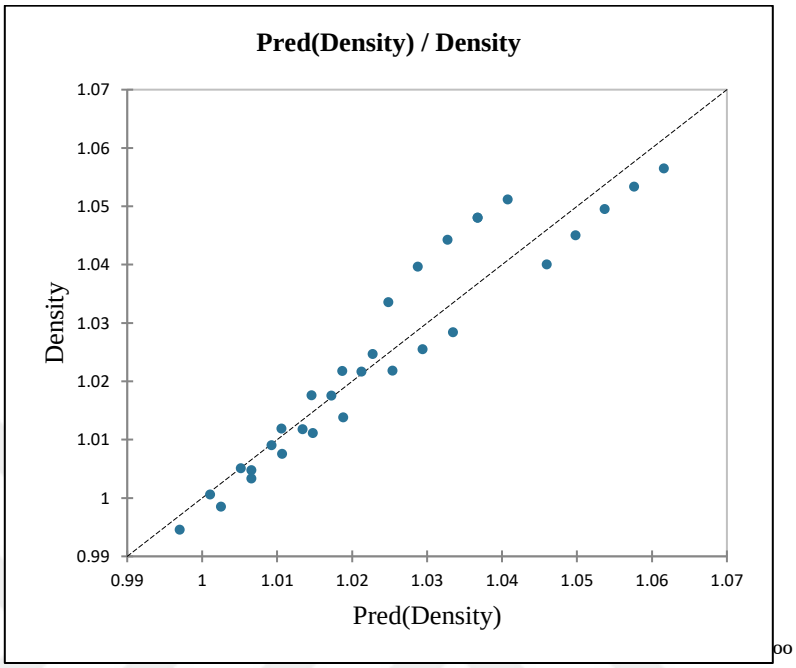

Figure 6.6. The compatibility of predicted values with measured values for equation 6.1

Figure 6.6 demonstrates the relationship in between the actual data and the predicted data for the corresponding empirical model (DM1). The y-axis in the figure represents the expected density values which are the measurements and the x-axis represents the results of the predictions calculated from the constructed model. Hence, the 45º line is where measured (expected) values and predictions are equal to each other. Therefore, if a data point gets close to the 45º line, the prediction is said to be accurate. It is observed from Figure 6.6 that almost all the data points are near or on the 45º line which means that most of the predictions via this empirical model are successful. It can also be argued that the perfectly acceptable error of the model is not originated by the model's great capability of prediction, but mostly due to comparably low alterations (even insignificant at dilute cases) in the density of nanofluids as compared to the corresponding base fluids.

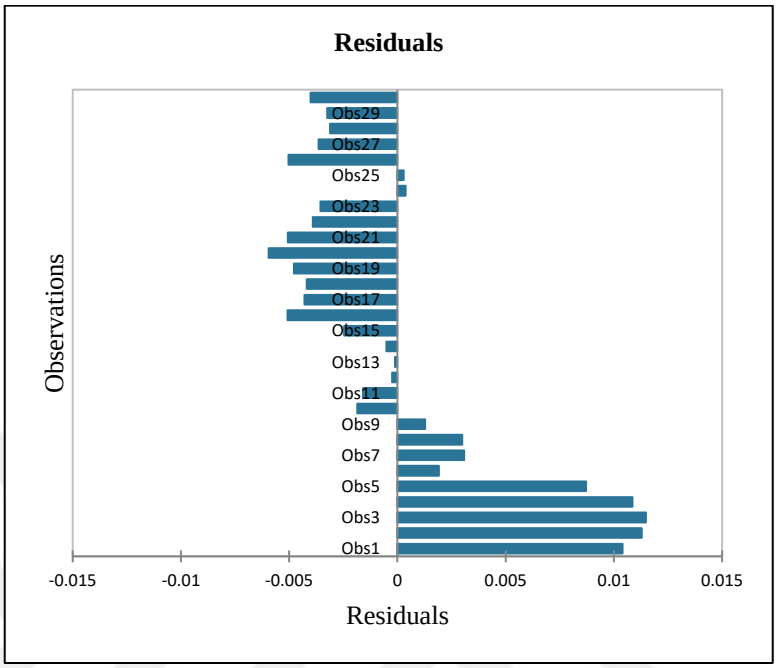

Figure 6.7. Residuals of all observations included in equation 6.1

Figure 6.7 illustrates the residuals that belong to each observation predicted by the model (DM1) individually. The residuals which represent the differences in between the actual value and the predicted value on the right-hand side are positive whereas those on the left-hand side are negative. Hence, the smaller the residual, the closer is the prediction to the expected value. Therefore, small residuals mean lower error of the constructed model and a better accuracy. As shown in Figure 6.7 the highest residuals were obtained as roughly 0.01 g/ml which is an indication of an adequate fit of the model (DM1) to the measured data.

Consequently, all of the models that are presented in Table 6.1 were fit to different data groups and subsequently several equations were obtained following the same steps as explained. Whereas DM1, DM2 and DM3 were fit specifically for each distinct nanoparticle-base fluid system, DM4, DM5 and DM6 were tried to fit to all types of nanofluids as those involve the density ratio of the nanofluid to the corresponding base fluid. The resulting empirical equations are presented in Table 6.2 along with representative errors and number of observations as well

as the details of the nanofluid such as the type of nanoparticle, base fluid and applied surfactant. The statistical analysis graphs associated with each empirical density model presented in Table 6.2 are given in Appendix A (Figures A.1-A.48).

Table 6.2. Empirical correlations for the estimation of nanofluid densities

Model no	**Obs no**	**Np type**	**Surfactant**	**Base fluid**	**Error (%)**	**Model**
DM 1	30	Fe_3O_4/ COP	Citric Acid	Water	0.4	$\rho_{nf} = 1.012 + 0.0198\emptyset - 4x10^{-4}T$
DM 1	80	Fe_3O_4/ POX	PAA 250kDa PAA 450kDa	Water	0.6	$\rho_{nf} = 1.013 + 0.0219\emptyset - 4.4x10^{-4}T$
DM 1	35	Fe_3O_4/ POX	PAA 450kDa	Water	0.11	$\rho_{nf} = 1.006 + 0.0165\emptyset - 4x10^{-4}T$
DM 1	45	Fe_3O_4/ POX	PAA 250kDa	Water	0.16	$\rho_{nf} = 1.008 + 0.116\emptyset - 4.8x10^{-4}T$
DM 1	110	Fe_3O_4	Citric Acid PAA 250kDa PAA 450kDa	Water	0.6	$\rho_{nf} = 1.013 + 0.0196\emptyset - 4.3x10^{-4}T$
DM 1	15	CuO	-	Water	0.1	$\rho_{nf} = 1.007 + 0.0137\emptyset - 4.3x10^{-4}T$
DM 1	125	Fe_3O_4 CuO	Citric Acid PAA 250kDa PAA 450kDa	Water	0.6	$\rho_{nf} = 1.012 + 0.0193\emptyset - 4.3x10^{-4}T$

Table 6.2. Empirical correlations for the estimation of nanofluid densities (Continued)

Model no	**Obs no**	**Np type**	**Surfactant**	**Base fluid**	**Error (%)**	**Model**
DM 2	6	Fe_3O_4/ COP	Citric Acid	Water	0.4	$\rho_{nf} = 3.0024\emptyset - 1.0028(1 - \emptyset)$
DM 2	16	Fe_3O_4/ POX	PAA 250kDa PAA 450kDa	Water	0.6	$\rho_{nf} = 2.7672\emptyset - 1.004(1 - \emptyset)$
DM 2	7	Fe_3O_4/ POX	PAA 450kDa	Water	0.09	$\rho_{nf} = 2.6279\emptyset - 0.997(1 - \emptyset)$
DM 2	9	Fe_3O_4/ POX	PAA 250kDa	Water	0.04	$\rho_{nf} = 11.784\emptyset - 0.999(1 - \emptyset)$
DM 2	22	Fe_3O_4	Citric Acid PAA 250kDa PAA 450kDa	Water	0.6	$\rho_{nf} = 2.961\emptyset - 1.004(1 - \emptyset)$
DM 2	3	CuO	-	Water	0.04	$\rho_{nf} = 2.25\emptyset - 0.998(1 - \emptyset)$
DM 2	25	Fe_3O_4 CuO	Citric Acid PAA 250kDa PAA 450kDa	Water	0.6	$\rho_{nf} = 2.922\emptyset - 1.0026(1 - \emptyset)$
DM 4	140	Fe_3O_4 CuO	Citric Acid PAA 250kDa PAA 450kDa	Water EG	0.7	$\frac{\rho_{nf}}{\rho_{bf}} = 1.0036 + 0.0192\emptyset - 3.45x10^{-5}T$
DM 5	28	Fe_3O_4 CuO	Citric Acid PAA 250kDa PAA 450kDa	Water EG	0.7	$\frac{\rho_{nf}}{\rho_{bf}} = 2.9\emptyset + 1.0028(1 - \emptyset)$

Table 6.2. Empirical correlations for the estimation of nanofluid densities (Continued)

Model no	Obs no	Np type	Surfactant	Base fluid	%Error	Model
DM3	30	Fe_3O_4/COP	Citric Acid	Water	0.3	$\rho_{nf} = 0.996 - 1.14x10^{-4}T - 3.9x10^{-6}T^2 + 0.037\emptyset - 0.005\emptyset^2 + 9.1x10^{-6}T\emptyset$
DM3	80	Fe_3O_4/POX	PAA 250kDa PAA 450kDa	Water	0.6	$\rho_{nf} = 0.997 - 3.94x10^{-5}T - 5.75x10^{-6}T^2 + 0.158\emptyset - 0.393\emptyset^2 + 4x10^{-4}T\emptyset$
DM3	35	Fe_3O_4/POX	PAA 450kDa	Water	0.06	$\rho_{nf} = 1.003 - 5.59x10^{-5}T - 4.26x10^{-6}T^2 - 0.0225\emptyset + 0.0917\emptyset^2 - 8.85x10^{-6}T\emptyset$
DM3	45	Fe_3O_4/POX	PAA 250kDa	Water	0.11	$\rho_{nf} = 1.002 - 8.81x10^{-6}T - 6.97x10^{-6}T^2 + 0.088\emptyset - 0.0064\emptyset^2 + 7.32x10^{-4}T\emptyset$
DM3	110	Fe_3O_4	Citric Acid PAA 250kDa PAA 450kDa	Water	0.6	$\rho_{nf} = 1.006 - 2.33x10^{-5}T - 5.23x10^{-6}T^2 + 0.0227\emptyset - 0.0015\emptyset^2 + 1.9x10^{-5}T\emptyset$

Table 6.2. Empirical correlations for the estimation of nanofluid densities (Continued)

Model no	Obs no	Np type	Surfactant	Base fluid	%Error	Model
DM3	15	CuO	-	Water	0.02	$\rho_{nf} = 1.002 + 2.05x10^{-5}T - 6.3x10^{-6}T^2 + 9.65x10^{-4}\emptyset + 0.007\emptyset^2 + 9.49x10^{-5}T\emptyset$
DM3	125	Fe_3O_4 CuO	Citric Acid PAA 250kDa PAA 450kDa	Water	0.6	$\rho_{nf} = 1.005 - 1.33x10^{-5}T - 5.35x10^{-6}T^2 + 0.017\emptyset + 5.6x10^{-4}\emptyset^2 + 1.9x10^{-5}T\emptyset$
DM6	140	Fe_3O_4 CuO	Citric Acid PAA 250kDa PAA 450kDa	Water EG	0.7	$\frac{\rho_{nf}}{\rho_{bf}} = 1.0035 + 7.03x10^{-5}T - 1.5x10^{-6}T^2 + 0.0118\emptyset + 2.59x10^{-3}\emptyset^2 + 2.4x10^{-5}T\emptyset$

As illustrated in Table 6.2, various types of nanoparticle-carrier fluid systems were tried to be fit to the base models both together and as separate groups and in each case the average absolute percent error calculated were under 1 percent. All the models that have been constructed based on empirical data collected during the present study perfectly predicted the densities of all kinds of nanofluids with extremely small errors. The results on the other hand indicated that the predictions are generally better when each nanoparticle-base fluid system and distinct models are examined separately, as residuals get higher when separate groups are combined. For instance, when 250 kDa and 450kDa polyacrylic acid coated ferrimagnetic magnetite/water nanofluids are examined separately, nearly all the data are close to or exactly on the 45º line. However, when all the measurements are used together as input, the data points scatter away from the 45º line. This observation can also be verified by considering the average absolute percent errors stated in Table 6.2. The errors of models formed for 250 kDa and 450 kDa PAA coated ferrimagnetic magnetite/water nanofluids are 0.16 and 0.11, respectively. On the other hand, the percent error of the model that considers both groups in combination was increased to 0.6 percent. Although, 0.6 percent is a promising outcome for an empirical model, the enhancement of percent error for the combined class of models should be kept in consideration when viscosity and thermal conductivity related models are examined. For all models, it can also be concluded that the notably small percent errors are mostly originated from the small alterations in density upon addition of nanoparticles especially for dilute cases. Another outcome that is revealed according to the results illustrated in Table 6.2 is the effect of temperature. It is concluded from the equation parameters that temperature has a relatively insignificant role for the prediction of density when compared to nanoparticle concentration. In conclusion, different data groups belong to both distinct nanoparticle-carrier fluid systems and their combinations were tried to fit to several types of models and the results showed that the percent error of the models remained nearly constant and calculated to be less than 1 percent regardless of the observation number, nanoparticle type (CuO or Fe_3O_4), average size, types of the surfactant (citric acid or PAA) and the base fluid (water or ethylene glycol). The reason behind this small amount of error encountered in each case was attributed to the exceedingly small changes in density upon addition of low concentration of nanoparticles. Accordingly, when nanofluids are preferred in heat transfer applications the effect of nanoparticles over the

density of the base fluid can be neglected and instead the density of base fluids can directly be used for process calculations especially for dilute cases. However, for concentrated nanofluids direct measurement or estimated values of densities should be taken into consideration as the enhancement might be significant.

As a consequence, results indicated that the formulation of empirical correlations for the density of nanofluids is possible for distinct nanoparticle-base fluid systems which are considered individually. However, the average absolute percent errors of the models tend to increase when different types of nanofluids are grouped together. By considering the empirical equations that have been modeled for the estimation of nanofluid densities, it can be stated that the average errors are around 0.7 percent. Additionally, according to the statistical analysis of the models (Figures A.13, A.27, A.41, A.43, A.45, A.47), DM1 and DM3 was shown to exhibit the most accurate results for an extended group of nanofluids as all the data points are close and regularly scattered over the 45º line.

6.2. VISCOSITY OF NANOFLUIDS

Previous studies on the viscosities of nanofluids revealed that the viscosities of base fluids enhanced remarkably upon the addition of nanoparticles and decreases with increasing temperature by following a similar trend with those of commonly used based fluids. In this section, the rheological behavior of various nanofluids with respect to both variable nanoparticle concentration and temperature has been investigated. In order to compare the effect of nanoparticle and base fluid types, 250 kDa and 450kDa polyacrylic acid coated ferrimagnetic magnetite/water nanofluids, 450kDa polyacrylic acid and citric acid coated superparamagnetic magnetite/water nanofluids, copper oxide/water nanofluids and copper oxide/ethylene glycol nanofluids were analyzed and the collected data was used as input for several base models to formulate generalized empirical correlations for the estimation of nanofluid viscosities. Results in general indicated that the viscosity of all nanofluids increased remarkably with increasing particle loading and decreased significantly with increasing temperature as expected. However, the enhancements obtained for viscosity is incomparably apparent when compared with density.

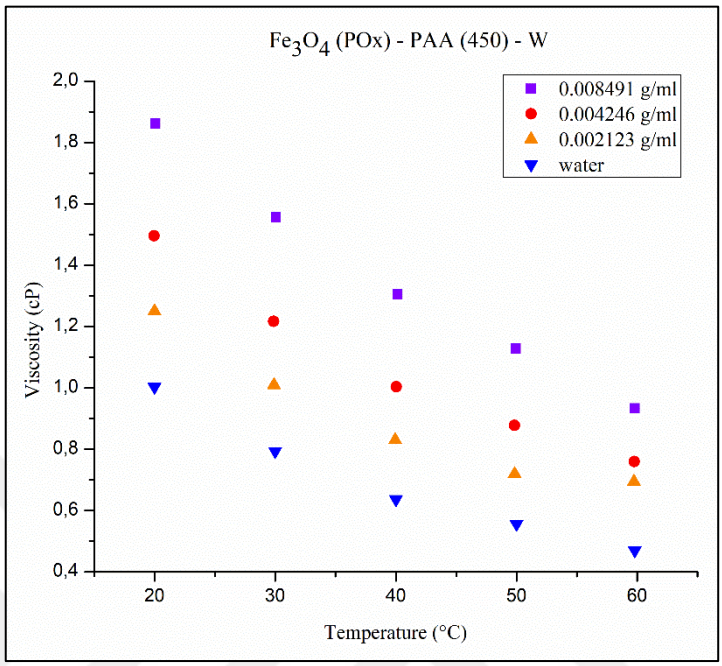

Figure 6.8. Influence of particle loading and temperature on the viscosity of 450kDa PAA coated ferrimagnetic magnetite/water nanofluids

In Figure 6.8, the viscosities of 450kDa polyacrylic acid coated ferrimagnetic magnetite/water nanofluids are presented as a function of both temperature and concentration of nanoparticles. It is clearly seen from the relevant figure that the viscosities of all nanofluids are higher than that of water at all temperatures, meaning that the addition of nanoparticles have led to a significant enhancement in the viscosity of the base fluid. Furthermore, the enhancement in the viscosities of nanofluids is increased with increasing concentration of nanoparticles. Moreover, viscosities of nanofluids decrease with increasing temperature, following a similar trend to that of water. At a constant temperature of 20°C, the viscosity enhancements of nanofluids having concentrations of 0.008491g/ml, 0.004246g/ml and 0.002123g/ml were found to be 86, 49 and 25 percent, respectively.

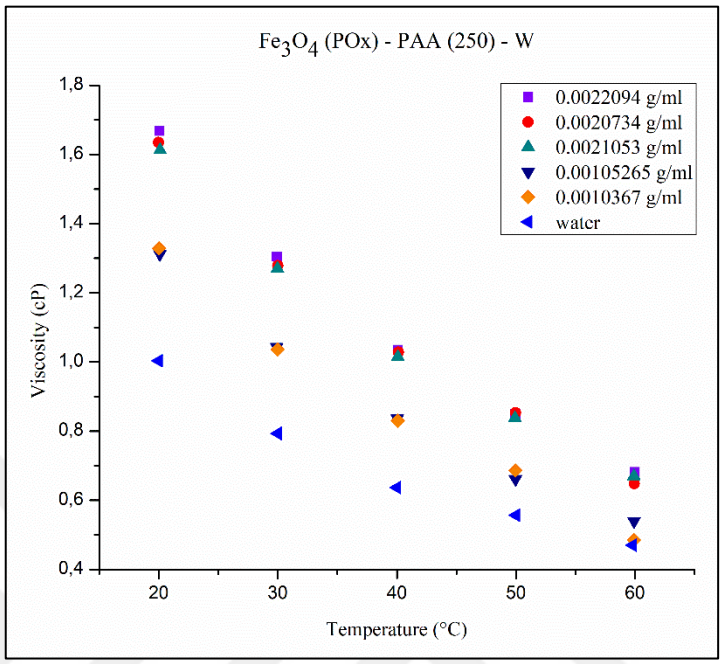

Figure 6.9. Influence of particle loading and temperature on the viscosity of 250kDa PAA coated ferrimagnetic magnetite/water nanofluids

Figure 6.9 also represents viscosity of aqueous magnetic nanofluids but containing 250kDa polyacrylic acid coated ferrimagnetic magnetite nanoparticles as a function of concentration and temperature. Similar to the previous case, the viscosity of water is enhanced upon the addition of nanoparticles and decreased with increasing temperature. It is also evident that nanofluids with similar concentrations exhibit similar viscosity enhancements which indicates the reliability of measurements. The maximum viscosity enhancement was obtained as 66 percent for the most concentrated nanofluid (0.0022094g/ml), at 20°C and the percent viscosity enhancements decreased with decreasing nanofluid concentration. Experimental results also revealed that a 30 percent viscosity enhancement is achievable even with extremely low nanoparticle concentrations (around 0.001g/ml). Furthermore, in order to account for the effect of the type of the surfactant, the nanofluid samples (450 kDa and 250 kDa PAA coated ferrimagnetic magnetite/water samples) were compared. The comparison of the two different nanofluids at similar nanoparticle concentrations (around 0.0021g/ml) has shown that

ferrimagnetic magnetite nanoparticles coated with 450kDa PAA have led to an enhancement of 25 percent while those coated with 250kDa PAA have shown a viscosity enhancement of 60 percent, indicating that 250kDa PAA coated nanoparticles have induced a much larger viscosity enhancement. Polymers with higher molecular weights exhibit higher viscosities, hence 450kDa PAA coated magnetite nanofluids were expected to exhibit relatively higher viscosities. However, results indicated the opposite trend. The unexpected trend of the rheological behavior of these nanofluids can be attributed to their colloidal stabilities which affect the uniform distribution of nanoparticles thus change the local concentrations within the samples as 450kDa PAA coated nanoparticles were relatively unstable as compared to 250 kDa PAA coated nanoparticles which exhibited better colloidal stability.

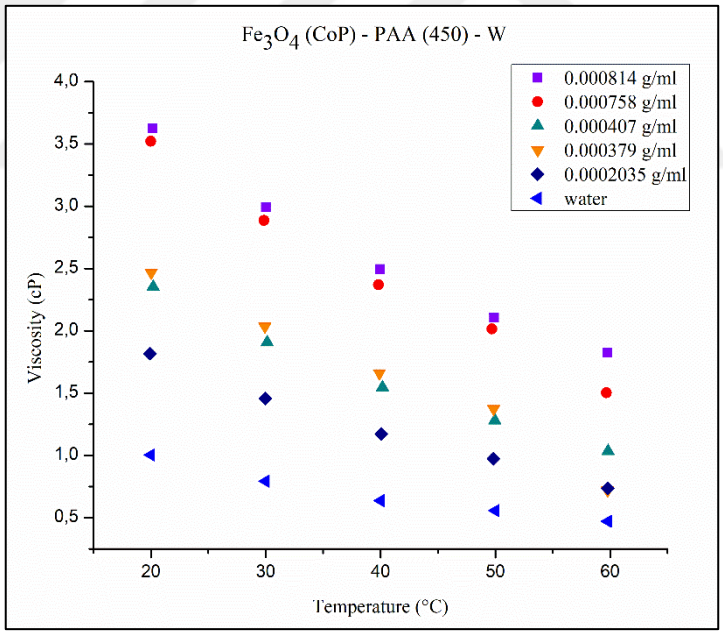

Figure 6.10. Influence of particle loading and temperature on the viscosity of 450kDa PAA coated superparamagnetic magnetite/water nanofluids

The nanofluids containing 450kDa polyacrylic acid coated magnetite nanoparticles that are presented in Figure 6.10 were synthesized via co-precipitation method and therefore possess smaller sizes. The expected trend of nanofluids with changing nanoparticle concentration and

temperature is observed again in Figure 6.10; the viscosity of water is enhanced clearly with increasing concentration of nanoparticles and decreased with increasing temperature. Nanofluids presented in Figure 6.10 serve also for revealing the effect of nanoparticle size over the viscosity of nanofluids. When comparing these nanoparticles with 450kDa coated ferrimagnetic nanoparticles which possess relatively larger sizes, it is observed that these nanoparticles having smaller sizes exhibited comparably greater viscosity enhancements at a much lower nanoparticle concentration. The viscosity enhancements of nanofluids with concentrations of 0.000814g/ml, 0.000758g/ml, 0.000407g/ml, 0.000379g/ml and 0.0002035g/ml were found to be 261, 250, 134, 146 and 81 percent, respectively at 20 ºC. The essential reason behind this extreme difference between the viscosity enhancements of 450kDa coated ferrimagnetic and superparamagnetic magnetite nanofluids can be attributed to the uniform distribution of superparamagnetic nanoparticles within the suspension as a consequence of a better colloidal stabilization.

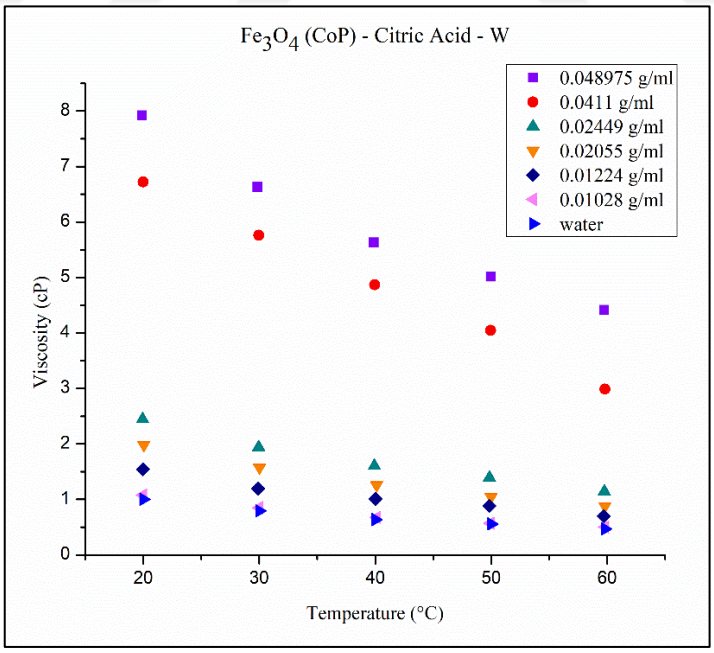

Figure 6.11. Influence of particle loading and temperature on the viscosity of citric acid coated superparamagnetic magnetite/water nanofluids

In Figure 6.11, viscosities of citric acid coated superparamagnetic magnetite/water nanofluids are demonstrated as a function of nanofluid concentration and temperature. It is observed again that the viscosity of water is remarkably enhanced with increasing concentration and decreased with increasing temperature by following a similar trend of water. The viscosity enhancements of nanofluids containing citric acid coated superparamagnetic nanoparticles were found to range from 7 to 690 percent when concentration of nanoparticles increased from 0.01028 g/ml to 0.048975 g/ml at 20°C, respectively. Hence, tremendous viscosity enhancements are obtained for highly concentrated citric acid coated magnetite/water nanofluids. The relevant case therefore is a strong evidence demonstrating the undeniably great impact of concentration of nanoparticles over the viscosity of base fluids

.

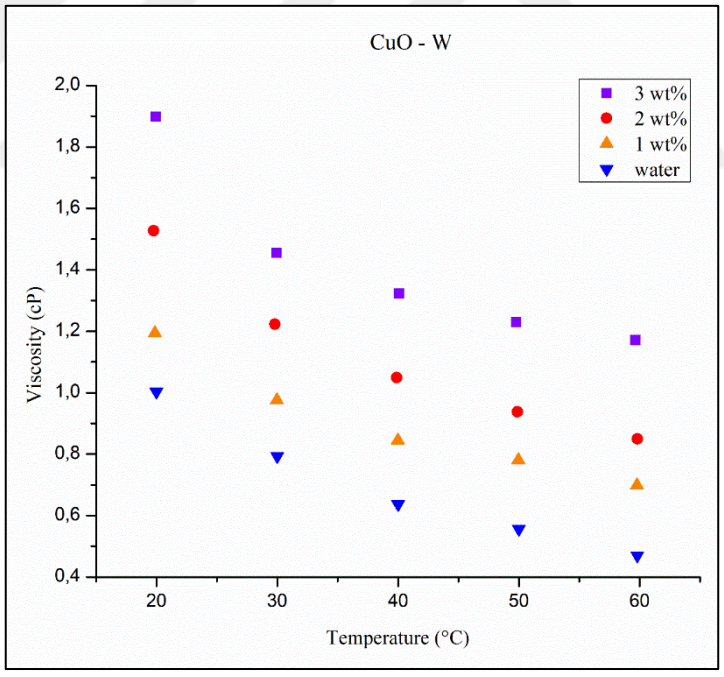

Figure 6.12. Influence of particle loading and temperature on the viscosity of copper oxide/water nanofluids

Finally, Figure 6.12 illustrates the effect of both nanoparticle concentration and temperature over the viscosities of copper oxide/water nanofluids. Similar to all previous experimental

results, the viscosity of water is enhanced with increasing nanoparticle loading and decreased with increasing temperature. The viscosity enhancements of copper oxide nanofluids with 3, 2 and 1 weight percent were found to be 89, 52 and 19 percent, respectively. at a constant temperature of 20°C. When comparing copper oxide and magnetite nanoparticles at similar concentrations, the results indicated that the addition of magnetite nanoparticles have generally led to a greater enhancement when compared to copper oxide nanoparticles. This outcome indicates that even at comparable concentrations different types of nanoparticles may lead to divergent viscosity enhancements for the same type of base fluid.

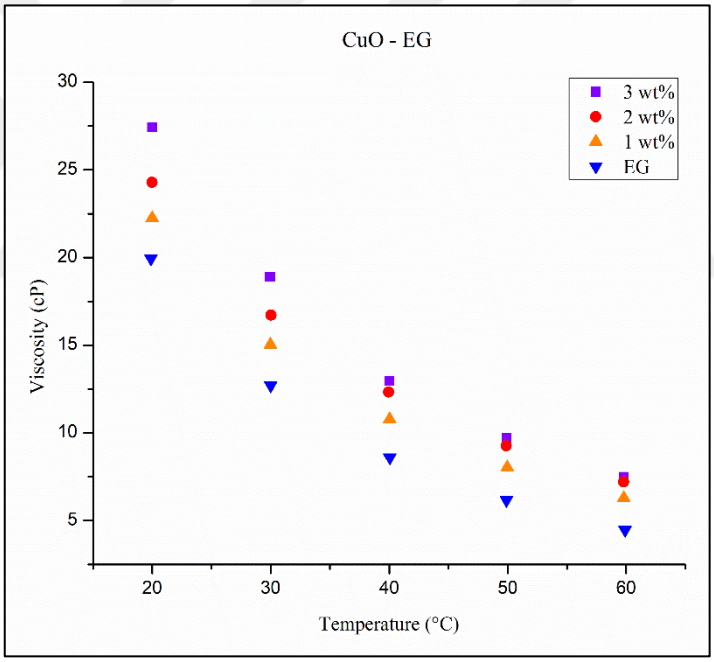

Figure 6.13. Influence of particle loading and temperature on the viscosity of copper oxide/ethylene glycol nanofluids

In order to reveal the effect of base fluid over the viscosity of nanofluids, measurements were performed for ethylene glycol-based copper oxide nanofluids which are presented in Figure 6.13. The results showed that the addition of copper oxide nanoparticles led to a considerable enhancement in the viscosity of ethylene glycol at all temperatures. Moreover. the relative

enhancements were found to be increasing with increasing concentration of nanoparticles. The viscosity enhancements relative to that of ethylene glycol were found to be 37, 22 and 12 percent for 3, 2 and 1 weight percent respectively, at a constant temperature of 20℃. The comparison of water and ethylene glycol-based copper oxide nanofluids with similar nanoparticle concentrations indicated that the viscosity of water is further enhanced at the same temperature. It can therefore be concluded that water is relatively more sensitive to the addition of nanoparticles than ethylene glycol is.

The results presented in this section of the study reveal the effects of different parameters such as the type and size of nanoparticles, type of surfactants and base fluids, over the viscosities of two commonly used base fluids namely water and ethylene glycol. It was observed for all nanofluids that the viscosities of base fluids enhanced remarkably upon the addition of nanoparticles and decreased with increasing temperature, following a similar trend with that of the corresponding base fluid. In addition, the comparison of the viscosity enhancements originated by different nanofluids have revealed that there is no specific behavior followed by each nanoparticle-base fluid system, but they rather possess genuine rheological behaviors. The maximum viscosity enhancement at a constant temperature of 20℃ was inherently observed with the most concentrated nanofluid (citric acid coated magnetite/water nanofluid with a concentration of 0.048975g/ml) and was found to be 590 percent. It is drastically evident that the addition of nanoparticles possesses an undeniably great role on the viscosities of common base fluids and therefore their effect must be considered in practical applications. Additionally, the rheological behavior of nanofluids is not as predictable as their densities. Thus, it is practically necessary to have empirical correlations for the estimation of nanofluid viscosities if direct measurement is not applicable. For this purpose, certain types of models that are presented in the literature were considered and the measured data was used as input for the formation of generalized empirical correlations.

Table 6. 3. Skeletal forms of the chosen models for the viscosity of nanofluids

Model number	**Correlation form**
VM 1	$\frac{\mu_{nf}}{\mu_{bf}} = A + B\emptyset$
VM 2	$\frac{\mu_{nf}}{\mu_{bf}} = Ae^{B\emptyset}$
VM 3	$\frac{\mu_{nf}}{\mu_{bf}} = \frac{1}{(1-\emptyset)^{A}}$
VM 4	$\frac{\mu_{nf}}{\mu_{bf}} = AT^{B}\emptyset^{C}$
VM 5	$\mu_{nf} = (A\emptyset^2 + B\emptyset + C)e^{-DT}$
VM 6	$\mu_{nf} = \frac{Ae^{B\emptyset}}{T}$
VM 7	$\mu_{nf} = A\emptyset + \frac{B}{T}$

The base models that are chosen for the estimation of the viscosities of nanofluids are presented in Table 6.3. In all of the models, *T* is the nanofluid temperature in degrees Celsius (℃) and ∅ is the concentration of nanoparticles in g/ml. It should be noted that models 1-3 consider the effect of nanoparticle concentration only and are valid at a constant temperature of 20℃, while the rest of the models consider the effects of both nanoparticle concentration and temperature. In order to construct the desired types of models, the viscosities of the nanofluids which were measured with changing nanoparticle concentration and temperature were introduced to XLSTAT as input, along with the desired model base. Consequently, the empirical data was computed and the equation parameters were obtained for each case. The average absolute percent errors of the models were calculated based on the residuals. The resulting models correlating the viscosities of different nanofluids to concentration and temperature are presented in Table 6.4. The statistical analysis graphs associated with each viscosity model presented in Table 6.4 are given in Appendix B (Figures B.1-B.120).

Table 6.4. Empirical correlations for the estimation of nanofluid viscosities

Model no	Obs no	Np type	Surfactant	Base fluid	Error (%)	Model
VM 1	11	Fe_3O_4/COP	Citric Acid PAA 450kDa	Water	54	$\frac{\mu_{nf}}{\mu_{bf}} = 1.846 + 93.995\emptyset$
VM 1	8	Fe_3O_4/POX	PAA 250kDa PAA 450kDa	Water	6	$\frac{\mu_{nf}}{\mu_{bf}} = 1.340 + 60.225\emptyset$
VM 1	3	Fe_3O_4/POX	PAA 450kDa	Water	1.2	$\frac{\mu_{nf}}{\mu_{bf}} = 1.063 + 94.401\emptyset$
VM 1	5	Fe_3O_4/POX	PAA 250kDa	Water	0.8	$\frac{\mu_{nf}}{\mu_{bf}} = 1.009 + 293.045\emptyset$
VM 1	19	Fe_3O_4	Citric Acid PAA 250kDa PAA 450kDa	Water	40	$\frac{\mu_{nf}}{\mu_{bf}} = 1.51 + 102.409\emptyset$
VM 1	3	CuO	-	Water	1.1	$\frac{\mu_{nf}}{\mu_{bf}} = 0.846 + 33.327\emptyset$
VM 1	22	Fe_3O_4 CuO	Citric Acid PAA 250kDa PAA 450kDa	Water	44	$\frac{\mu_{nf}}{\mu_{bf}} = 1.422 + 84.743\emptyset$
VM 1	3	CuO	-	EG	1.1	$\frac{\mu_{nf}}{\mu_{bf}} = 0.977 + 11.395\emptyset$

Table 6.4. Empirical correlations for the estimation of nanofluid viscosities (Continued)

Model no	Obs no	Np type	Surfactant	Base fluid	Error (%)	Model
VM 1	6	CuO	-	Water EG	12	$\frac{\mu_{nf}}{\mu_{bf}} = 0.967 + 19.277\emptyset$
VM 2	11	Fe_3O_4/COP	Citric Acid PAA 450kDa	Water	43	$\frac{\mu_{nf}}{\mu_{bf}} = 1.763e^{29.971\emptyset}$
VM 2	8	Fe_3O_4/POX	PAA 250kDa PAA 450kDa	Water	9	$\frac{\mu_{nf}}{\mu_{bf}} = 1.356e^{36.797\emptyset}$
VM 2	3	Fe_3O_4/POX	PAA 450kDa	Water	2	$\frac{\mu_{nf}}{\mu_{bf}} = 1.125e^{59.603\emptyset}$
VM 2	5	Fe_3O_4/POX	PAA 250kDa	Water	0.7	$\frac{\mu_{nf}}{\mu_{bf}} = 1.068e^{199.296\emptyset}$
VM 2	19	Fe_3O_4	Citric Acid PAA 250kDa PAA 450kDa	Water	30	$\frac{\mu_{nf}}{\mu_{bf}} = 1.562e^{32.809\emptyset}$
VM 2	3	CuO	-	Water	0.14	$\frac{\mu_{nf}}{\mu_{bf}} = 0.957e^{22.002\emptyset}$
VM 2	22	Fe_3O_4 CuO	Citric Acid PAA 250kDa PAA 450kDa	Water	35	$\frac{\mu_{nf}}{\mu_{bf}} = 1.352e^{34.506\emptyset}$

Table 6.4. Empirical correlations for the estimation of nanofluid viscosities (Continued)

Model no	Obs no	Np type	Surfactant	Base fluid	Error (%)	Model
VM 2	3	CuO	-	EG	0.9	$\frac{\mu_{nf}}{\mu_{bf}} = 0.996e^{9.314\emptyset}$
VM 2	6	CuO	-	Water EG	12	$\frac{\mu_{nf}}{\mu_{bf}} = 1.023e^{13.639\emptyset}$
VM 3	11	Fe_3O_4/COP	Citric Acid PAA 450kDa	Water	37	$\frac{\mu_{nf}}{\mu_{bf}} = \frac{1}{(1-\emptyset)^{42.072}}$
VM 3	8	Fe_3O_4/POX	PAA 250kDa PAA 450kDa	Water	16	$\frac{\mu_{nf}}{\mu_{bf}} = \frac{1}{(1-\emptyset)^{86.554}}$
VM 3	3	Fe_3O_4/POX	PAA 450kDa	Water	5.3	$\frac{\mu_{nf}}{\mu_{bf}} = \frac{1}{(1-\emptyset)^{75.681}}$
VM 3	5	Fe_3O_4/POX	PAA 250kDa	Water	1.8	$\frac{\mu_{nf}}{\mu_{bf}} = \frac{1}{(1-\emptyset)^{232.992}}$
VM 3	19	Fe_3O_4	Citric Acid PAA 250kDa PAA 450kDa	Water	32	$\frac{\mu_{nf}}{\mu_{bf}} = \frac{1}{(1-\emptyset)^{42.119}}$
VM 3	3	CuO	-	Water	1.3	$\frac{\mu_{nf}}{\mu_{bf}} = \frac{1}{(1-\emptyset)^{20.053}}$

Table 6.4. Empirical correlations for the estimation of nanofluid viscosities (Continued)

Model no	Obs no	Np type	Surfactant	Base fluid	Error (%)	Model
VM 3	22	Fe_3O_4 CuO	Citric Acid PAA 250kDa PAA 450kDa	Water	35	$\frac{\mu_{nf}}{\mu_{bf}} = \frac{1}{(1-\emptyset)^{41.011}}$
VM 3	3	CuO	-	EG	0.9	$\frac{\mu_{nf}}{\mu_{bf}} = \frac{1}{(1-\emptyset)^{9.035}}$
VM 3	6	CuO	-	Water EG	12	$\frac{\mu_{nf}}{\mu_{bf}} = \frac{1}{(1-\emptyset)^{14.248}}$
VM 4	55	Fe_3O_4/COP	Citric Acid PAA 450kDa	Water	75	$\frac{\mu_{nf}}{\mu_{bf}} = 10.637T^{1.73x10^{-5}}\emptyset^{0.233}$
VM 4	40	Fe_3O_4/POX	PAA 250kDa PAA 450kDa	Water	7	$\frac{\mu_{nf}}{\mu_{bf}} = 5.057T^{-5.9x10^{-7}}\emptyset^{0.201}$
VM 4	15	Fe_3O_4/POX	PAA 450kDa	Water	2	$\frac{\mu_{nf}}{\mu_{bf}} = 6.059T^{0.081}\emptyset^{0.298}$
VM 4	25	Fe_3O_4/POX	PAA 250kDa	Water	5	$\frac{\mu_{nf}}{\mu_{bf}} = 10.847T^{-7.89x10^{-7}}\emptyset^{0.315}$

Table 6.4. Empirical correlations for the estimation of nanofluid viscosities (Continued)

Model no	Obs no	Np type	Surfactant	Base fluid	Error (%)	Model
VM 4	95	Fe_3O_4	Citric Acid PAA 250kDa PAA 450kDa	Water	54	$\frac{\mu_{nf}}{\mu_{bf}} = 18.463T^{0.038}\emptyset^{0.422}$
VM 4	15	CuO	-	Water	5	$\frac{\mu_{nf}}{\mu_{bf}} = 3.868T^{0.222}\emptyset^{0.415}$
VM 4	110	Fe_3O_4 CuO	Citric Acid PAA 250kDa PAA 450kDa	Water	55	$\frac{\mu_{nf}}{\mu_{bf}} = 11.014T^{0.055}\emptyset^{0.348}$
VM 4	15	CuO	-	EG	7	$\frac{\mu_{nf}}{\mu_{bf}} = 2.77T^{4.4x10^{-7}}\emptyset^{0.177}$
VM 4	30	CuO	-	Water EG	12	$\frac{\mu_{nf}}{\mu_{bf}} = 4.497T^{4.7x10^{-7}}\emptyset^{0.274}$
VM 5	55	Fe_3O_4/COP	Citric Acid PAA 450kDa	Water	23	$\mu_{nf} = (7866.5\emptyset^2 - 221.01\emptyset + 3.732)e^{-0.018T}$
VM 5	40	Fe_3O_4/POX	PAA 250kDa PAA 450kDa	Water	8	$\mu_{nf} = (-5871.8\emptyset^2 + 172.113\emptyset + 1.832)e^{-0.02T}$

Table 6.4. Empirical correlations for the estimation of nanofluid viscosities (Continued)

Model no	Obs no	Np type	Surfactant	Base fluid	Error (%)	Model
VM 5	15	Fe_3O_4/POX	PAA 450kDa	Water	0.02	$\mu_{nf} = (-4184.8\emptyset^2 + 184.108\emptyset + 1.356)e^{-0.017T}$
VM 5	25	Fe_3O_4/POX	PAA 250kDa	Water	2	$\mu_{nf} = (-37145.5\emptyset^2 + 582.313\emptyset + 1.497)e^{-0.023T}$
VM 5	95	Fe_3O_4	Citric Acid PAA 250kDa PAA 450kDa	Water	27	$\mu_{nf} = (7065.8\emptyset^2 - 155.261\emptyset + 2.963)e^{-0.018T}$
VM 5	15	CuO	-	Water	4	$\mu_{nf} = (720.85\emptyset^2 + 11.731\emptyset + 1.334)e^{-0.014T}$
VM 5	110	Fe_3O_4 CuO	Citric Acid PAA 250kDa PAA 450kDa	Water	28	$\mu_{nf} = (7823.4\emptyset^2 - 199.396\emptyset + 3.043)e^{-0.018T}$
VM 5	15	CuO	-	EG	4	$\mu_{nf} = (3256.8\emptyset^2 + 287.363\emptyset + 39.115)e^{-0.034T}$

Table 6.4. Empirical correlations for the estimation of nanofluid viscosities (Continued)

Model no	Obs no	Np type	Surfactant	Base fluid	Error (%)	Model
VM 6	55	Fe_3O_4/COP	Citric Acid PAA 450kDa	Water	44	$\mu_{nf} = \frac{39.494e^{31.359\emptyset}}{T}$
VM 6	40	Fe_3O_4/POX	PAA 250kDa PAA 450kDa	Water	13	$\mu_{nf} = \frac{29.961e^{45.498\emptyset}}{T}$
VM 6	15	Fe_3O_4/POX	PAA 450kDa	Water	16	$\mu_{nf} = \frac{25.925e^{62.9\emptyset}}{T}$
VM 6	25	Fe_3O_4/POX	PAA 250kDa	Water	10	$\mu_{nf} = \frac{23.729e^{200.49\emptyset}}{T}$
VM 6	95	Fe_3O_4	Citric Acid PAA 250kDa PAA 450kDa	Water	30	$\mu_{nf} = \frac{35.182e^{34.064\emptyset}}{T}$
VM 6	15	CuO	-	Water	19	$\mu_{nf} = \frac{22.75e^{21.756\emptyset}}{T}$
VM 6	110	Fe_3O_4 CuO	Citric Acid PAA 250kDa PAA 450kDa	Water	33	$\mu_{nf} = \frac{30.246e^{36.005\emptyset}}{T}$

Table 6.4. Empirical correlations for the estimation of nanofluid viscosities (Continued)

Model no	Obs no	Np type	Surfactant	Base fluid	Error (%)	Model
VM 6	15	CuO	-	EG	6	$\mu_{nf} = \frac{393.965e^{9.134\emptyset}}{T}$
VM 7	55	Fe_3O_4/ COP	Citric Acid PAA 450kDa	Water	60	$\mu_{nf} = 70.697\emptyset + \frac{44.416}{T}$
VM 7	40	Fe_3O_4/ POX	PAA 250kDa PAA 450kDa	Water	8	$\mu_{nf} = 67.377\emptyset + \frac{28.603}{T}$
VM 7	15	Fe_3O_4/ POX	PAA 450kDa	Water	6	$\mu_{nf} = 79.461\emptyset + \frac{24.274}{T}$
VM 7	25	Fe_3O_4/ POX	PAA 250kDa	Water	6	$\mu_{nf} = 165.703\emptyset + \frac{25.219}{T}$
VM 7	95	Fe_3O_4	Citric Acid PAA 250kDa PAA 450kDa	Water	43	$\mu_{nf} = 77.024\emptyset + \frac{35.84}{T}$
VM 7	15	CuO	-	Water	5	$\mu_{nf} = 26.641\emptyset + \frac{20.119}{T}$

Table 6.4. Empirical correlations for the estimation of nanofluid viscosities (Continued)

Model no	**Obs no**	**Np type**	**Surfactant**	**Base fluid**	**Error (%)**	**Model**
VM 7	110	Fe_3O_4 CuO	Citric Acid PAA 250kDa PAA 450kDa	Water	45	$\mu_{nf} = 64.348\emptyset + \frac{33.657}{T}$
VM 7	15	CuO	-	EG	10	$\mu_{nf} = 36.034\emptyset + \frac{462.569}{T}$

The most striking result that is displayed by Table 6.4 is probably the remarkable average percent errors of the constructed models. It is observed from the related table that most of the average errors are hardly below 5 percent. Moreover, the presence of equations with tremendously high average errors cannot be ignored. The great number of errors that the models reveal is mostly originated from the sensitivity of viscosity to the addition of nanoparticles, as well as to temperature. The empirical data had already shown that unlike density, viscosity is considerably affected by both of the variables, and this fact is also reflected on the constructed models. It is evident from the results that the assembling of different nanoparticle-base fluid systems into a single equation leads to an increase in the average absolute percent error. Models considering the viscosity of a single nanofluid system have relatively lower percent errors, while those in which multiple nanofluids are considered possess much higher percent errors. For instance, the comparison of the viscosity enhancements of copper oxide suspensions in water and ethylene glycol had already proven that the two of the base fluids were affected differently upon the addition of nanoparticles. It was stated that the relative viscosity enhancements observed with water were much greater than those observed with ethylene glycol at all temperatures, showing that water was relatively more sensitive to the addition of nanoparticles

than ethylene glycol. Consequently, the errors of the equations are relatively small when water and ethylene glycol-based copper oxide nanofluids are considered separately in diverse equations, however the percent error is increased when both groups are combined. Among all the models that have been constructed considering the different types of nanoparticles individually, there is one that attracts great attention because of its tremendous error that arises in each case, regardless of the type of model. As illustrated in Table 6.4, all the models in which citric acid coated superparamagnetic magnetite/water nanofluids are included, exhibit high absolute percent errors. The reason behind this high amount of error encountered with these nanofluids in each type of model is that they include highly concentrated and dilute samples all together. Thus, the concentration data that is used during the construction of relevant models comprise a relatively wide concentration range when compared to the rest of the samples. The case is not observed with any other system-specific model since the concentrations of the rest of the nanofluids were relatively closer to each other and they did not contain highly concentrated samples due to the drawbacks opposed by the synthesis and stability. Hence, the latter reveals another significant criterion that should be considered during the construction of the models; the concentration range of the nanofluids. As a result, this indicates that different models should be constructed for nanofluids with different concentration ranges, even when considering nanofluids of identical type.

In conclusion, empirical data on the viscosities of distinct types of nanofluids have revealed consistently in each case that, unlike density, viscosity is strongly affected by the addition of nanoparticles. Results have also shown that viscosity is not solely affected by the addition of nanoparticles, but each individual parameter, including the concentration range, possesses a huge role on the rheological behavior of nanofluids and this makes the estimation of their viscosity extremely difficult. Even if a common trend of increasing viscosity is observed upon increasing concentration in all cases, the relative enhancements in each nanofluid system were found to be distinct and unique. Hence, the augmentation in the percent errors of the models that is encountered when assembling different types of nanofluids, or nanofluids with different concentration ranges together, might be attributed to the fact that each nanofluids viscosity is affected differently and follows a genuine route with respect to changing concentration and

temperature. The models that are constructed by combining nanofluids with distinct properties therefore fail to predict their viscosities due to the genuine and unpredictable rheological behavior of nanofluids as well as their dependence on many parameters such as the type and size of nanoparticles, concentration of nanoparticles, type of surfactant and type of the base fluid. The results therefore point out that the construction of system-specific correlations tend to possess relatively lower percent errors and hence, they tend to be more reliable. Thus, when correlating the viscosities of nanofluids to their volume fractions or temperatures they should be considered as exclusive groups rather than combinations, in order to decrease the average percent errors and to increase the accuracies of the models.

Considering all the models that have been formulated by combining different types of nanoparticle-base fluid systems, the average absolute percent errors of all models evidently suggest that the construction of a generalized model that is able to predict the rheological behavior of any kind of nanofluid is quite difficult. By considering the related statistical analysis results (Figures B.13, B.31, B.49, B.67, B.85, B.101, B.117), the model that exhibits the best performance for estimating the viscosity of different types of nanofluids appears to be VM5, which presented an inconvenient average absolute error of 28 percent. However, this outcome is not applicable for processes in which precise data is necessary. Consequently, it is evident even with the limited amount of data that was considered in the scope of this study that the formation of a generalized model is not possible without complicated correlations.

6.3. THERMAL CONDUCTIVITY OF NANOFLUIDS

Thermal conductivity is one of the most essential thermophysical properties of a substance and is directly related to heat transfer. Since most solids possess much greater thermal conductivities than conventional heat transfer fluids, suspensions of small solid particles in these fluids are reasonably expected to increase the thermal conductivities, and in parallel, the related heat transfer capability. The extensive amount of studies on the investigation of the thermal conductivity of nanofluids however seems to be more complex and controversial when compared to density or viscosity. Although a vast majority of research that are presented in the

literature demonstrated enhancements in the thermal conductivity of base fluids, there are some results indicating deteriorations in the thermal conductivity of corresponding base fluids, upon addition of nanoparticles. Experimental measurements of different nanoparticle-base fluid systems have shown over the years that thermal conductivity does not present a similar trend that is observed in all cases, but it is rather unique for different systems. Thermal conductivity of a base fluid may enhance or deteriorate upon the addition of nanoparticles or upon increasing working temperature, depending on the nanoparticle-base fluid system. The following part of the study is focused on investigating the thermal conductivity of several nanoparticle-base fluid systems as a function of nanoparticle concentration and temperature. The nanofluids that are examined during this section of the study include citric acid coated superparamagnetic magnetite/water, silver/water. copper oxide/water and copper oxide/ethylene glycol nanofluids. Whereas the thermal conductivities of water and ethylene glycol-based copper oxide suspensions were measured experimentally, the thermal conductivities of magnetite/water and silver/water were taken from previous studies of Altan et. al. [104]

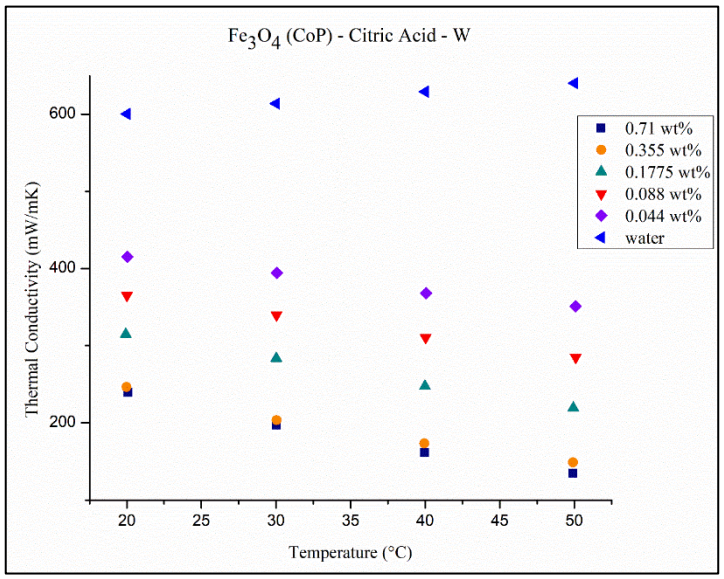

Figure 6.14. Influence of particle loading and temperature on the thermal conductivity of citric acid coated superparamagnetic magnetite/water nanofluids

In Figure 6.14 the thermal conductivity of citric acid coated superparamagnetic magnetite/water nanofluids are presented as a function of both concentration of nanoparticles and temperature. The results indicated that the addition of citric acid coated magnetite nanoparticles has induced a significant deterioration in the thermal conductivity of water. Moreover, the amount of deterioration in the thermal conductivity is increased with increasing concentration of nanoparticles. The percent deteriorations that are caused by the addition of magnetite nanoparticles are in the range of 31 and 60 percent, which is increasing with increasing concentration. at a constant temperature of 20°C. Furthermore, the increase in the deterioration of thermal conductivity increases with increasing temperature, resulting in a much greater deterioration at a higher temperature of 60°C. Most importantly, the nanofluids follow a different temperature dependency than that of the base fluid (water) as the thermal conductivity of water increases but of nanofluid decreases as with increasing temperature.

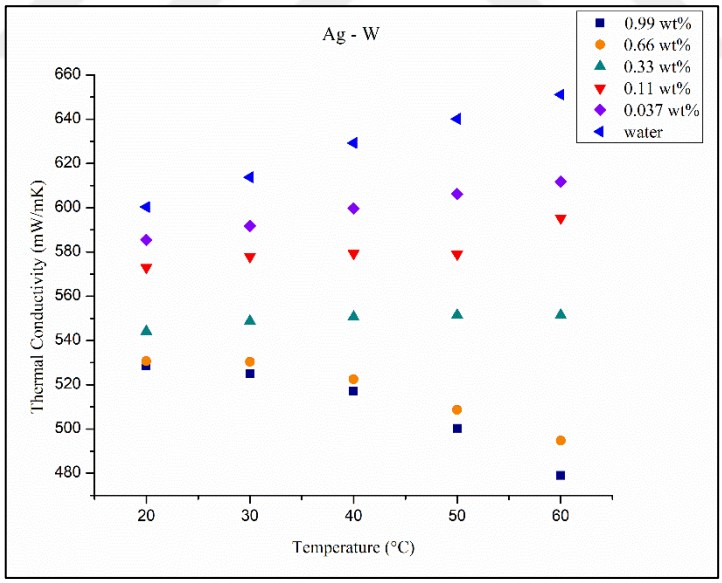

Figure 6.15. Influence of particle loading and temperature on the thermal conductivity of silver/water nanofluids

Figure 6.15 displays the thermal conductivity of silver/water nanofluids as a function of nanoparticle concentration and temperature. It is observed from Figure 6.15 that the thermal

conductivity of silver based aqueous nanofluids are less than that of water at all temperatures indicating that the addition of silver nanoparticles led to a reduction in the thermal conductivity of the base fluid. When examining the thermal conductivity trend at a constant temperature, with changing nanoparticle concentration, it is observed again that the increase in the nanoparticle loading leads to a further deterioration in the thermal conductivity. The percent deteriorations at a constant temperature of 20℃ were found to be 2.5, 5, 9, 11.6 and 11.9 percent, indicating an increasing trend upon increasing nanoparticle loading. The relative decrease in the thermal conductivity further increases with increasing temperature as the nanofluid exhibits a slightly different trend than that of water. Whereas nanofluids with relatively higher concentrations follow opposite trends with water, as a function of temperature, the trend of the nanofluid approaches to that of water as its concentration is decreased. When comparing magnetite and silver nanoparticle suspensions with similar weight percent's, it is observed that magnetite nanoparticles have led to a much greater deterioration in the thermal conductivity of water. This might be attributed to the effect of surfactant, as well as the effects arising by virtue of the quite different nature of nanoparticles.

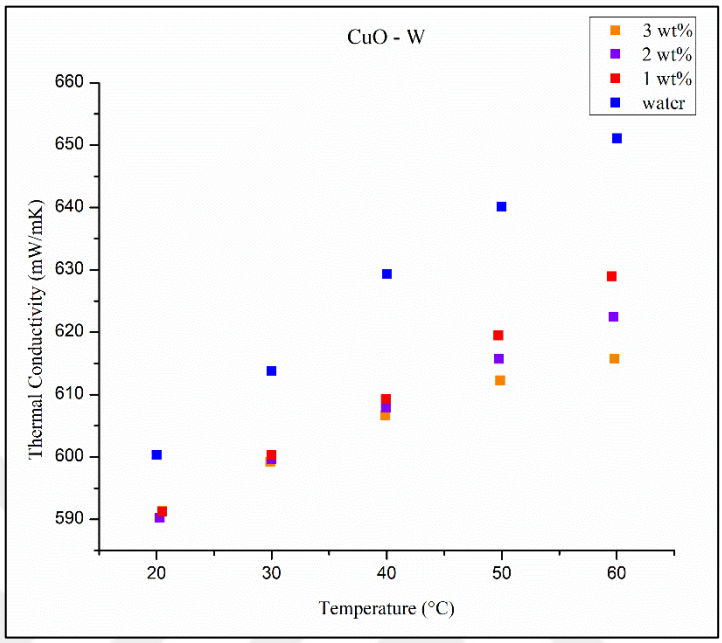

Figure 6.16. Influence of particle loading and temperature on the thermal conductivity of copper oxide/water nanofluids

The deterioration in the thermal conductivity of water with increasing particle loading is also observed in Figure 6.16 in which thermal conductivities of copper oxide/water nanofluids are displayed with respect to altering nanoparticle concentration and temperature. The thermal conductivities of all nanofluids are clearly less that of water at all conditions. The trend of copper oxide nanofluids is revealed to be a bit different from those of magnetite and silver nanofluids. Whereas the alterations emerging from different concentrations were more distinctly detectable in Figures 6.14 and 6.15 at all temperatures, it is observed from Figure 6.16 that the effect of concentration is explicitly revealed at relatively higher temperatures. Data points scattered around 60℃ show clearly that the increased particle loading has led to a further decrease in the thermal conductivity of water. The amount of deterioration in the thermal conductivity of the base fluid was found to be around 1.5 percent, at a constant temperature of 20℃, for all copper oxide/water nanofluids. Moreover, the maximum amount of deterioration which was found to be 5.4 percent, belongs obviously to the most concentrated nanofluid (3 wt. percent) and is observed at 60℃. The comparison of copper oxide/water nanofluids with the rest of water-based

suspensions indicate that much smaller reductions were obtained in the thermal conductivity of water by the addition of copper oxide nanoparticles as compared to magnetite and silver nanoparticles.

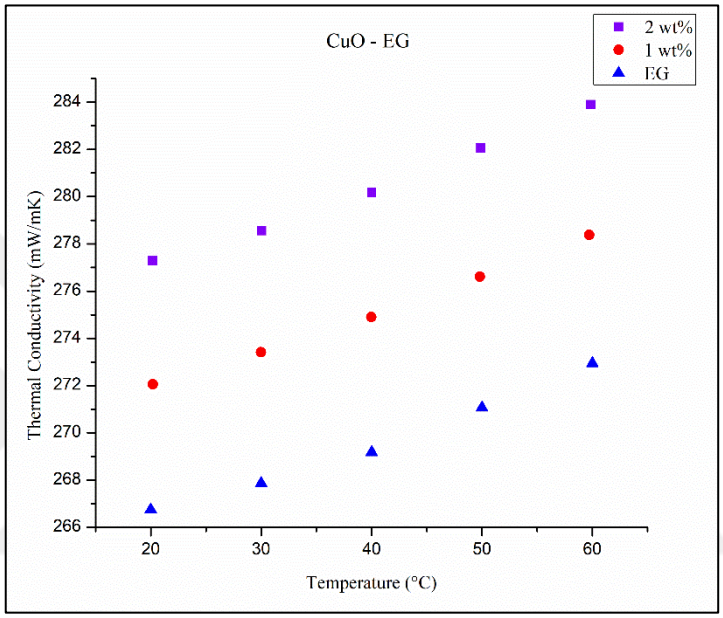

Figure 6.17. Influence of particle loading and temperature on the thermal conductivity of copper oxide/ethylene glycol nanofluids

In Figure 6.17 in which ethylene glycol-based copper oxide suspensions are considered, it is observed that in contrast to all water based nanofluids, the thermal conductivity of ethylene glycol is enhanced upon the addition of nanoparticles. Moreover, the increase in the particle loading has led to a further enhancement in the thermal conductivity of the base fluid. The percent enhancements associated with 1 and 2 weight percent copper oxide/ethylene glycol nanofluids were found to be 2 and 4 percent, respectively. Figure 6.17 as a result serves to demonstrate one more time that the effect of nanoparticles over the base fluid thermal conductivity is rather unpredictable. Hence, the thermal conductivity of a base fluid may enhance or deteriorate upon the addition of nanoparticles, depending on the nanoparticle-base fluid system that is being considered.

Considering the empirical data that has been collected via measurement of thermal conductivities of distinct nanoparticle-base fluid systems, the possibility of forming an empirical model to predict the nanofluid thermal conductivity was investigated. The base models that were chosen for the estimation of the thermal conductivity of nanofluids are listed in Table 6.5.

Table 6.5. Skeletal forms of the chosen models for the thermal conductivity of nanofluids

Model number	**Correlation form**
TM 1	$\frac{k_{nf}}{k_{bf}} = A + BT + CT^2$
TM 2	$\frac{k_{nf}}{k_{bf}} = 1 + A\emptyset + BT\emptyset$
TM 3	$\frac{k_{nf}}{k_{bf}} = 1 + B\emptyset^C T^D$
TM 4	$\frac{k_{nf}}{k_{bf}} = A + B\emptyset$
TM 5	$\frac{k_{nf}}{k_{bf}} = Ae^{B\emptyset + CT}$
TM 6	$\frac{k_{nf}}{k_{bf}} = Ae^{B\emptyset^C + DT}$

In all models that are presented in Table 6.5, T is the nanofluid temperature in degrees Celsius (°C) and $\emptyset$ is the concentration of nanoparticles in weight percent. It should be noted that TM 1 and TM 4 account only for the effects of temperature or concentration respectively, whereas the rest of the models consider the effects of nanoparticle concentration and temperature together.

In order to construct the desired types of models, the thermal conductivity data of the nanofluids which were measured with respect to both varying nanoparticle concentration and temperature were used as input along with the selected type of equation. Consequently, the empirical data were computed through non-linear regression and the equation parameters were obtained for

each model. The average absolute percent errors of the models were calculated based on residuals. Moreover, the process was repeated by considering different data groups, in order to see the effect of assembling different types of nanofluids on the estimation capabilities and accuracies of the models. The resulting models correlating the thermal conductivities of different nanofluids to their concentration and temperature are presented in Table 6.6. The statistical analysis graphs associated with each thermal conductivity correlation presented in Table 6.6 are given in Appendix C (Figures C.1-C.66).

Table 6.6. Empirical correlations for the estimation of nanofluid thermal conductivities

Model no	**Obs no**	**Np type**	**Surfactant**	**Base fluid**	**Error (%)**	**Model**
TM 1	15	CuO	-	Water	0.3	$\frac{k_{nf}}{k_{bf}} = 1.0082 - 1.296x10^{-3}T + 7.045x10^{-6}T^2$
TM 1	25	Ag	-	Water	5.7	$\frac{k_{nf}}{k_{bf}} = 0.96 - 1.896x10^{-3}T - 2.254x10^{-6}T^2$
TM 1	20	Fe_3O_4	Citric Acid	Water	28	$\frac{k_{nf}}{k_{bf}} = 0.698 - 9.653x10^{-3}T + 5.63x10^{-5}T^2$
TM 1	60	CuO Ag Fe_3O_4	Citric acid	Water	42	$\frac{k_{nf}}{k_{bf}} = 1.145 - 0.0233T + 3.044x10^{-4}T^2$
TM 1	10	CuO	-	EG	1	$\frac{k_{nf}}{k_{bf}} = 1.027 + 2.015x10^{-4}T - 2.39x10^{-6}T^2$

Table 6.6. Empirical correlations for the estimation of nanofluid thermal conductivities (Continued)

Model no	Obs no	Np type	Surfactant	Base fluid	Error (%)	Model
TM 1	25	CuO	-	Water EG	3	$\frac{k_{nf}}{k_{bf}} = 1.017 - 7.88x10^{-4}T + 4.45x10^{-6}T^2$
TM 2	15	CuO	-	Water	0.8	$\frac{k_{nf}}{k_{bf}} = 1 + 1.35x10^{-4}\emptyset - 3.486x10^{-4}T\emptyset$
TM 2	25	Ag	-	Water	4.5	$\frac{k_{nf}}{k_{bf}} = 1 - 0.061\emptyset - 4.133x10^{-3}T\emptyset$
TM 2	20	Fe_3O_4	Citric Acid	Water	74	$\frac{k_{nf}}{k_{bf}} = 1 - 0.908\emptyset - 0.013T\emptyset$
TM 2	60	CuO Ag Fe_3O_4	Citric acid	Water	58	$\frac{k_{nf}}{k_{bf}} = 1 - 0.083\emptyset - 1.073x10^{-4}T\emptyset$
TM 2	10	CuO	-	EG	0.04	$\frac{k_{nf}}{k_{bf}} = 1 + 0.0199\emptyset + 7.378x10^{-6}T\emptyset$
TM 2	25	CuO	-	Water EG	2.8	$\frac{k_{nf}}{k_{bf}} = 1 + 5.28x10^{-3}\emptyset - 2.54x10^{-4}T\emptyset$

Table 6.6. Empirical correlations for the estimation of nanofluid thermal conductivities (Continued)

Model no	Obs no	Np type	Surfactant	Base fluid	Error (%)	Model
TM 3	15	CuO	-	Water	0.2	$\frac{k_{nf}}{k_{bf}} = 1 - 8.14x10^{-4}\emptyset^{0.261}T^{0.943}$
TM 3	20	Fe_3O_4	Citric Acid	Water	8	$\frac{k_{nf}}{k_{bf}} = 1 - 0.247\emptyset^{0.210}T^{0.332}$
TM 3	35	CuO Fe_3O_4	Citric acid	Water	49	$\frac{k_{nf}}{k_{bf}} = 1 - 0.144\emptyset^{-0.247}T^{0.177}$
TM 3	10	CuO	-	EG	0.04	$\frac{k_{nf}}{k_{bf}} = 1 + 0.019\emptyset^{0.974}T^{0.018}$
TM 3	25	CuO	-	Water EG	2.4	$\frac{k_{nf}}{k_{bf}} = 1 - 1.78x10^{-11}\emptyset^{15.548}T^{1.164}$
TM 4	3	CuO	-	Water	0.08	$\frac{k_{nf}}{k_{bf}} = 0.984 + 1.117x10^{-4}\emptyset$
TM 4	5	Ag	-	Water	1.6	$\frac{k_{nf}}{k_{bf}} = 0.962 - 0.097\emptyset$
TM 4	5	Fe_3O_4	Citric Acid	Water	10	$\frac{k_{nf}}{k_{bf}} = 0.637 - 0.402\emptyset$
TM 4	13	CuO Ag Fe_3O_4	Citric acid	Water	27	$\frac{k_{nf}}{k_{bf}} = 0.708 - 0.104\emptyset$
TM 4	5	CuO	-	Water EG	2	$\frac{k_{nf}}{k_{bf}} = 1.014 - 6.14x10^{-3}\emptyset$

Table 6.6. Empirical correlations for the estimation of nanofluid thermal conductivities (Continued)

Model no	Obs no	Np type	Surfactant	Base fluid	Error (%)	Model
TM 5	15	CuO	-	Water	0.3	$\frac{k_{nf}}{k_{bf}} = 1.006e^{-0.00378\emptyset - 7.55x10^{-4}T}$
TM 5	25	Ag	-	Water	2.2	$\frac{k_{nf}}{k_{bf}} = 1.034e^{-0.170\emptyset - 2.28x10^{-3}T}$
TM 5	20	Fe_3O_4	Citric Acid	Water	12	$\frac{k_{nf}}{k_{bf}} = 0.896e^{-1.275\emptyset - 0.012T}$
TM 5	60	CuO Ag Fe_3O_4	Citric acid	Water	38	$\frac{k_{nf}}{k_{bf}} = 0.679e^{0.135\emptyset - 1.36x10^{-4}T}$
TM 5	10	CuO	-	EG	0.04	$\frac{k_{nf}}{k_{bf}} = 1.001e^{0.019\emptyset + 8.65x10^{-6}T}$
TM 5	25	CuO	-	Water EG	2.7	$\frac{k_{nf}}{k_{bf}} = 1.033e^{-0.012\emptyset - 4.31x10^{-4}T}$
TM 6	15	CuO	-	Water	0.3	$\frac{k_{nf}}{k_{bf}} = 0.810e^{0.213\emptyset^{-0.032} - 7.55x10^{-4}T}$

Table 6.6. Empirical correlations for the estimation of nanofluid thermal conductivities (Continued)

Model no	Obs no	Np type	Surfactant	Base fluid	Error (%)	Model
TM 6	25	Ag	-	Water	1.7	$\frac{k_{nf}}{k_{bf}} = 1.141e^{-0.253\emptyset^{0.330}-2.28x10^{-3}T}$
TM 6	60	CuO Ag Fe_3O_4	Citric acid	Water	38	$\frac{k_{nf}}{k_{bf}} = 0.685e^{0.117\emptyset^{1.119}-1.21x10^{-4}T}$
TM 6	10	CuO	-	EG	0.04	$\frac{k_{nf}}{k_{bf}} = 0.958e^{0.063\emptyset^{0.385}+8.65x10^{-6}T}$
TM 6	25	CuO	-	Water EG	2.7	$\frac{k_{nf}}{k_{bf}} = 0.463e^{0.789\emptyset^{-0.021}-4.32x10^{-4}T}$

It is observed from Table 6.6 that most of the models that correlate the relative thermal conductivities of nanofluids to nanoparticle concentration and temperature exhibit reasonably acceptable amount of percent errors when compared to viscosity models. Most of the models that are constructed considering a single type of nanoparticle-base fluid system has resulted in errors less than 5 percent, except for models that consider citric acid coated magnetite nanofluids. Regarding the percent errors of the models that have been constructed considering a single nanoparticle-base fluid system, it is observed that citric acid coated nanoparticles are the only class that led to a maximum amount of error. The considerable amount of errors that are aroused by citric acid coated nanoparticles may again be attributed to the presence of both highly concentrated and relatively dilute samples. Additionally, the experimental results had shown that the magnetic nanofluid with the lowest concentration caused a 31 percent

deterioration in the thermal conductivity of water, whereas the deteriorations caused by the most concentrated silver and copper oxide nanofluids were found to be 11.9 and 1.5 percent, respectively. at a constant temperature of 20℃. The tremendous difference between the thermal conductivity alterations of nanofluids were naturally reflected on the errors of the models. According to the statistical analysis results of the models that consider different types of nanofluids together, all the data points are randomly scattered and mostly not even close to the 45º line. The increase in the percent errors of the models that consider different types of nanofluids was expected as it was also observed in density and viscosity. As a consequence, the assembly of different types of nanoparticles again lead to relatively inadequate and inaccurate models. Hence, for the estimation of the thermal conductivity of nanofluids, system-specific models should be preferred. It is observed from Table 6.6 that the percent errors of the system specific modes that are designed considering only silver/water and copper/oxide nanofluids bear acceptable amount of errors. As for magnetite nanofluids, the construction of different models for different concentration ranges may improve the errors of the estimations. Although the assemble of different types of nanoparticles suspended in the same base fluid results in poor estimations, considering the same type of nanoparticles suspended in different types of base fluids also cause enhanced errors. By considering the models which are designed by the combination of data measured for copper oxide nanoparticles in water and ethylene glycol, it is observed in each case that the percent errors are fairly acceptable as the corresponding percent absolute errors were around 2-3 percent. However, the obtained percent error that seems fairly acceptable is probably as a consequence of relatively low alterations in the thermal conductivities of copper oxide nanofluids and not because of the accuracy of the models. The failure of the models in estimating the expected values can also be observed by considering the related statistical analysis figures that are presented in Appendix C (Figures C.1-C.66). Despite the low percent errors of the models. the related figures expose that the estimated data points are randomly scattered and are mostly far away from the 45º line. Additionally, the addition of copper oxide nanoparticles has revealed opposite effects on different base fluids (deteriorated the thermal conductivity of water and enhanced the thermal conductivity of ethylene glycol), thus the failure of the corresponding models were obviously an expected outcome.

The resulting model parameters that are presented in Table 6.6 in addition reveal that the effect of concentration should be taken into account in conjunction with temperature. When analyzing the statistical graphs that belong to TM 1, in which the effect of temperature is considered only, it can be observed again that most of the data points are far from the 45ºline, meaning that the related model fails at estimating the expected values. The statistical analysis results that belong to TM4 on the other hand, reveal that considering the effect of nanoparticle concentration alone is not effective. However, the models that consider both the effect of temperature and concentration yield relatively lower absolute percent errors for unique nanoparticle-base fluid systems. The average percent errors and analysis results of the models that include the effects of both nanoparticle concentration and temperature indicate that they are more successful in estimating the expected values. The latter can be observed from the promising results of TM2, TM3, TM5 and TM6 in which both effects are considered.

In conclusion, models that are constructed by the aim of estimating the thermal conductivity of nanofluids have been found to be more promising than those constructed for their viscosity estimation. The analysis of the results indicates that the effects of both nanoparticle concentration and temperature should be considered in order to obtain better predictions and enhance the accuracy of the models. The resulting percent errors of the models however, drastically increased when different types of nanoparticle-base fluid systems were assembled in a single model. This was expected as the alterations induced by different types of nanofluids have been found to be dissimilar. Thus. the design of a model that can estimate the thermal conductivity of all nanofluids, regardless of their type and unique properties, appears to be impossible which is exactly apparent even with the quite limited data measured and used during this study for the formation of empirical models. The results however indicated that the construction of system-specific models have the possibility to exhibit relatively better estimations. The latter was strongly observed with system specific models that were constructed for silver and copper oxide nanofluids. However, citric acid coated magnetite nanofluids had shown that the construction of system-specific models might not always result in successful models especially for extended range of concentrations. The excessive percent errors of the system-specific models that were constructed considering magnetite nanofluids were attributed

to the gathering of nanofluids with quite different concentrations. Hence, the design of separate correlations considering different concentration ranges can be proposed to overcome the relevant complication.

In conclusion, among all the models that have been constructed by assembling different types of nanofluids together, TM4 with an average absolute error of 27 percent was found to exhibit the least amount of error. However, regarding the related statistical analysis result (Figure C.41) it was observed that the relatively low amount of error associated with TM4 is not originated from the accuracy of the model but from the relatively less amount of data included during its construction, as it considers the effect of concentration only. The related statistical analysis results (Figures C.7, C.19, C.29, C.41, C.51, C.61) furthermore revealed that none of the models present an adequate performance for estimating the thermal conductivity of an extended range of nanofluids. Hence, the formation of an accurate, precise and a generalized model appears to be complicated.

7.CONCLUSION

Nanofluids are colloidal suspensions of ultrafine particles in the size range of 1-100 nm in convenient carrier fluids which have been shown to exhibit extraordinary properties by virtue of their exceedingly small sizes. One of the most frequently discussed implementations of these newly engineered fluids is their potential usage in applications involving heat transfer. The enhancements in the thermophysical properties of conventional heat transfer fluids (i.e. water and ethylene glycol) by the addition of nanoparticles and accordingly the possibility of obtaining advanced heat transfer performance, made nanofluids to be referred as new generation heat transfer fluids. The usage of these innovative fluids in practical applications requires however a deep investigation of their properties. Among all, thermophysical properties such as density, viscosity and thermal conductivity are the most essential ones that should be investigated as those strongly affect the heat transfer performance of a fluid. Therefore, the thermophysical properties of nanofluids have been investigated by numerous researchers and the results have revealed that the thermophysical properties of conventional fluids are strongly affected by the addition of nanoparticles. This alteration is actually found to depend considerably on various parameters such as the type, size and concentration of the nanoparticles, the type of surfactant used for obtaining colloidal stabilization and inherently the type of the base fluid.

Furthermore, it is known that thermophysical properties of nanofluids are not described by classical theories as they are not conventional suspensions. However, the estimation of their thermophysical properties are requisites for evaluating their effect over the heat transfer performance. Although, there exist several models to estimate system specific thermophysical properties of nanofluids, generalized empirical correlations which are capable of predicting the required thermophysical properties of a broad range of nanofluids are not available where direct measurement is not applicable or possible.

Consequently, the initial aim of this study was to investigate the thermophysical properties of various nanofluids via direct measurement techniques. In order to account for the effects of different parameters, various types of nanoparticle-base fluid systems were synthesized and corresponding thermophysical properties were measured with respect to both changing particle loading and temperature. Another purpose of this study was to formulate generalized empirical correlations for the density, viscosity and thermal conductivity of nanofluids with altering temperature and particle concentration by using the collected empirical data.

First of all, the density measurements of nanofluids have shown a common trend of enhancement upon addition of nanoparticles which was found to increase with the concentration of nanoparticles and decrease with temperature. Although, the density enhancements were more pronounced for nanofluids that possess relatively high concentrations, dilute systems were shown to be almost unaffected. The formulation of estimation models for the density of nanofluids illustrated that the average absolute percent error of the models was generally under 1 percent, regardless of the nanofluid system that was considered. However, the errors of the models were relatively increased when different groups of nanofluids were combined. The extremely low percent errors associated with the density models were attributed to the exceedingly small alterations in density as result of low concentrations of nanofluids used in the scope of this work. Eventually, it is proposed to assume the base fluid properties where relatively low concentration of nanofluids are used for applications. Nevertheless, if the application requires accuracy and precision then the best feasible options are to use one of the proposed empirical correlations especially in the form of DM 2 due to its simplicity to estimate if not possible to measure the density of the nanofluid directly. It is also necessary to note that the relevant results are only valid for extremely low concentrations of nanoparticles and most probably subjected to change at higher concentrations.

On the other hand, viscosity measurements of synthesized nanofluids have revealed a significant increase in the viscosity of the base fluid by the addition of nanoparticles and a considerable decrease with increasing temperature. Experimental measurements of various types of nanoparticle-base fluid systems revealed that unlike density, viscosity is drastically affected by

the addition of nanoparticles, even at extremely low nanoparticle loadings. Although a common trend of increasing viscosity was observed with increasing nanoparticle concentration for all nanofluids, the relative viscosity enhancement of each nanofluid system was found to be unique. The tremendous alterations in the viscosity of the base fluids were inherently reflected on the results of the models. Hence, the percent errors were highly augmented when different types of nanofluids were considered together. Viscosity models have in addition shown that not only the assembling of different types of nanofluids leads to augmented errors, but the assembling of nanofluids with different concentrations also cause a significant increase in the percent absolute error of the model. Hence, it was concluded that each nanofluid' viscosity is affected differently and follows a genuine route with both altering concentration and temperature. The failure of the viscosity models was attributed to the genuine and unpredictable rheological behavior of nanofluids as a consequence of numerous parameters such as the type and size of nanoparticles, concentration of nanofluid, the type of surfactant and the type of the base fluid. To sum up, results illustrated that it is almost impossible to construct a model that is successful in predicting the expected values as viscosity is highly affected by all variables, especially by the concentration of nanoparticles and temperature. In order to enhance the estimation capabilities of the resulting models, the formulation of system specific as well as concentration range specific models could be proposed. It is therefore proposed to directly measure the viscosities of nanofluids that will be used in heat transfer applications, to obtain the most reliable results.

Thermal conductivity measurements of distinct nanofluids have revealed that the addition of nanoparticles has a significant effect over the thermal conductivity of the corresponding base fluids. The results indicated that the thermal conductivity of nanofluids does not have a common trend, but it may exhibit an increasing or decreasing trend upon the addition of nanoparticles, as well as by increasing temperature.

Whereas thermal conductivity of water was deteriorated upon the addition of nanoparticles, regardless of the nanoparticle type, that of ethylene glycol was enhanced by the addition of copper oxide nanoparticles. Moreover, the assembling of different types of nanofluids in a single equation resulted again in an augmentation in the percent errors of the models, as expected. This

fact was attributed to the genuine alterations caused by different types of nanofluids. The fact that the thermal conductivity followed an unpredictable route with respect to variable concentration and temperature, expectedly led to the inaccuracy of the related empirical models. On the other hand, correlations that were designed considering a single type of nanoparticle-base fluid systems presented promising results as shown by related absolute percent errors. Furthermore, as in the case of viscosity, the grouping of different nanofluids with various concentrations exhibited models with high errors, as thermal conductivity was found to be highly sensitive to the addition of nanoparticles. Hence, in order to enhance the accuracy of the empirical models, the generation of system specific and concentration range specific models which include the effects of both concentration and temperature could be proposed. The design of a model that can estimate the thermal conductivity of all nanofluids however, appears to be impossible since each nanoparticle-base fluid system alters the thermal conductivity of the base fluid differently. Although the outcomes of system specific models have been found to be promising especially for dilute nanofluid systems, the direct measurement of thermal conductivity is suggested for more precise and accurate results.

In conclusion, when considering nanofluids in heat transfer applications, it is proposed that the density of the base fluid can be used in the related calculations, as the effect of nanoparticles over the density of base fluids was found to be almost negligible for dilute cases. However. neither viscosity nor the thermal conductivity of the base fluid can be used in relevant calculations as they are both significantly affected by the addition of nanoparticles, as well as by the nature of the constituents of nanofluids. Although system specific correlations have shown promising estimation capabilities, results certainly indicate that the design of a generalized correlation that can estimate the viscosity or the thermal conductivity of all types of nanofluids is extremely difficult and possibly requires complicated approaches. Hence, in order to avoid significant errors and to evaluate the accurate heat transfer performance of a system, viscosity or the thermal conductivity of nanofluids should be measured prior to use.

As a future work, the enormous amount of data that is present in the literature may be collected and tested with relatively more complex models by considering additional variables such as the

size or even the morphology of nanoparticles in order to completely evaluate the possibility of generating system specific or generalized correlations for the estimation of thermophysical properties.

REFERENCES

1. Thermal Conductivity of Materials and Chemical Elements [cited 2021 Apr 23]. Available from: https://www.nuclear-power.net/nuclear-engineering/heat-transfer/thermal-conduction/thermal-conductivity/thermal-conductivity-of-materials-and-chemical-elements/

2. Das SK, Choi SUS, Patel HE. Heat transfer in nanofluids - A review. *Heat Transfer Engineering*. 2006;27(10):3–19.

3. Choi SUS, Eastman JA. Enhancing Thermal Conductivity of Fluids with Nanoparticles. *ASME International Mechanical Engineering Congress & Exposition*. 1995.

4. Sivashanmugam P. Application of Nanofluids in Heat Transfer. An Overview of Heat *Transfer Phenomena*. 2012;

5. Chandrasekar M, Suresh S, Chandra Bose A. Experimental investigations and theoretical determination of thermal conductivity and viscosity of Al2O3/water nanofluid. *Experimental Thermal and Fluid Science*. 2009;34(2):210–6.

6. Garg J, Poudel B, Chiesa M, Gordon JB, Ma JJ, Wang JB, et al. Enhanced thermal conductivity and viscosity of copper nanoparticles in ethylene glycol nanofluid. *Journal of Applied Physics*. 2008;103(7).

7. Duangthongsuk W, Wongwises S. Measurement of temperature-dependent thermal conductivity and viscosity of TiO2-water nanofluids. *Experimental Thermal and Fluid Science*. 2009;33(4):706–14.

8. Mahian O, Kianifar A, Wongwises S. Dispersion of ZnO Nanoparticles in a Mixture of Ethylene Glycol-Water, Exploration of Temperature-Dependent Density, and Sensitivity Analysis. *Journal of Cluster Science*. 2013;24(4):1103–14.

9. Pastoriza-Gallego MJ, Casanova C, Páramo R, Barbés B, Legido JL, Piñeiro MM. A study on stability and thermophysical properties (density and viscosity) of Al2 O3 in water nanofluid. *Journal of Applied Physics*. 2009;106(6).

10. Li Z, Asadi S, Karimipour A, Abdollahi A, Tlili I. Experimental study of temperature and mass fraction effects on thermal conductivity and dynamic viscosity of SiO2-oleic acid/liquid paraffin nanofluid. *International Communications in Heat and Mass Transfer*. 2020;110.

11. Banisharif A, Aghajani M, van Vaerenbergh S, Estellé P, Rashidi A. Thermophysical properties of water ethylene glycol (WEG) mixture-based Fe3O4 nanofluids at low concentration and temperature. *Journal of Molecular Liquids*. 2020;302:112606.

12. P. Keblinski a,*,1, S.R. Phillpot b, S.U.S. Choi c,* JAE b. Mechanisms of heat fow in suspensions of nano-sized particles (nanofuids). *International Journal of Heat and Mass Transfer*. 2002;2:1411–4.

13. Kleinstreuer C, Feng Y. Experimental and theoretical studies of nanofluid thermal conductivity enhancement: a review. *Nanoscale Research Letters*. 2011;6(1):1–13.

14. Yu W, Choi SUS. The role of interfacial layers in the enhanced thermal conductivity of nanofluids: A renovated Hamilton-Crosser model. *Journal of Nanoparticle Research*. 2004;6(4):355–61.

15. Rudyak VY, Minakov A v. Thermophysical properties of nanofluids. *European Physical Journal E*. 2018;41(1):1–12.

16. Eastman JA, Phillpot SR, Choi SUS, Keblinski P. Thermal Transport in Nanofluids. *Annual Review of Materials Research*. 2004;34(1):219–46.

17. Evans W, Prasher R, Fish J, Meakin P, Phelan P, Keblinski P. Effect of aggregation and interfacial thermal resistance on thermal conductivity of nanocomposites and colloidal nanofluids. *International Journal of Heat and Mass Transfer*. 2008;51:1431–8.

18. Keblinski P, Prasher R, Eapen J. Thermal conductance of nanofluids: Is the controversy over? *Journal of Nanoparticle Research*. 2008;10(7):1089–97.

19. Philip J, Shima PD, Raj B. Enhancement of thermal conductivity in magnetite based nanofluid due to chainlike structures. *Applied Physics Letters*. 2007;91(20):2005–8.

20. Philip J, Shima PD. Thermal properties of nanofluids. *Advances in Colloid and Interface Science.* 2012;183–184:30–45.

21. Vajjha RS, Das DK. A review and analysis on influence of temperature and concentration of nanofluids on thermophysical properties, heat transfer and pumping power. International Journal of Heat and Mass Transfer [Internet]. 2012;55(15–16):4063–78.

22. Pryazhnikov MI, Minakov A v., Rudyak VY, Guzei D v. Thermal conductivity measurements of nanofluids. *International Journal of Heat and Mass Transfer*. 2017;104:1275–82.

23. Mahbubul IM, Saidur R, Amalina MA. Latest developments on the viscosity of nanofluids. *International Journal of Heat and Mass Transfer*. 2012;55(4):874–85.

24. What are Nanoparticles? Definition, Size, Uses and Properties - TWI. [cited 2021 Apr 21]. Available from: https://www.twi-global.com/technical-knowledge/faqs/what-are-nanoparticles

25. nanoparticle | Definition, Size Range, & Applications | Britannica [Internet]. [cited 2021 Apr 21]. Available from: https://www.britannica.com/science/nanoparticle#ref288108

26. Khan I, Saeed K, Khan I. Nanoparticles: Properties, applications and toxicities. Arabian *Journal of Chemistry*. 2019;12(7):908–31.

27. Guo D, Xie G, Luo J. Mechanical properties of nanoparticles: Basics and applications. *Journal of Physics D: Applied Physics*. 2014;47(1).

28. Singh AK, Raykar VS. Microwave synthesis of silver nanofluids with polyvinylpyrrolidone (PVP) and their transport properties. *Colloid and Polymer Science*. 2008;286(14–15):1667–73.

29. Alqadi MK, Abo Noqtah OA, Alzoubi FY, Alzouby J, Aljarrah K. PH effect on the aggregation of silver nanoparticles synthesized by chemical reduction. *Materials Science- Poland*. 2014;32(1):107–11.

30. Borgohain K, Singh J. Quantum size effects in CuO nanoparticles. *Physical Review B - Condensed Matter and Materials Physics*. 2000;61(16):11093–6.

31. Quantum size effects | Article about quantum size effects by The Free Dictionary. [cited 2021 Apr 21]. Available from: https://encyclopedia2.thefreedictionary.com/quantum+size+effects

32. Lin S, Bai G, Liu Z, Xu Z, Hu Z. Photonics and Optoelectronics of Low-Dimensional Materials. *Advances in Condensed Matter Physics*. 2018 Jan 1;2018.

33. Ramos M, Ortiz-Jordan L, Hurtado-Macias A, Flores S, Elizalde-Galindo JT, Rocha C, et al. Hardness and elastic modulus on six-fold symmetry gold nanoparticles. *Materials.* 2013;6(1):198–205.

34. Buffat P, Borel JP. Size effect on the melting temperature of gold particles. *Physical Review A*. 1976;13(6):2287–98.

35. Akbari M, Afrand M, Arshi A, Karimipour A. An experimental study on rheological behavior of ethylene glycol based nanofluid: Proposing a new correlation as a function of silica concentration and temperature. *Journal of Molecular Liquids* [Internet]. 2017;233:352–7. Available from: http://dx.doi.org/10.1016/j.molliq.2017.03.020

36. Ashik UPM, Kudo S, Hayashi J. An Overview of Metal Oxide Nanostructures. Synthesis of Inorganic Nanomaterials. *Elsevier Ltd*.; 2018. 19–57.

37. Yu W, Xie H. A review on nanofluids: Preparation, stability mechanisms, and applications. *Journal of Nanomaterials*. 2012;2012.

38. Yuan Y, Rende D, Altan CL, Bucak S, Ozisik R, Borca-Tasciuc DA. Effect of surface modification on magnetization of iron oxide nanoparticle colloids. *Langmuir*. 2012;28(36):13051–9.

39. Ilyas SU, Pendyala R, Marneni N. Stability of Nanofluids. *Topics in Mining, Metallurgy and Materials Engineering*. 2017. 1–31.

40. Sezer N, Atieh MA, Koç M. A comprehensive review on synthesis, stability, thermophysical properties, and characterization of nanofluids. *Powder Technology*. 2019;344:404–31.

41. Ruan B, Jacobi AM. Ultrasonication effects on thermal and rheological properties of carbon nanotube suspensions. *Nanoscale Research Letters*. 2012;7:1–14.

42. The I, Of E, Volume N, The C. Chapter – 3 Preparation and Estimation of Nanofluid Properties 3.1 Introduction. C(1998):24–58.

43. Salavati-Niasari M, Davar F, Mir N. Synthesis and characterization of metallic copper nanoparticles via thermal decomposition. *Polyhedron*. 2008;27(17):3514–8.

44. Simeonidis K, Mourdikoudis S, Moulla M, Tsiaoussis I, Martinez-Boubeta C, Angelakeris M, et al. Controlled synthesis and phase characterization of Fe-based nanoparticles obtained by thermal decomposition. *Journal of Magnetism and Magnetic Materials*. 2007;316(2 SPEC. ISS.):2–5.

45. Ealias AM, Saravanakumar MP. A review on the classification, characterisation, synthesis of nanoparticles and their application. *IOP Conference Series: Materials Science and Engineering*. 2017;263(3).

46. Ijaz I, Gilani E, Nazir A, Bukhari A. Detail review on chemical, physical and green synthesis, classification, characterizations and applications of nanoparticles. *Green Chemistry Letters and Reviews*. 2020;13(3):59–81.

47. Altan CL, Gurten B, Sommerdijk NAJM, Bucak S. Deterioration in effective thermal conductivity of aqueous magnetic nanofluids. *Journal of Applied Physics*. 2014;116(22).

48. Byrappa K, Adschiri T. Hydrothermal technology for nanotechnology. Progress in Crystal Growth and Characterization of Materials. 2007;53(2):117–66.

49. Nam NH, Luong NH. Nanoparticles: Synthesis and applications. Materials for Biomedical Engineering: Inorganic Micro- and Nanostructures. *Elsevier Inc*.; 2019. 211–240.

50. Hydrothermal Synthesis Method For Nanoparticle - antsLAB. [cited 2021 Apr 21]. Available from: https://www.antslab.in/hydrothermal-synthesis-method/

51. Singh RN, Madhu, Awasthi R. Alcohol Fuel Cells. In: New and Future Developments in Catalysis: Batteries, Hydrogen Storage and Fuel Cells. *Elsevier B.V.*; 2013. p. 453–78.

52. Lu AH, Salabas EL, Schüth F. Magnetic nanoparticles: Synthesis, protection, functionalization, and application. *Angewandte Chemie - International Edition*. 2007;46(8):1222–44.

53. Liu S, Ma C, Ma MG, Xu F. Magnetic nanocomposite adsorbents. Composite Nanoadsorbents. *Elsevier Inc.*; 2018. 295–316.

54. Dembski S, Schneider C, Christ B, Retter M. Core-shell nanoparticles and their use for in vitro and in vivo diagnostics. Core-Shell Nanostructures for Drug Delivery and Theranostics. Elsevier Ltd; 2018. 119–141.

55. Varanda LC, De Souza CGS, Perecin CJ, De Moraes DA, De Queiróz DF, Neves HR, et al. Inorganic and organic-inorganic composite nanoparticles with potential biomedical applications: Synthesis challenges for enhanced performance. Materials for Biomedical Engineering: Bioactive Materials, Properties, and Applications. 2019. 47–99.

56. Prasad S, Kumar V, Kirubanandam S, Barhoum A. Engineered nanomaterials: Nanofabrication and surface functionalization. Emerging Applications of Nanoparticles and Architectural Nanostructures: Current Prospects and Future Trends. *Elsevier Inc.*; 2018. 305–340.

57. Rappole JH. 1. Introduction. The Avian Migrant. 2016;1–24.

58. Wong K V., De Leon O. Applications of nanofluids: Current and future. *Advances in Mechanical Engineering*. 2010;2010.

59. Laurent S, Forge D, Port M, Roch A, Robic C, Vander Elst L, et al. Magnetic iron oxide nanoparticles: Synthesis, stabilization, vectorization, physicochemical characterizations and biological applications. *Chemical Reviews*. 2008;108(6):2064–110.

60. Singh D, Mehta B, Asfer M. Investigations on Convective Heat Transfer of Ferrofluids for the Application of Cooling of Photovoltaic Systems. *Journal of Energy and Environmental Sustainability*. 2017;4(February):45–51.

61. Duangthongsuk W, Wongwises S. Effect of thermophysical properties models on the predicting of the convective heat transfer coefficient for low concentration nanofluid. *International Communications in Heat and Mass Transfer*. 2008;35(10):1320–6.

62. Yu W, France DM, Routbort JL, Choi SUS. Review and comparison of nanofluid thermal conductivity and heat transfer enhancements. *Heat Transfer Engineering*. 2008;29(5):432–60.

63. Eastman JA, Choi SUS, Li S, Yu W, Thompson LJ. Anomalously increased effective thermal conductivities of ethylene glycol-based nanofluids containing copper nanoparticles. *Applied Physics Letters*. 2001;78(6):718–20.

64. MAXWELL JC. Maxwell_1873_Treatise_Preface. 1873.

65. Masoumi N, Sohrabi N, Behzadmehr A. A new model for calculating the effective viscosity of nanofluids. *Journal of Physics D: Applied Physics*. 2009;42(5).

66. Murshed SMS, Leong KC, Yang C. Thermophysical and electrokinetic properties of nanofluids - A critical review. *Applied Thermal Engineering*. 2008;28(17–18):2109–25.

67. Zhang Z, He W, Zheng J, Wang G, Ji J. Rice Husk Ash-Derived Silica Nanofluids: Synthesis and Stability Study. *Nanoscale Research Letters*. 2016;11(1).

68. Zhu HT, Zhang CY, Tang YM, Wang JX. Novel synthesis and thermal conductivity of CuO nanofluid. *Journal of Physical Chemistry* C. 2007;111(4):1646–50.

69. Khanafer K, Vafai K. A critical synthesis of thermophysical characteristics of nanofluids. *International Journal of Heat and Mass Transfer*. 2011;54(19–20):4410–28.

70. Cengel YA, Ghajar AJ. Cengel_heat_and_mass_transfer_5ed_rev. 2015.

71. El Bécaye Maïga S, Palm SJ, Nguyen CT, Roy G, Galanis N. Heat transfer enhancement by using nanofluids in forced convection flows. *International Journal of Heat and Fluid Flow*. 2005;26(4 SPEC. ISS.):530–46.

72. Li Q, Xuan Y. Convective heat transfer and flow characteristics of Cu-water nanofluid. 2002;45(4).

73. Duangthongsuk W, Wongwises S. An experimental study on the heat transfer performance and pressure drop of TiO2-water nanofluids flowing under a turbulent flow regime. *International Journal of Heat and Mass Transfer*. 2010;53(1–3):334–44.

74. Haddad Z, Oztop HF, Abu-Nada E, Mataoui A. A review on natural convective heat transfer of nanofluids. *Renewable and Sustainable Energy Reviews*. 2012;16(7):5363–78.

75. Li CH, Peterson GP. Experimental studies of natural convection heat transfer of Al 2O3/DI water nanoparticle suspensions (Nanofluids). *Advances in Mechanical Engineering*. 2010;2010.

76. Ho CJ, Liu WK, Chang YS, Lin CC. Natural convection heat transfer of alumina-water nanofluid in vertical square enclosures: An experimental study. *International Journal of Thermal Sciences*. 2010;49(8):1345–53.

77. Khanafer K, Vafai K, Lightstone M. Buoyancy-driven heat transfer enhancement in a two-dimensional enclosure utilizing nanofluids. *International Journal of Heat and Mass Transfer*. 2003;46(19):3639–53.

78. Kim J, Kang YT, Choi CK. Analysis of convective instability and heat transfer characteristics of nanofluids. *Physics of Fluids*. 2004;16(7):2395–401.

79. Putra N, Roetzel W, Das SK. Natural convection of nano-fluids. *Heat and Mass Transfer/Waerme- und Stoffuebertragung*. 2003;39(8–9):775–84.

80. Vajjha RS, Das DK, Mahagaonkar BM. Density measurement of different nanofluids and their comparison with theory. *Petroleum Science and Technology*. 2009;27(6):612–24.

81. Murshed SMS, Leong KC, Yang C. Investigations of thermal conductivity and viscosity of nanofluids. *International Journal of Thermal Sciences*. 2008;47(5):560–8.

82. Naik MT, Ranga Janardhana G, Vijaya Kumar Reddy K, Subba Reddy B. Experimental investigation into rheological property of copper oxide nanoparticles suspended in propylene glycol-water based fluids. *Journal of Engineering and Applied Sciences*. 2010;5(6):29–34.

83. Said Z, Sajid H M, Kamyar A, Saidur R. Experimental investigation on the stability and density of TiO2, Al2O3, SiO2 and TiSiO4. *IOP Conference Series: Earth and Environmental Science*. 2013;16(1).

84. Naddaf A, Zeinali Heris S. Density and rheological properties of different nanofluids based on diesel oil at different mass concentrations: An experimental study. Journal of *Thermal Analysis and Calorimetry*. 2019;135(2):1229–42.

85. Kole M, Dey TK. Viscosity of alumina nanoparticles dispersed in car engine coolant. *Experimental Thermal and Fluid Science*. 2010;34(6):677–83.

86. Namburu PK, Kulkarni DP, Dandekar A, Das DK. Experimental investigation of viscosity and specific heat of silicon dioxide nanofluids. *Micro and Nano Letters*. 2007;2(3):67–71.

87. Hemmat Esfe M, Saedodin S. An experimental investigation and new correlation of viscosity of ZnO-EG nanofluid at various temperatures and different solid volume fractions. *Experimental Thermal and Fluid Science*. 2014;55:1–5.

88. Pak BC, Cho YI. Hydrodynamic and heat transfer study of dispersed fluids with submicron metallic oxide particles. *Experimental Heat Transfer*. 1998;11(2):151–70.

89. Toghraie D, Alempour SM, Afrand M. Experimental determination of viscosity of water based magnetite nanofluid for application in heating and cooling systems. *Journal of Magnetism and Magnetic Materials.* 2016;417:243–8.

90. Li J, Li Z, Wang B. Experimental viscosity measurements for copper oxide nanoparticle suspensions. *Tsinghua Science and Technology*. 2002;7(2):198–201.

91. Syam Sundar L, Singh MK, Sousa ACM. Investigation of thermal conductivity and viscosity of Fe3O4 nanofluid for heat transfer applications. *International Communications in Heat and Mass Transfer*. 2013;44:7–14.

92. Nguyen CT, Desgranges F, Roy G, Galanis N, Maré T, Boucher S, et al. Temperature and particle-size dependent viscosity data for water-based nanofluids – Hysteresis phenomenon. *International Journal of Heat and Fluid Flow*. 2007;28(6):1492–506.

93. He Y, Jin Y, Chen H, Ding Y, Cang D, Lu H. Heat transfer and flow behaviour of aqueous suspensions of TiO2 nanoparticles (nanofluids) flowing upward through a vertical pipe. *International Journal of Heat and Mass Transfer*. 2007;50(11–12):2272–81.

94. Chevalier J, Tillement O, Ayela F. Rheological properties of nanofluids flowing through microchannels. *Applied Physics Letters*. 2007;91(23):1–4.

95. Suganthi KS, Rajan KS. Metal oxide nanofluids: Review of formulation, thermo-physical properties, mechanisms, and heat transfer performance. *Renewable and Sustainable Energy Reviews*. 2017;76(October 2015):226–55.

96. Das SK, Putra N, Thiesen P, Roetzel W. Temperature dependence of thermal conductivity enhancement for nanofluids. *Journal of Heat Transfer*. 2003;125(4):567–74.

97. Kwak K, Kim C. Viscosity and thermal conductivity of copper oxide nanofluid dispersed in ethylene glycol. Vol. 17, *Korea Australia Rheology Journal*. 2005. p. 35–40.

98. Parekh K, Lee HS. Magnetic field induced enhancement in thermal conductivity of magnetite nanofluid. *Journal of Applied Physics*. 2010;107(9):7–10.

99. Gavili A, Zabihi F, Isfahani TD, Sabbaghzadeh J. The thermal conductivity of water base ferrofluids under magnetic field. *Experimental Thermal and Fluid Science*. 2012;41:94–8.

100. Karimi A, Afghahi SSS, Shariatmadar H, Ashjaee M. Experimental investigation on thermal conductivity of MFe2O4 (M = Fe and Co) magnetic nanofluids under influence of magnetic field. *Thermochimica Acta*. 2014;598:59–67.

101. Yu W, Xie H, Chen L, Li Y. Enhancement of thermal conductivity of kerosene-based Fe3O4 nanofluids prepared via phase-transfer method. *Colloids and Surfaces A: Physicochemical and Engineering Aspects*. 2010;355(1–3):109–13.

102. Altan CL, Bucak S. The effect of Fe3O4 nanoparticles on the thermal conductivities of various base fluids. *Nanotechnology*. 2011;22(28).

103. Altan CL, Elkatmis A, Yüksel M, Aslan N, Bucak S. Enhancement of thermal conductivity upon application of magnetic field to Fe3O4 nanofluids. *Journal of Applied Physics*. 2011;110(9).

104. Seyhan M, Altan CL, Gurten B, Bucak S. The effect of functionalized silver nanoparticles over the thermal conductivity of base fluids. *AIP Advances*. 2017;7(4).

105. Philip J, Shima PD, Raj B. Evidence for enhanced thermal conduction through percolating structures in nanofluids. *Nanotechnology*. 2008;19(30).

106. Nabeel Rashin M, Hemalatha J. Magnetic and ultrasonic studies on stable cobalt ferrite magnetic nanofluid. *Ultrasonics*. 2014;54(3):834–40.

107. Wang XQ, Mujumdar AS. Heat transfer characteristics of nanofluids: a review. *International Journal of Thermal Sciences*. 2007;46(1):1–19.

108. Sharifpur M, Yousefi S, Meyer JP. A new model for density of nanofluids including nanolayer. *International Communications in Heat and Mass Transfer*. 2016;78:168–74.

109. Montazer E, Salami E, Yarmand H, Chowdhury ZZ, Dahari M, Kazi SN, et al. Development of a new density correlation for carbon-based nanofluids using response surface methodology. *Journal of Thermal Analysis and Calorimetry*. 2018;132(2):1399–407.

110. Kulkarni DP, Das DK, Chukwu GA. Temperature dependent rheological property of copper oxide nanoparticles suspension (nanofluid). *Journal of Nanoscience and Nanotechnology*. 2006;6(4):1150–4.

111. Hemmat Esfe M, Afrand M, Gharehkhani S, Rostamian H, Toghraie D, Dahari M. An experimental study on viscosity of alumina-engine oil: Effects of temperature and nanoparticles concentration. *International Communications in Heat and Mass Transfer* [Internet]. 2016;76:202–8. Available from: http://dx.doi.org/10.1016/j.icheatmasstransfer.2016.05.013

112. Einstein A. Investigations On the Theory of The Brownian Movement. 1956;

113. Brinkman HC. The viscosity of concentrated suspensions and solutions. *The Journal of Chemical Physics*. 1952;20(4):571.

114. Donald A. Drew SLP. Theory of Multicomponent Fluids [cited 2021 May 8]. Available from: https://books.google.com.tr/books?hl=en&lr=&id=sccFCAAAQBAJ&oi=fnd&pg=PR9&dq=D.A.Drew,S.L.+Passman,TheoryofMulti-Component+Fluids,+Springer,+Berlin,+1999&ots=Sn-RLVZPbV&sig=_Q2WMB1k9jYXrJVUVAXzcnvREOI&redir_esc=y#v=onepage&q&f=false

115. Batchelor GK. The effect of Brownian motion on the bulk stress in a suspension of spherical particles. *Journal of Fluid Mechanics*. 1977;83(1):97–117.

116. Wang X, Xu X, Choi SUS. Thermal conductivity of nanoparticle-fluid mixture. *Journal of thermophysics and heat transfer*. 1999;13(4):474–80.

117. Frankel NA, Acrivos A. On the viscosity of a concentrated suspension of solid spheres. *Chemical Engineering Science*. 1967;22(6):847–53.

118. Tseng WJ, Lin KC. Rheology and colloidal structure of aqueous TiO2 nanoparticle suspensions. *Materials Science and Engineering A*. 2003 Aug 25;355(1–2):186–92.

119. Chen H, Ding Y, He Y, Tan C. Rheological behaviour of ethylene glycol based titania nanofluids. *Chemical Physics Letters*. 2007 Aug 27;444(4–6):333–7.

120. Zadkhast M, Toghraie D, Karimipour A. Developing a new correlation to estimate the thermal conductivity of MWCNT-CuO/water hybrid nanofluid via an experimental investigation. *Journal of Thermal Analysis and Calorimetry*. 2017;129(2):859–67.

121. Hemmat Esfe M, Karimipour A, Yan WM, Akbari M, Safaei MR, Dahari M. Experimental study on thermal conductivity of ethylene glycol based nanofluids containing Al2O3 nanoparticles. *International Journal of Heat and Mass Transfer*. 2015;88:728–34.

122. Hamilton RL, Crosser OK. Thermal conductivity of heterogeneous two-component systems. *I & EC Fundamentals 1*. 1962;187–191.

123. Wasp EJ, Kenny JP, Gandhi RL. Solid-liquid flow slurry pipeline transportation. [cited 2021 May 9]. Available from: https://www.worldcat.org/title/solid-liquid-flow-slurry-pipeline-transportation/oclc/2859489

124. Yu W, Choi SUS. The role of interfacial layers in the enhanced thermal conductivity of nanofluids: A renovated Hamilton-Crosser model. *Journal of Nanoparticle Research*. 2003;6(4):355–61.

125. Timofeeva E V., Gavrilov AN, McCloskey JM, Tolmachev Y V., Sprunt S, Lopatina LM, et al. Thermal conductivity and particle agglomeration in alumina nanofluids: Experiment and theory. *Physical Review E - Statistical, Nonlinear, and Soft Matter Physics*. 2007 Dec 28;76(6).

126. Rohini Priya K, Suganthi KS, Rajan KS. Transport properties of ultra-low concentration CuO-water nanofluids containing non-spherical nanoparticles. *International Journal of Heat and Mass Transfer*. 2012;55(17–18):4734–43.

127. Bucak S, Rende D. Colloid and Surface Chemistry: A Laboratory Guide for Exploration of the Nano World [cited 2021 May 7]. Available from: https://www.routledge.com/Colloid-and-Surface-Chemistry-A-Laboratory-Guide-for-Exploration-of-the/Bucak-Rende/p/book/9780367379018

128. Zhu H, Han D, Meng Z, Wu D, Zhang C. Preparation and thermal conductivity of cuo nanofluid via a wet chemical method. *Nanoscale Research Letters*. 2011;6(1):2–7.

APPENDIX A

Table A.1. Skeletal forms of the chosen models for the density of nanofluids

Model number	Correlation form
DM 1	$\rho_{nf} = A + B\emptyset + CT$
DM 2	$\rho_{nf} = A\emptyset + B(1 - \emptyset)$
DM 3	$\rho_{nf} = A + BT + CT^2 + D\emptyset + E\emptyset^2 + FT\emptyset$
DM 4	$\frac{\rho_{nf}}{\rho_{bf}} = A + B\emptyset + CT$
DM 5	$\frac{\rho_{nf}}{\rho_{bf}} = A\emptyset + B(1 - \emptyset)$
DM 6	$\frac{\rho_{nf}}{\rho_{bf}} = A + BT + CT^2 + D\emptyset + E\emptyset^2 + FT\emptyset$

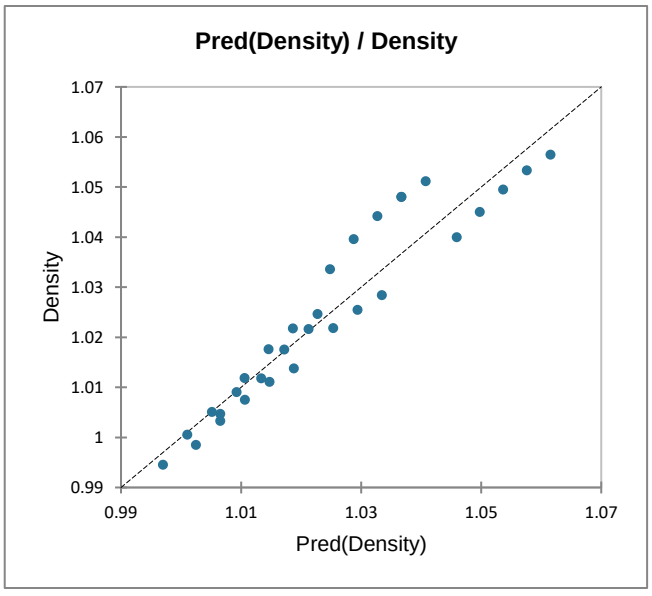

Figure A.1. The compatibility of predicted values with measured values for DM 1 concerning citric acid coated superparamagnetic Fe_3O_4/water nanofluids

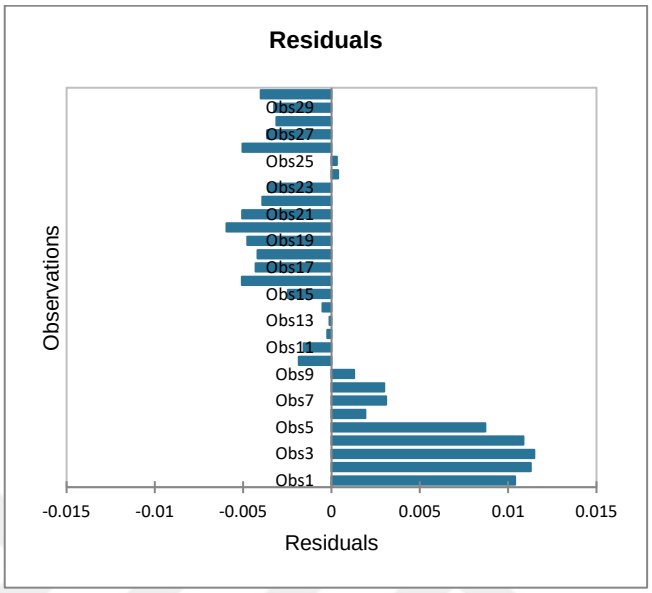

Figure A.2. Residuals of observations for DM 1 concerning citric acid coated superparamagnetic Fe_3O_4/water nanofluids

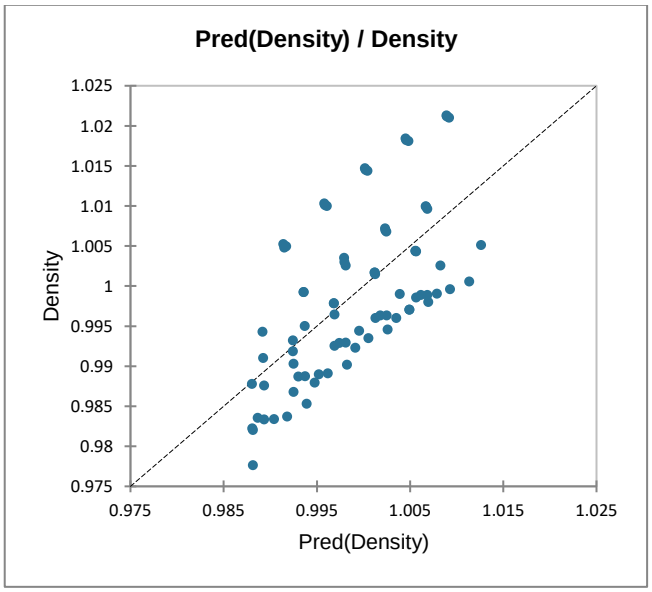

Figure A.3. The compatibility of predicted values with measured values for DM 1 concerning 250 and 450kDa PAA coated ferrimagnetic Fe_3O_4/water nanofluids

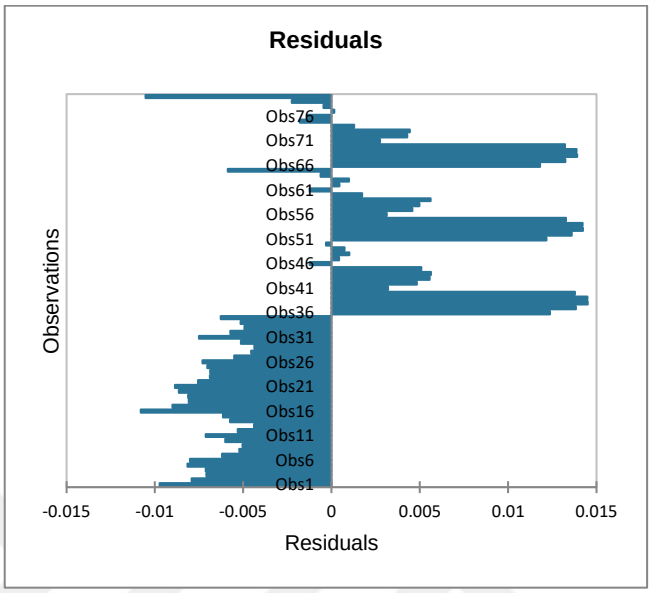

Figure A.4. Residuals of observations for DM 1 concerning 250 and 450kDa PAA coated ferrimagnetic Fe_3O_4/water nanofluids

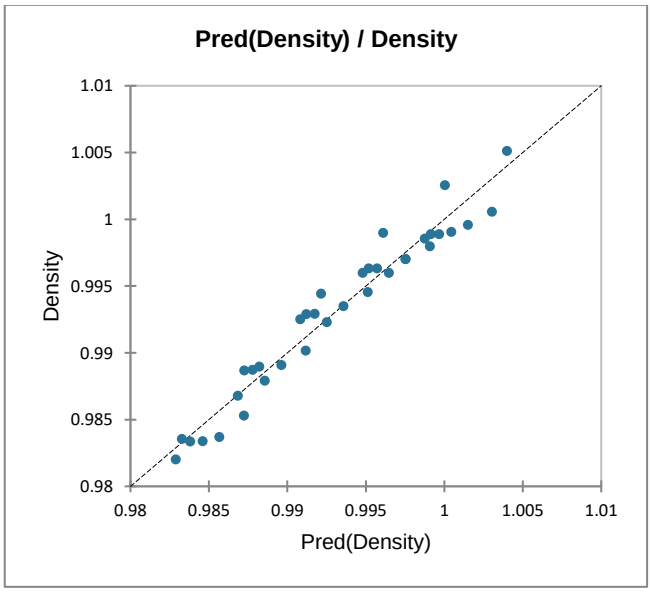

Figure A.5. The compatibility of predicted values with measured values for DM 1 concerning 450kDa PAA coated ferrimagnetic Fe_3O_4/water nanofluids

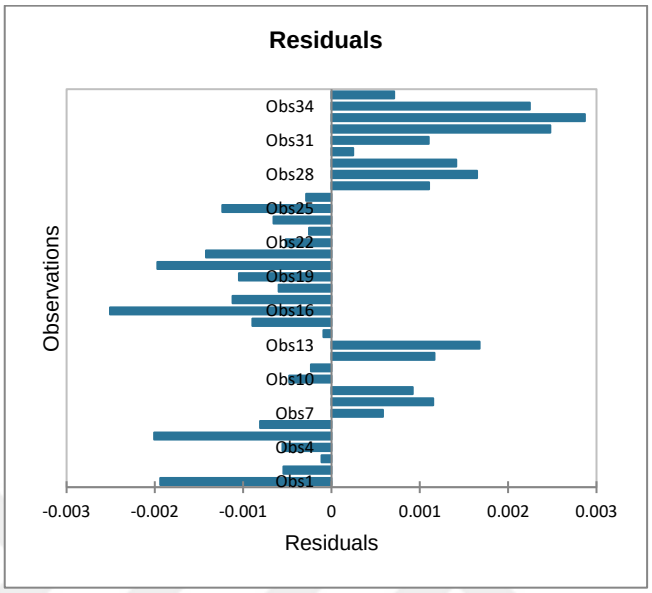

Figure A.6. Residuals of observations for DM 1 concerning 450kDa PAA coated ferrimagnetic Fe_3O_4/water nanofluids

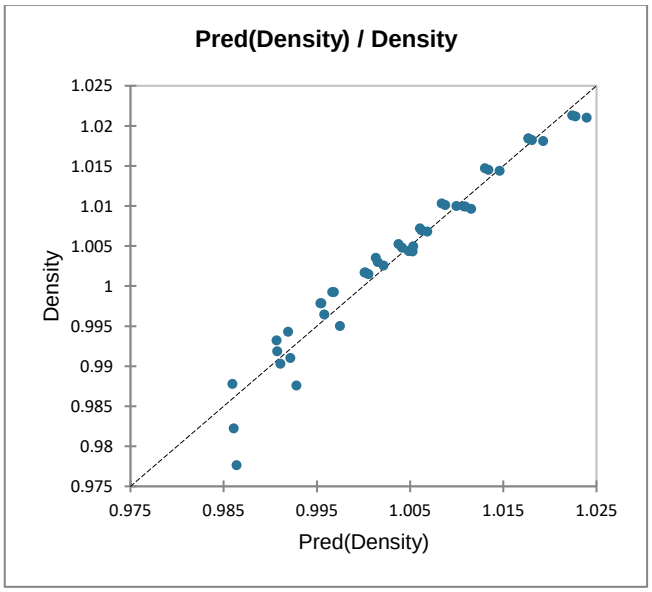

Figure A.7. The compatibility of predicted values with measured values for DM 1 concerning 250kDa PAA coated ferrimagnetic Fe_3O_4/water nanofluids

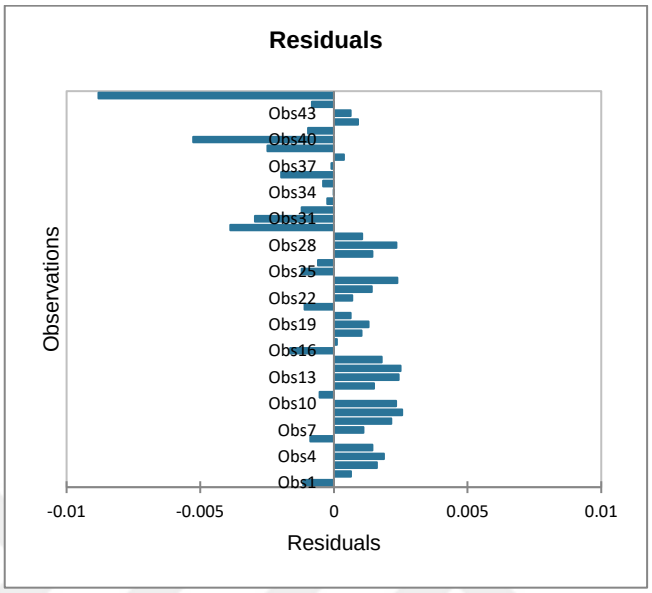

Figure A.8. Residuals of observations for DM 1 concerning 250kDa PAA coated ferrimagnetic Fe_3O_4/water nanofluids

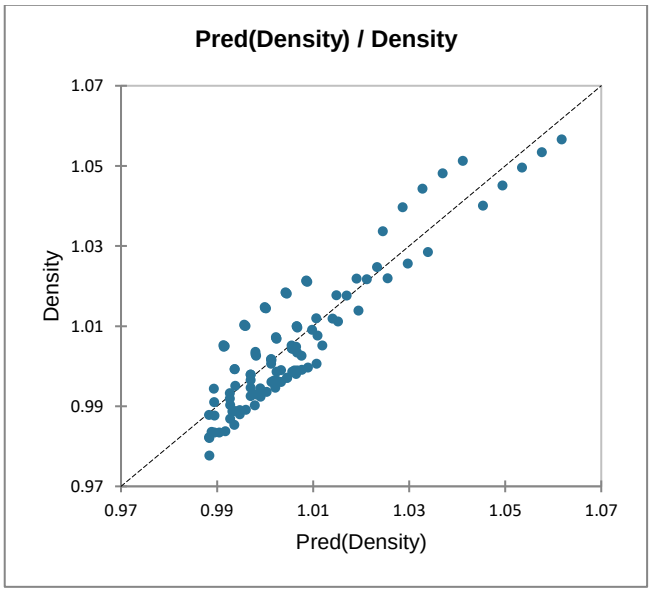

Figure A.9. The compatibility of predicted values with measured values for DM 1 concerning all Fe_3O_4/water nanofluids

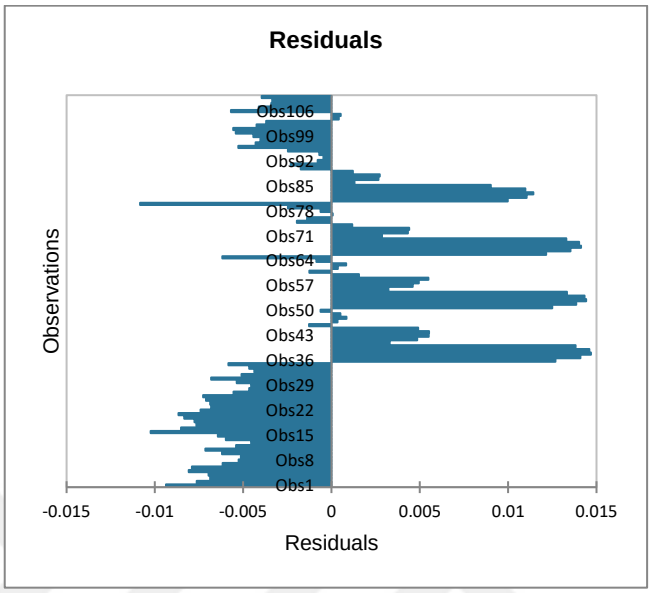

Figure A.10. Residuals of observations for DM 1 concerning all Fe_3O_4/water nanofluids

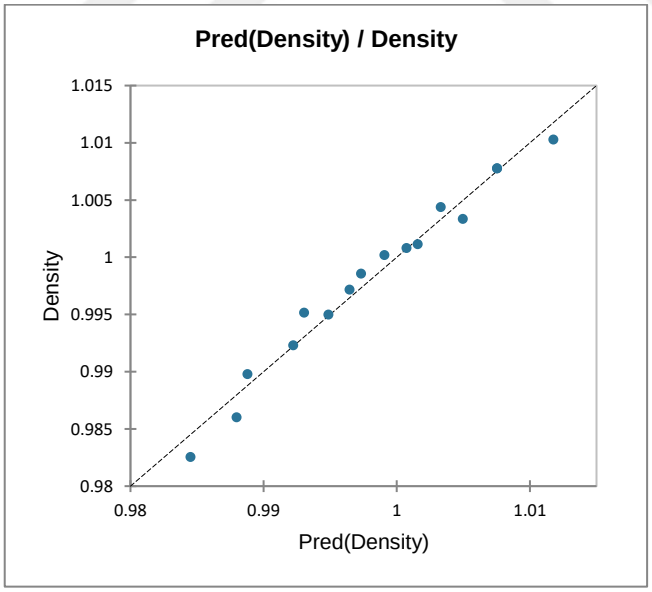

Figure A.11. The compatibility of predicted values with measured values for DM 1 concerning CuO/water nanofluids

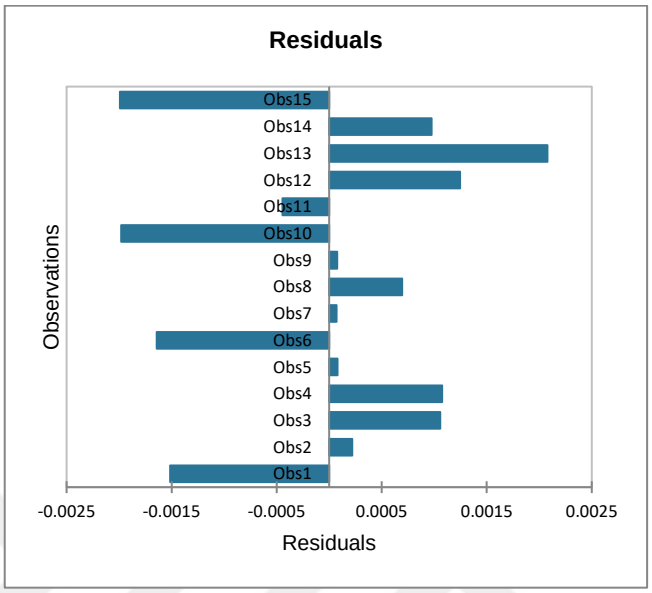

Figure A.12. Residuals of observations for DM 1 concerning CuO/water nanofluids

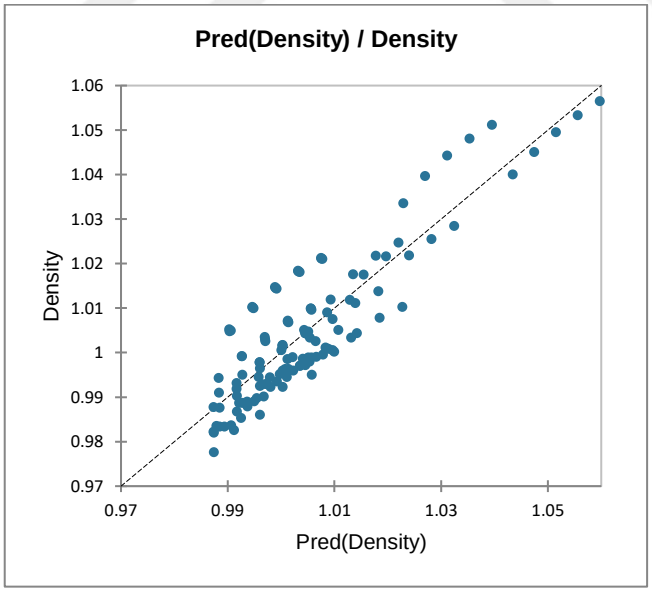

Figure A.13. The compatibility of predicted values with measured values for DM 1 concerning all Fe_3O_4 and CuO/water nanofluids together

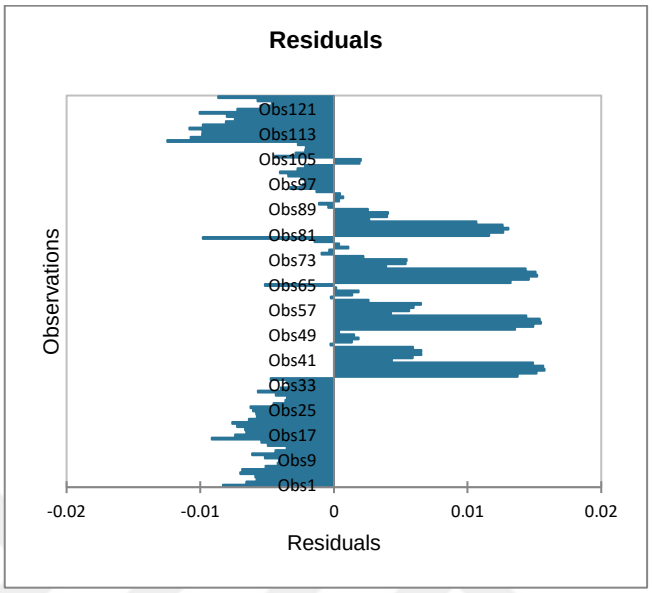

Figure A.14. Residuals of observations for DM 1 concerning all Fe_3O_4 and CuO/water nanofluids together

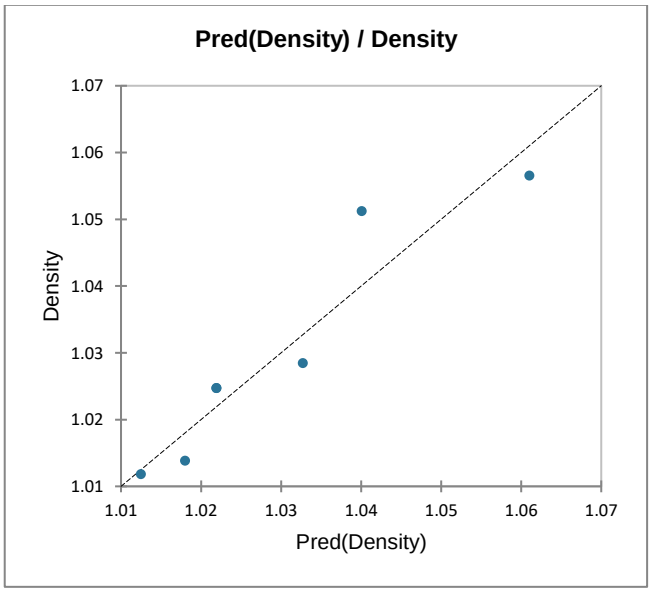

Figure A.15. The compatibility of predicted values with measured values for DM 2 concerning citric acid coated superparamagnetic Fe_3O_4/water nanofluids

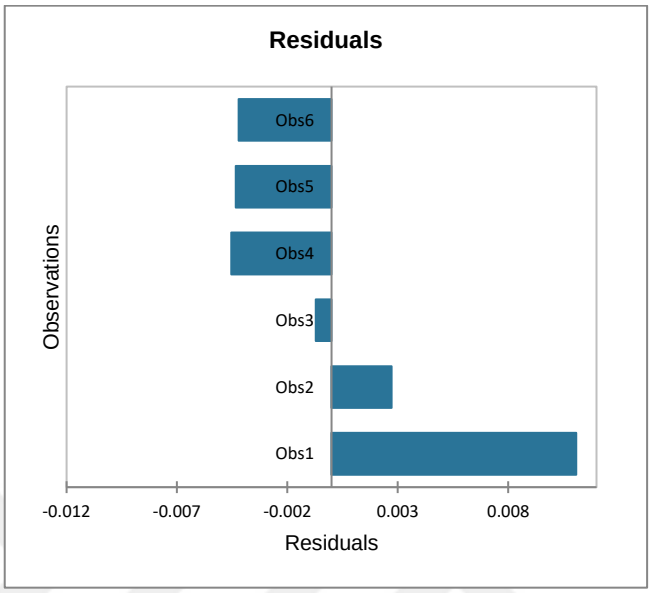

Figure A.16. Residuals of observations for DM 2 concerning citric acid coated superparamagnetic Fe_3O_4/water nanofluids

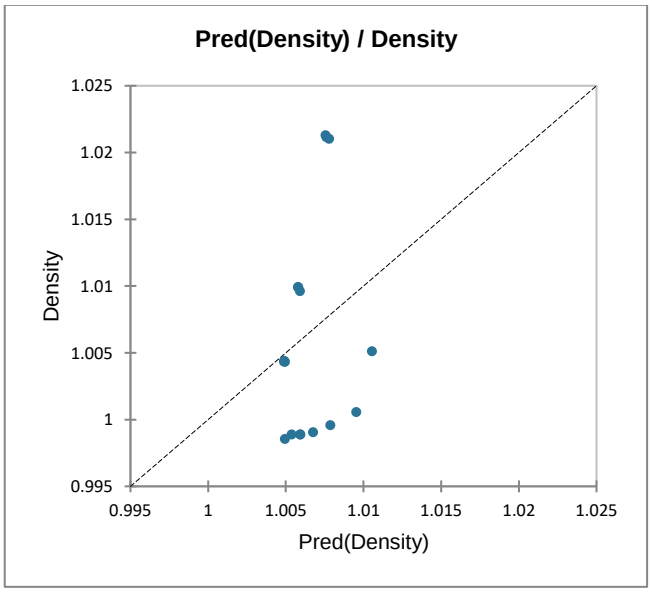

Figure A.17. The compatibility of predicted values with measured values DM 2 concerning 250 and 450kDa PAA coated ferrimagnetic Fe_3O_4/water nanofluids

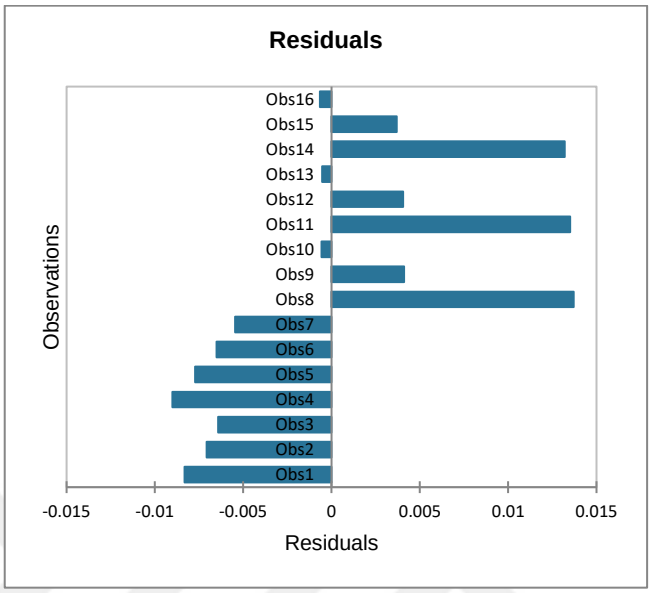

Figure A.18. Residuals of observations for DM 2 concerning 250 and 450kDa PAA coated ferrimagnetic Fe_3O_4/water nanofluids

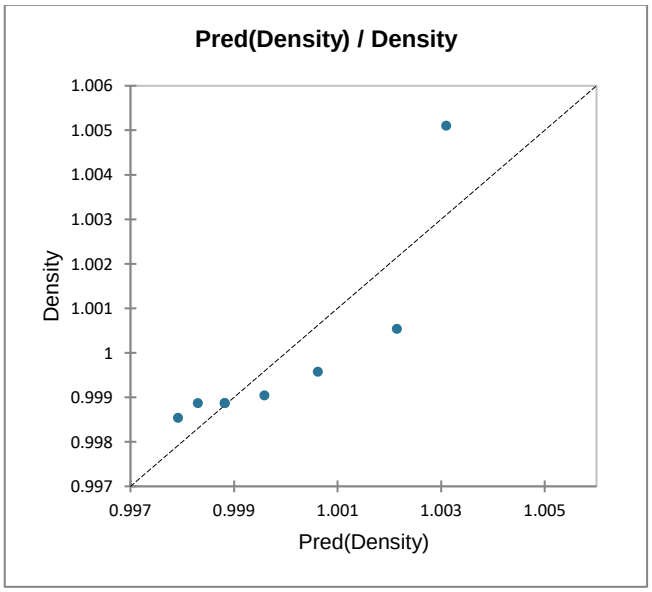

Figure A.19. The compatibility of predicted values with measured values DM 2 concerning 450kDa PAA coated ferrimagnetic Fe_3O_4/water nanofluids

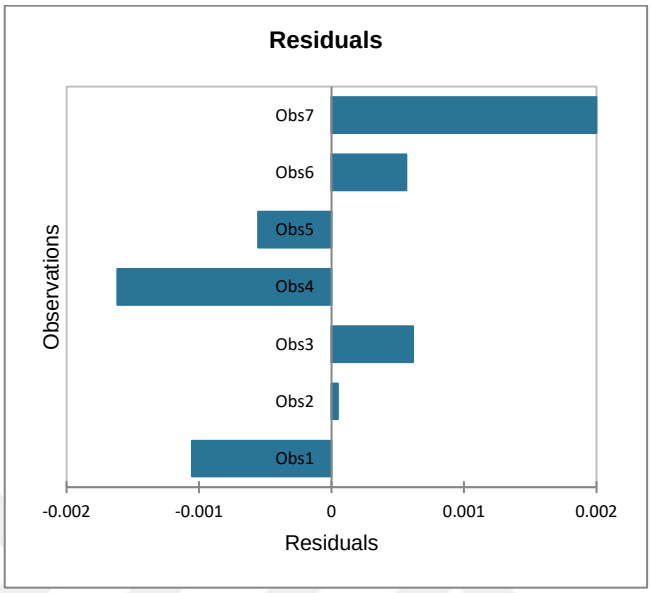

Figure A.20. Residuals of observations for DM 2 concerning 450kDa PAA coated ferrimagnetic Fe_3O_4/water nanofluids

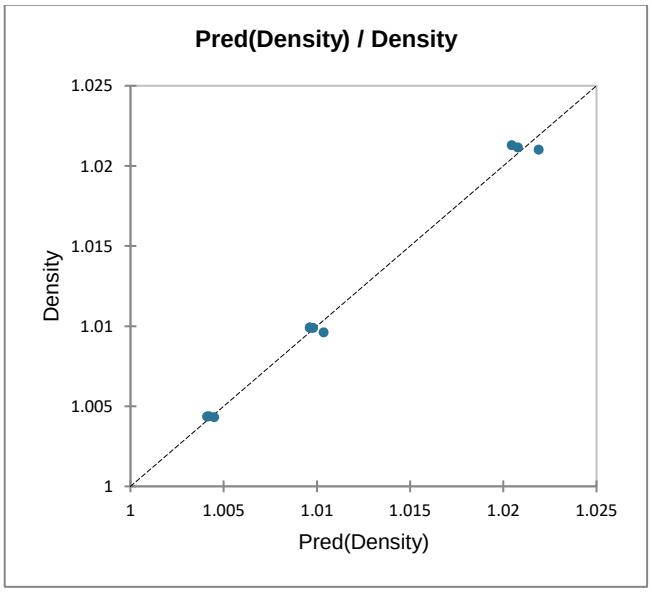

Figure A.21. The compatibility of predicted values with measured values for DM 2 concerning 250kDa PAA coated ferrimagnetic Fe_3O_4/water nanofluids

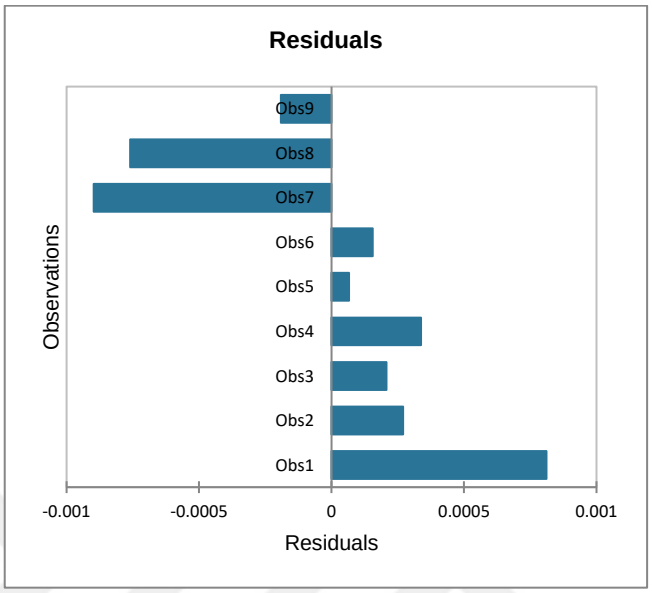

Figure A.22. Residuals of observations for DM 2 concerning 250kDa PAA coated ferrimagnetic Fe_3O_4/water nanofluids

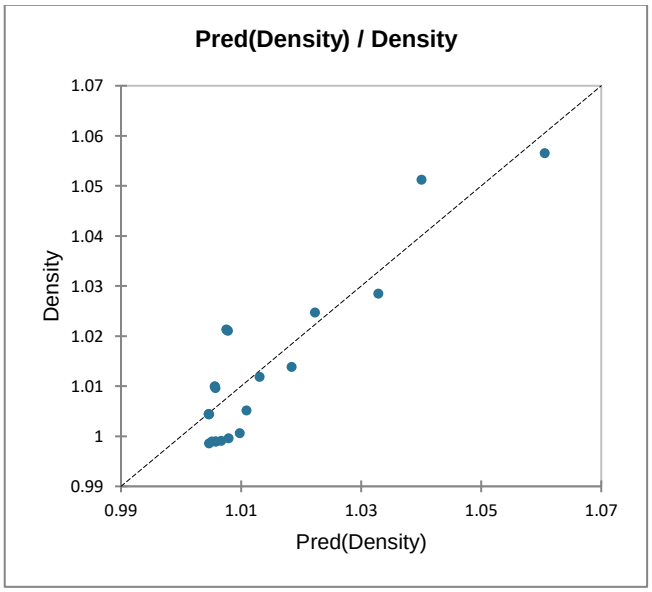

Figure A.23. The compatibility of predicted values with measured values for DM 2 concerning all Fe_3O_4/water nanofluids

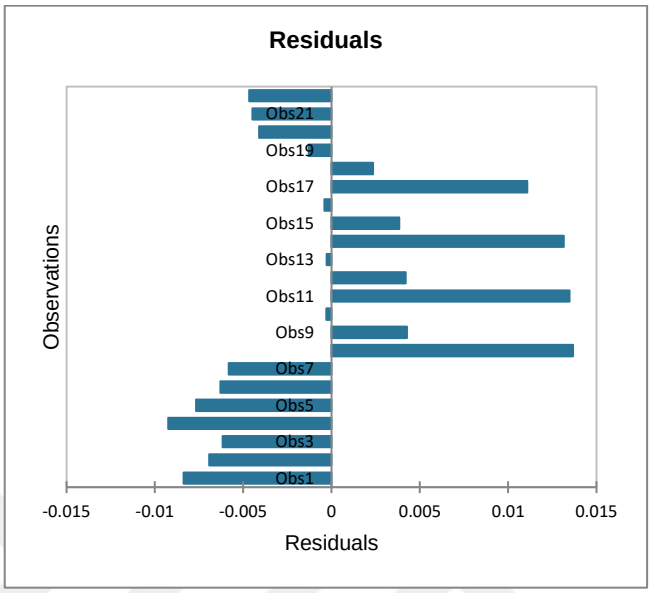

Figure A.24. Residuals of observations for DM 2 concerning all Fe_3O_4/water nanofluids

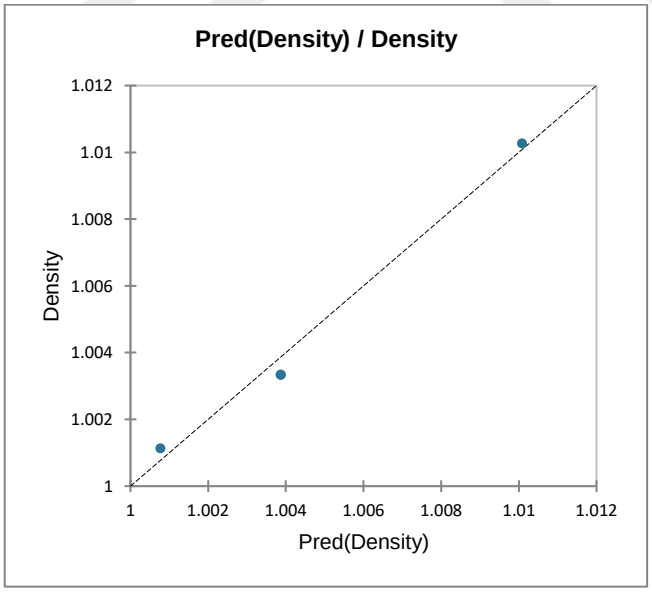

Figure A.25. The compatibility of predicted values with measured values for DM 2 concerning CuO/water nanofluids

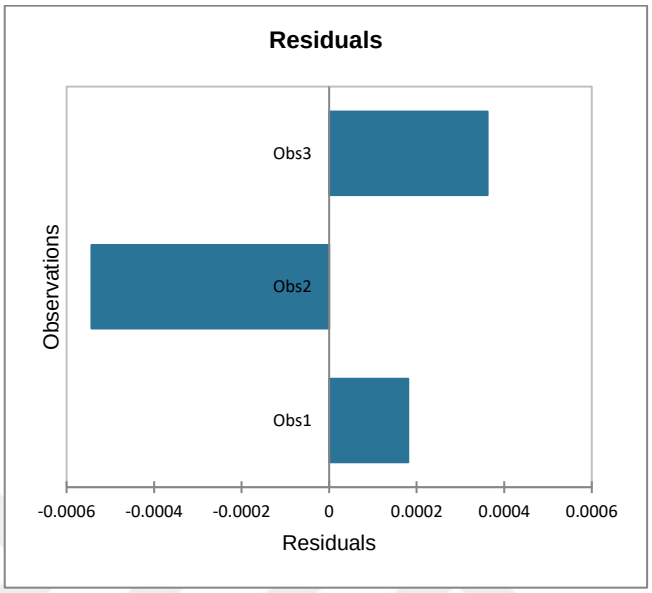

Figure A.26. Residuals of observations for DM 2 concerning CuO/water nanofluids

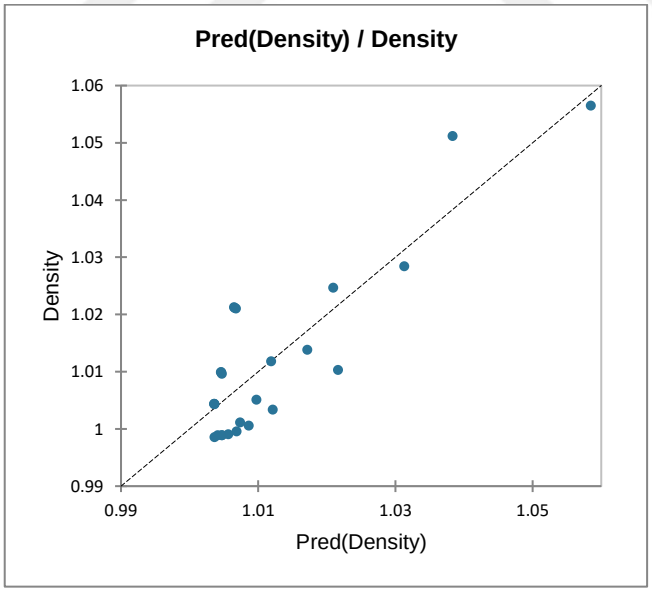

Figure A.27. The compatibility of predicted values with measured values for DM 2 concerning all Fe_3O_4 and CuO/water nanofluids together

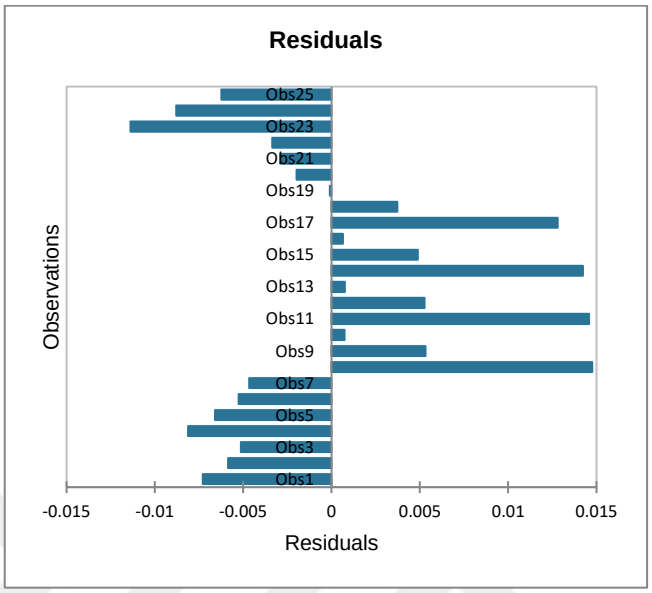

Figure A.28. Residuals of observations for DM 2 concerning all Fe_3O_4 and CuO/water nanofluids together

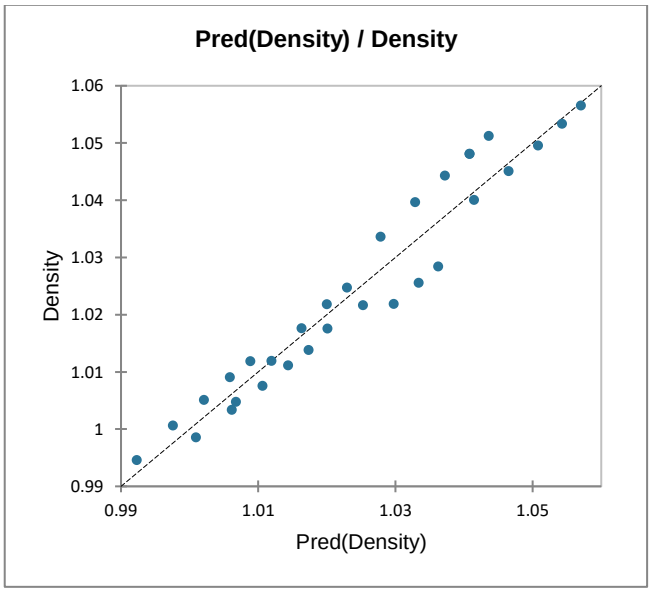

Figure A.29. The compatibility of predicted values with measured values for DM 3 concerning citric acid coated superparamagnetic Fe_3O_4/water nanofluids

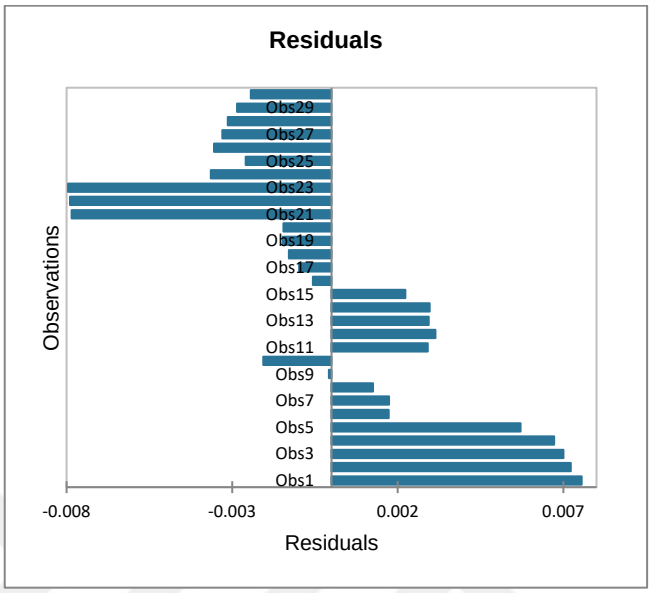

Figure A.30. Residuals of observations for DM 3 concerning citric acid coated superparamagnetic Fe_3O_4/water nanofluids

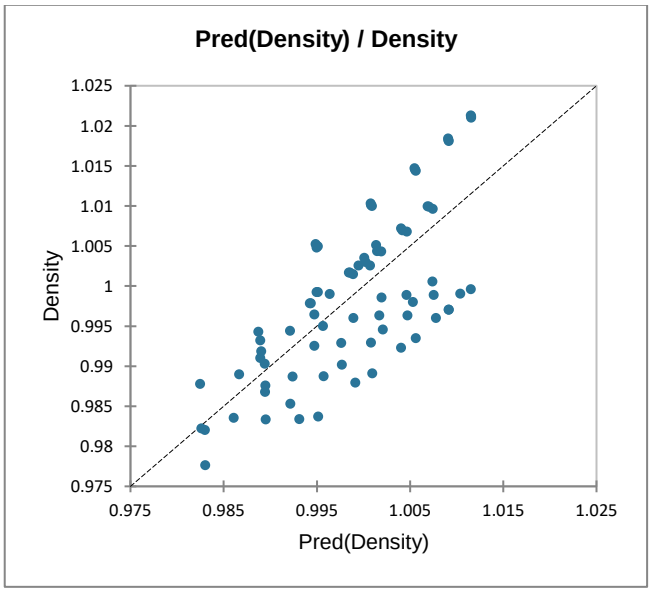

Figure A.31. The compatibility of predicted values with measured values for DM 3 concerning 250 and 450kDa PAA coated ferrimagnetic Fe_3O_4/water nanofluids

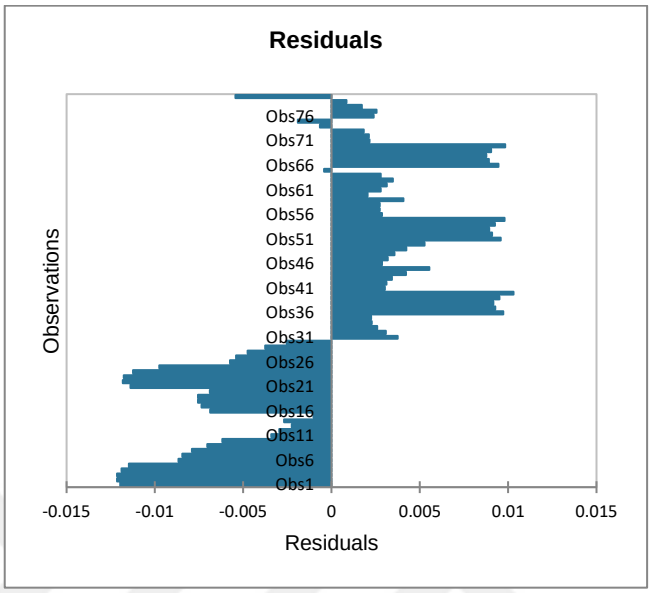

Figure A.32. Residuals of observations for DM 3 concerning 250 and 450kDa PAA coated ferrimagnetic Fe_3O_4/water nanofluids

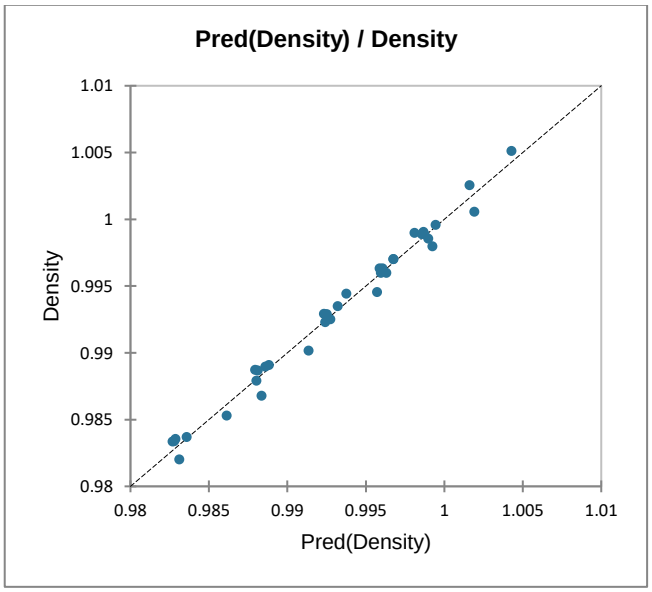

Figure A.33. The compatibility of predicted values with measured values for DM 3 concerning 450kDa PAA coated ferrimagnetic Fe_3O_4/water nanofluids

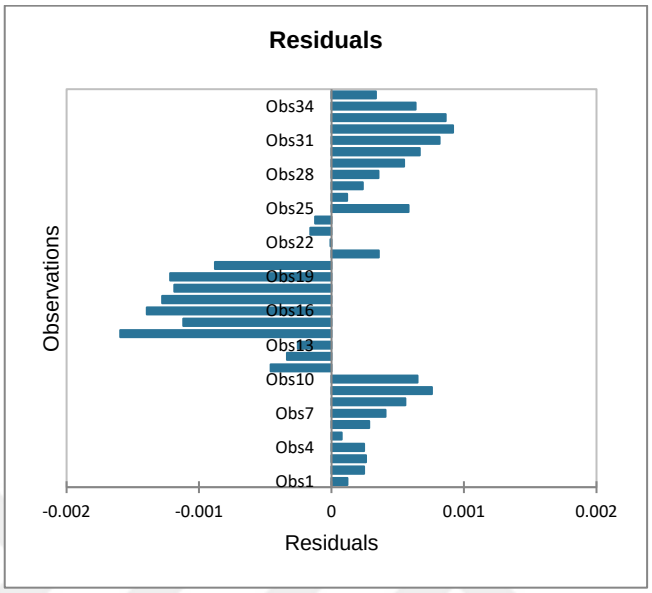

Figure A.34. Residuals of observations for DM 3 concerning 450kDa PAA coated ferrimagnetic Fe_3O_4/water nanofluids

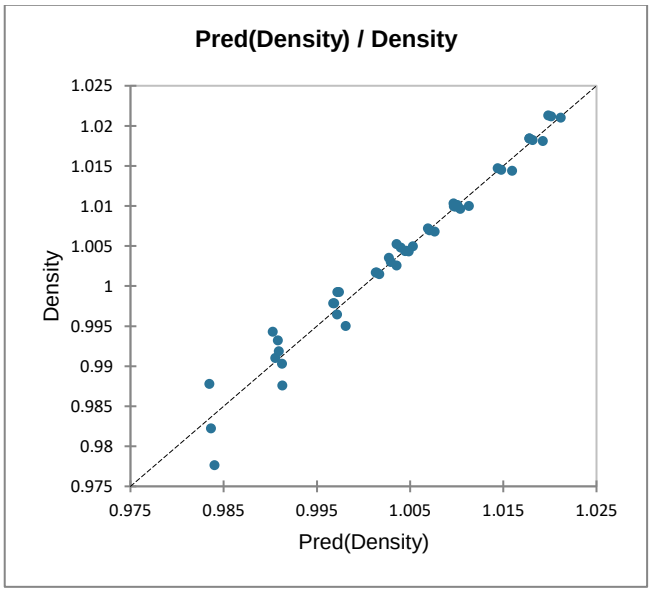

Figure A.35. The compatibility of predicted values with measured values for DM 3 concerning 250kDa PAA coated ferrimagnetic Fe_3O_4/water nanofluids

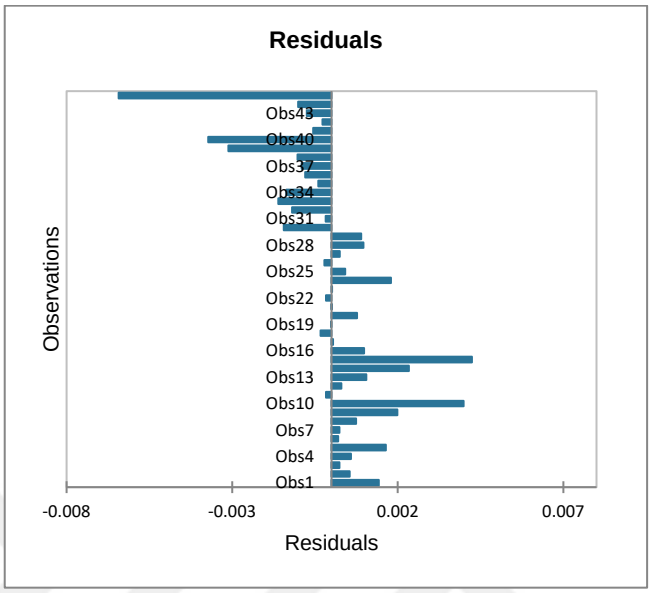

Figure A.36. Residuals of observations for DM 3 concerning 250kDa PAA coated ferrimagnetic Fe_3O_4/water nanofluids

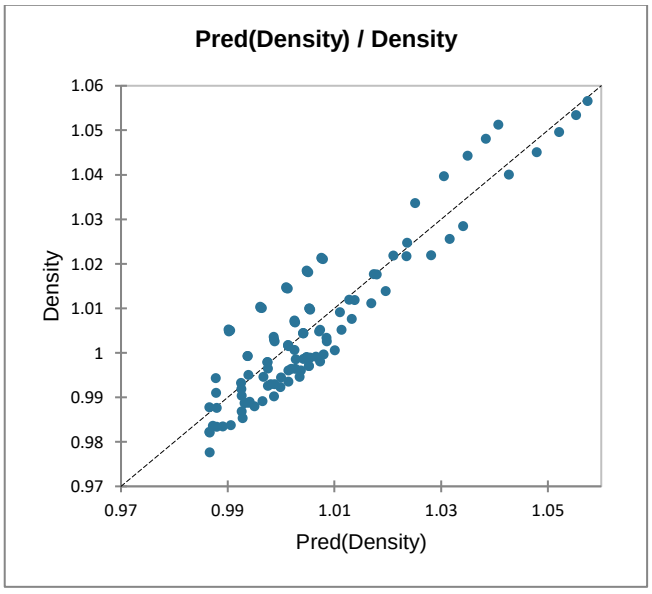

Figure A.37. The compatibility of predicted values with measured values for DM 3 concerning all Fe_3O_4/water nanofluids

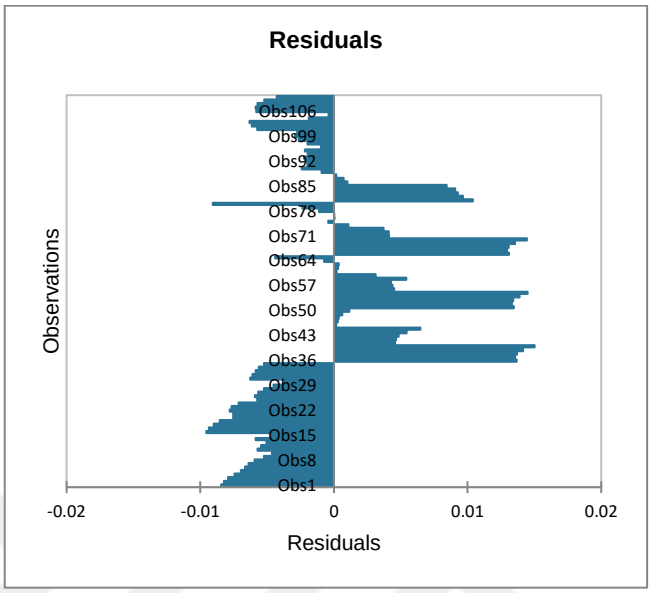

Figure A.38. Residuals of observations for DM 3 concerning all Fe_3O_4/water nanofluids

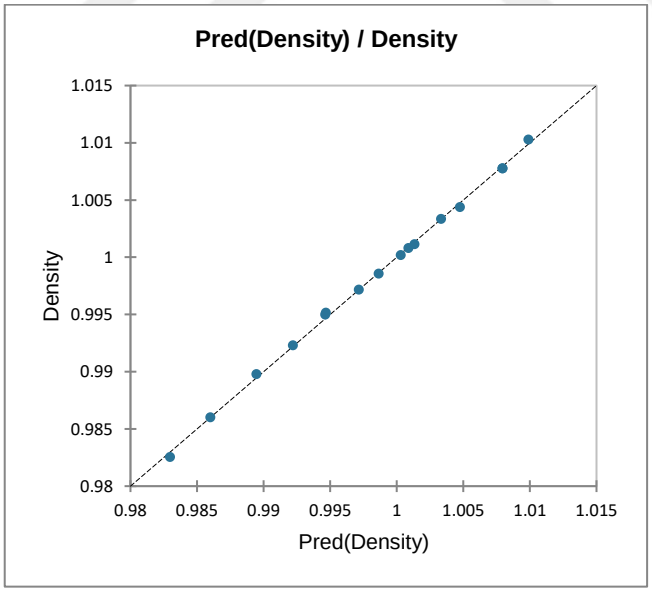

Figure A.39. The compatibility of predicted values with measured values for DM 3 concerning CuO/water nanofluids

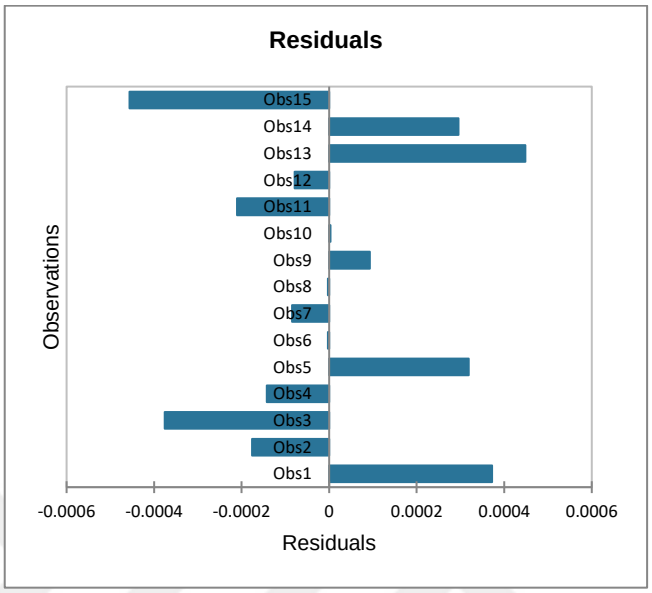

Figure A.40. Residuals of observations for DM 3 concerning CuO/water nanofluids

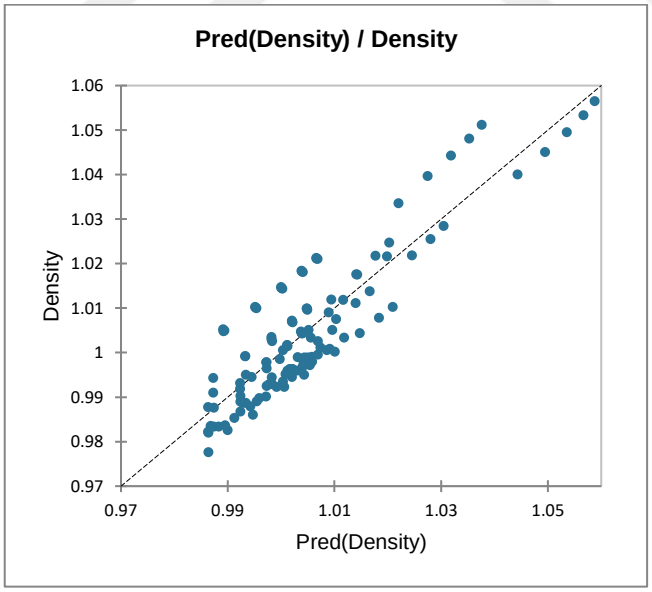

Figure A.41. The compatibility of predicted values with measured values for DM 3 concerning all Fe_3O_4 and CuO/water nanofluids together

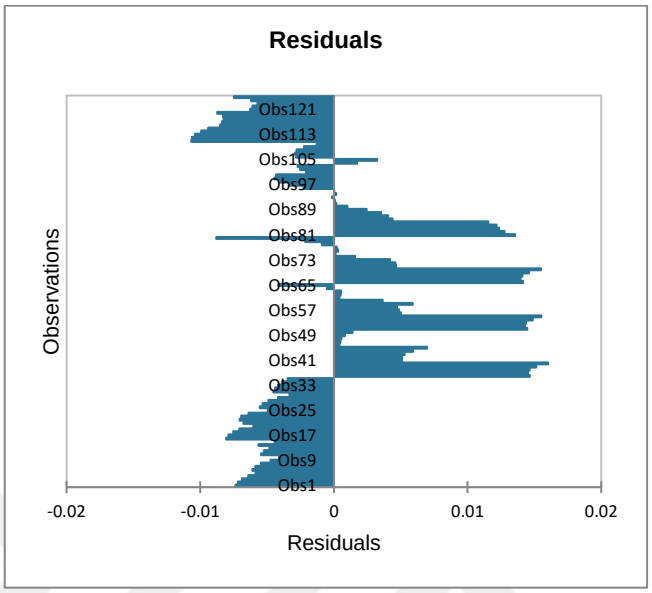

Figure A.42. Residuals of observations for DM 3 concerning all Fe_3O_4 and CuO/water nanofluids together

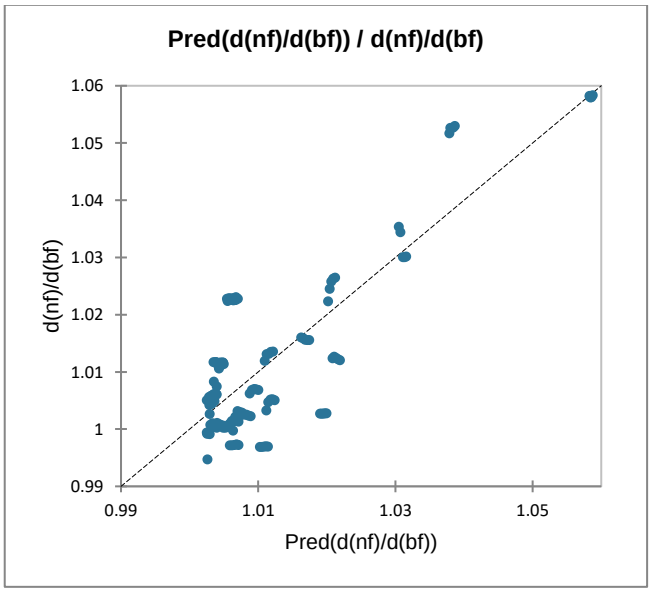

Figure A.43. The compatibility of predicted values with measured values for DM 4 concerning all nanofluids together

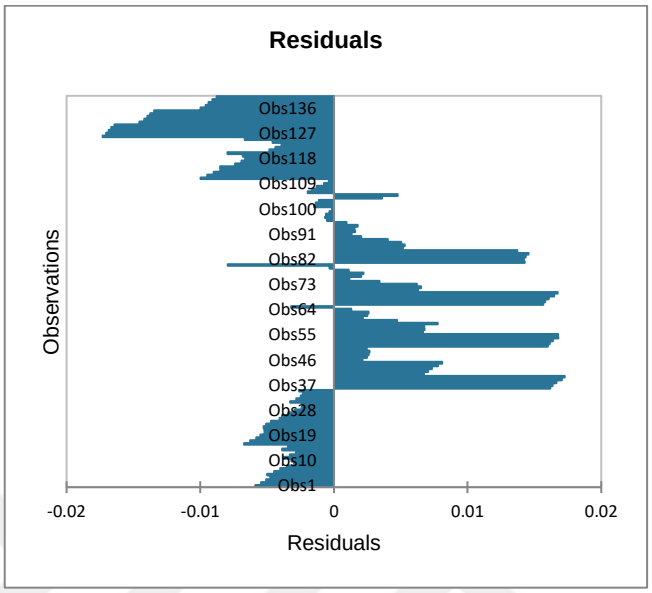

Figure A.44. Residuals of observations for DM 4 concerning all nanofluids together

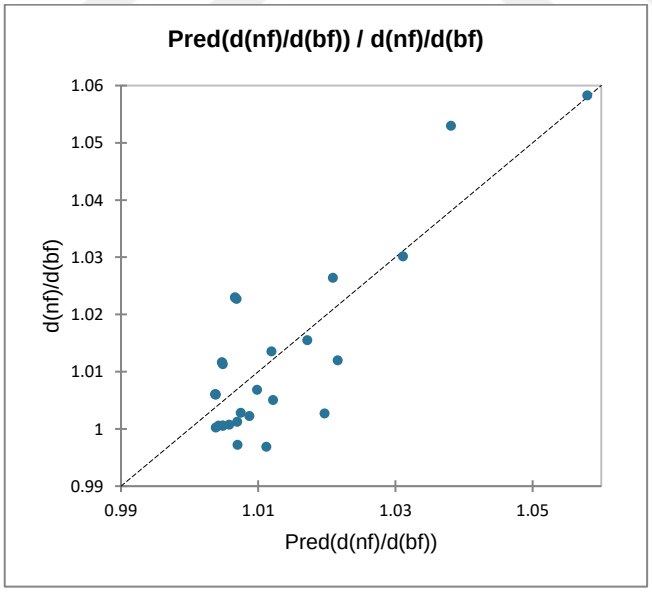

Figure A.45. The compatibility of predicted values with measured values for DM 5 concerning all nanofluids together

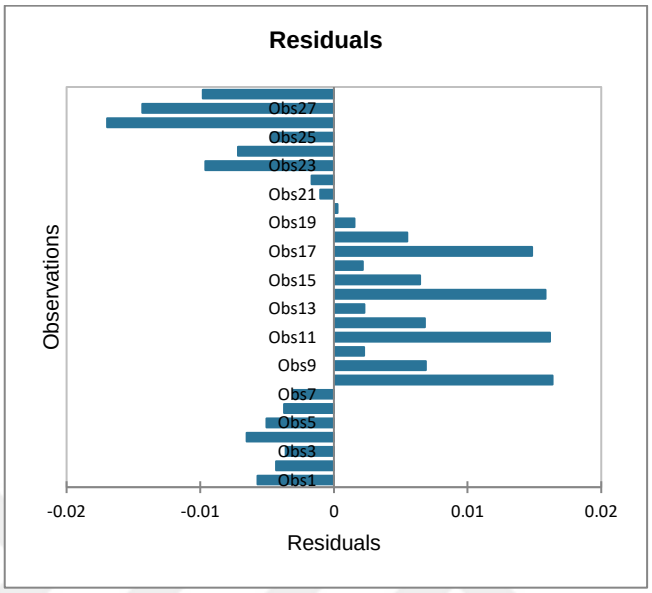

Figure A.46. Residuals of observations for DM 5 concerning all nanofluids together

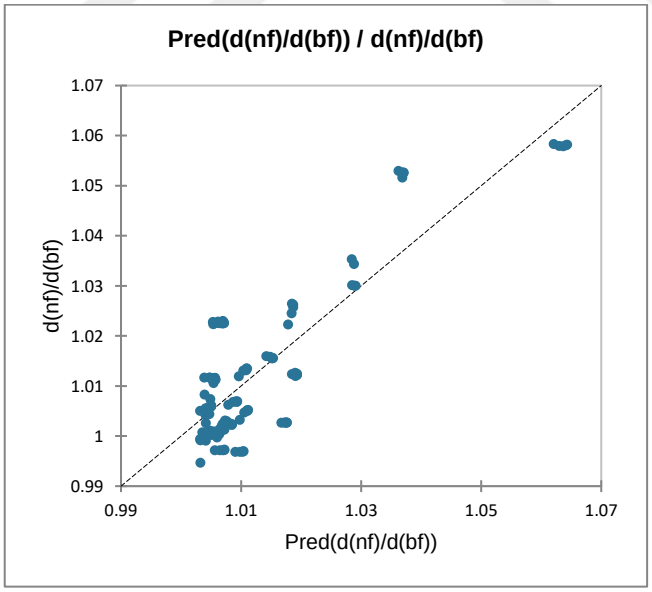

Figure A.47. The compatibility of predicted values with measured values for DM 6 concerning all nanofluids together

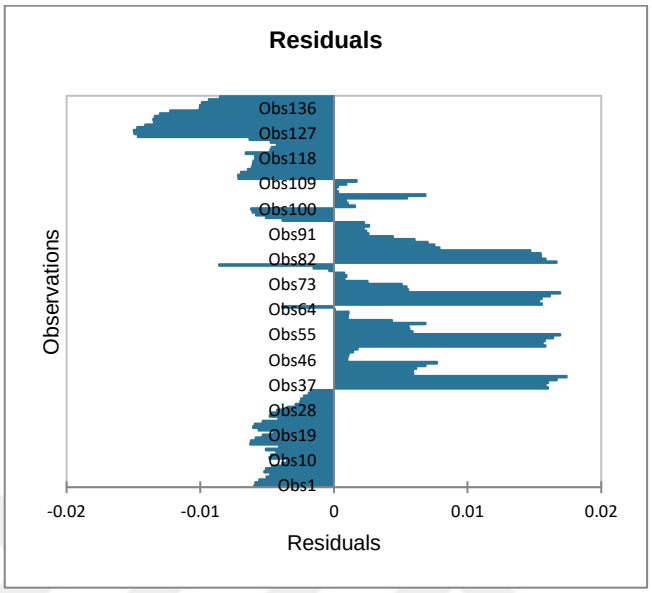

Figure A.48. Residuals of observations for DM 6 concerning all nanofluids together

APPENDIX B

Table B.1. Skeletal forms of the chosen models for the viscosity of nanofluids

Model number	**Correlation form**
VM 1	$\frac{\mu_{nf}}{\mu_{bf}} = A + B\emptyset$
VM 2	$\frac{\mu_{nf}}{\mu_{bf}} = Ae^{B\emptyset}$
VM 3	$\frac{\mu_{nf}}{\mu_{bf}} = \frac{1}{(1-\emptyset)^{A}}$
VM 4	$\frac{\mu_{nf}}{\mu_{bf}} = AT^{B}\emptyset^{C}$
VM 5	$\mu_{nf} = (A\emptyset^{2} + B\emptyset + C)e^{-DT}$
VM 6	$\mu_{nf} = \frac{Ae^{B\emptyset}}{T}$
VM 7	$\mu_{nf} = A\emptyset + \frac{B}{T}$

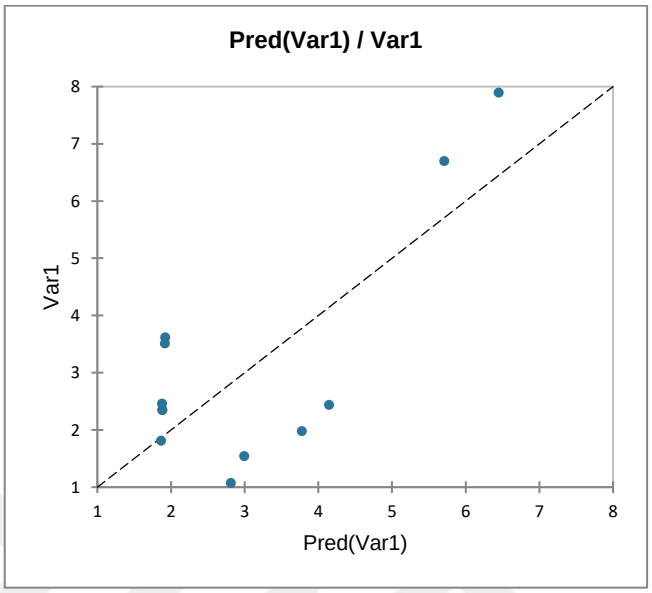

Figure B.1. The compatibility of predicted values with measured values for VM 1 concerning all superparamagnetic Fe_3O_4/water nanofluids

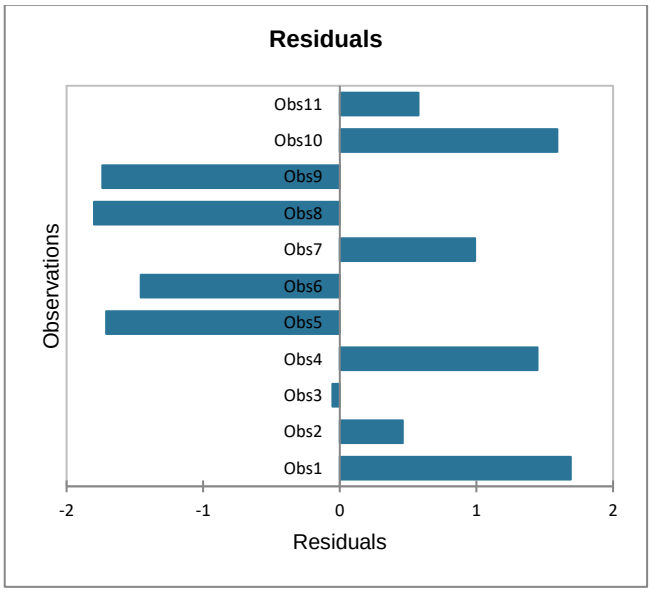

Figure B.2. Residuals of observations for VM 1 concerning all superparamagnetic Fe_3O_4/water nanofluids

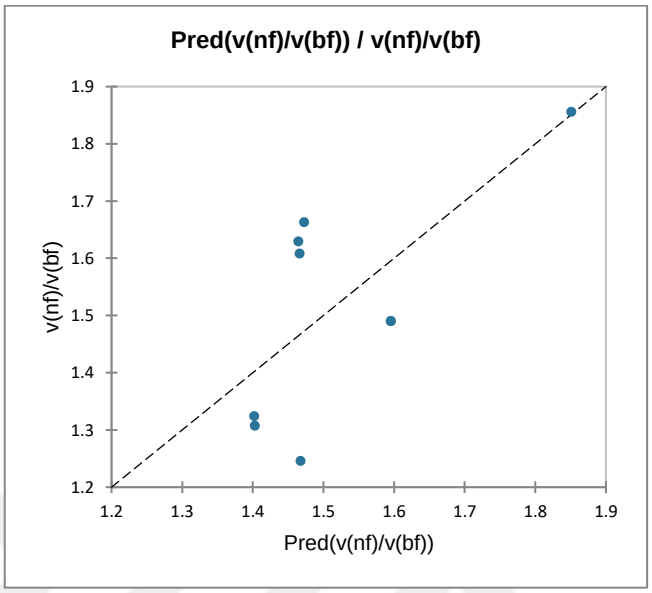

Figure B.3. The compatibility of predicted values with measured values for VM 1 concerning all ferrimagnetic Fe_3O_4/water nanofluids

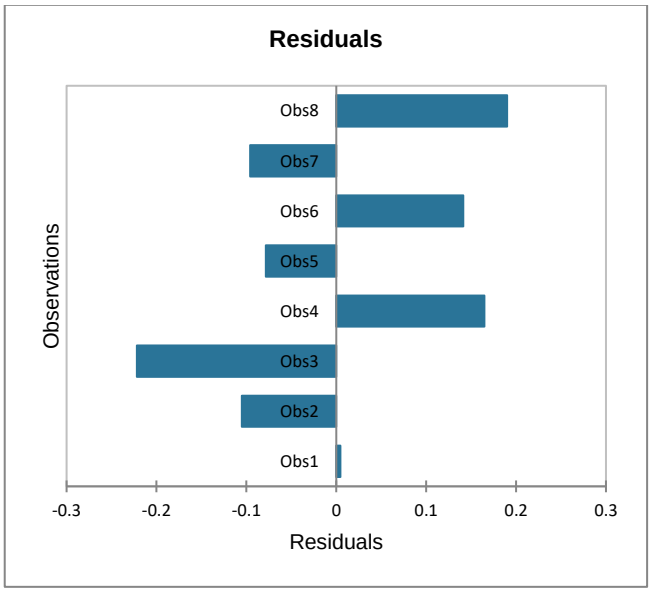

Figure B.4. Residuals of observations for VM 1 concerning all ferrimagnetic Fe_3O_4/water nanofluids

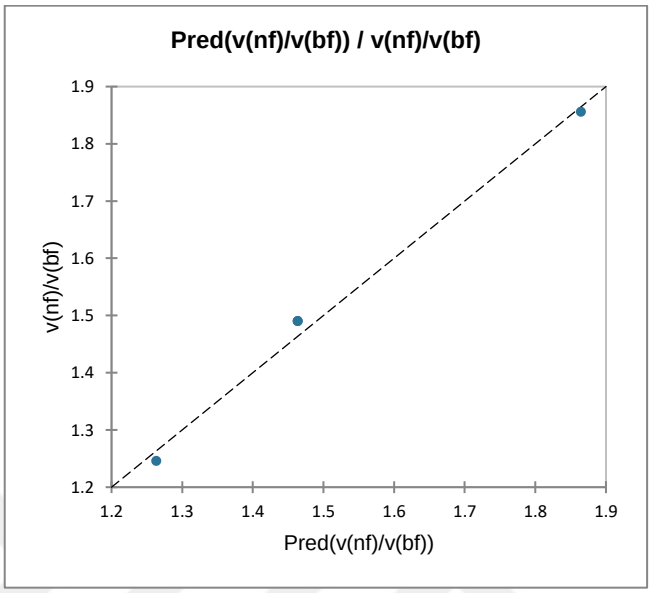

Figure B.5. The compatibility of predicted values with measured values for VM 1 concerning 450kDa PAA coated ferrimagnetic Fe_3O_4/water nanofluids

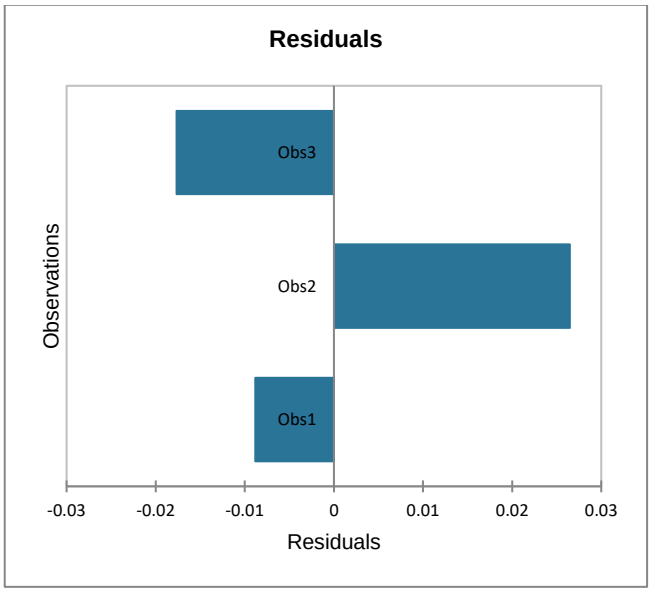

Figure B.6. Residuals of observations for VM 1 concerning 450kDa PAA coated ferrimagnetic Fe_3O_4/water nanofluids

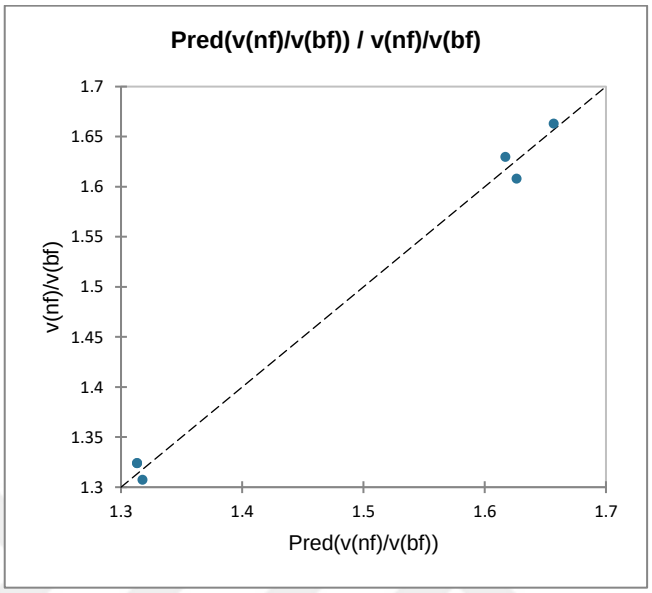

Figure B.7. The compatibility of predicted values with measured values for VM 1 concerning 250kDa PAA coated ferrimagnetic Fe_3O_4/water nanofluids

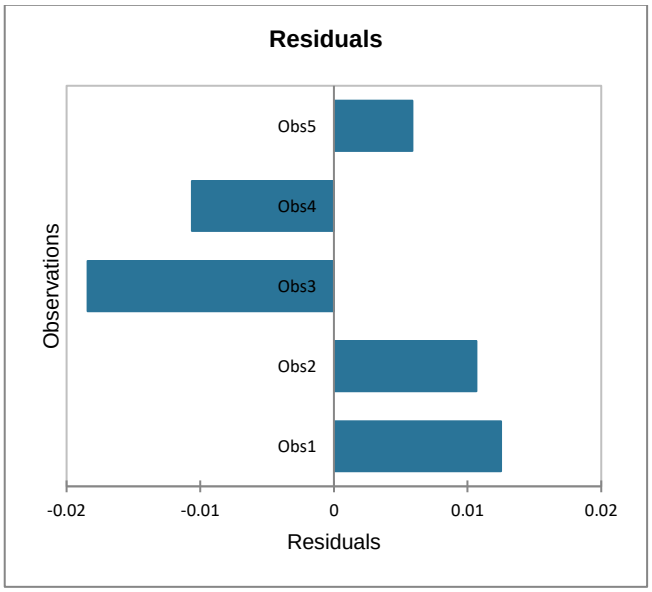

Figure B.8. Residuals of observations for VM 1 concerning 250kDa PAA coated ferrimagnetic Fe_3O_4/water nanofluids

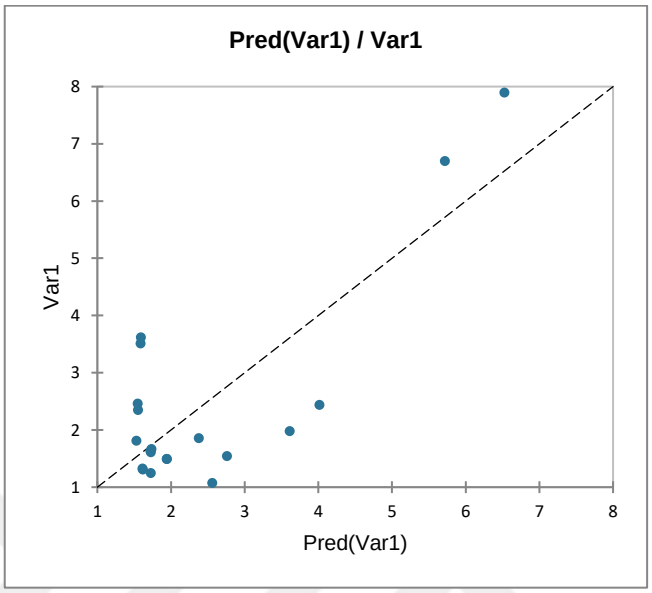

Figure B.9. The compatibility of predicted values with measured values for VM 1 concerning all Fe_3O_4/water nanofluids

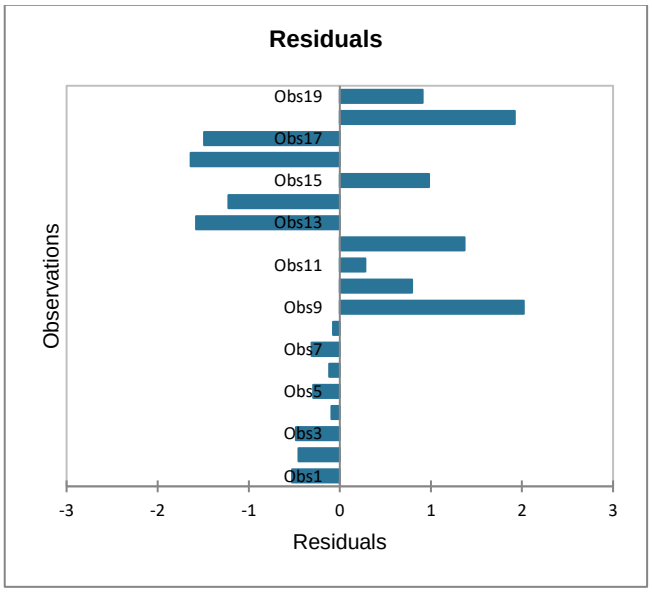

Figure B.10. Residuals of observations for VM 1 concerning all Fe_3O_4/water nanofluids

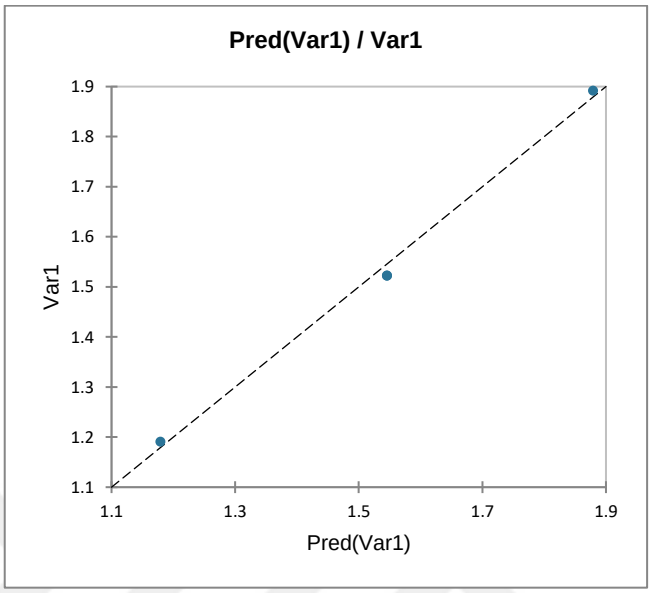

Figure B.11. The compatibility of predicted values with measured values for VM 1 concerning CuO/water nanofluids

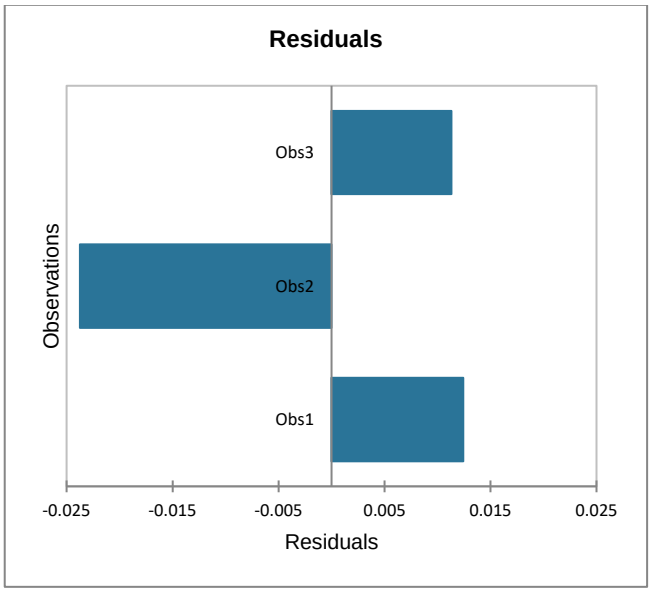

Figure B.12. Residuals of observations for VM 1 concerning CuO/water nanofluids

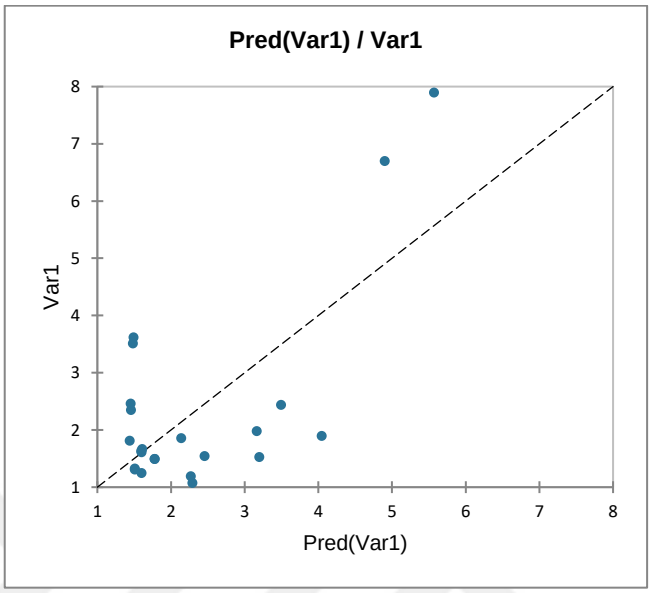

Figure B.13. The compatibility of predicted values with measured values for VM 1 concerning all Fe_3O_4 and CuO/water nanofluids together

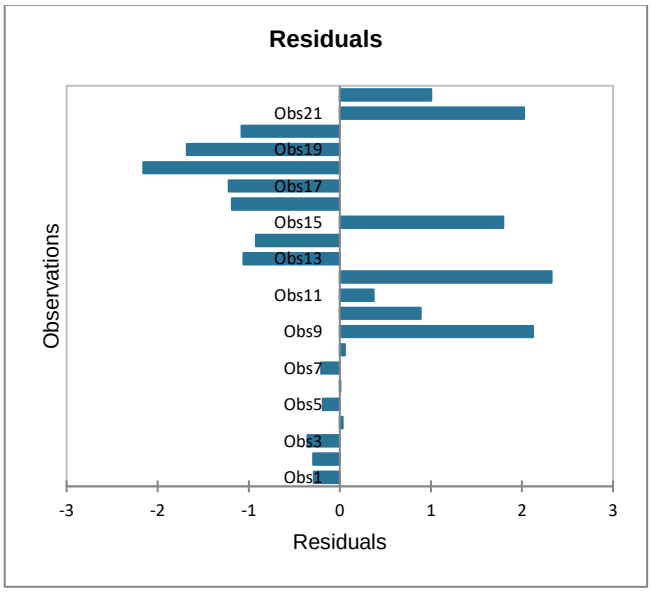

Figure B.14. Residuals of observations for VM 1 concerning all Fe_3O_4 and CuO/water nanofluids together

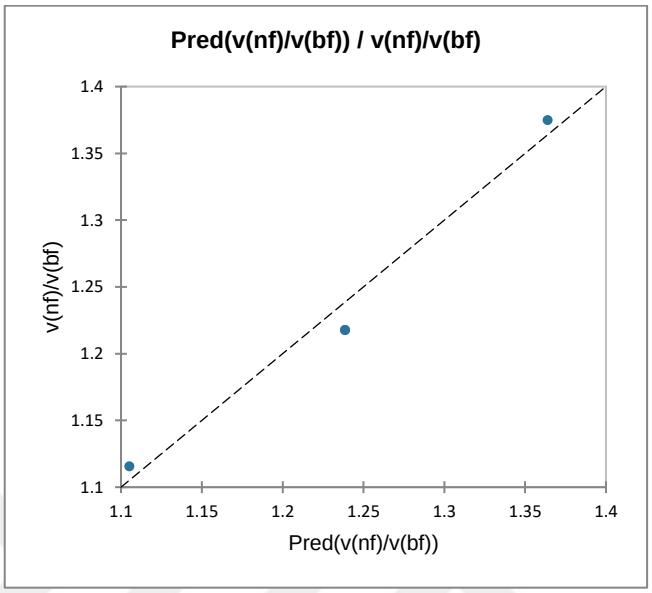

Figure B.15. The compatibility of predicted values with measured values for VM 1 concerning CuO/ethylene glycol nanofluids

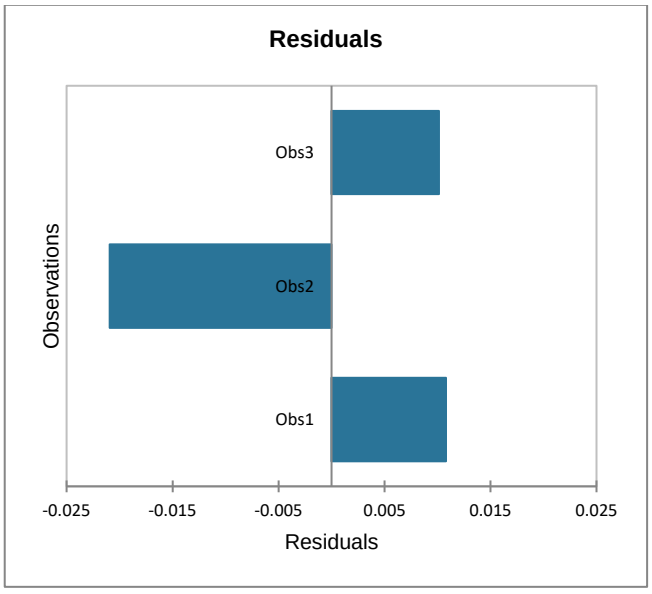

Figure B.16. Residuals of observations for VM 1 concerning CuO/ethylene glycol nanofluids

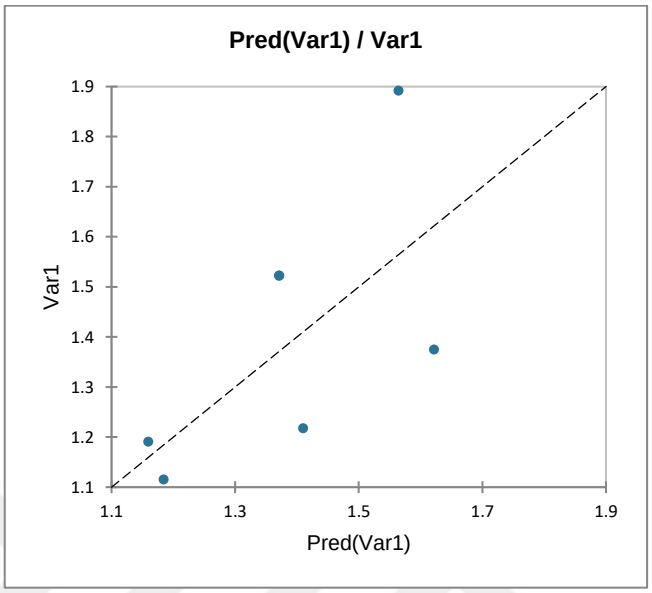

Figure B.17. The compatibility of predicted values with measured values for VM 1 concerning all CuO nanofluids

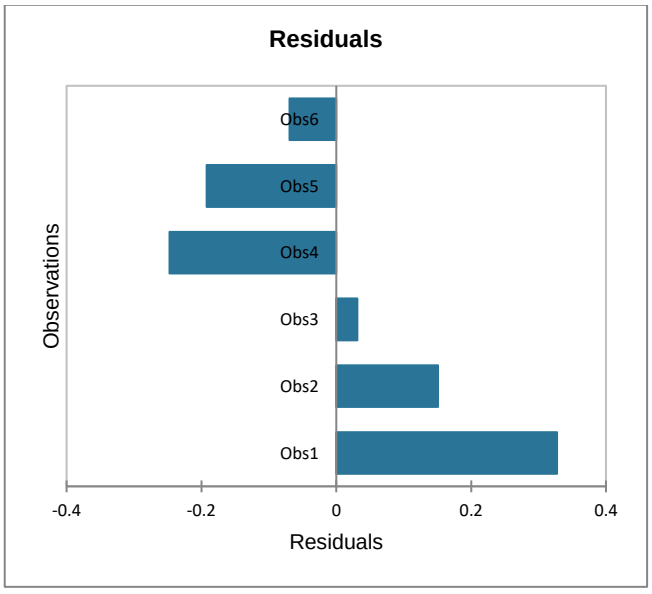

Figure B.18. Residuals of observations for VM 1 concerning all CuO nanofluids

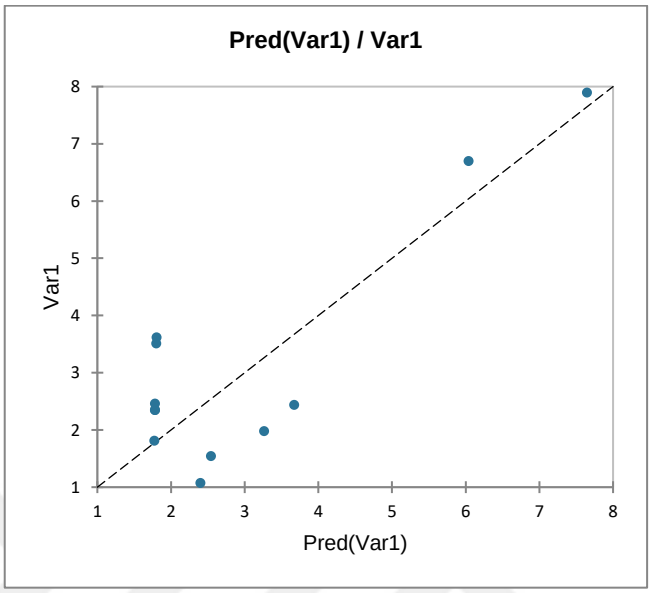

Figure B.19. The compatibility of predicted values with measured values for VM 2 concerning all superparamagnetic Fe_3O_4/water nanofluids

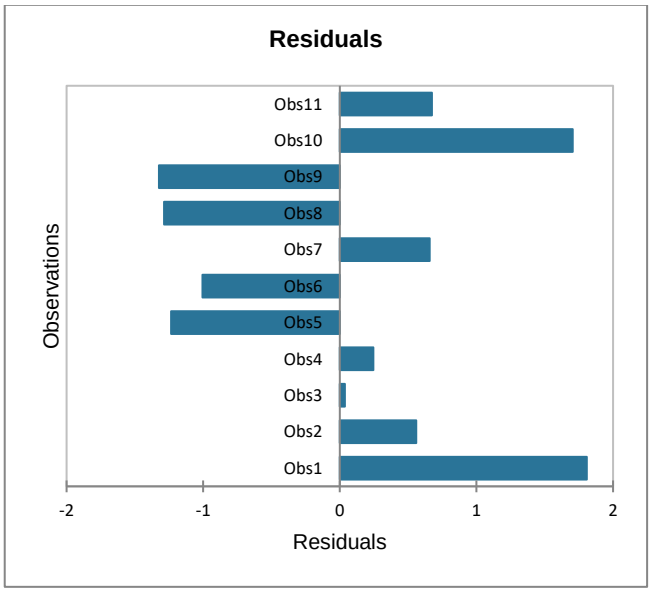

Figure B.20. Residuals of observations for VM 2 concerning all superparamagnetic Fe_3O_4/water nanofluids

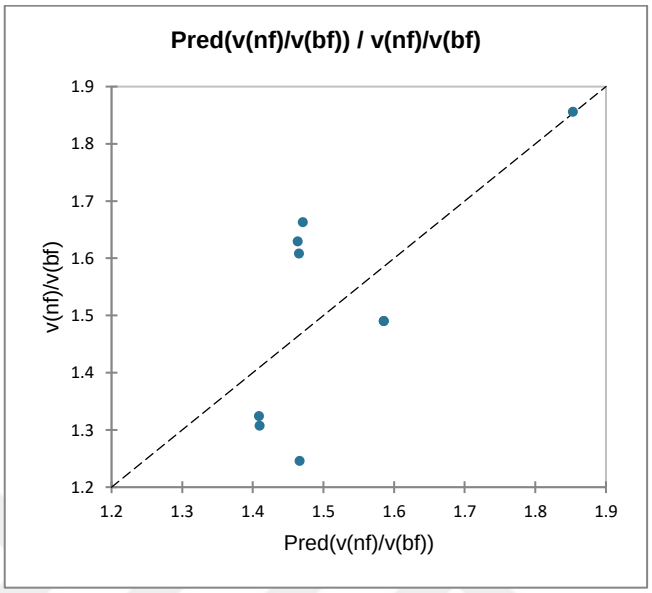

Figure B.21. The compatibility of predicted values with measured values for VM 2 concerning all ferrimagnetic Fe_3O_4/water nanofluids

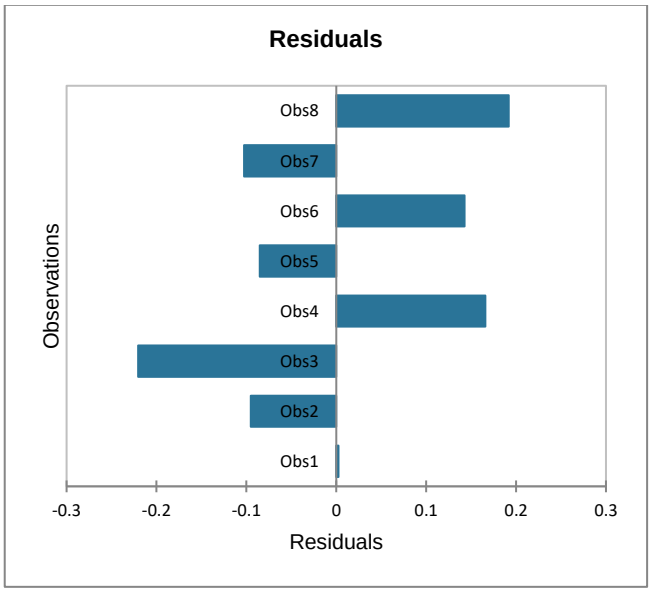

Figure B.22. Residuals of observations for VM 2 concerning all ferrimagnetic Fe_3O_4/water nanofluids

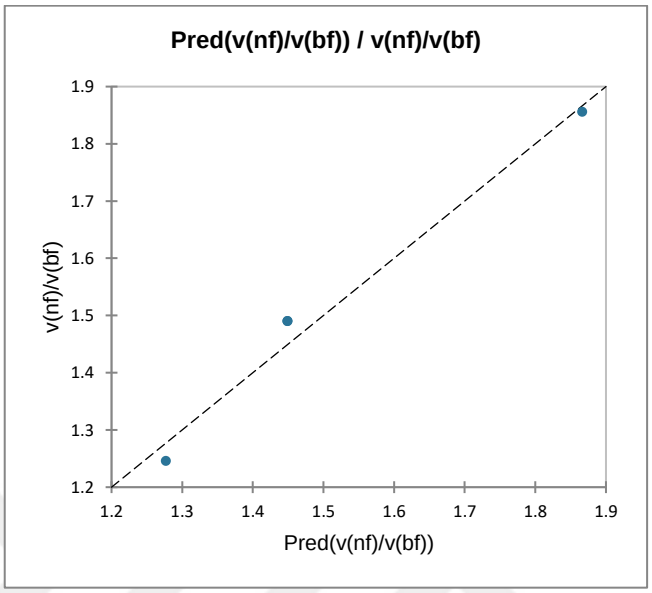

Figure B.23. The compatibility of predicted values with measured values for VM 2 concerning 450kDa PAA coated ferrimagnetic Fe_3O_4/water nanofluids

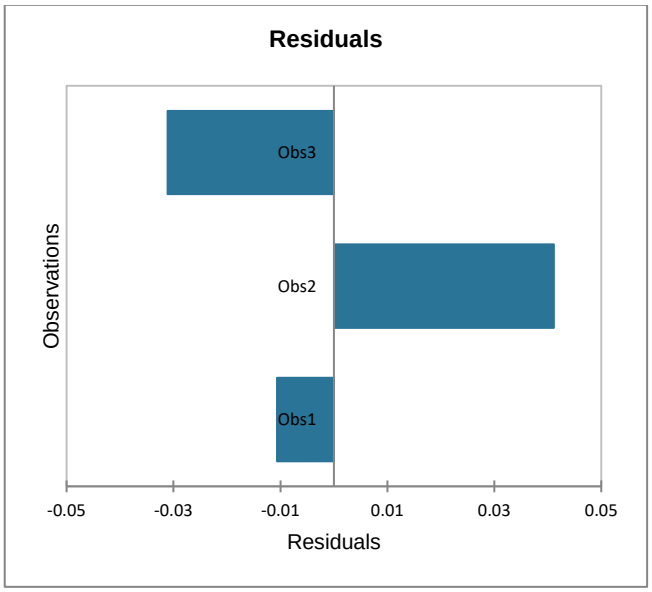

Figure B.24. Residuals of observations for VM 2 concerning 450kDa PAA coated ferrimagnetic Fe_3O_4/water nanofluids

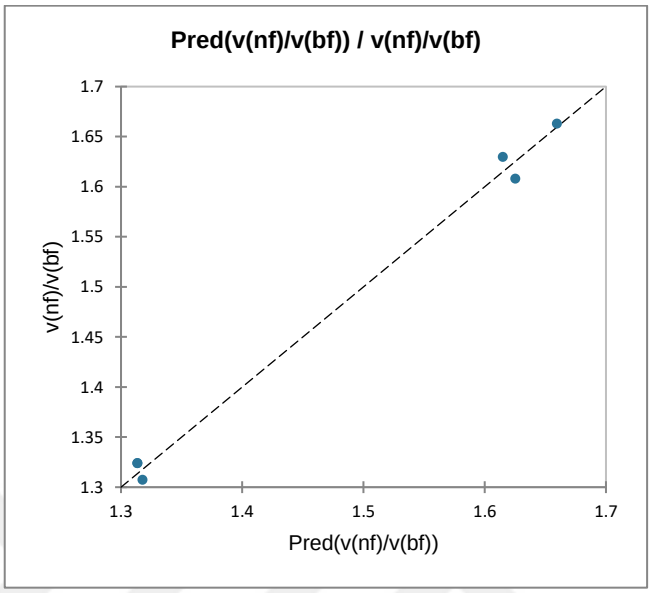

Figure B.25. The compatibility of predicted values with measured values for VM 2 concerning 250kDa PAA coated ferrimagnetic Fe_3O_4/water nanofluids

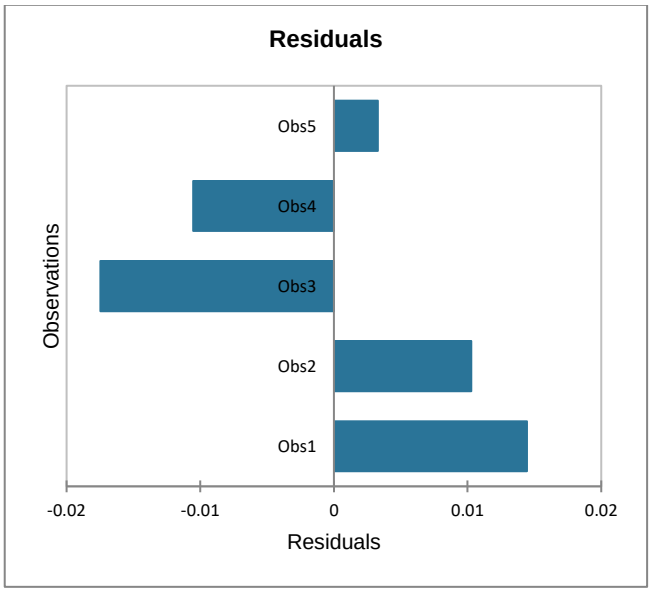

Figure B.26. Residuals of observations for VM 2 concerning 250kDa PAA coated ferrimagnetic Fe_3O_4/water nanofluids

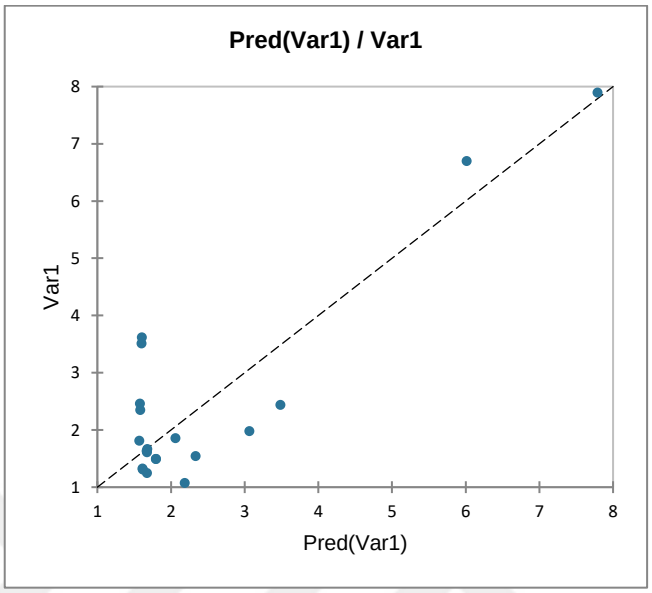

Figure B.27. The compatibility of predicted values with measured values for VM 2 concerning all Fe_3O_4/water nanofluids

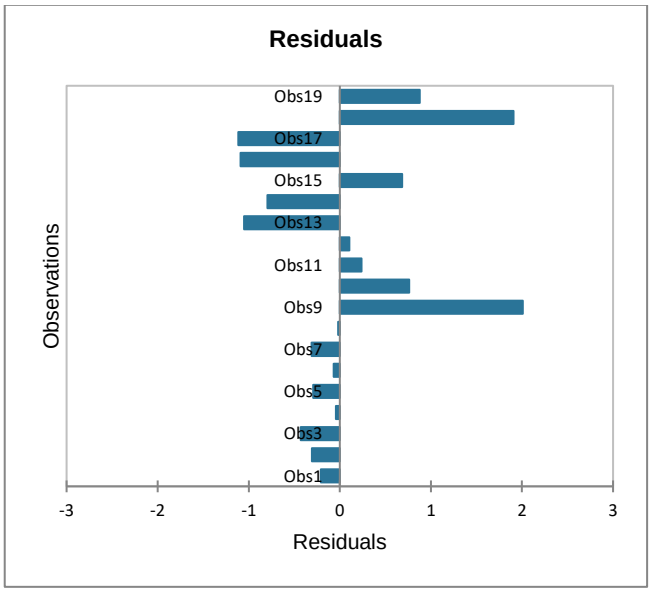

Figure B.28. Residuals of observations for VM 2 concerning all Fe_3O_4/water nanofluids

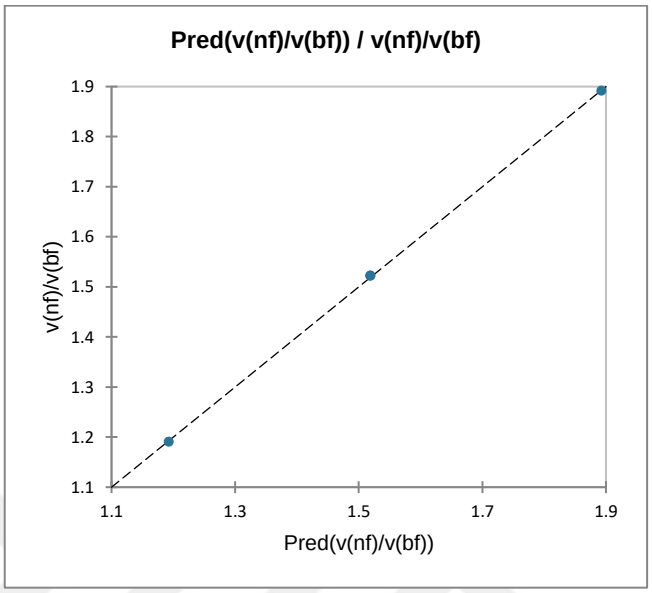

Figure B.29. The compatibility of predicted values with measured values for VM 2 concerning CuO/water nanofluids

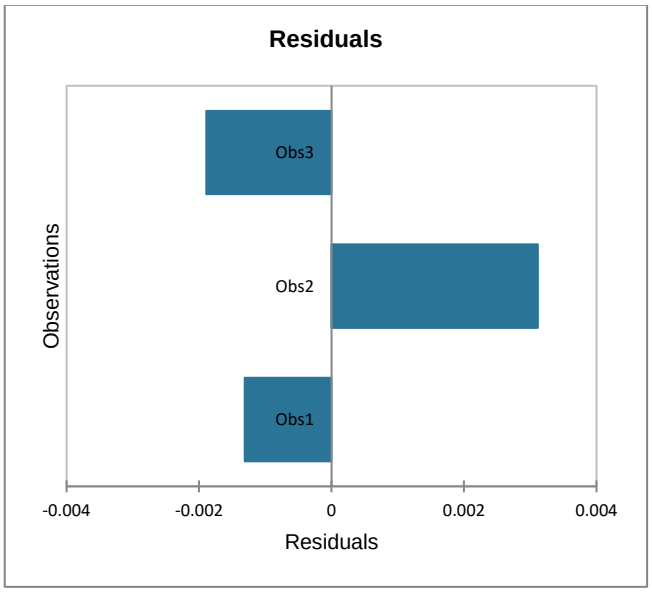

Figure B.30. Residuals of observations for VM 2 concerning CuO/water nanofluids

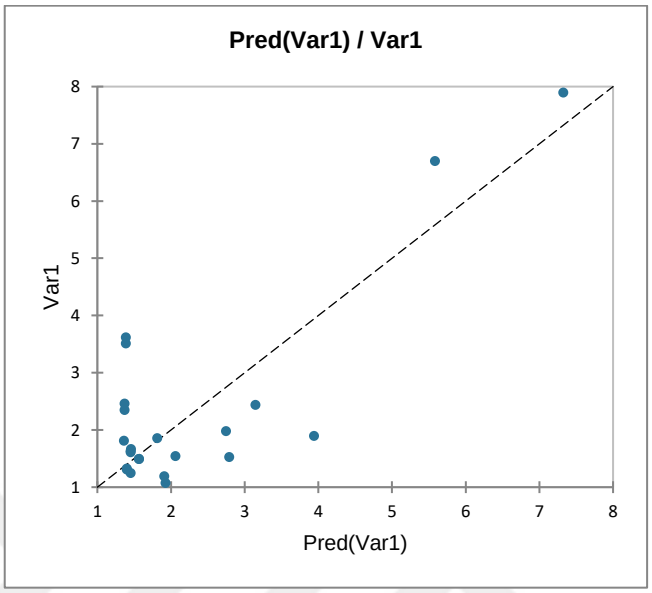

Figure B.31. The compatibility of predicted values with measured values for VM 2 concerning all Fe_3O_4 and CuO/water nanofluids together

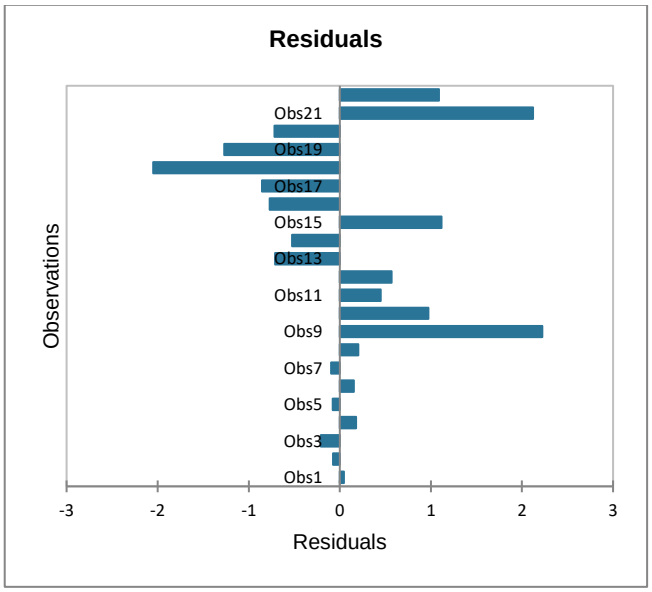

Figure B.32. Residuals of observations for VM 2 concerning all Fe_3O_4 and CuO/water nanofluids together

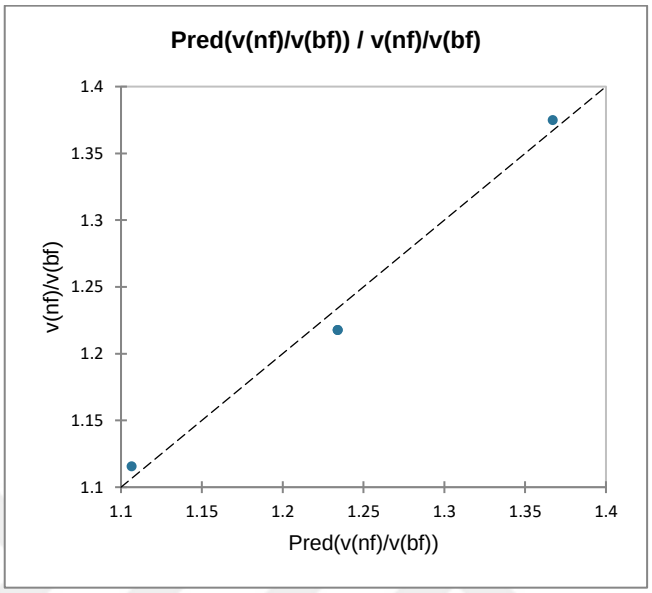

Figure B.33. The compatibility of predicted values with measured values for VM 2 concerning CuO/ethylene glycol nanofluids

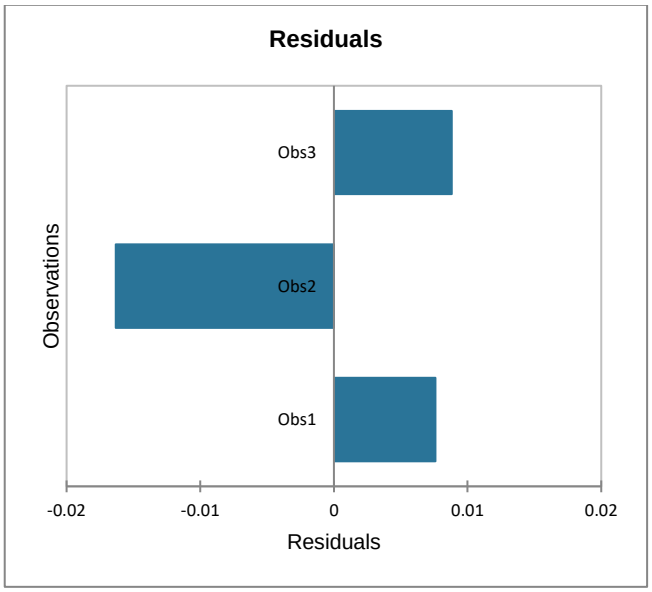

Figure B.34. Residuals of observations for VM 2 concerning CuO/ethylene glycol nanofluids

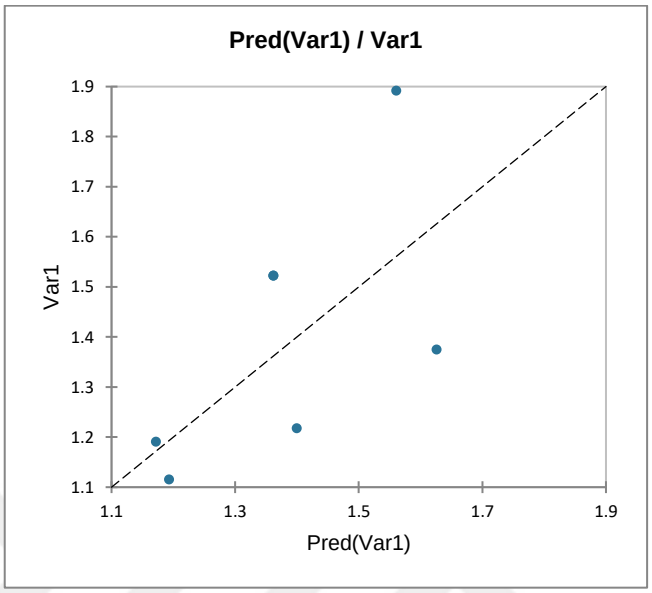

Figure B.35. The compatibility of predicted values with measured values for VM 2 concerning all CuO nanofluids

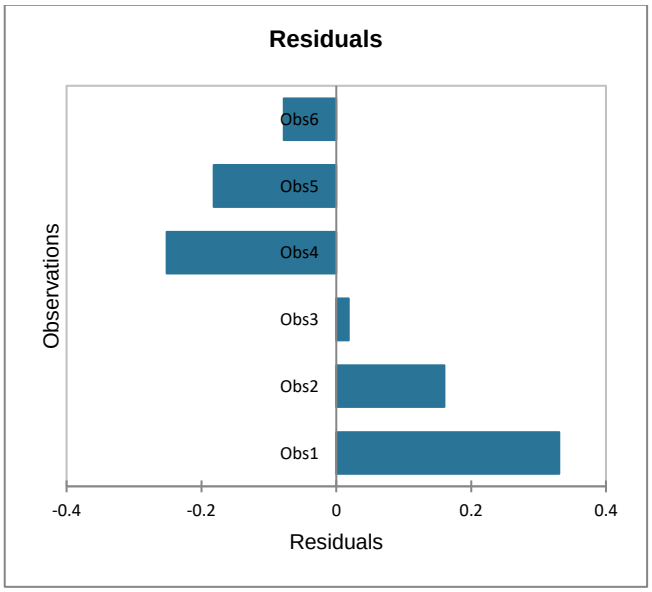

Figure B.36. Residuals of observations for VM 2 concerning all CuO nanofluids

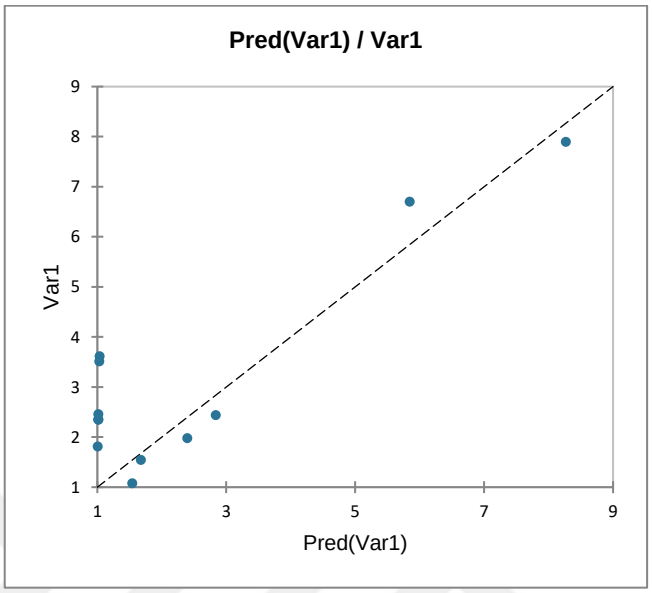

Figure B.37. The compatibility of predicted values with measured values for VM 3 concerning all superparamagnetic Fe_3O_4/water nanofluids

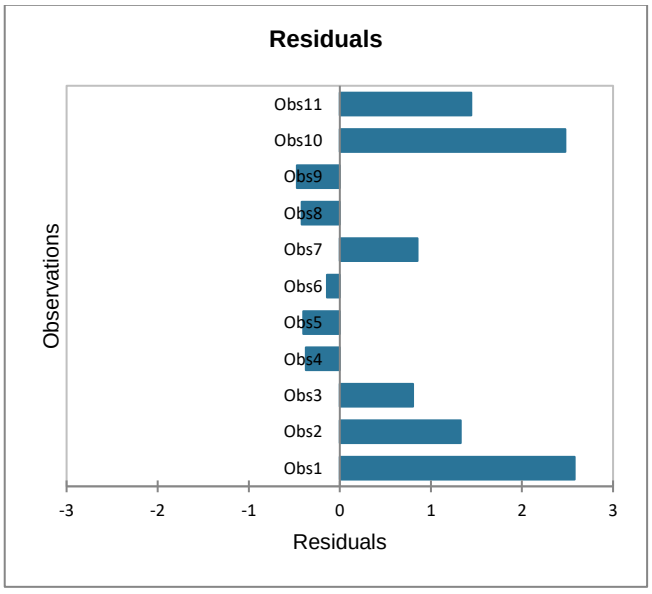

Figure B.38. Residuals of observations for VM 3 concerning all superparamagnetic Fe_3O_4/water nanofluids

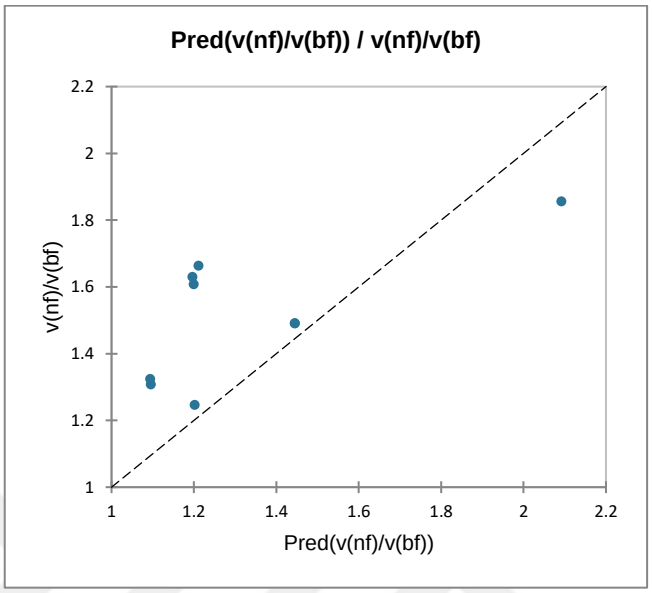

Figure B.39. The compatibility of predicted values with measured values for VM 3 concerning all ferrimagnetic Fe_3O_4/water nanofluids

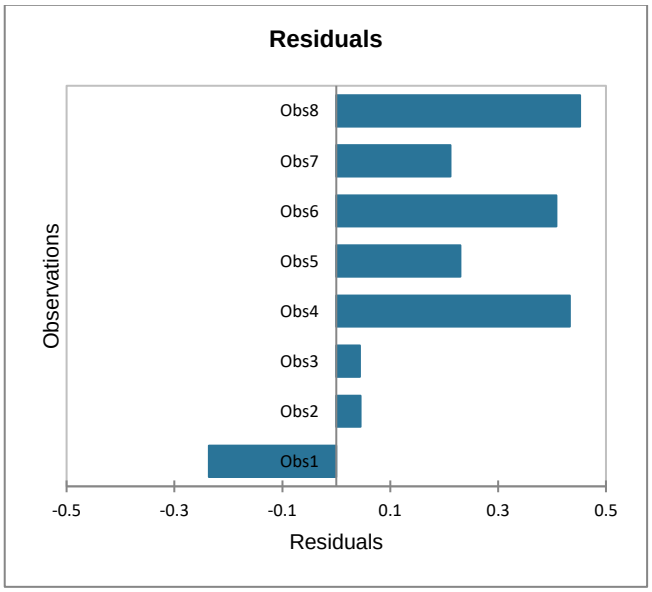

Figure B.40. Residuals of observations for VM 3 concerning all ferrimagnetic Fe_3O_4/water nanofluids

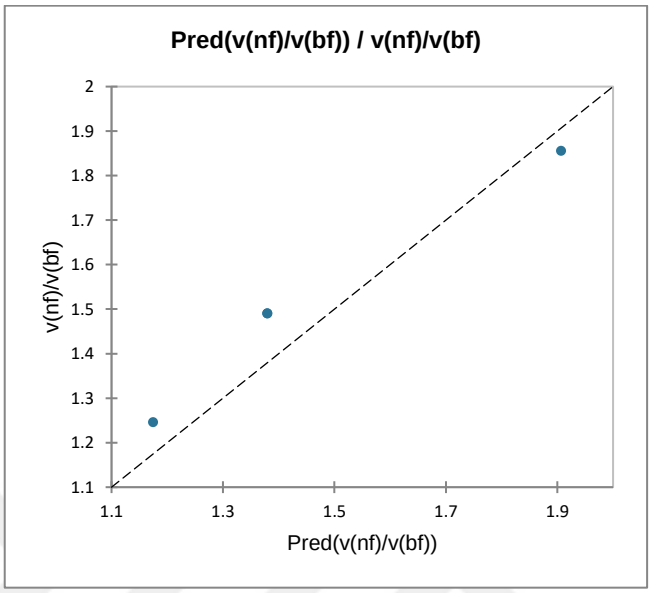

Figure B.41. The compatibility of predicted values with measured values for VM 3 concerning 450kDa PAA coated ferrimagnetic Fe_3O_4/water nanofluids

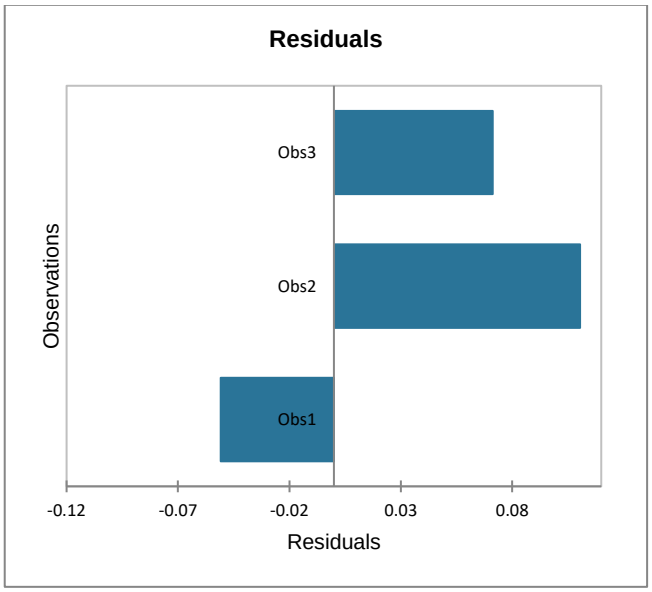

Figure B.42. Residuals of observations for VM 3 concerning 450kDa PAA coated ferrimagnetic Fe_3O_4/water nanofluids

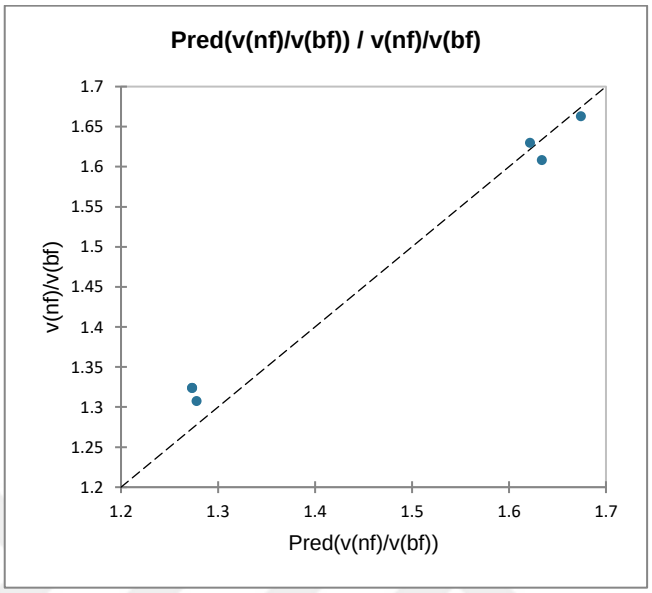

Figure B.43. The compatibility of predicted values with measured values for VM 3 concerning 250kDa PAA coated ferrimagnetic Fe_3O_4/water nanofluids

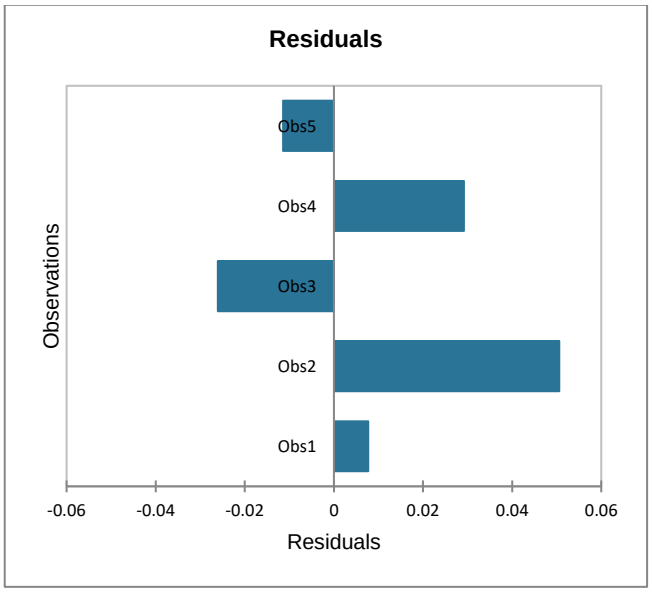

Figure B.44. Residuals of observations for VM 3 concerning 250kDa PAA coated ferrimagnetic Fe_3O_4/water nanofluids

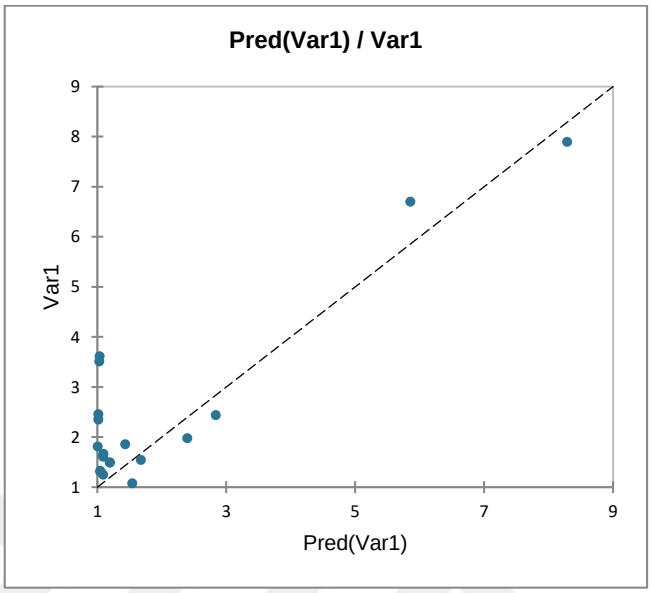

Figure B.45. The compatibility of predicted values with measured values for VM 3 concerning all Fe_3O_4/water nanofluids

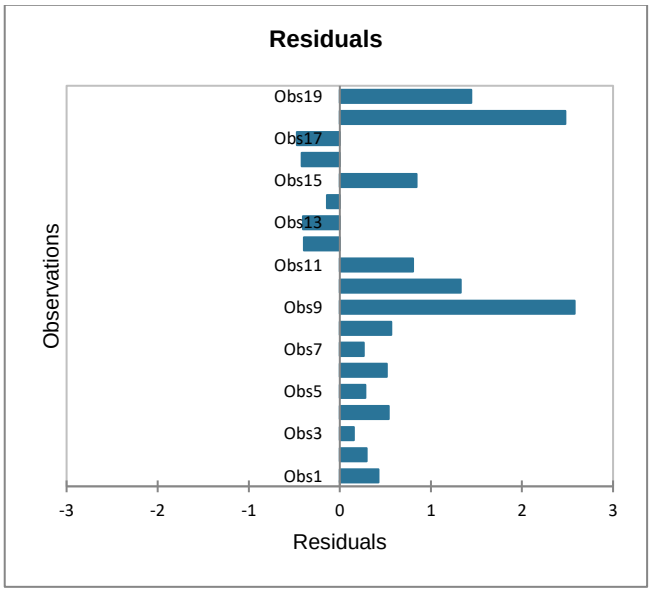

Figure B.46. Residuals of observations for VM 3 concerning all Fe_3O_4/water nanofluids

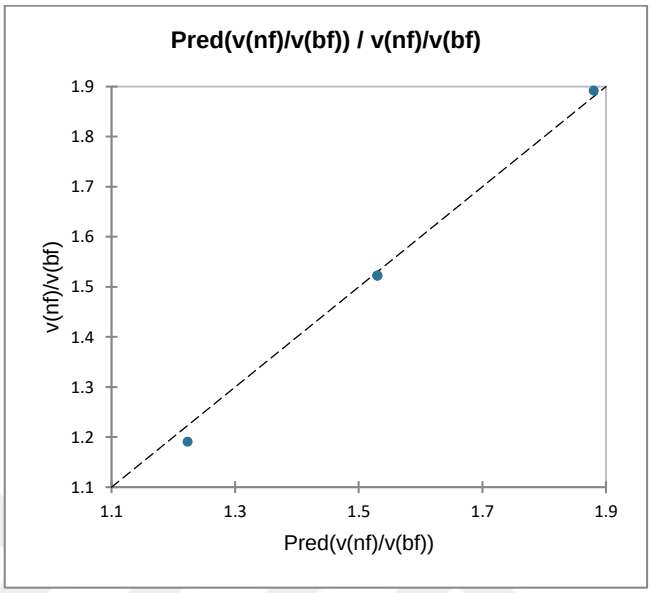

Figure B.47. The compatibility of predicted values with measured values for VM 3 concerning CuO/water nanofluids

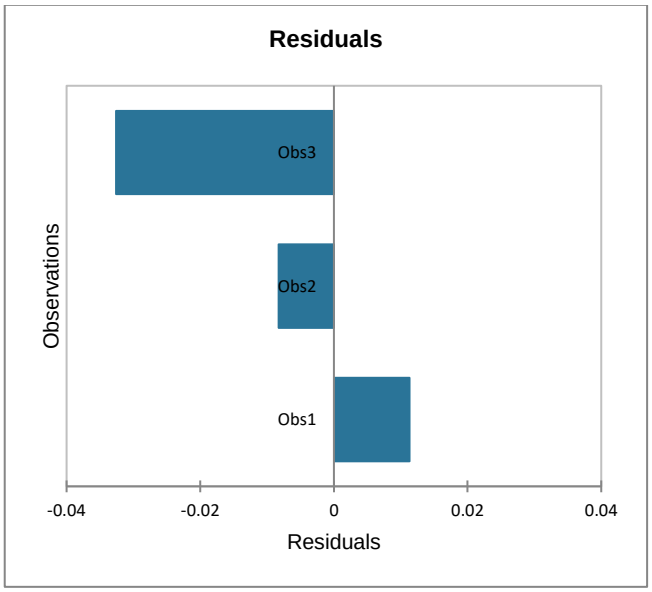

Figure B.48. Residuals of observations for VM 3 concerning CuO/water nanofluids

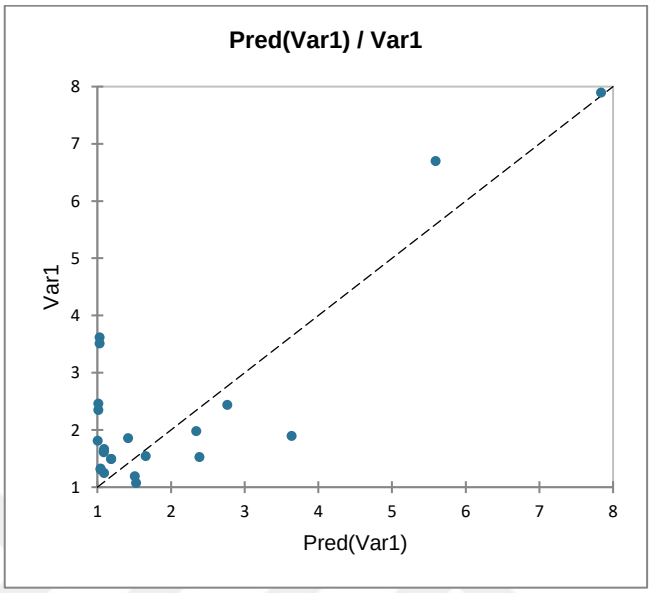

Figure B.49. The compatibility of predicted values with measured values for VM 3 concerning all Fe_3O_4 and CuO/water nanofluids together

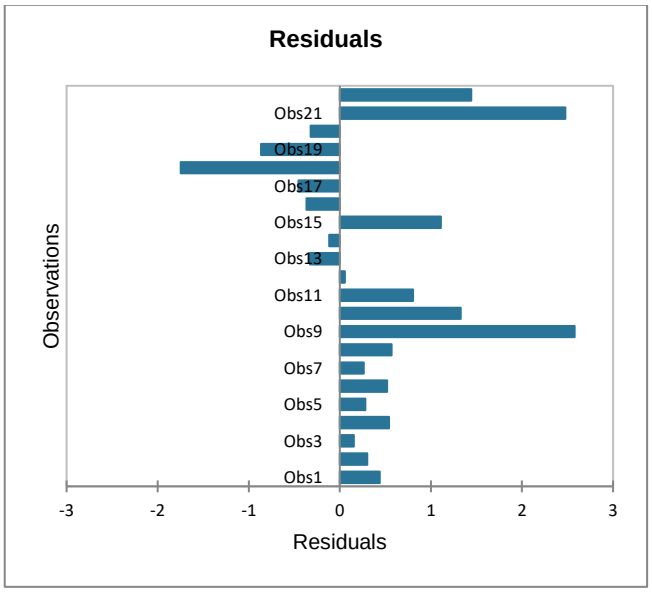

Figure B.50. Residuals of observations for VM 3 concerning all Fe_3O_4 and CuO/water nanofluids together

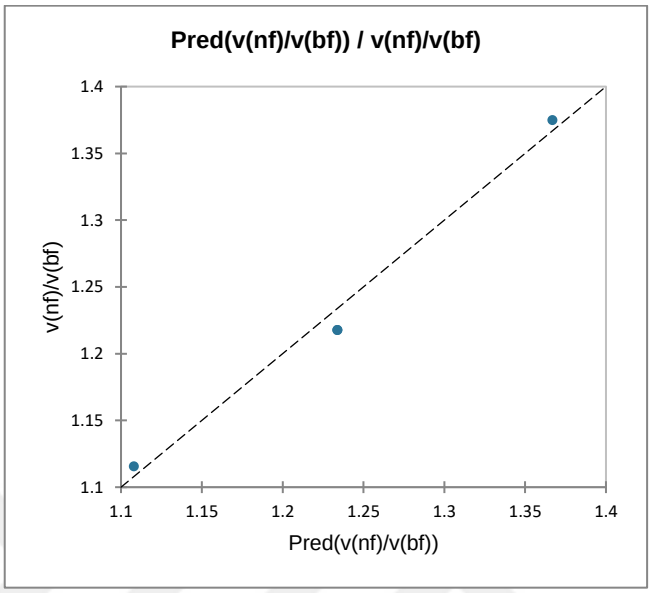

Figure B.51. The compatibility of predicted values with measured values for VM 3 concerning CuO/ethylene glycol nanofluids

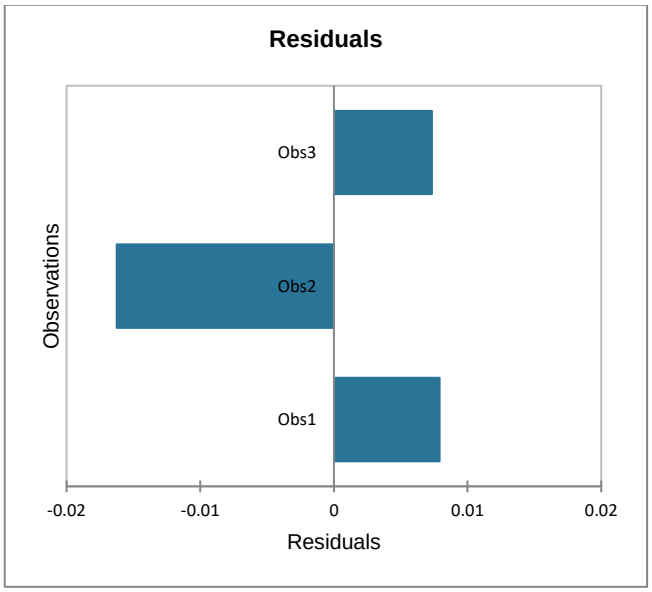

Figure B.52. Residuals of observations for VM 3 concerning CuO/ethylene glycol nanofluids

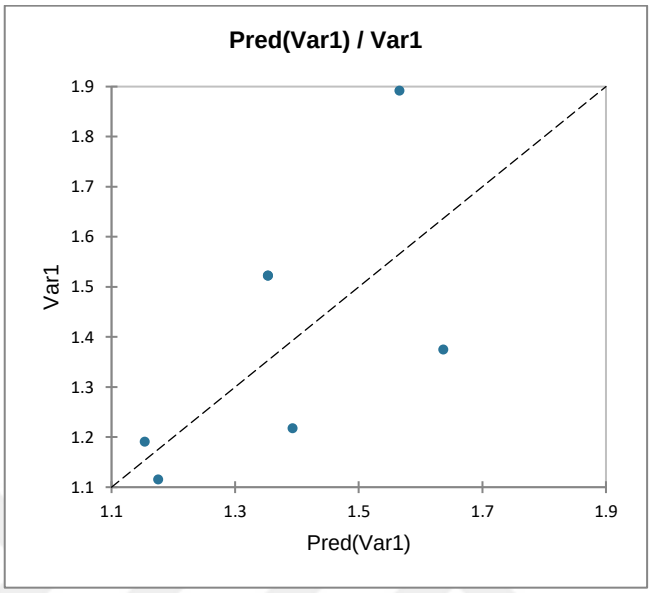

Figure B.53. The compatibility of predicted values with measured values for VM 3 concerning all CuO nanofluids

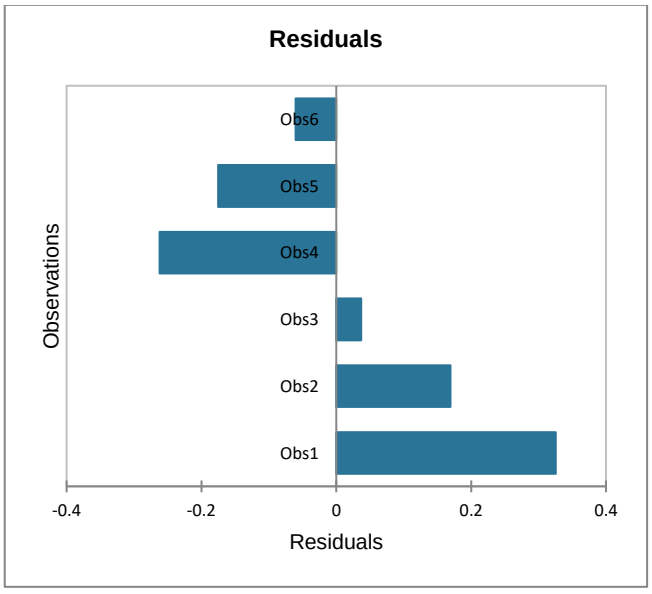

Figure B.54. Residuals of observations for VM 3 concerning all CuO nanofluids

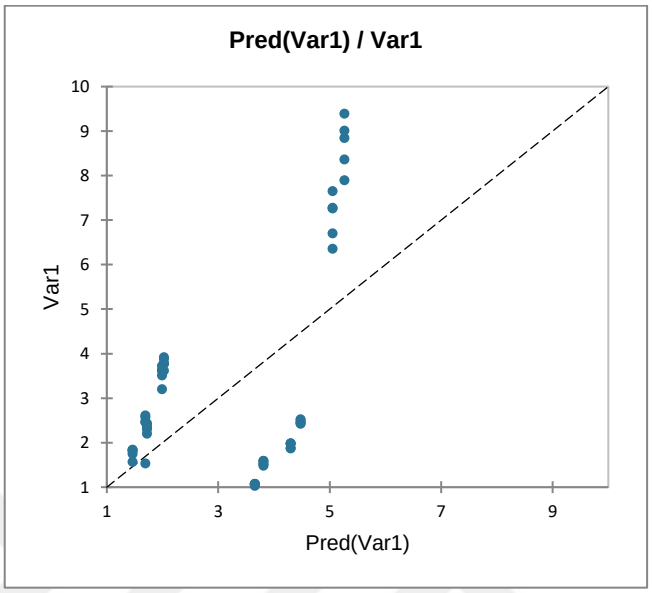

Figure B.55. The compatibility of predicted values with measured values for VM 4 concerning all superparamagnetic Fe_3O_4/water nanofluids

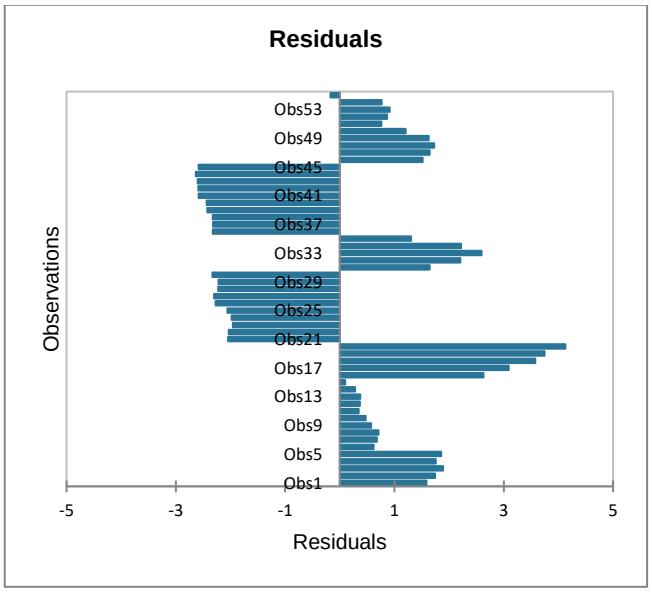

Figure B.56. Residuals of observations for VM 4 concerning all superparamagnetic Fe_3O_4/water nanofluids

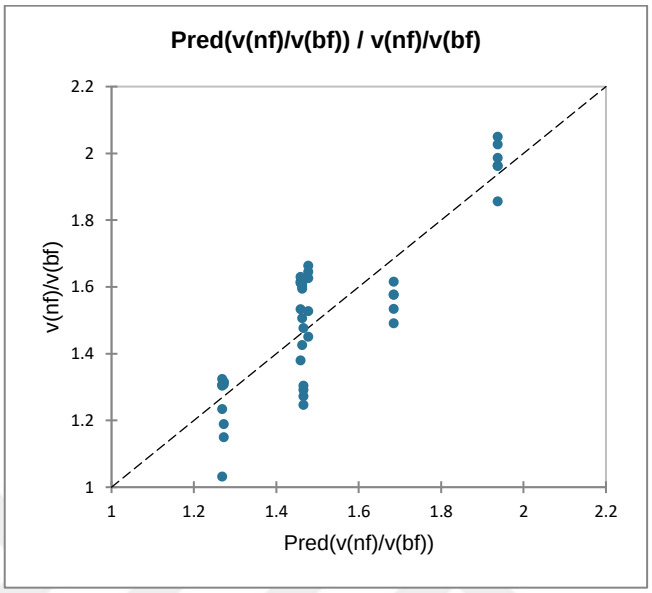

Figure B.57. The compatibility of predicted values with measured values for VM 4 concerning all ferrimagnetic Fe_3O_4/water nanofluids

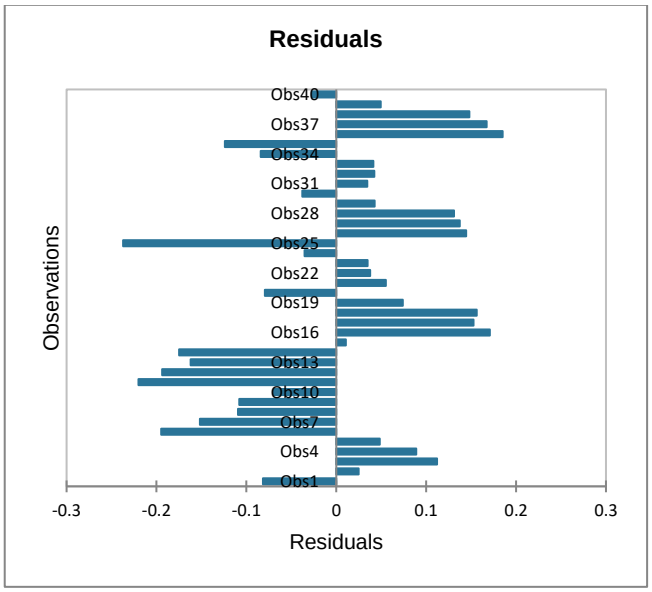

Figure B.58. Residuals of observations for VM 4 concerning all ferrimagnetic Fe_3O_4/water nanofluids

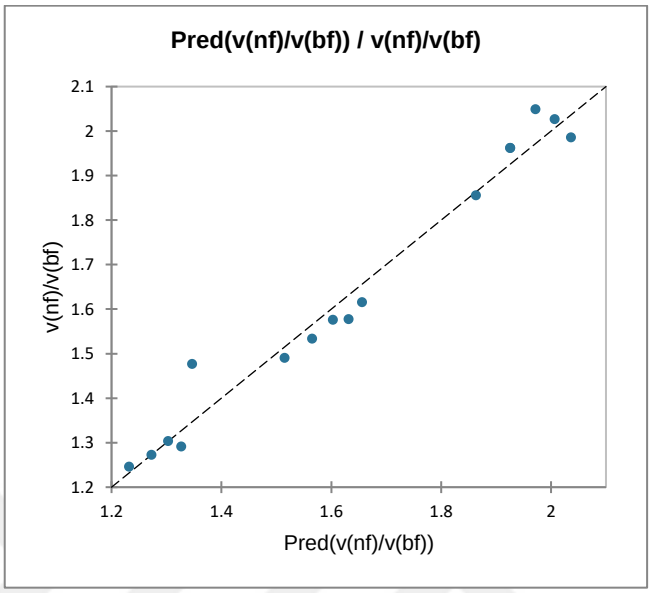

Figure B.59. The compatibility of predicted values with measured values for VM 4 concerning 450kDa PAA coated ferrimagnetic Fe_3O_4/water nanofluids

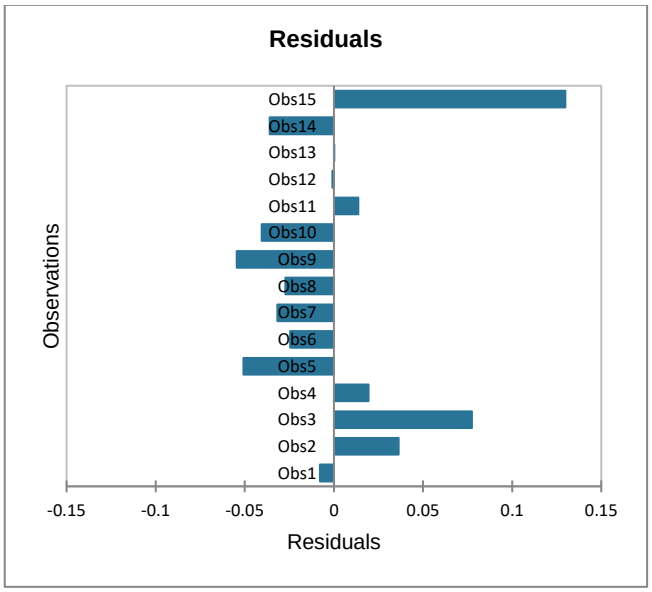

Figure B.60. Residuals of observations for VM 4 concerning 450kDa PAA coated ferrimagnetic Fe_3O_4/water nanofluids

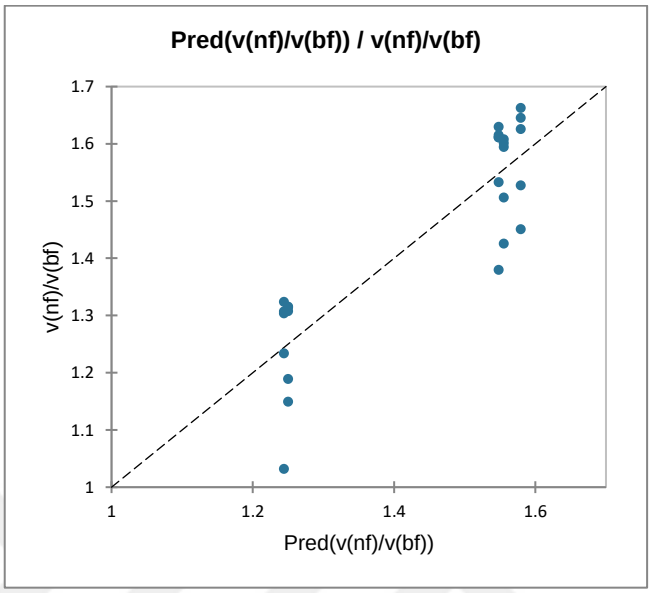

Figure B.61. The compatibility of predicted values with measured values for VM 4 concerning 250kDa PAA coated ferrimagnetic Fe_3O_4/water nanofluids

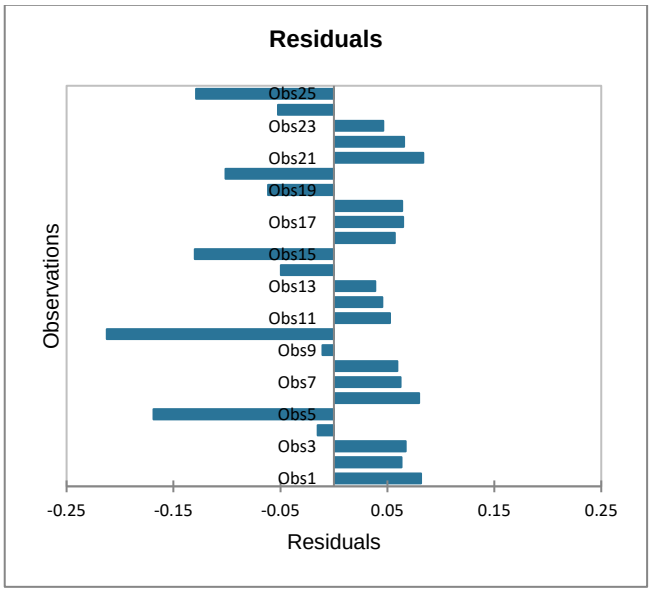

Figure B.62. Residuals of observations for VM 4 concerning 250kDa PAA coated ferrimagnetic Fe_3O_4/water nanofluids

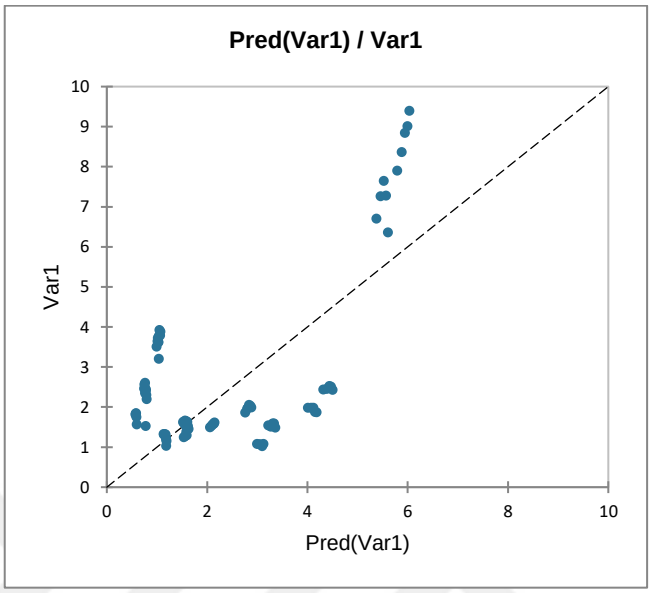

Figure B.63. The compatibility of predicted values with measured values for VM 4 concerning all Fe_3O_4/water nanofluids

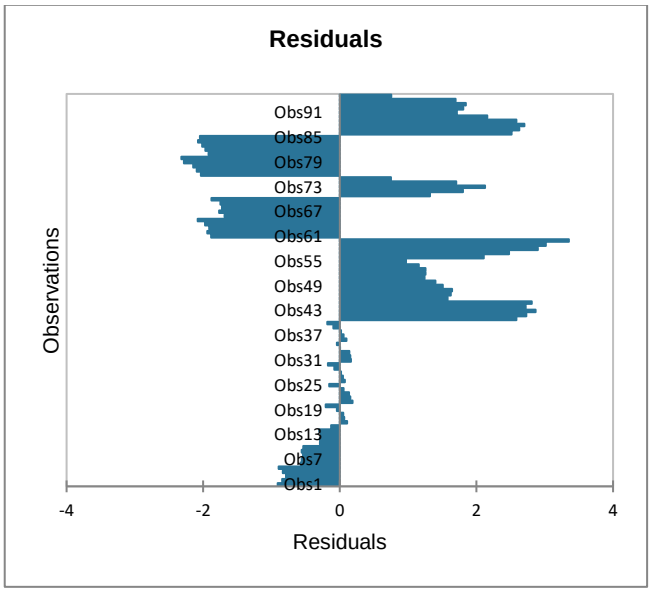

Figure B.64. Residuals of observations for VM 4 concerning all Fe_3O_4/water nanofluids

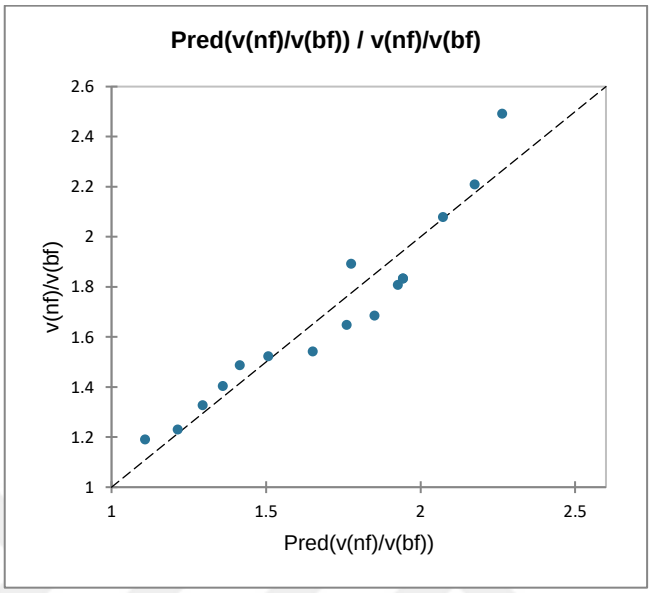

Figure B.65. The compatibility of predicted values with measured values for VM 3 concerning CuO/water nanofluids

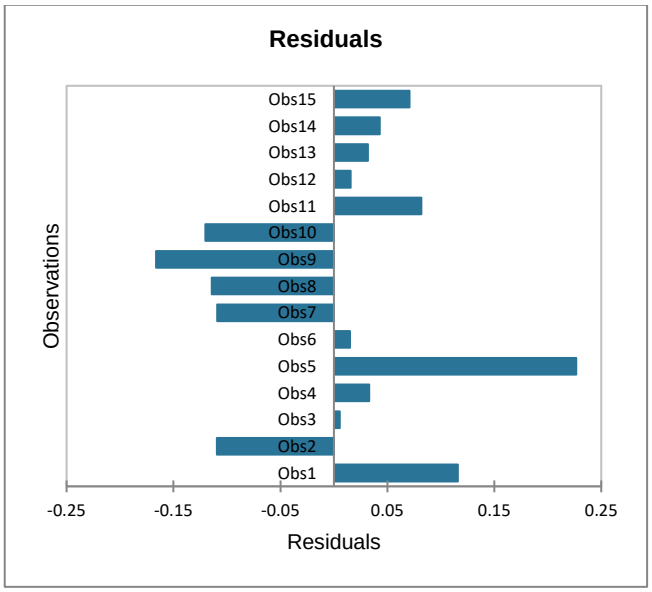

Figure B.66. Residuals of observations for VM 4 concerning CuO/water nanofluids

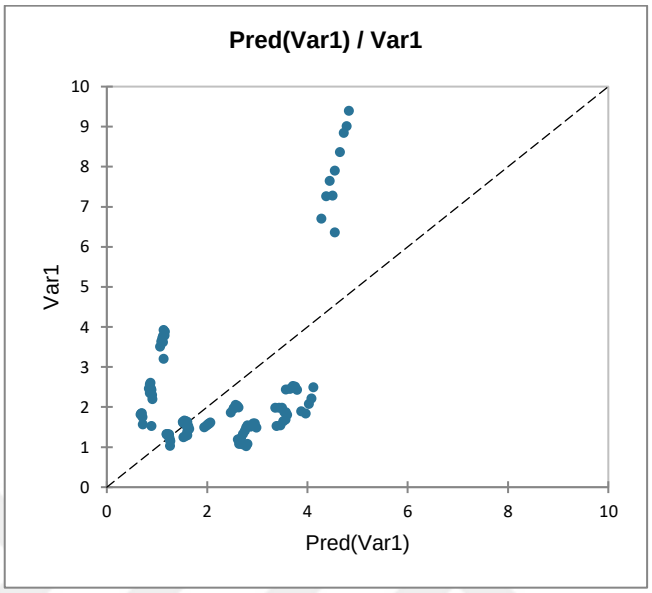

Figure B.67. The compatibility of predicted values with measured values for VM 4 concerning all Fe_3O_4 and CuO/water nanofluids together

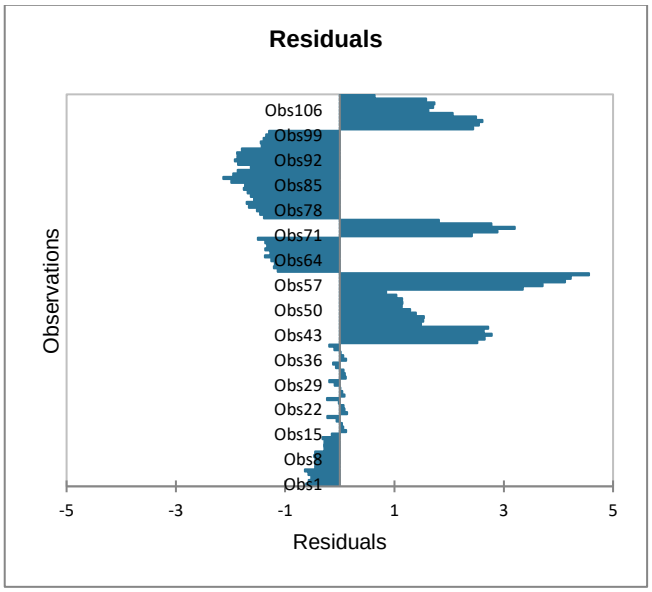

Figure B.68. Residuals of observations for VM 4 concerning all Fe_3O_4 and CuO/water nanofluids together

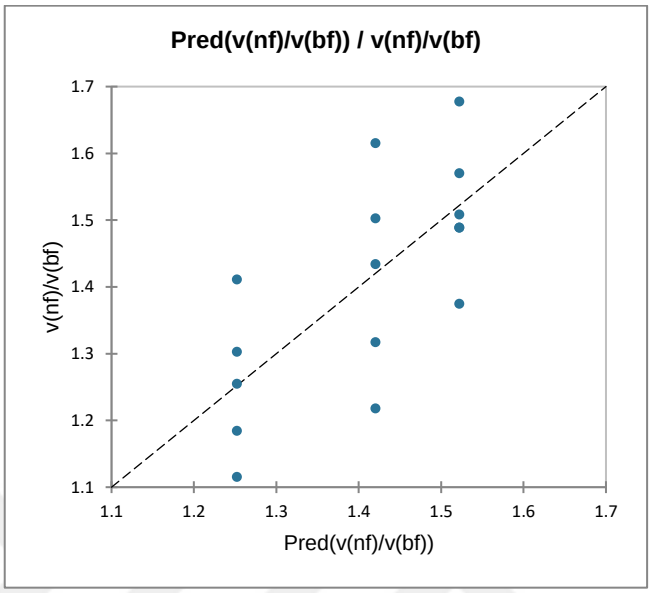

Figure B.69. The compatibility of predicted values with measured values for VM 4 concerning CuO/ethylene glycol nanofluids

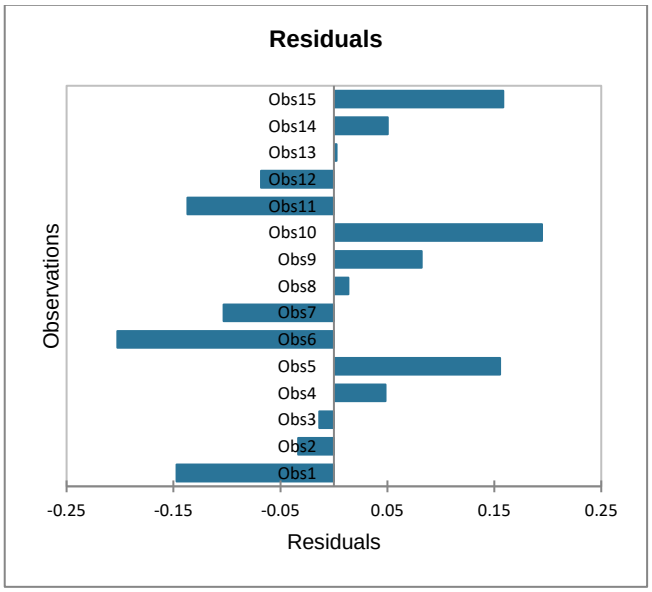

Figure B.70. Residuals of observations for VM 4 concerning CuO/ethylene glycol nanofluids

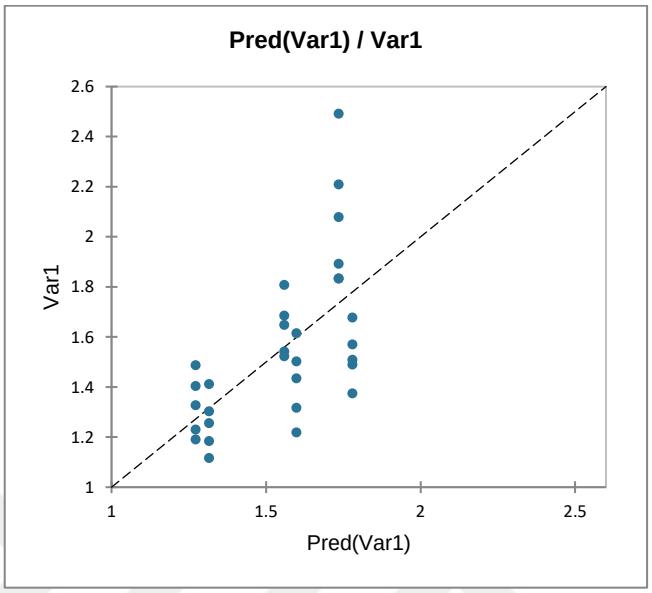

Figure B.71. The compatibility of predicted values with measured values for VM 4 concerning all CuO nanofluids

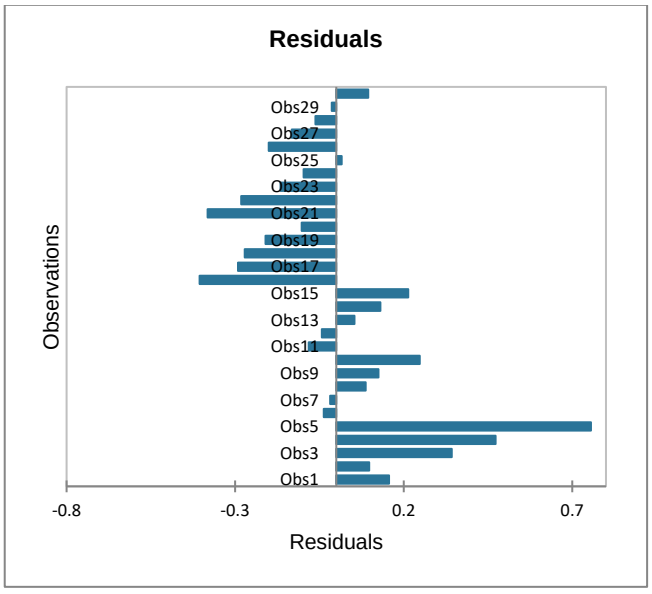

Figure B.72. Residuals of observations for VM 4 concerning all CuO nanofluids

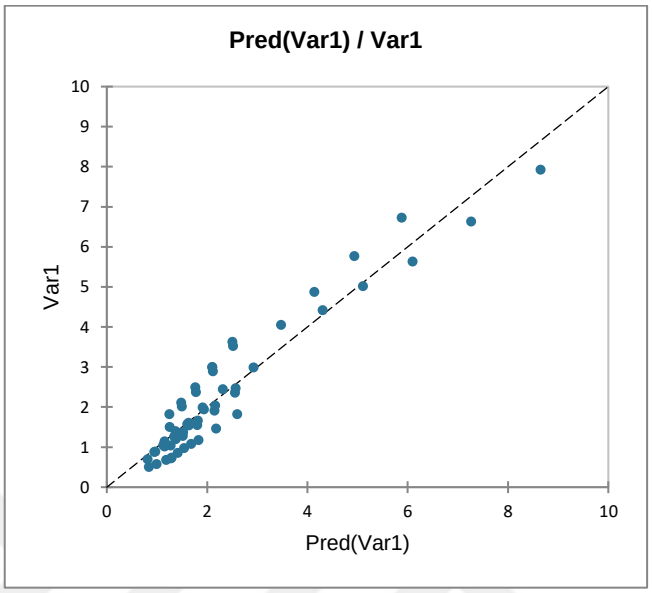

Figure B.73. The compatibility of predicted values with measured values for VM 5 concerning all superparamagnetic Fe_3O_4/water nanofluids

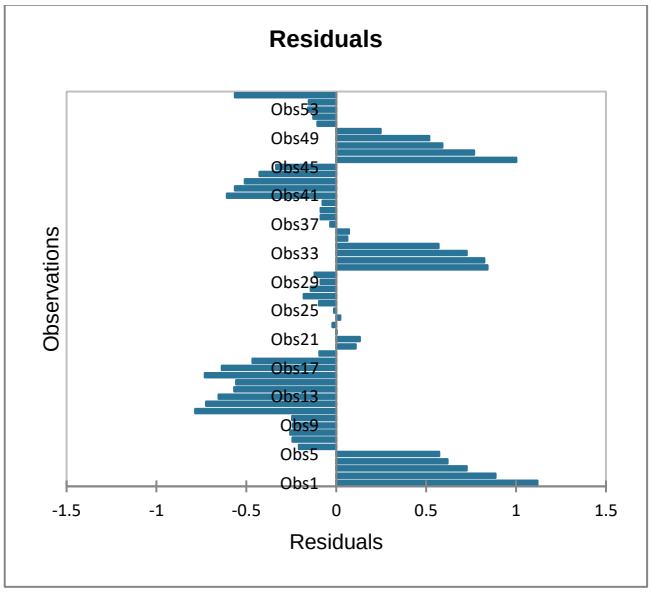

Figure B.74. Residuals of observations for VM 5 concerning all superparamagnetic Fe_3O_4/water nanofluids

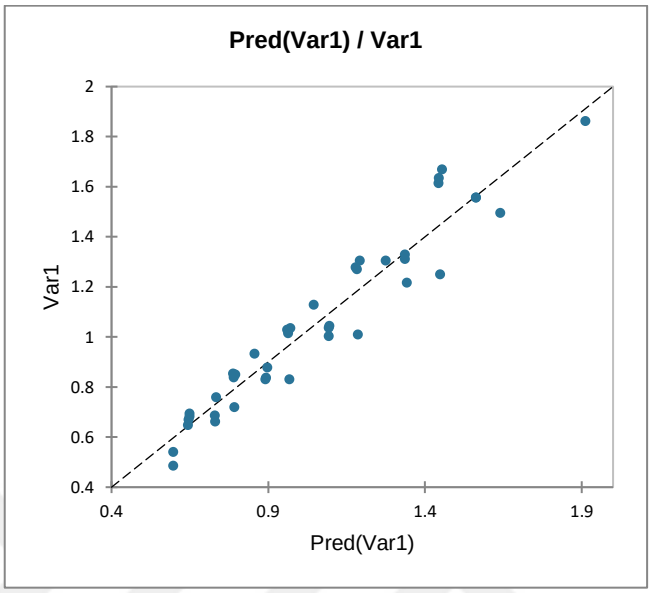

Figure B.75. The compatibility of predicted values with measured values for VM 5 concerning all ferrimagnetic Fe_3O_4/water nanofluids

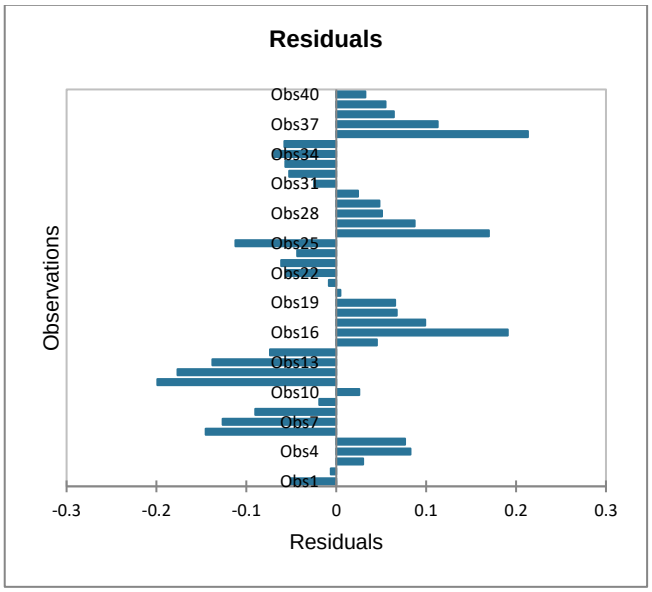

Figure B.76. Residuals of observations for VM 5 concerning all ferrimagnetic Fe_3O_4/water nanofluids

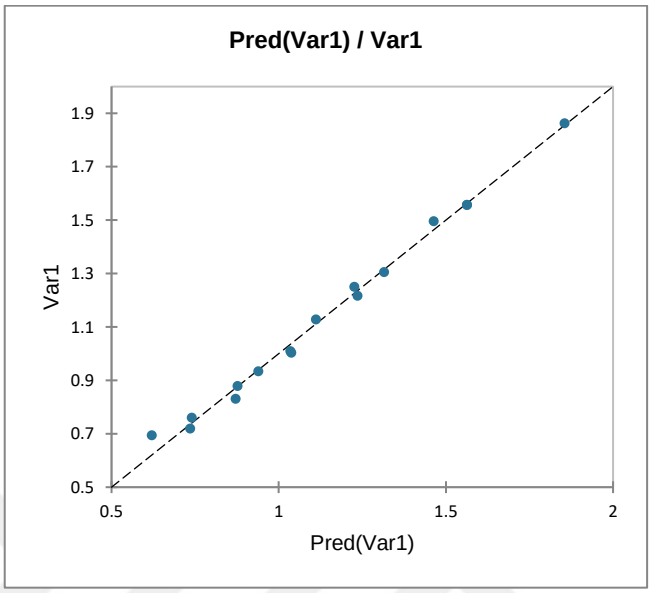

Figure B.77. The compatibility of predicted values with measured values for VM 5 concerning 450kDa PAA coated ferrimagnetic Fe_3O_4/water nanofluids

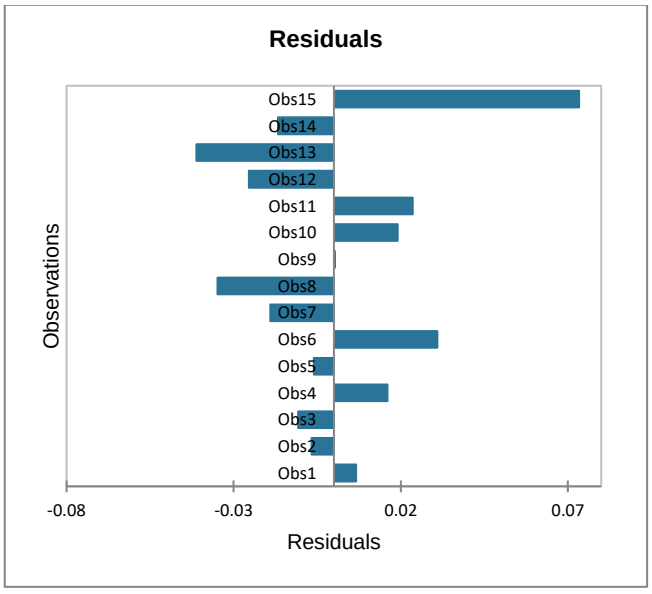

Figure B.78. Residuals of observations for VM 5 concerning 450kDa PAA coated ferrimagnetic Fe_3O_4/water nanofluids

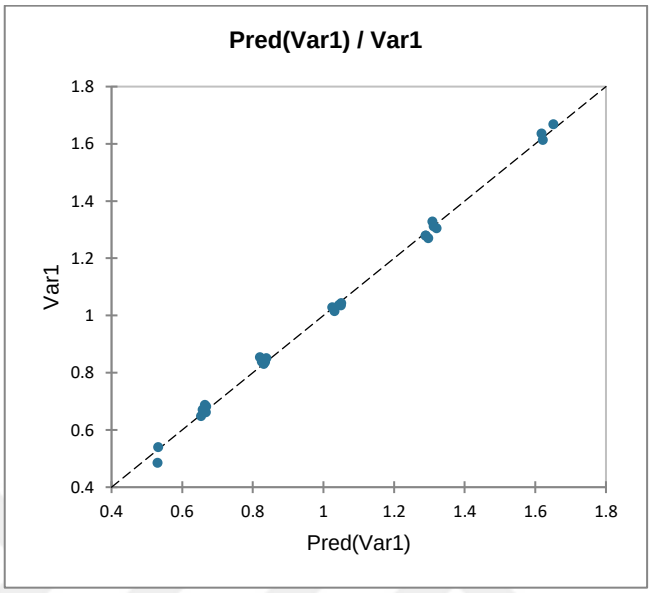

Figure B.79. The compatibility of predicted values with measured values for VM 5 concerning 250kDa PAA coated ferrimagnetic Fe_3O_4/water nanofluids

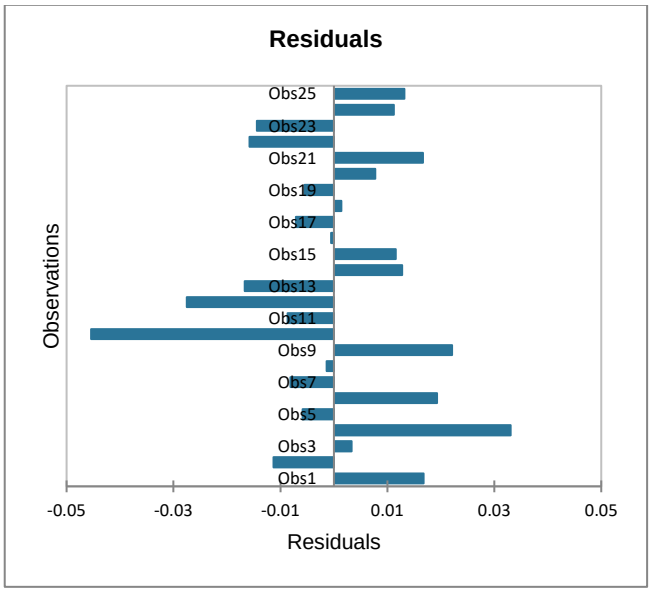

Figure B.80. Residuals of observations for VM 5 concerning 250kDa PAA coated ferrimagnetic Fe_3O_4/water nanofluids

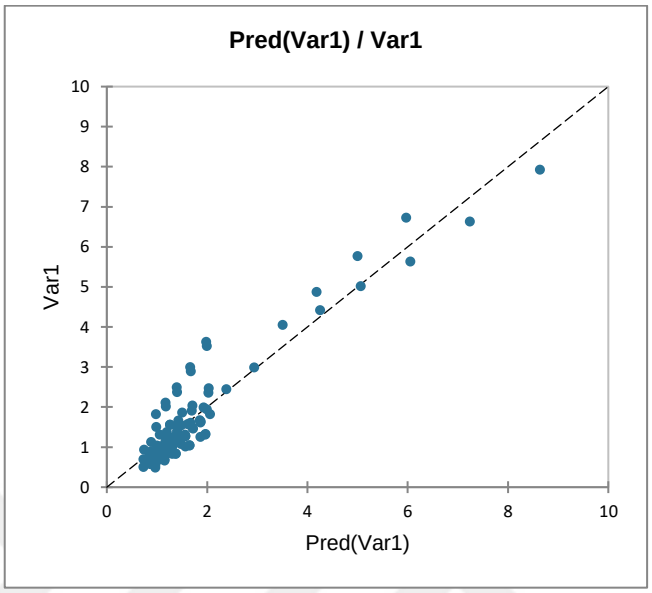

Figure B.81. The compatibility of predicted values with measured values for VM 5 concerning all Fe_3O_4/water nanofluids

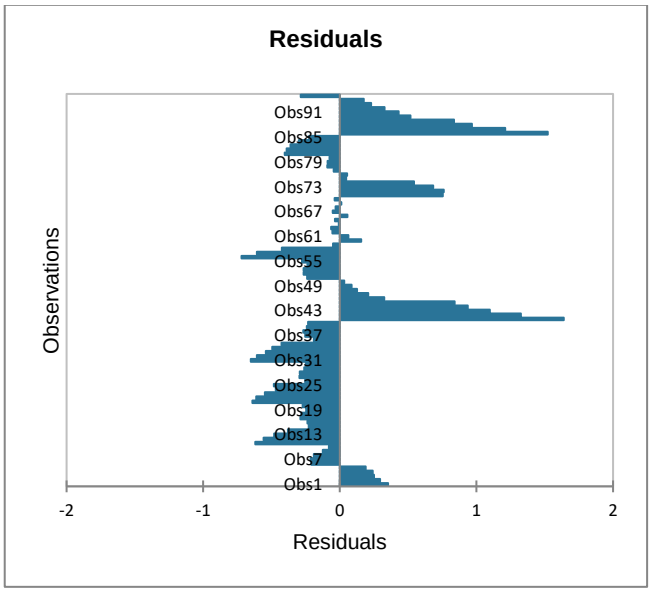

Figure B.82. Residuals of observations for VM 5 concerning all Fe_3O_4/water nanofluids

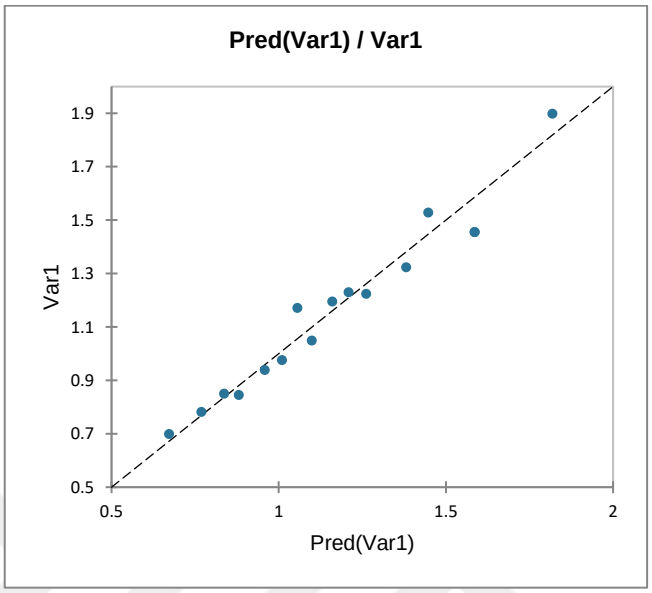

Figure B.83. The compatibility of predicted values with measured values for VM 5 concerning CuO/water nanofluids

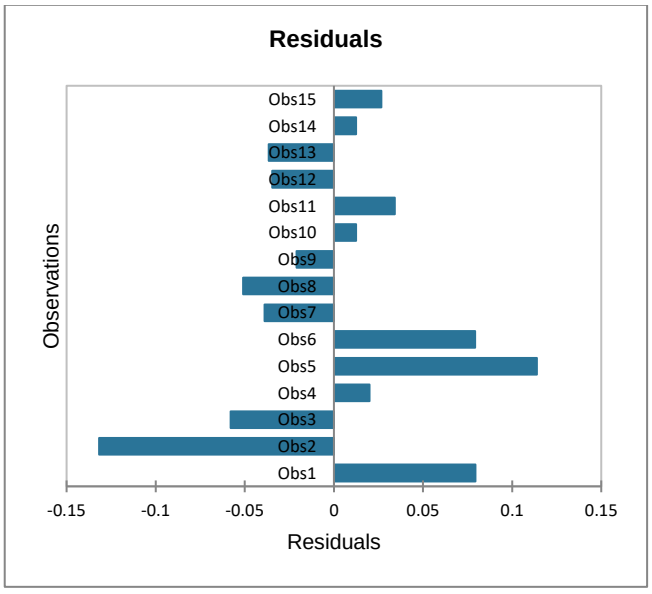

Figure B.84. Residuals of observations for VM 5 concerning CuO/water nanofluids

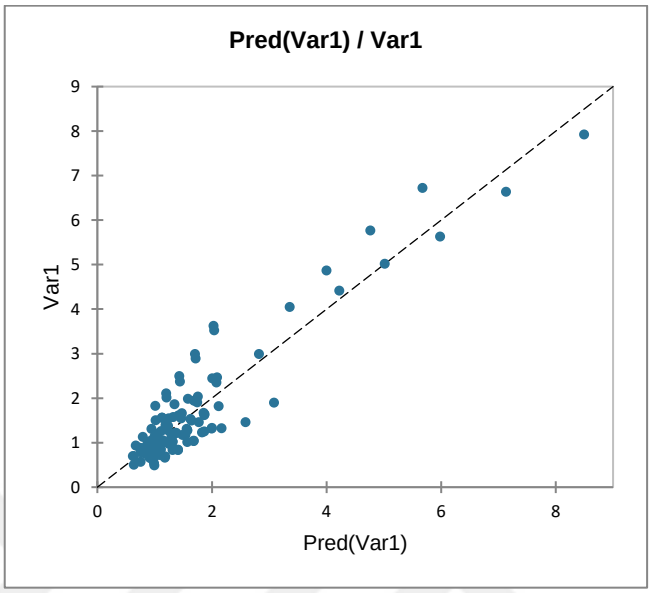

Figure B.85. The compatibility of predicted values with measured values for VM 5 concerning all Fe_3O_4 and CuO/water nanofluids together

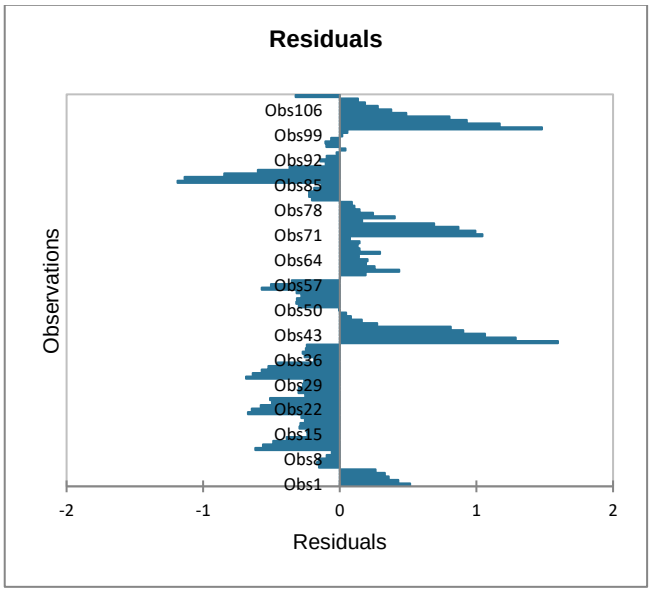

Figure B.86. Residuals of observations for VM 5 concerning all Fe_3O_4 and CuO/water nanofluids together

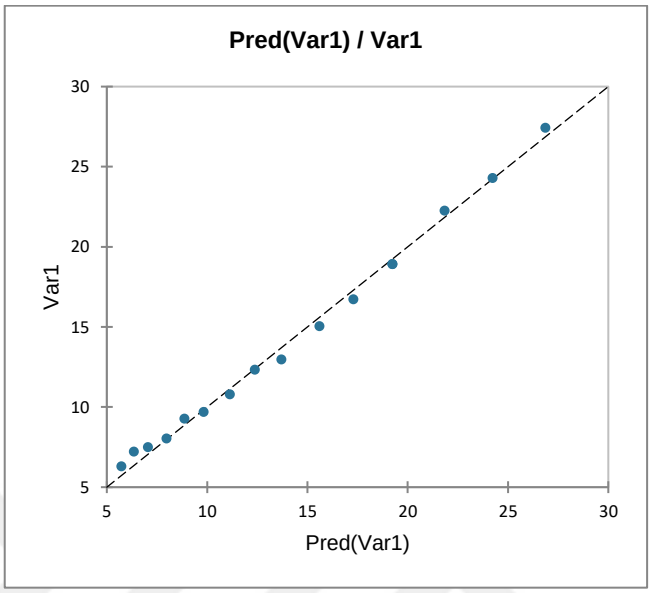

Figure B.87. The compatibility of predicted values with measured values for VM 5 concerning CuO/ethylene glycol nanofluids

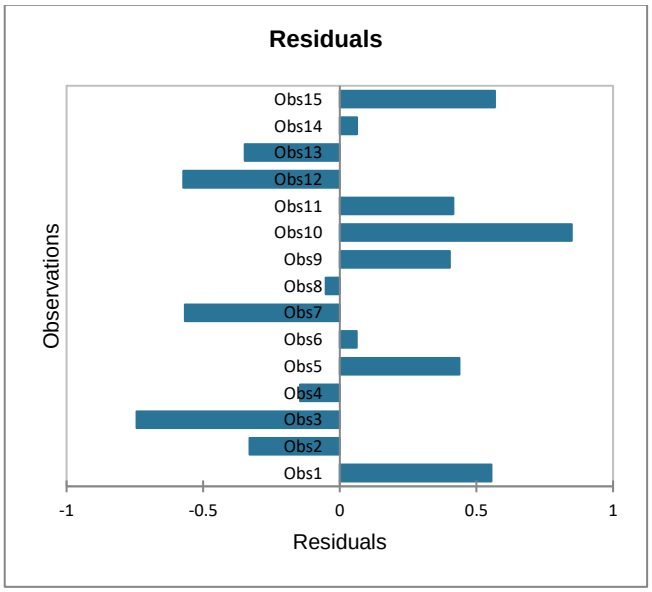

Figure B.88. Residuals of observations for VM 5 concerning CuO/ethylene glycol nanofluids

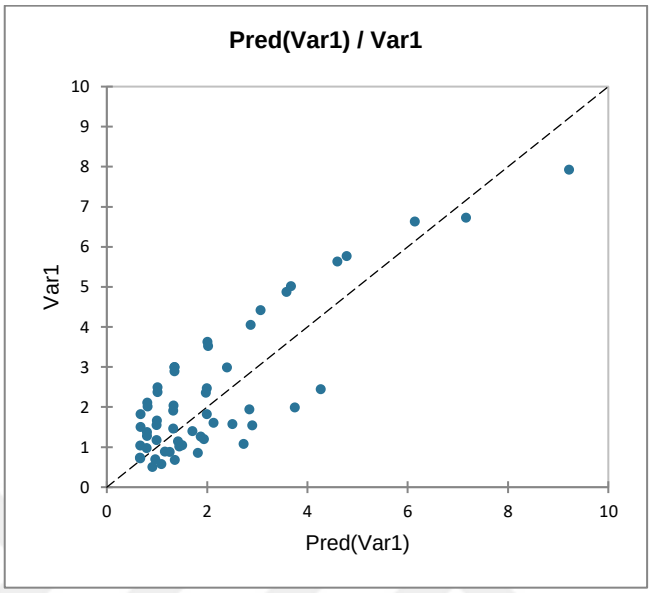

Figure B.89. The compatibility of predicted values with measured values for VM 6 concerning all superparamagnetic Fe_3O_4/water nanofluids

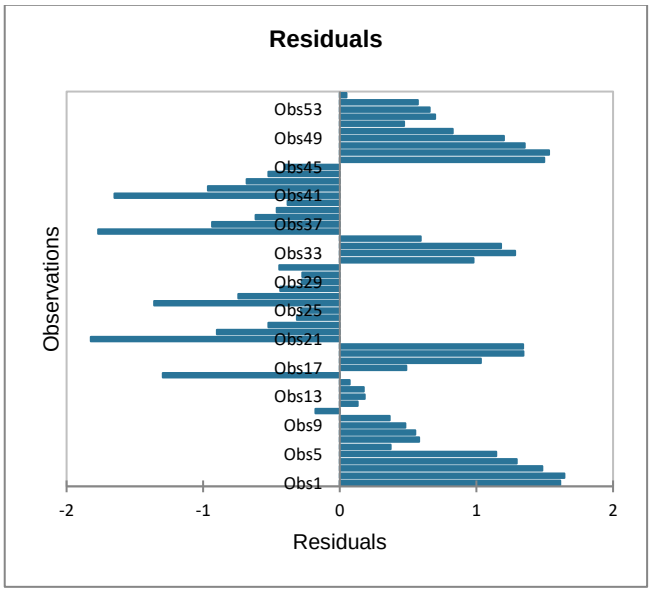

Figure B.90. Residuals of observations for VM 6 concerning all superparamagnetic Fe_3O_4/water nanofluids

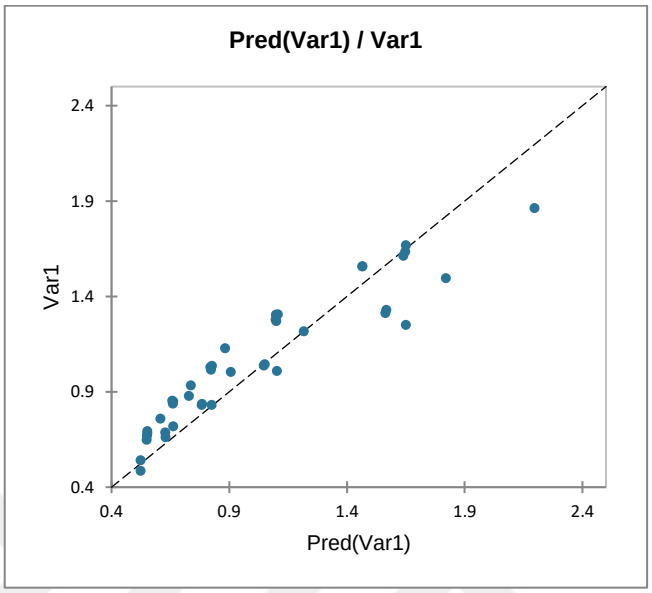

Figure B.91. The compatibility of predicted values with measured values for VM 6 concerning all ferrimagnetic Fe_3O_4/water nanofluids

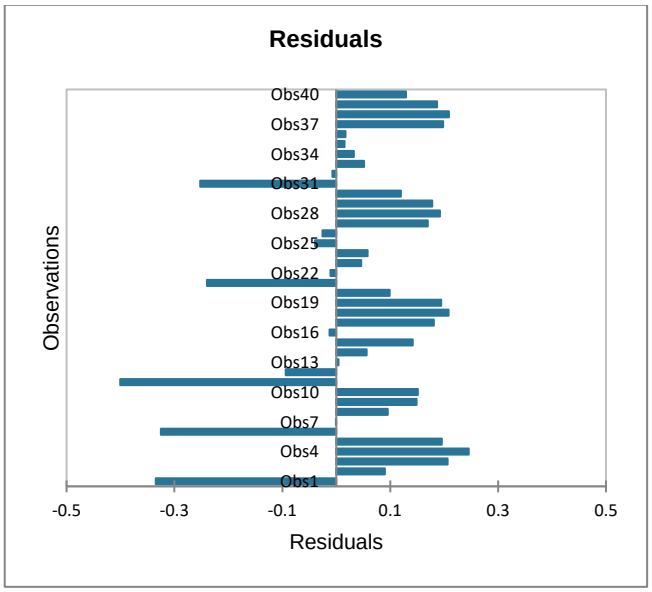

Figure B.92. Residuals of observations for VM 6 concerning all ferrimagnetic Fe_3O_4/water nanofluids

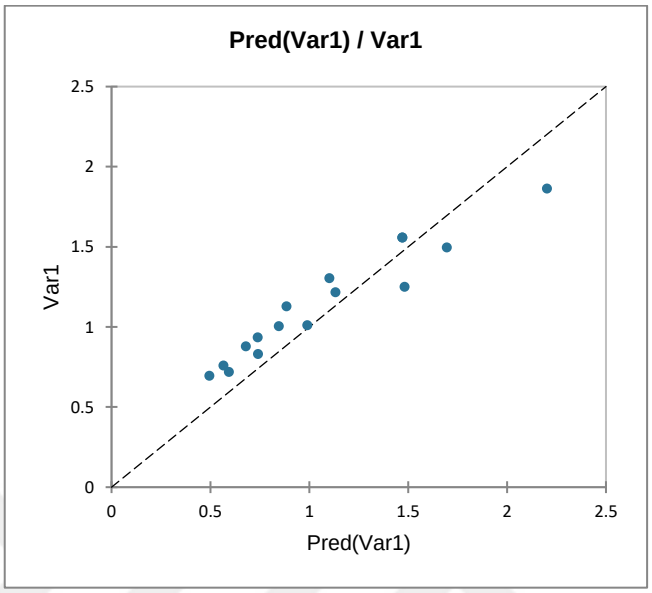

Figure B.93. The compatibility of predicted values with measured values for VM 6 concerning 450kDa PAA coated ferrimagnetic Fe_3O_4/water nanofluids

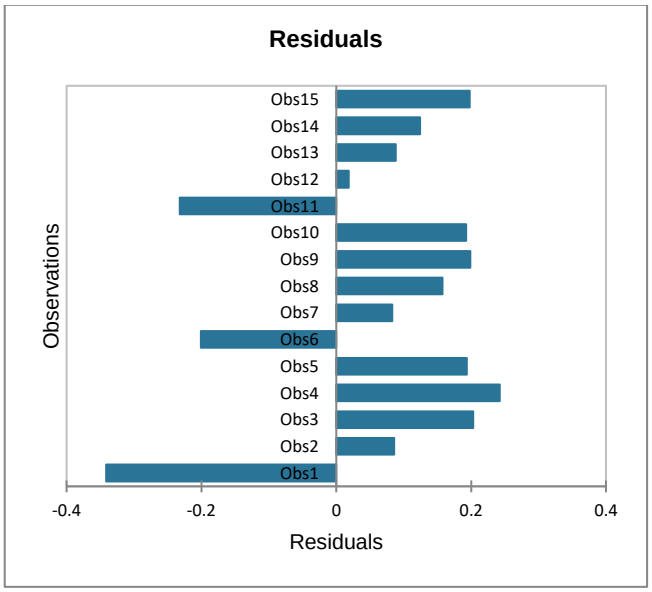

Figure B.94. Residuals of observations for VM 6 concerning 450kDa PAA coated ferrimagnetic Fe_3O_4/water nanofluids

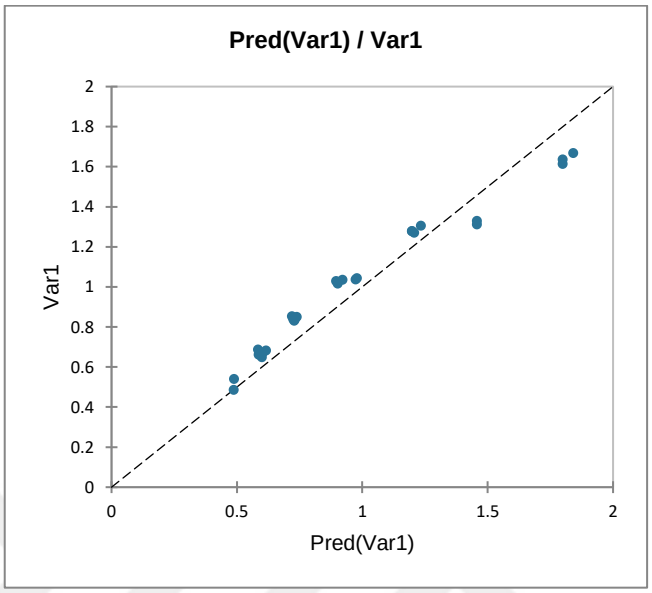

Figure B.95. The compatibility of predicted values with measured values for VM 6 concerning 250kDa PAA coated ferrimagnetic Fe_3O_4/water nanofluids

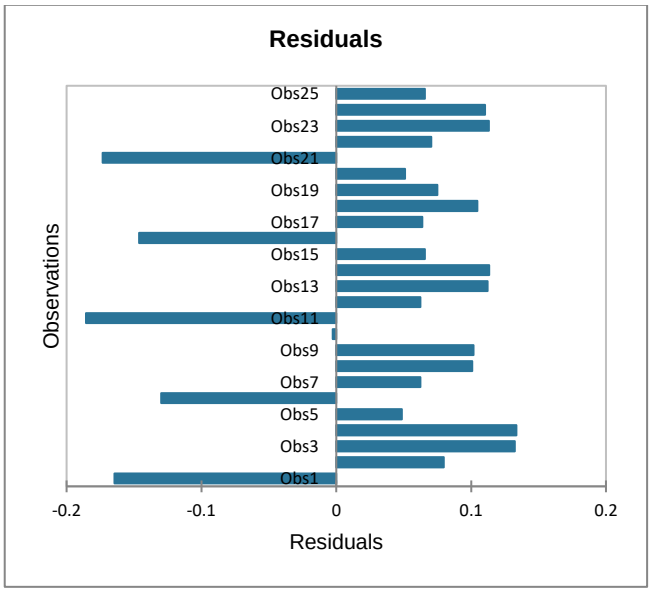

Figure B.96. Residuals of observations for VM 6 concerning 250kDa PAA coated ferrimagnetic Fe_3O_4/water nanofluids

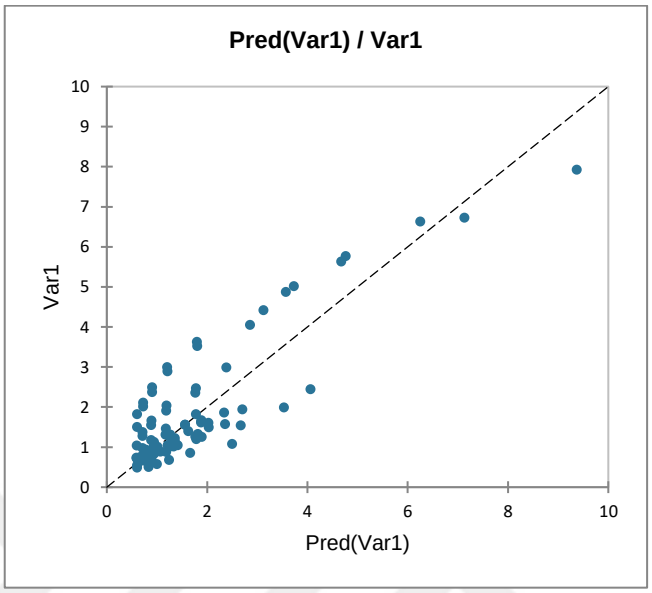

Figure B.97. The compatibility of predicted values with measured values for VM 6 concerning all Fe_3O_4/water nanofluids

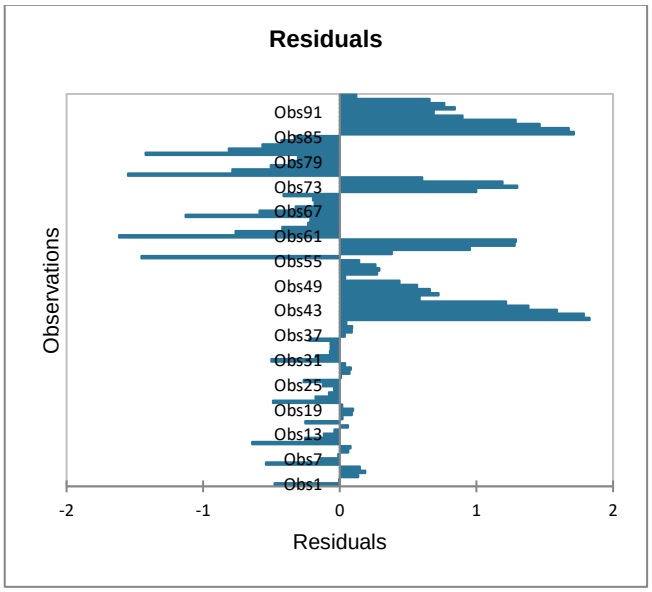

Figure B.98. Residuals of observations for VM 6 concerning all Fe_3O_4/water nanofluids

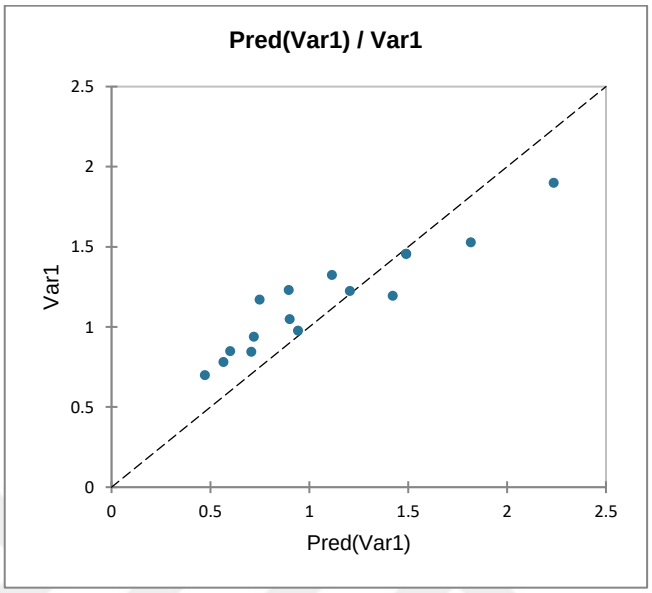

Figure B.99. The compatibility of predicted values with measured values for VM 6 concerning CuO/water nanofluids

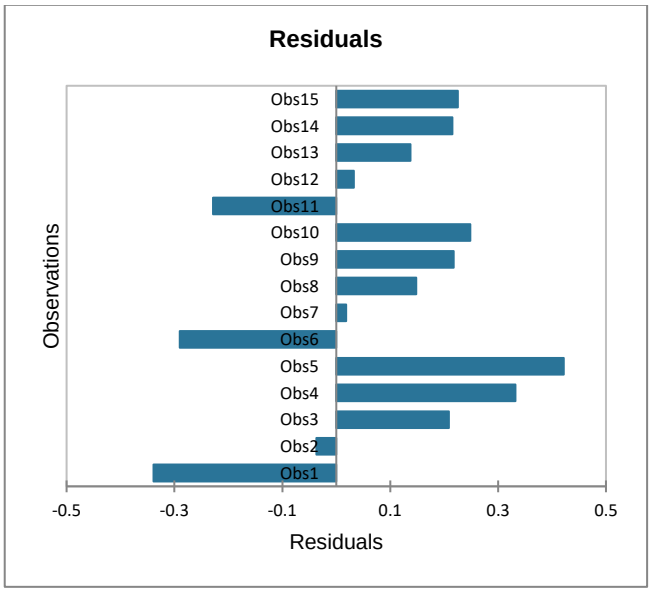

Figure B.100. Residuals of observations for VM 6 concerning CuO/water nanofluids

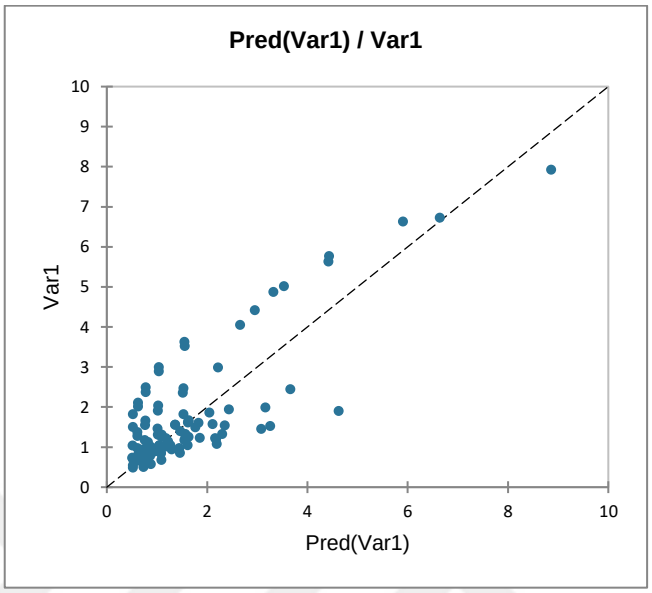

Figure B.101. The compatibility of predicted values with measured values for VM 6 concerning all Fe_3O_4 and CuO/water nanofluids together

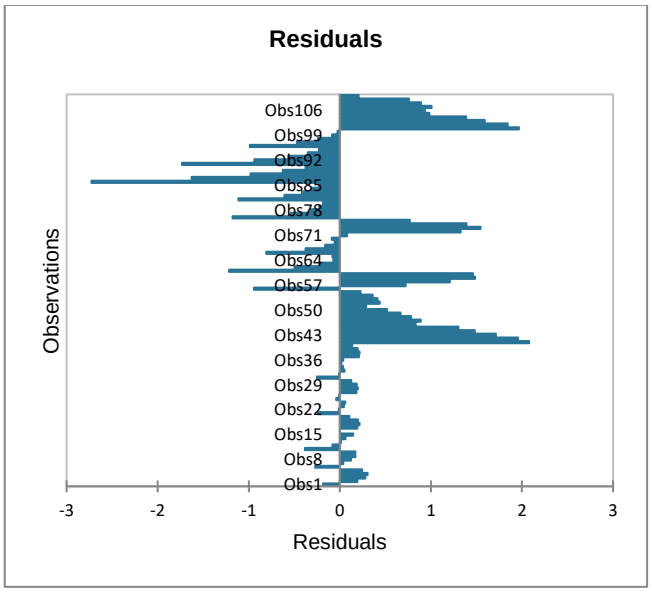

Figure B.102. Residuals of observations for VM 6 concerning all Fe_3O_4 and CuO/water nanofluids together

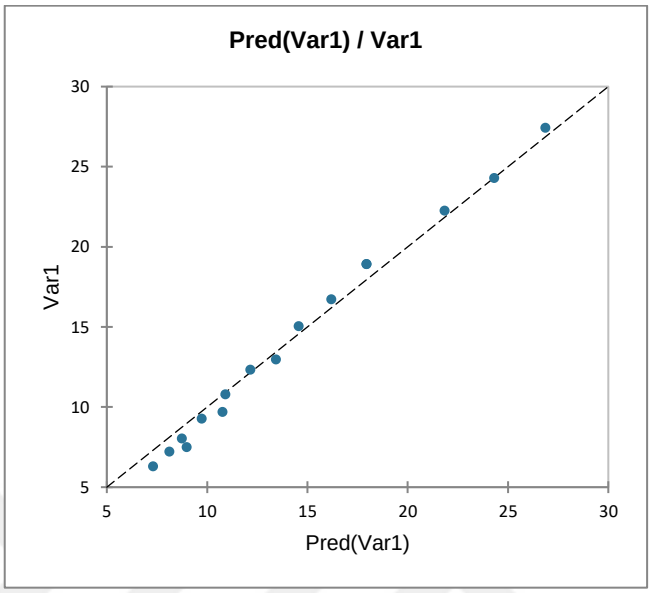

Figure B.103. The compatibility of predicted values with measured values for VM 6 concerning CuO/ethylene glycol nanofluids

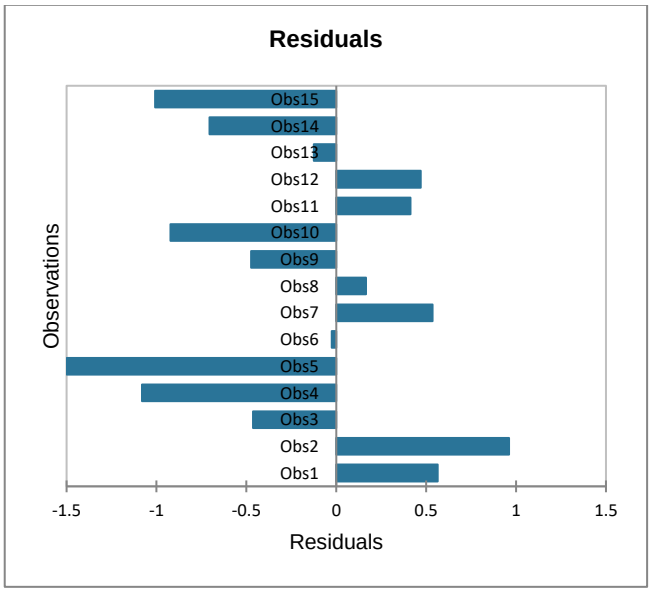

Figure B.104. Residuals of observations for VM 6 concerning CuO/ethylene glycol nanofluids

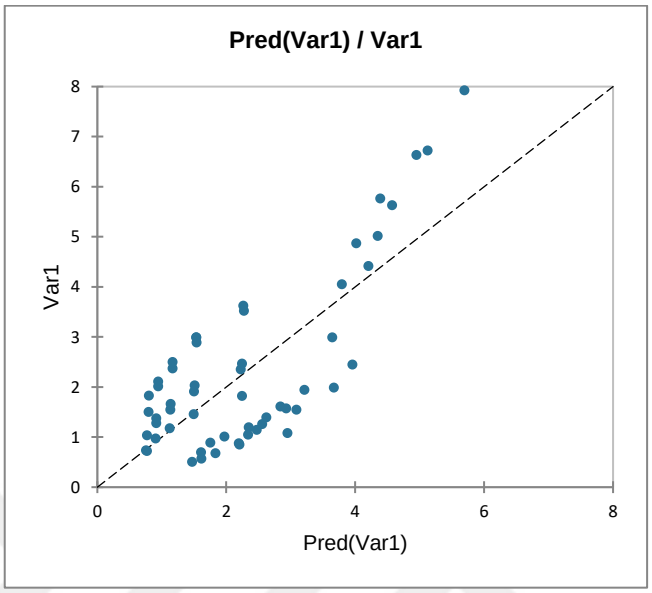

Figure B.105. The compatibility of predicted values with measured values for VM 7 concerning all superparamagnetic Fe_3O_4/water nanofluids

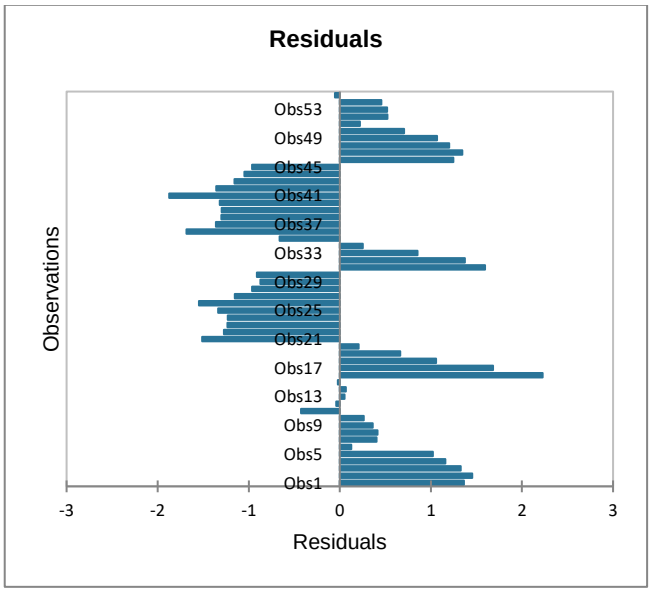

Figure B.106. Residuals of observations for VM 7 concerning all superparamagnetic Fe_3O_4/water nanofluids

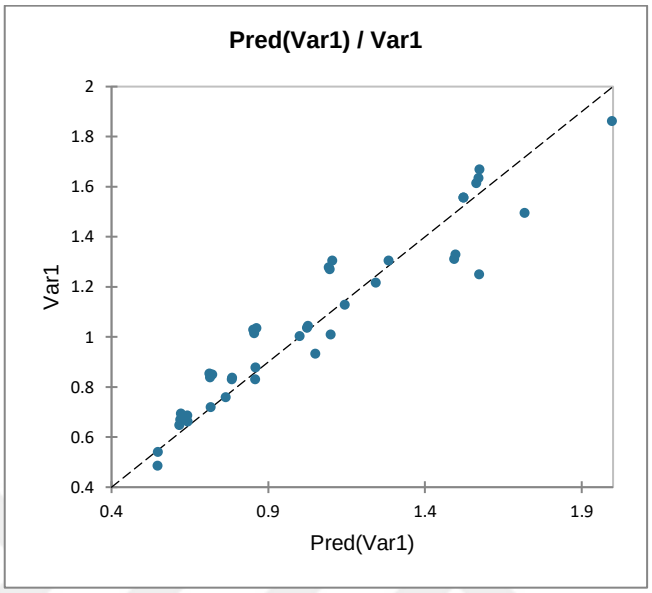

Figure B.107. The compatibility of predicted values with measured values for VM 7 concerning all ferrimagnetic Fe_3O_4/water nanofluids

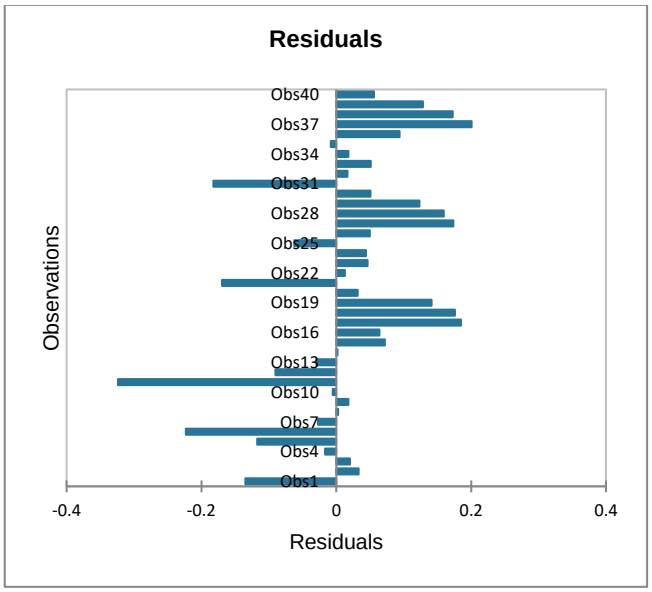

Figure B.108. Residuals of observations for VM 7 concerning all ferrimagnetic Fe_3O_4/water nanofluids

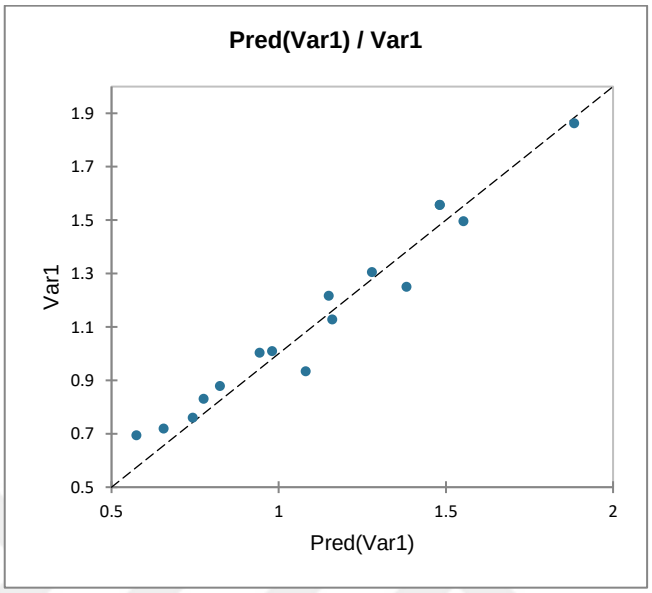

Figure B.109. The compatibility of predicted values with measured values for VM 7 concerning 450kDa PAA coated ferrimagnetic Fe_3O_4/water nanofluids

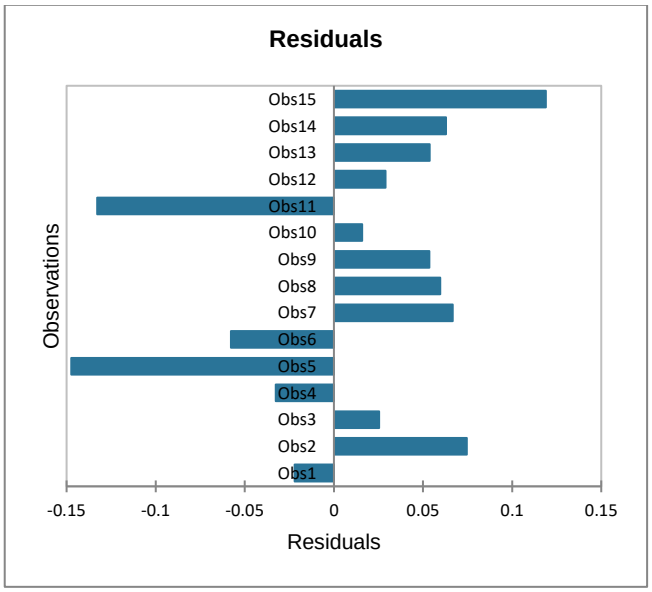

Figure B.110. Residuals of observations for VM 7 concerning 450kDa PAA coated ferrimagnetic Fe_3O_4/water nanofluids

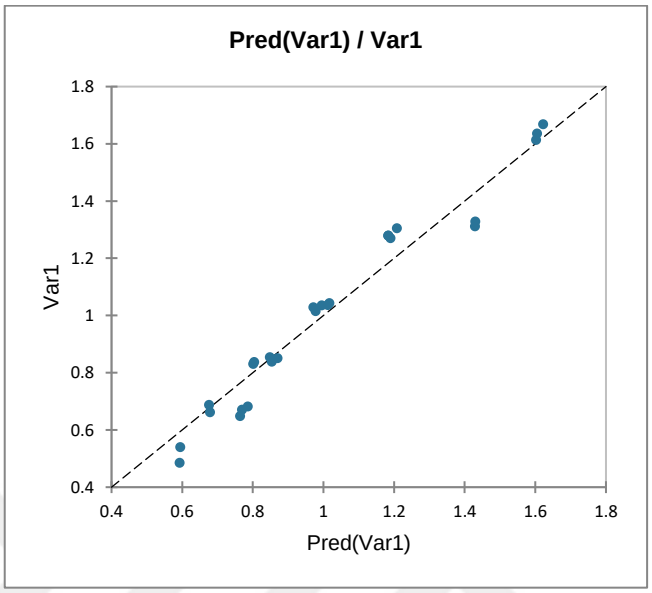

Figure B.111. The compatibility of predicted values with measured values for VM 7 concerning 250kDa PAA coated ferrimagnetic Fe_3O_4/water nanofluids

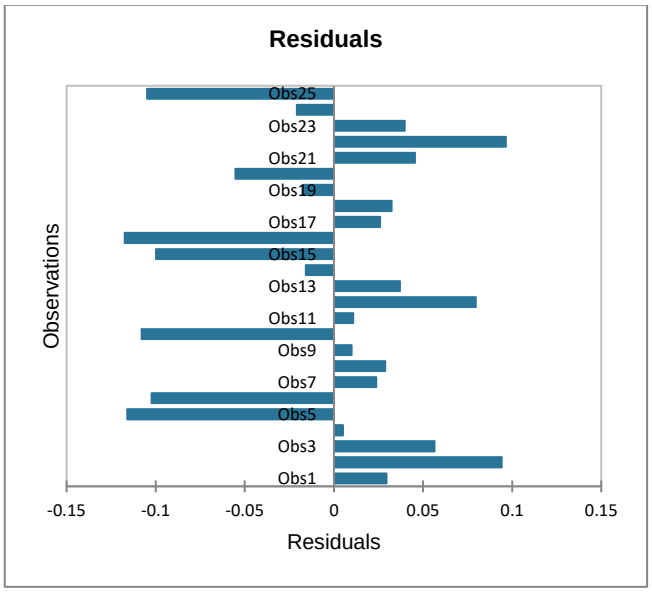

Figure B.112. Residuals of observations for VM 7 concerning 250kDa PAA coated ferrimagnetic Fe_3O_4/water nanofluids

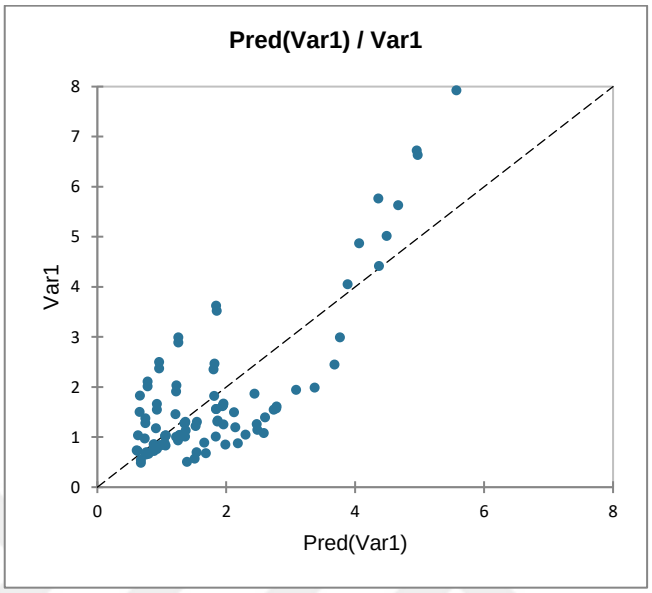

Figure B.113. The compatibility of predicted values with measured values for VM 7 concerning all Fe_3O_4/water nanofluids

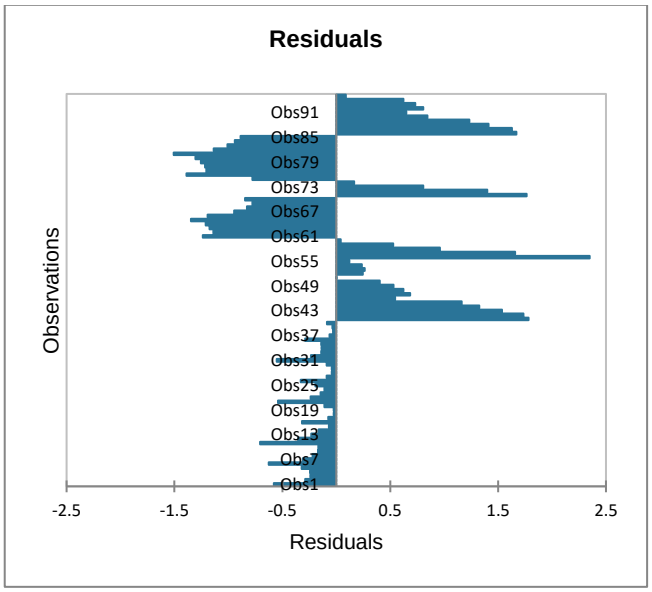

Figure B.114. Residuals of observations for VM 7 concerning all Fe_3O_4/water nanofluids

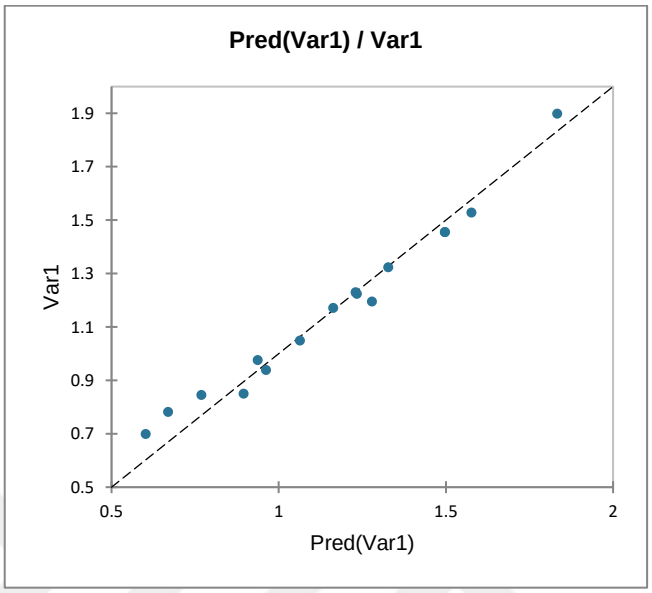

Figure B.115. The compatibility of predicted values with measured values for VM 7 concerning CuO/water nanofluids

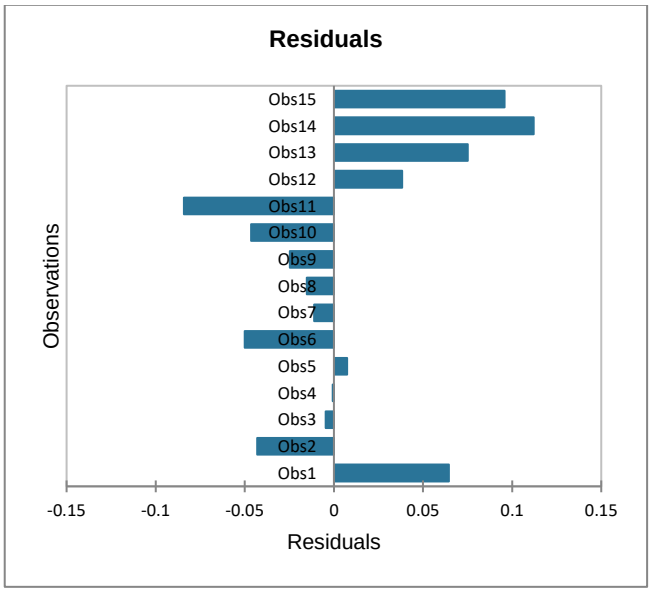

Figure B.116. Residuals of observations for VM 7 concerning CuO/water nanofluids

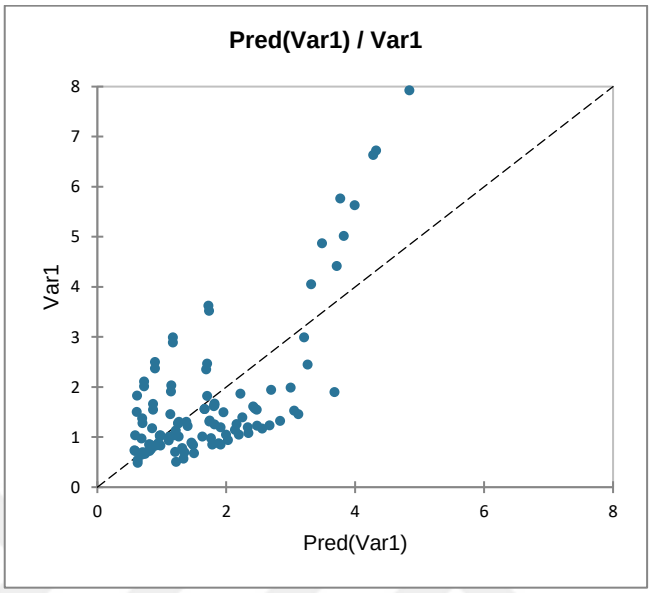

Figure B.117. The compatibility of predicted values with measured values VM 7 concerning all Fe_3O_4 and CuO/water nanofluids together

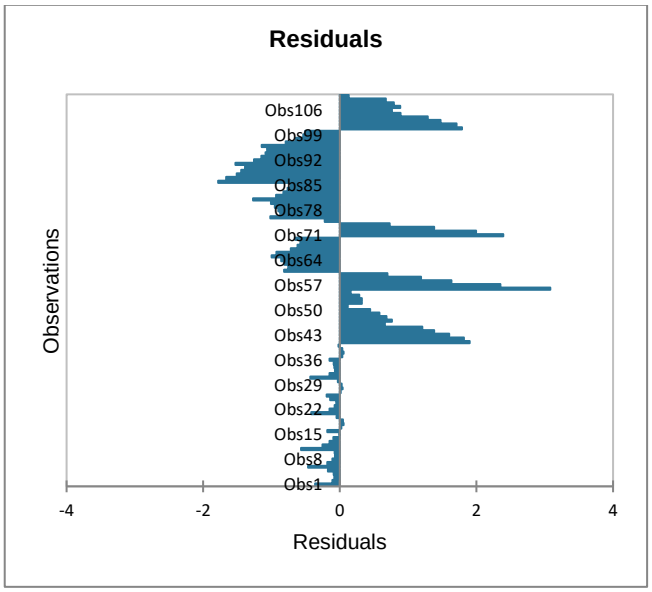

Figure B.118. Residuals of observations for VM 7 concerning all Fe_3O_4 and CuO/water nanofluids together

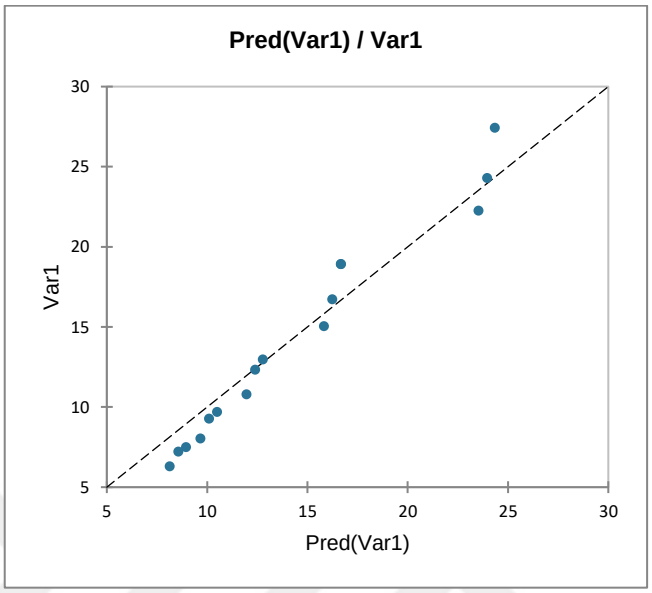

Figure B.119. The compatibility of predicted values with measured values for VM 7 concerning CuO/ethylene glycol nanofluids

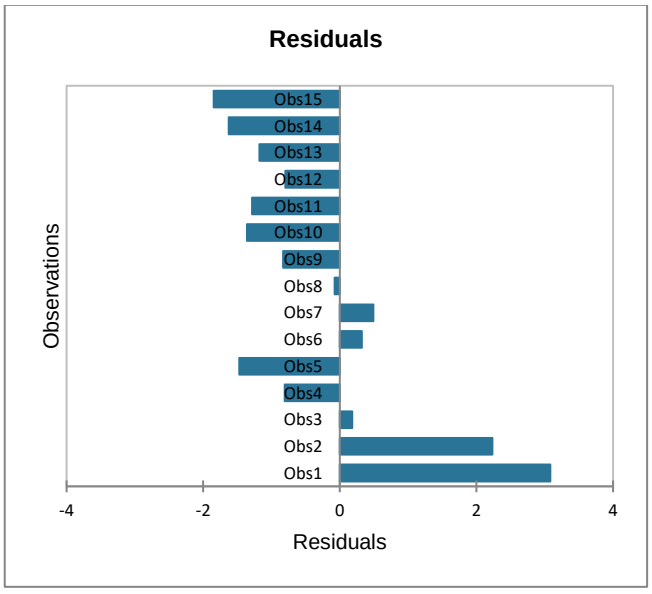

Figure B.120. Residuals of observations for VM 7 concerning CuO/ethylene glycol nanofluids

APPENDIX C

Table C.1. Skeletal forms of the chosen models for the thermal conductivity of nanofluids

Model number	**Correlation form**
TM 1	$\frac{k_{nf}}{k_{bf}} = A + BT + CT^2$
TM 2	$\frac{k_{nf}}{k_{bf}} = 1 + A\emptyset + BT\emptyset$
TM 3	$\frac{k_{nf}}{k_{bf}} = 1 + B\emptyset^C T^D$
TM 4	$\frac{k_{nf}}{k_{bf}} = A + B\emptyset$
TM 5	$\frac{k_{nf}}{k_{bf}} = Ae^{B\emptyset + CT}$
TM 6	$\frac{k_{nf}}{k_{bf}} = Ae^{B\emptyset^C + DT}$

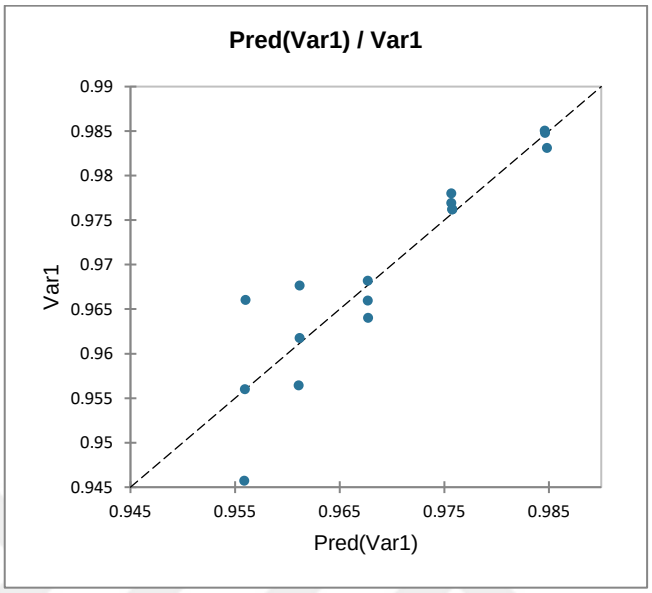

Figure C.1. The compatibility of predicted values with measured values for TM 1 concerning CuO/water nanofluids

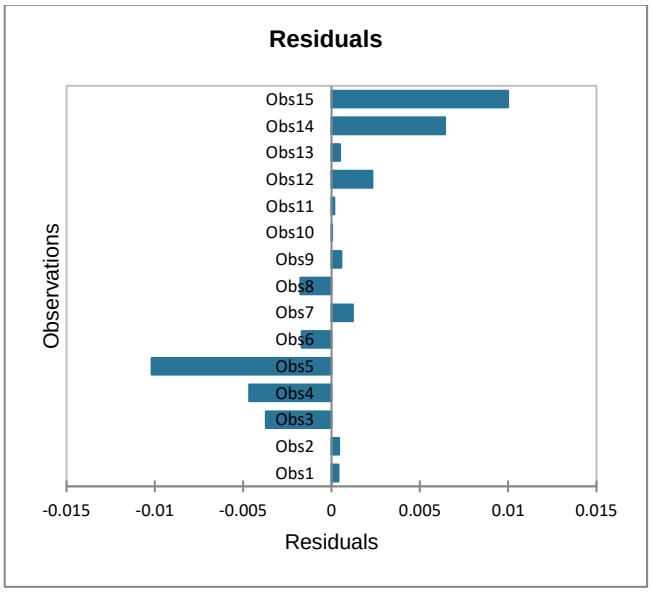

Figure C.2. Residuals of observations for TM 1 concerning CuO/water nanofluids

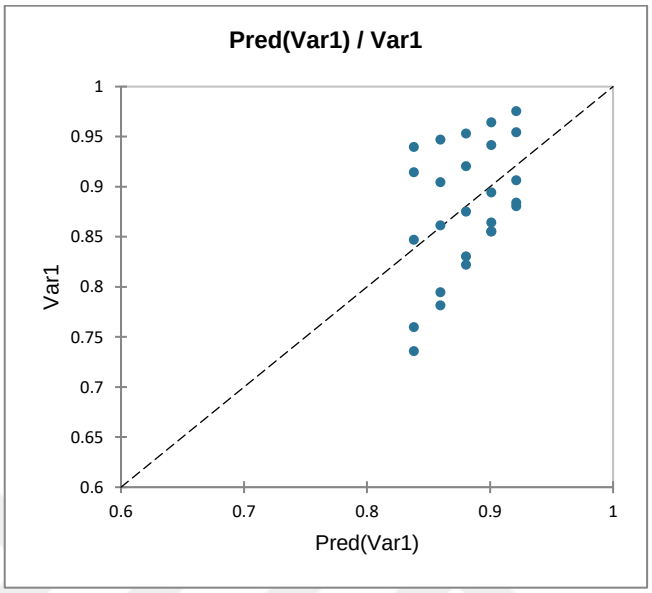

Figure C.3. The compatibility of predicted values with measured values for TM 1 concerning Ag/water nanofluids

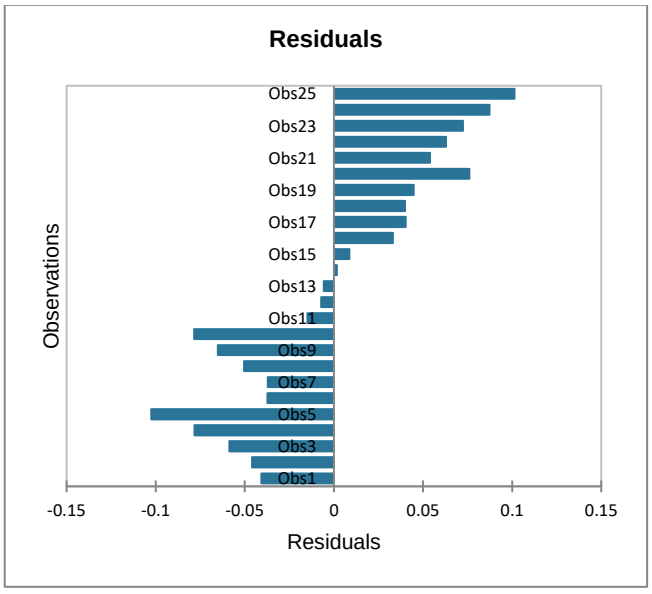

Figure C.4. Residuals of observations for TM 1 concerning Ag/water nanofluids

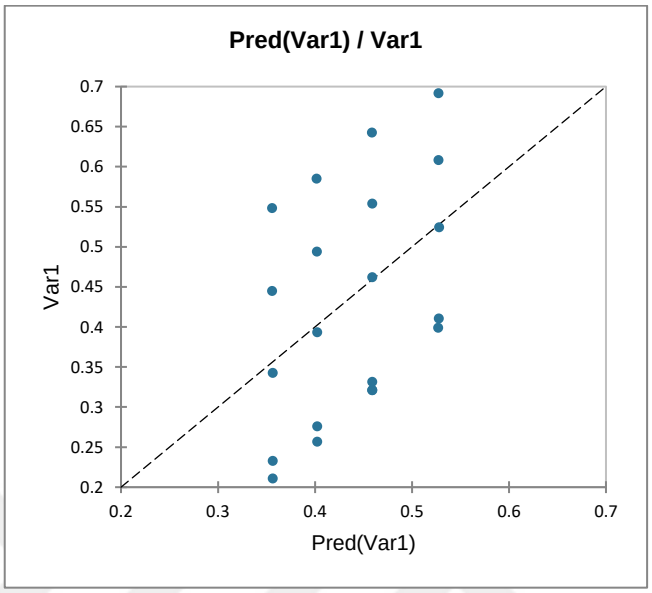

Figure C.5. The compatibility of predicted values with measured values for TM 1 concerning citric acid coated superparamagnetic Fe_3O_4/water nanofluids

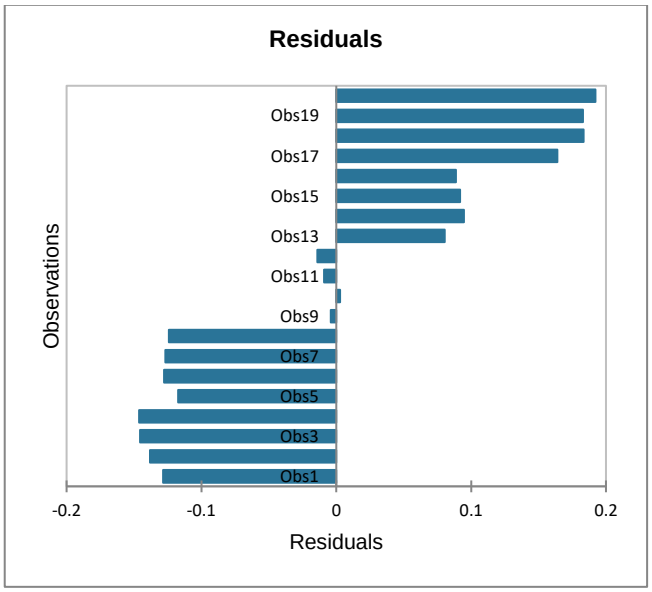

Figure C.6. Residuals of observations for TM 1 concerning citric acid coated superparamagnetic Fe_3O_4/water nanofluids

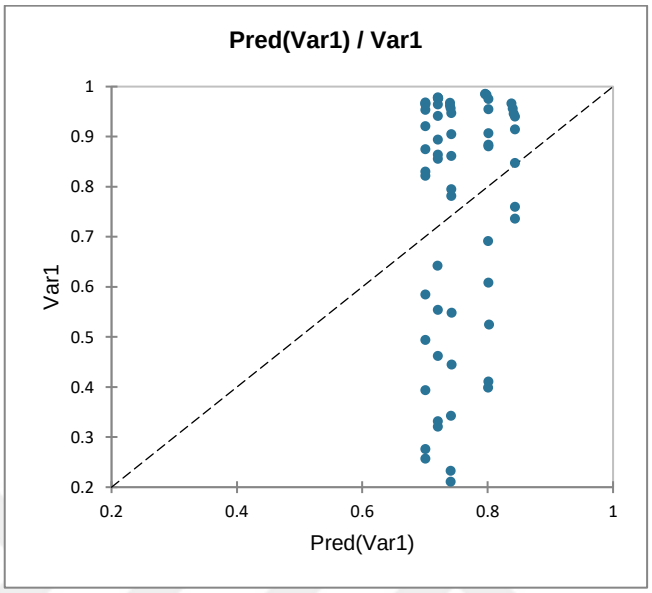

Figure C.7. The compatibility of predicted values with measured values for TM 1 concerning water-based Ag. Fe_3O_4 and CuO nanofluids together

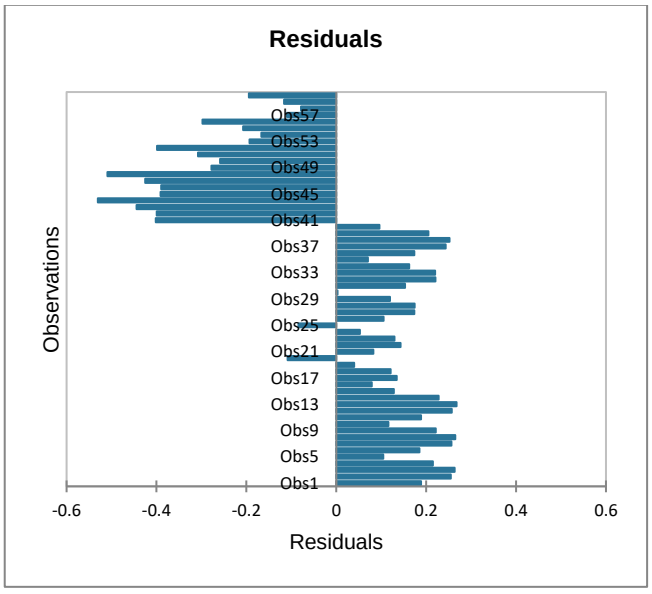

Figure C.8. Residuals of observations for TM 1 concerning water-based Ag. Fe_3O_4 and CuO nanofluids together

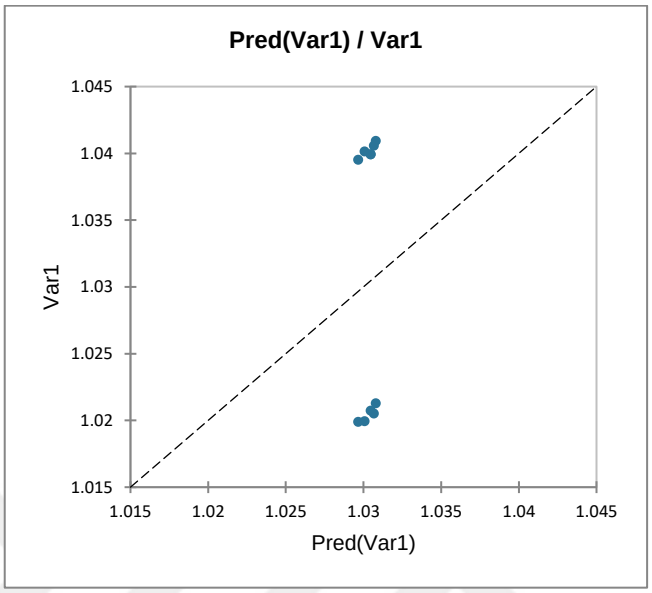

Figure C.9. The compatibility of predicted values with measured values for TM 1 concerning CuO/ethylene glycol nanofluids

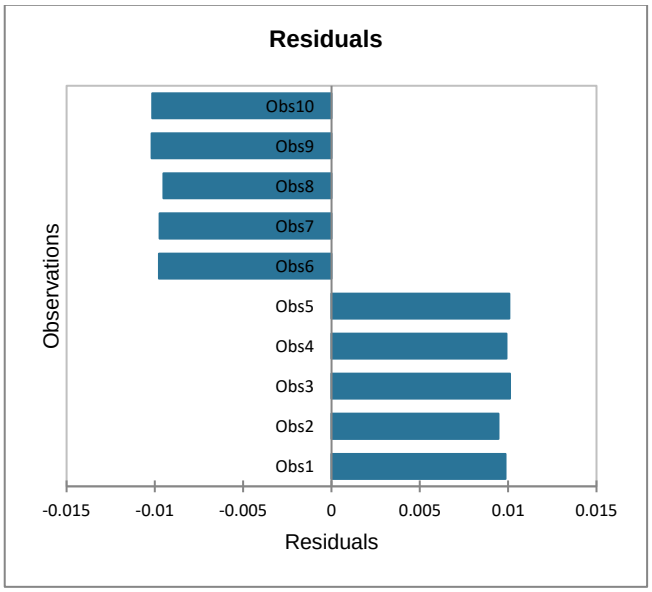

Figure C.10. Residuals of observations for TM 1 concerning CuO/ethylene glycol nanofluids

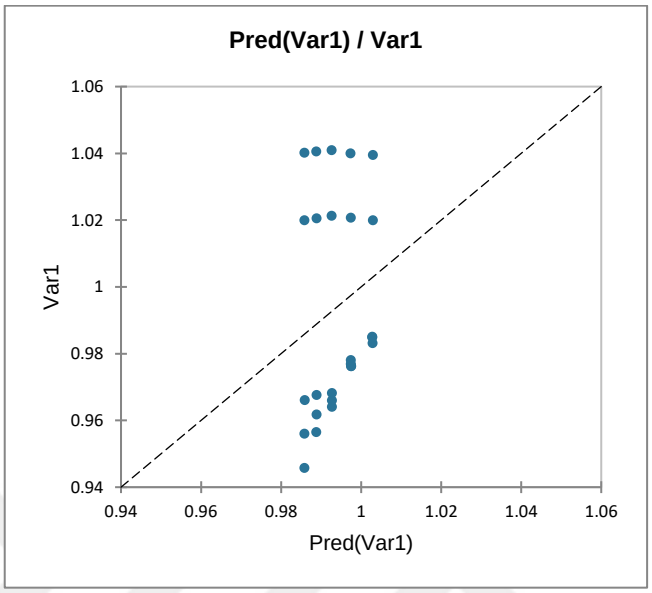

Figure C.11. The compatibility of predicted values with measured values for TM 1 concerning all CuO nanofluids

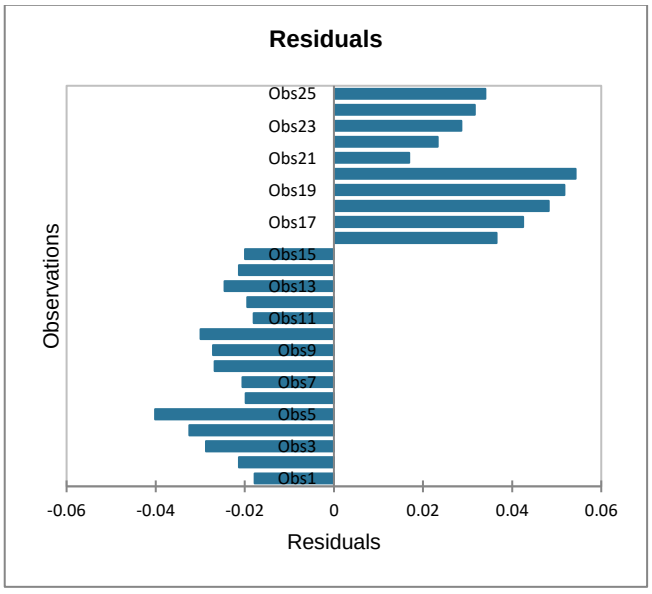

Figure C.12. Residuals of observations for TM 1 concerning all CuO nanofluids

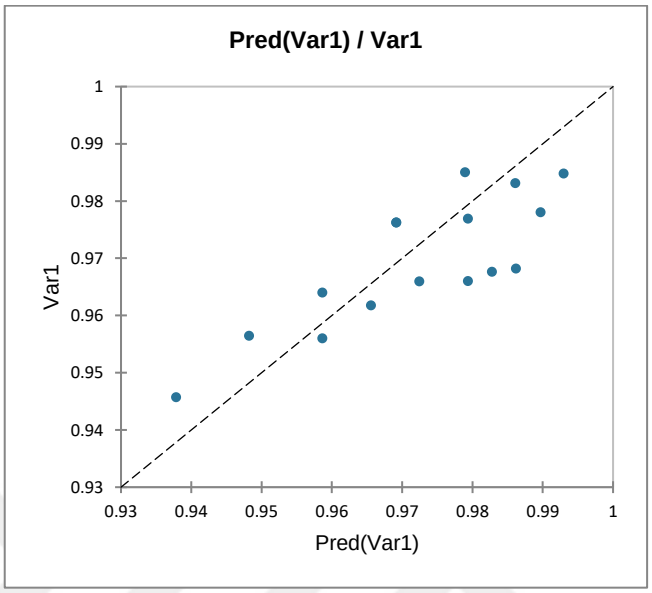

Figure C.13. The compatibility of predicted values with measured values for TM 2 concerning CuO/water nanofluids

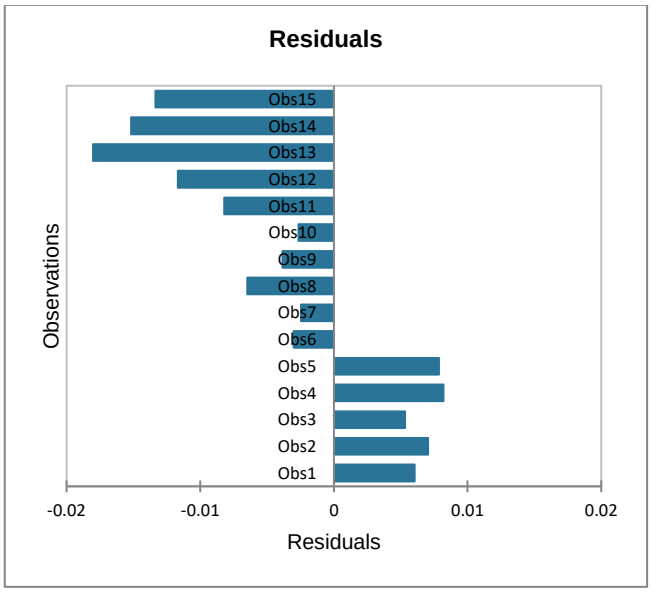

Figure C.14. Residuals of observations for TM 2 concerning CuO/water nanofluids

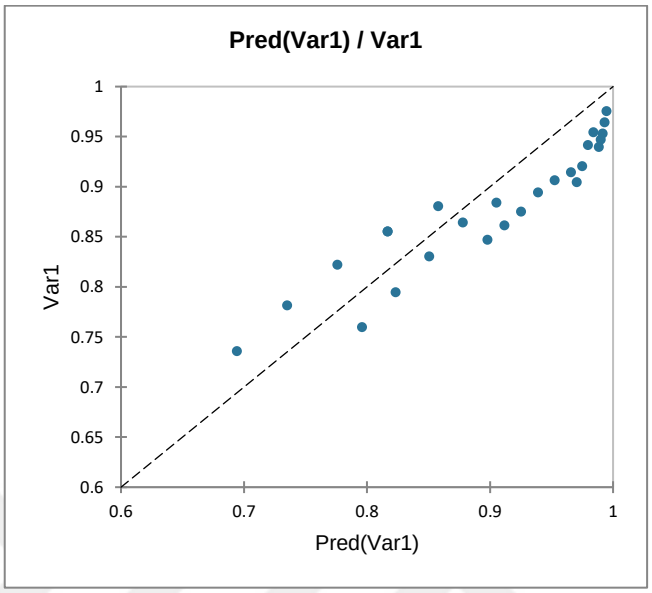

Figure C.15. The compatibility of predicted values with measured values for TM 2 concerning Ag/water nanofluids

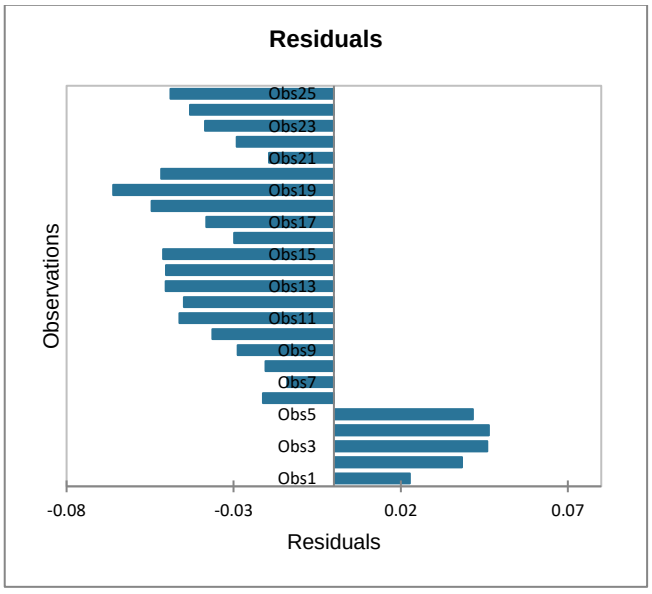

Figure C.16. Residuals of observations for TM 2 concerning Ag/water nanofluids

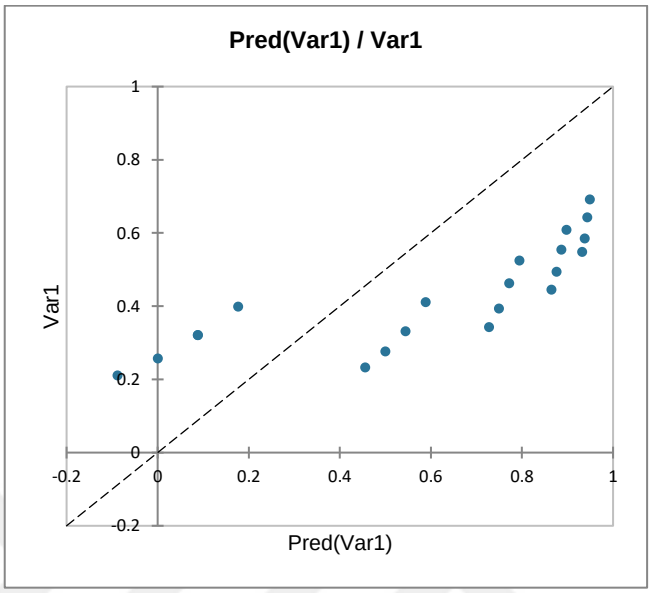

Figure C.17. The compatibility of predicted values with measured values for TM 2 concerning citric acid coated superparamagnetic Fe_3O_4/water nanofluids

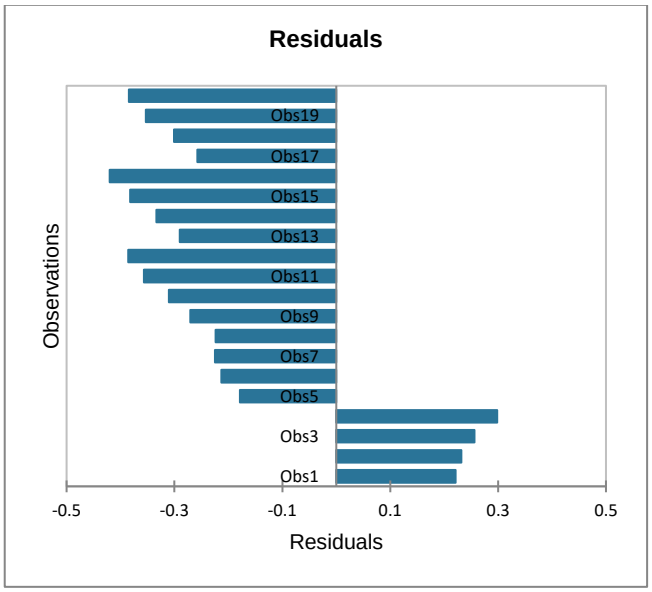

Figure C.18. Residuals of observations for TM 2 concerning citric acid coated superparamagnetic Fe_3O_4/water nanofluids

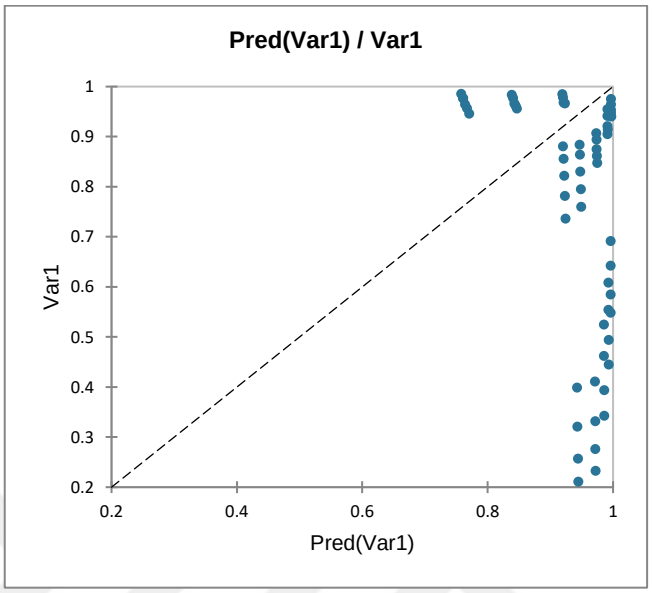

Figure C.19. The compatibility of predicted values with measured values for TM 2 concerning water-based Ag. Fe_3O_4 and CuO nanofluids together

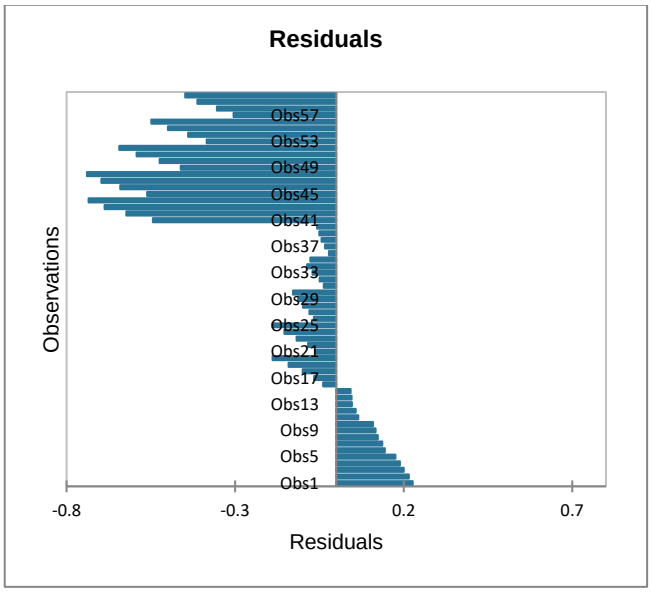

Figure C.20. Residuals of observations for TM 2 concerning water-based Ag. Fe_3O_4 and CuO nanofluids together

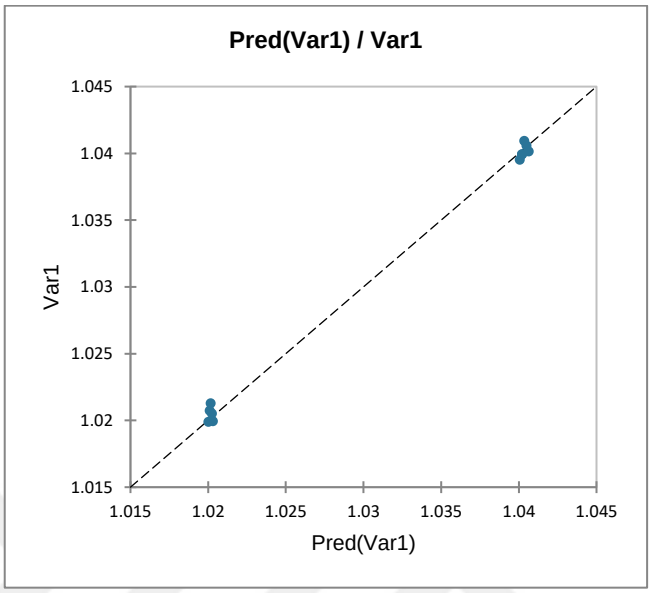

Figure C.21. The compatibility of predicted values with measured values for TM 2 concerning CuO/ethylene glycol nanofluids

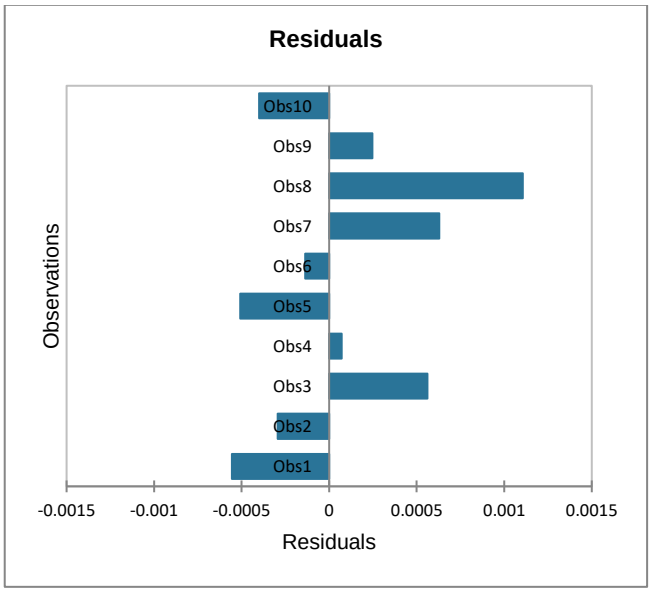

Figure C.22. Residuals of observations for TM 2 concerning CuO/ethylene glycol nanofluids

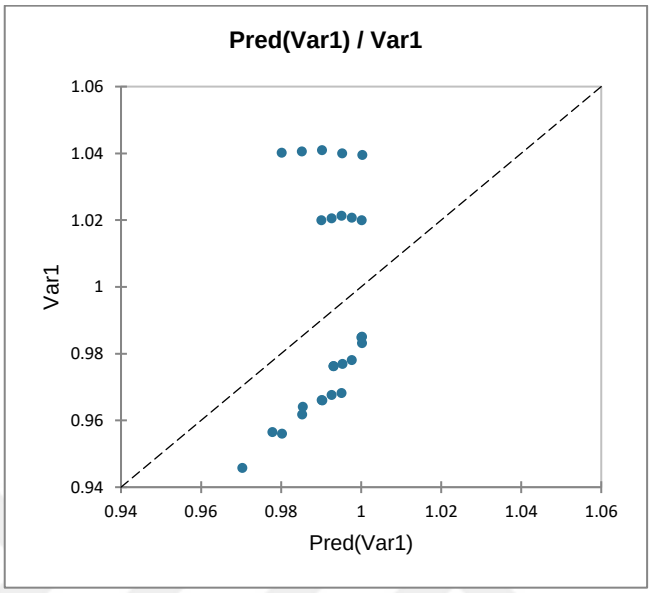

Figure C.23. The compatibility of predicted values with measured values for TM 2 concerning all CuO nanofluids

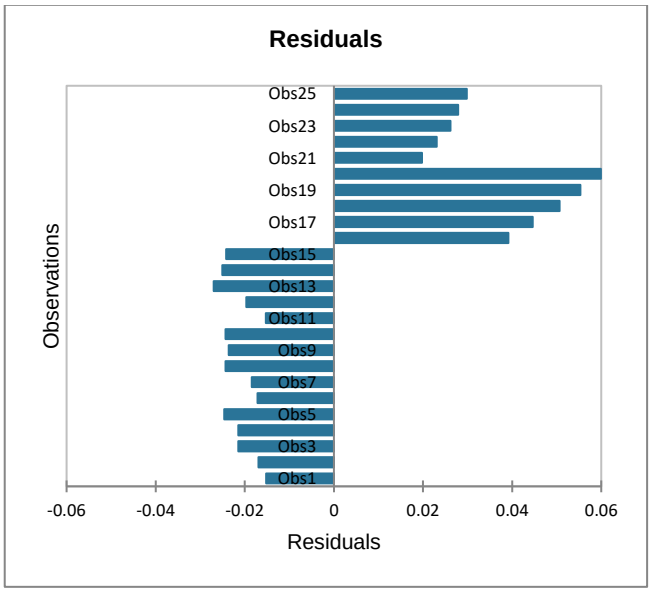

Figure C.24. Residuals of observations for TM 2 concerning all CuO nanofluids

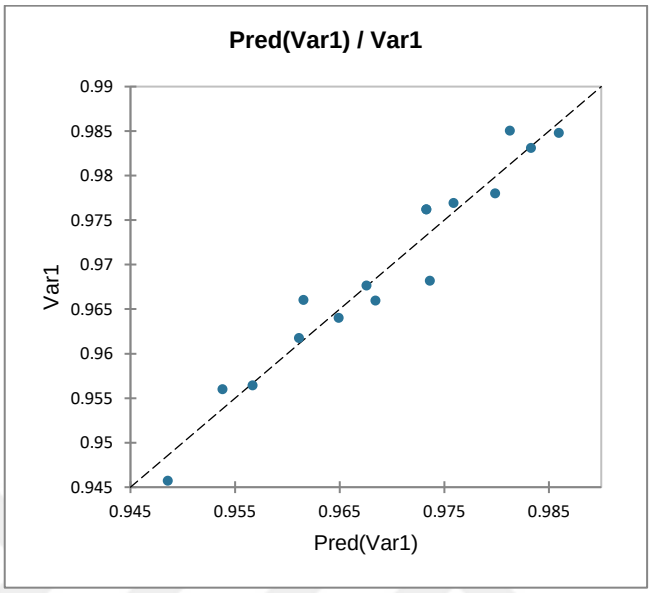

Figure C.25. The compatibility of predicted values with measured values for TM 3 concerning CuO/water nanofluids

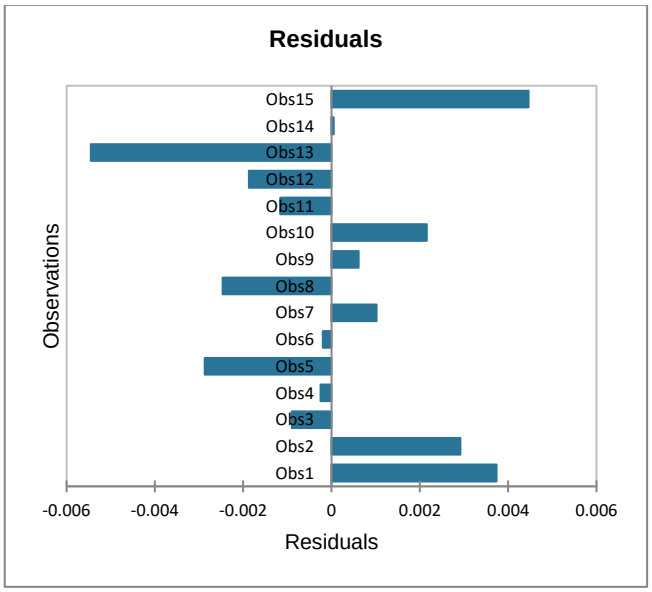

Figure C.26. Residuals of observations for TM 3 concerning CuO/water nanofluids

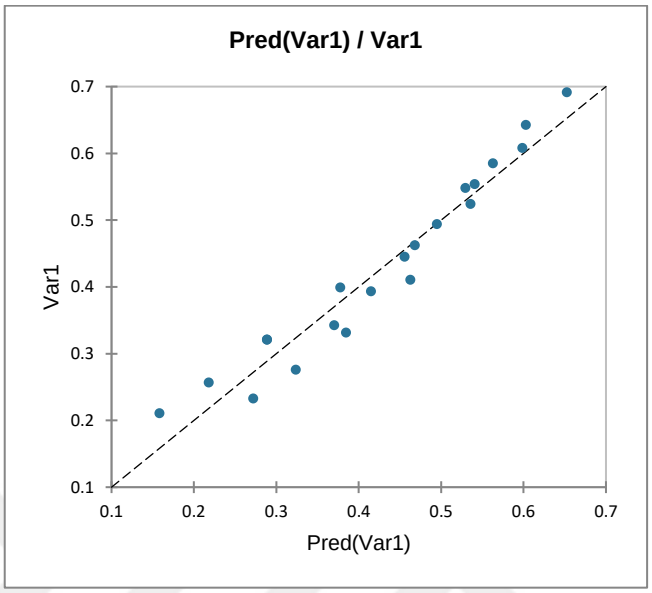

Figure C.27. The compatibility of predicted values with measured values for TM 3 concerning citric acid coated superparamagnetic Fe_3O_4/water nanofluids

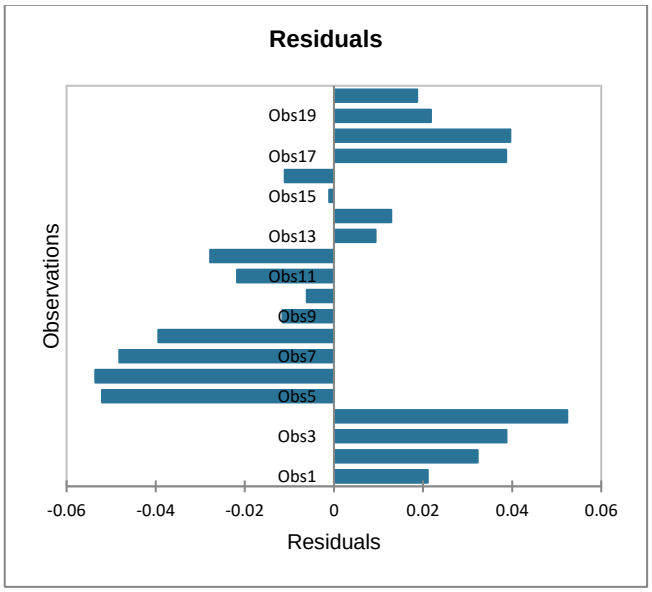

Figure C.28. Residuals of observations for TM 3 concerning citric acid coated superparamagnetic Fe_3O_4/water nanofluids

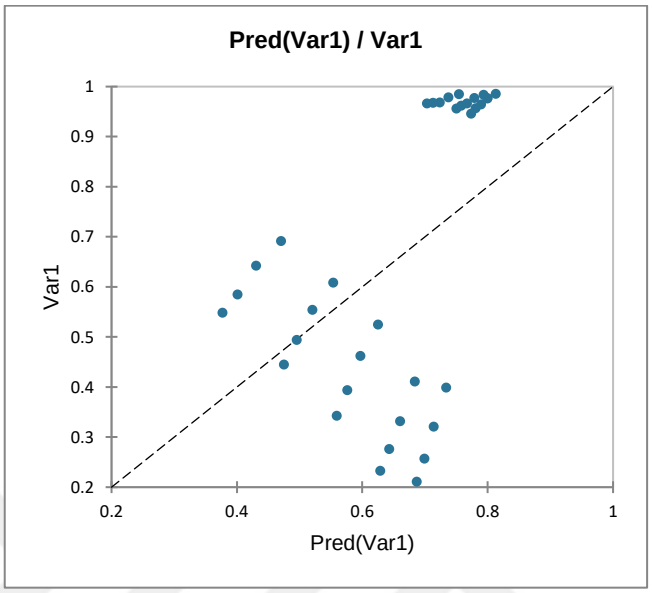

Figure C.29. The compatibility of predicted values with measured values for TM 3 concerning water-based Fe_3O_4 and CuO nanofluids together

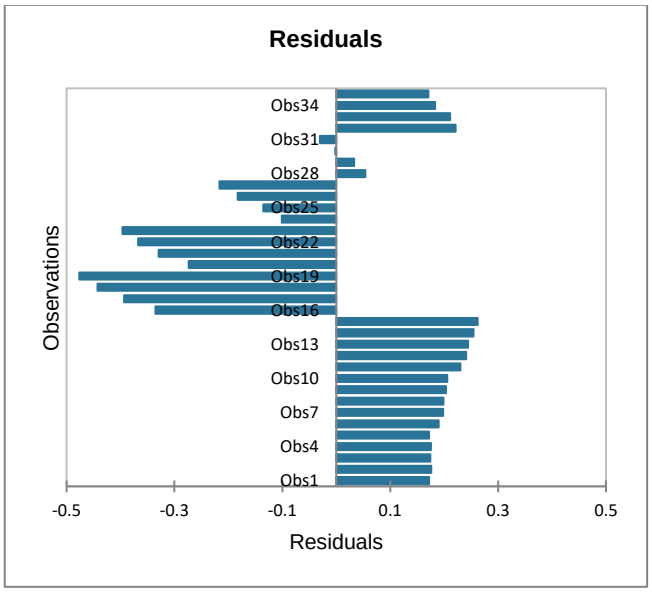

Figure C.30. Residuals of observations for TM 3 concerning water-based Fe_3O_4 and CuO nanofluids together

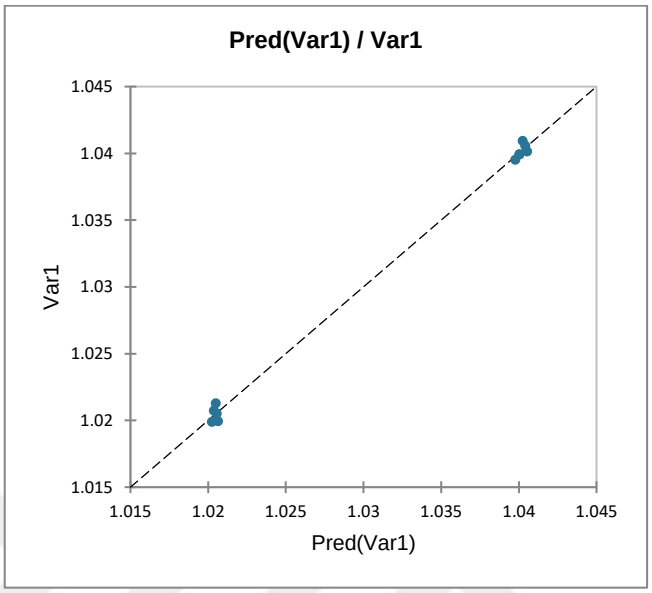

Figure C.31. The compatibility of predicted values with measured values for TM 3 concerning CuO/ethylene glycol nanofluids

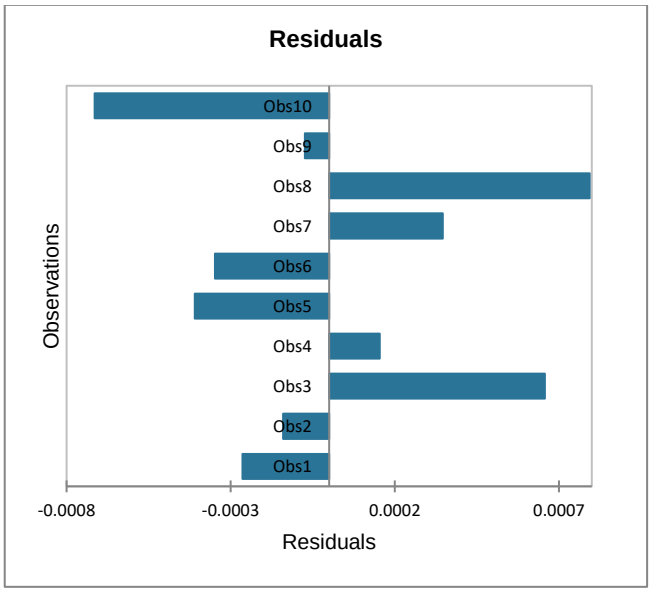

Figure C.32. Residuals of observations for TM 3 concerning CuO/ethylene glycol nanofluids

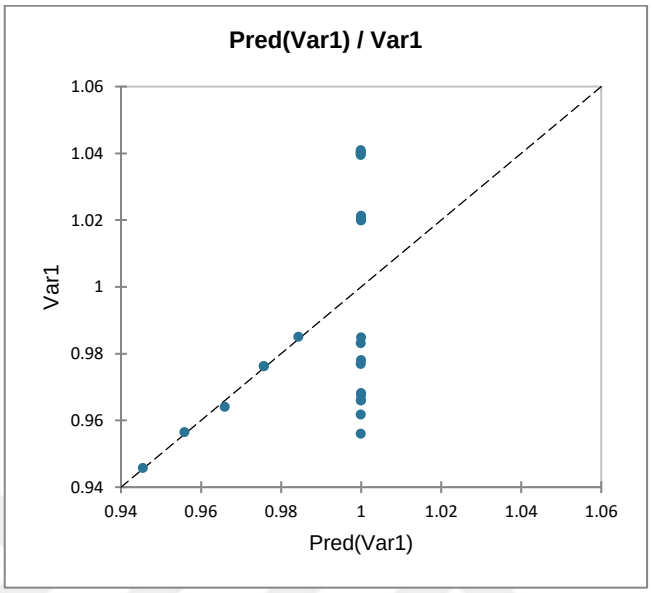

Figure C.33. The compatibility of predicted values with measured values for TM 3 concerning all CuO nanofluids

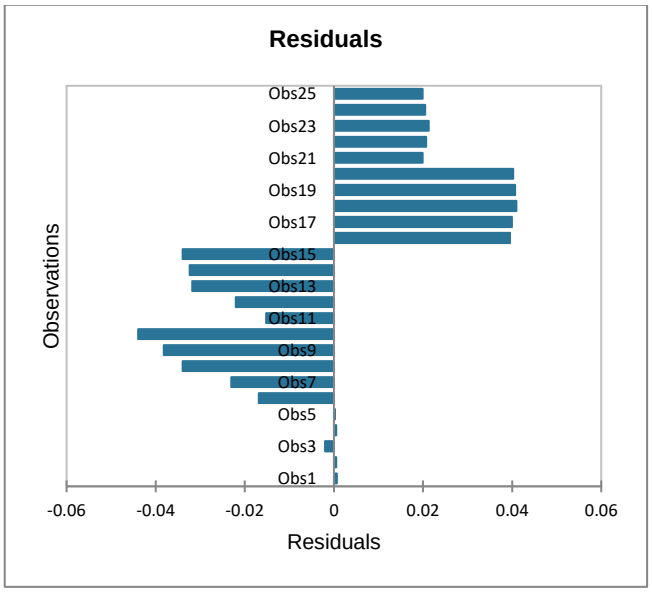

Figure C.34. Residuals of observations for TM 3 concerning all CuO nanofluids

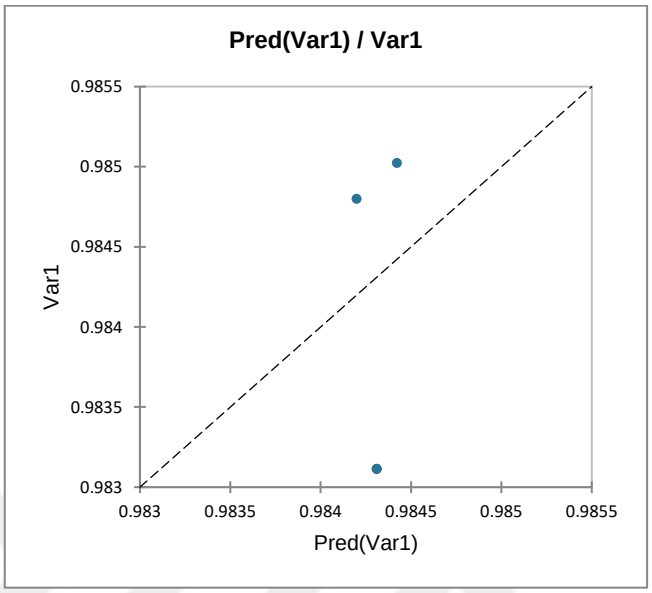

Figure C.35. The compatibility of predicted values with measured values for TM 4 concerning CuO/water nanofluids

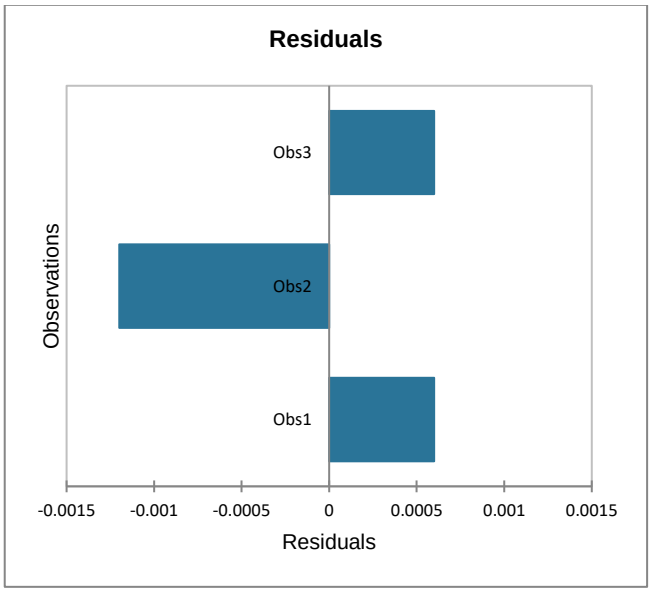

Figure C.36. Residuals of observations for TM 4 concerning CuO/water nanofluids

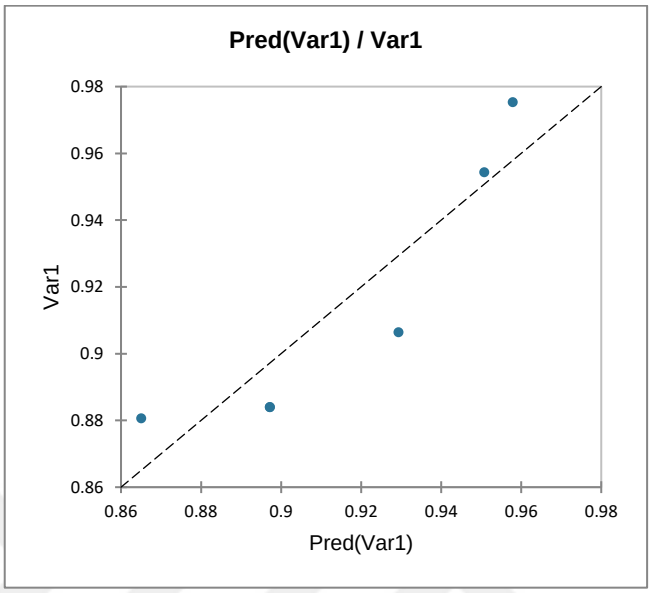

Figure C.37. The compatibility of predicted values with measured values for TM 4 concerning Ag/water nanofluids

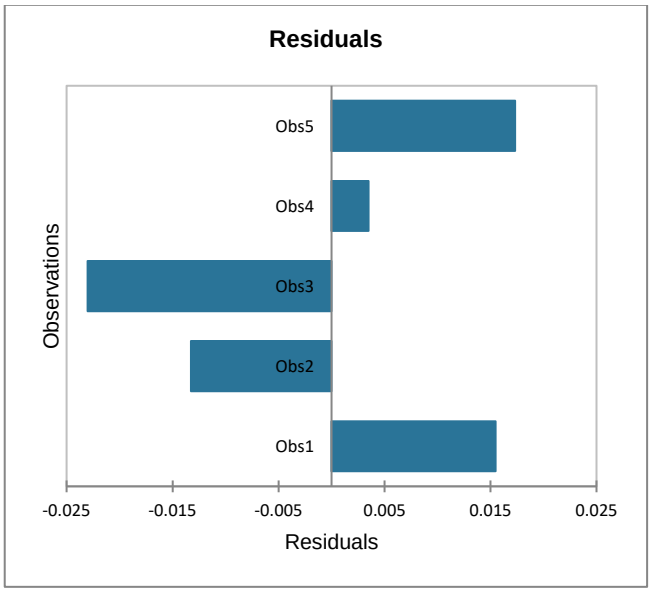

Figure C.38. Residuals of observations for TM 4 concerning Ag/water nanofluids

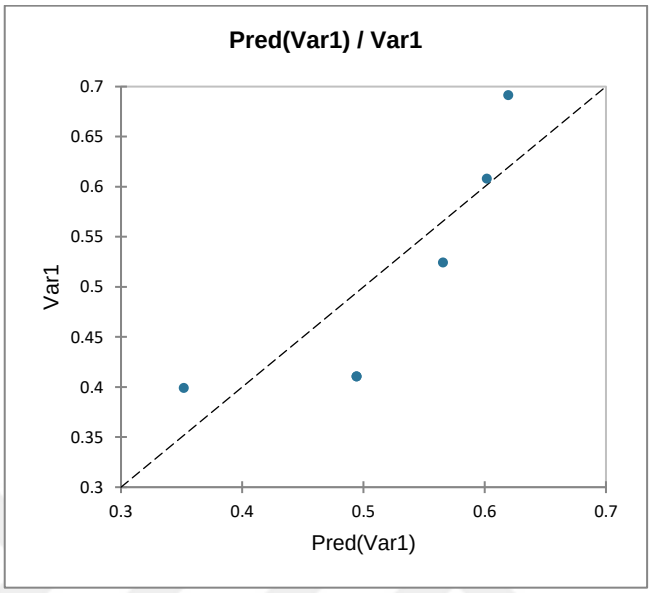

Figure C.39. The compatibility of predicted values with measured values for TM 4 concerning citric acid coated superparamagnetic Fe_3O_4/water nanofluids

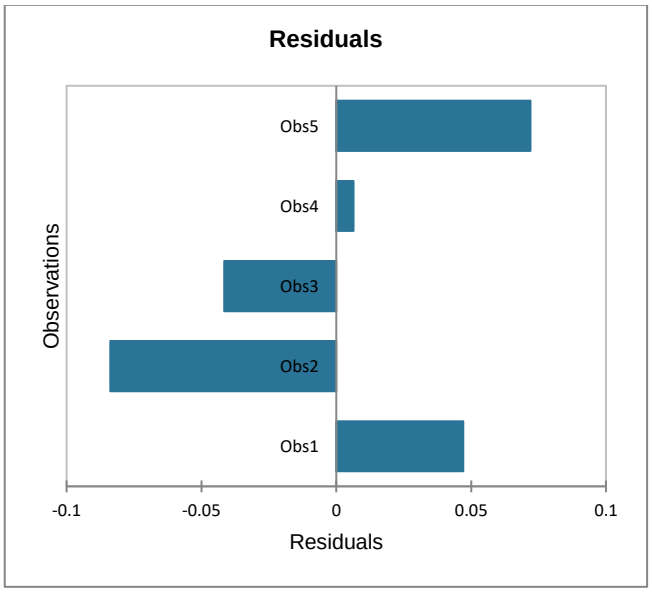

Figure C.40. Residuals of observations for TM 4 concerning citric acid coated superparamagnetic Fe_3O_4/water nanofluids

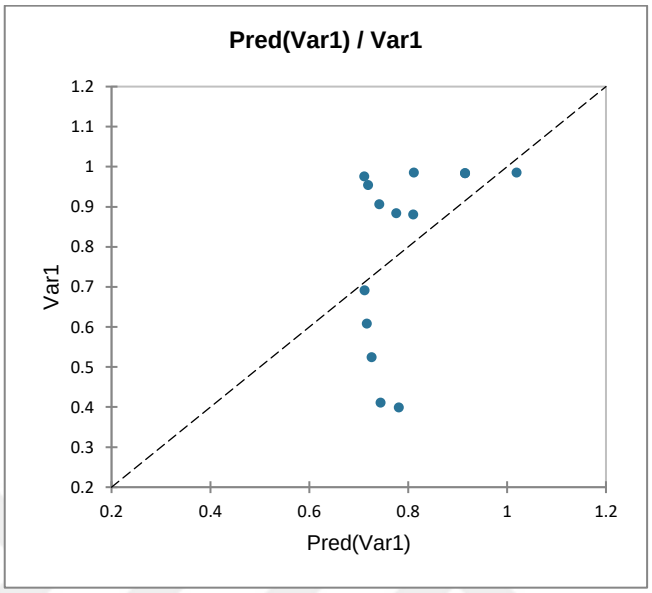

Figure C.41. The compatibility of predicted values with measured values for TM 4 concerning water-based Ag. Fe_3O_4 and CuO nanofluids together

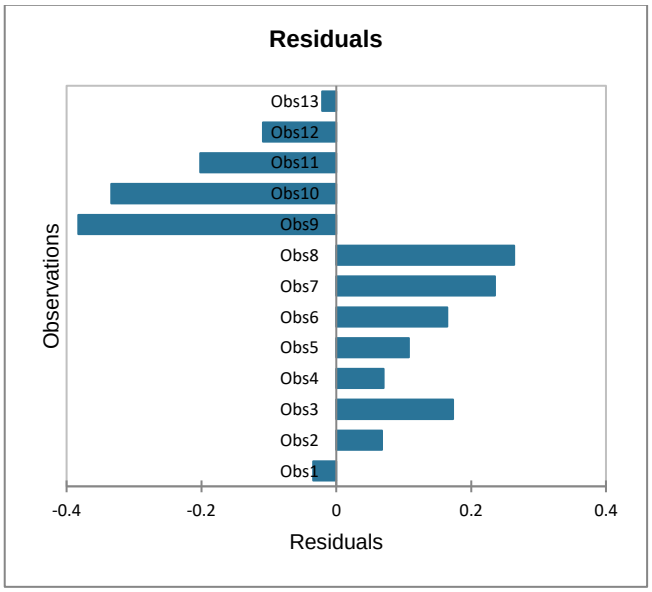

Figure C.42. Residuals of observations for TM 4 concerning water-based Ag. Fe_3O_4 and CuO nanofluids together

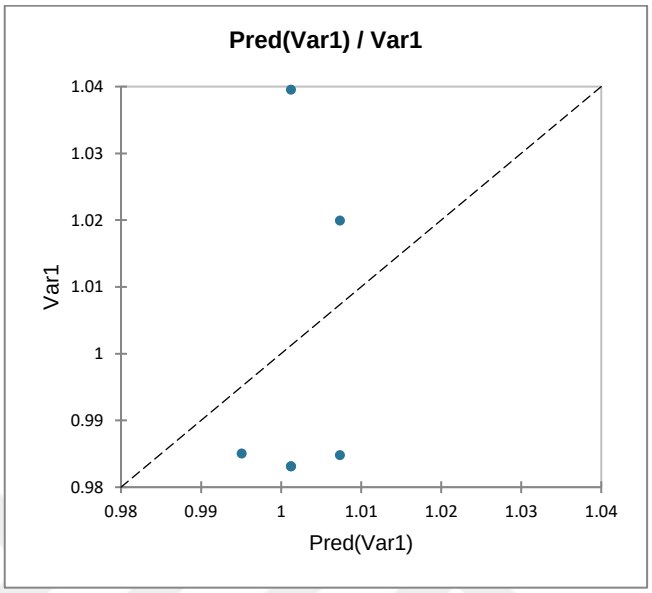

Figure C.43. The compatibility of predicted values with measured values for TM 4 concerning all CuO nanofluids

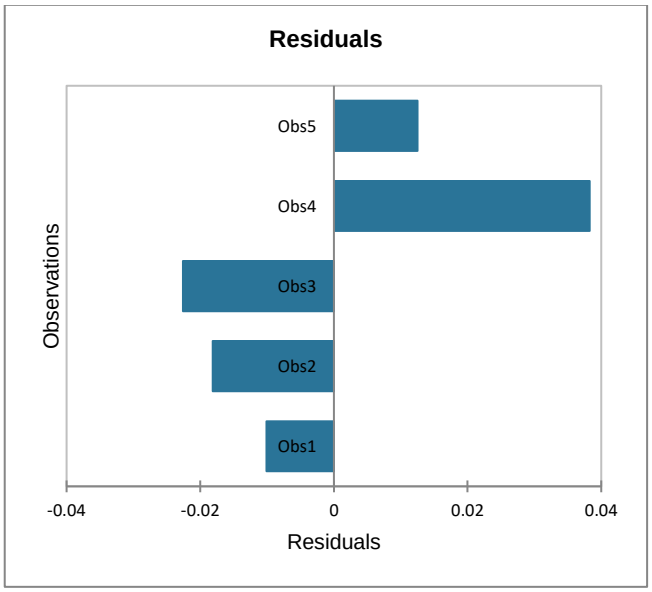

Figure C.44. Residuals of observations for TM 4 concerning all CuO nanofluids

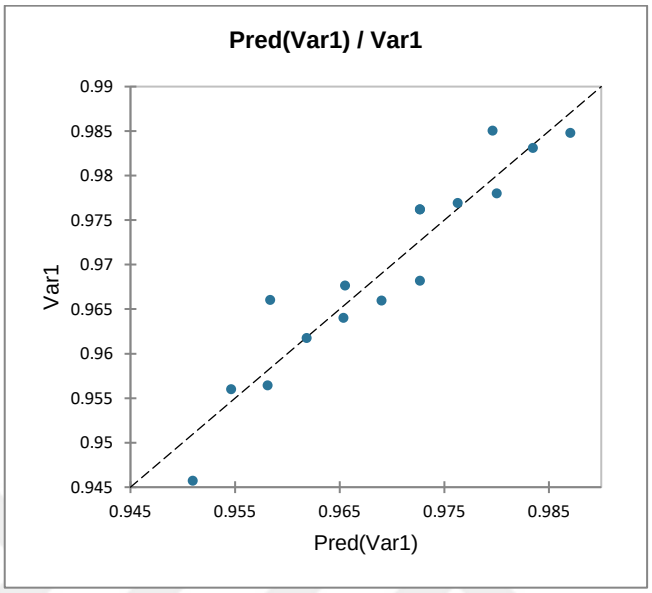

Figure C.45. The compatibility of predicted values with measured values for TM 5 concerning CuO/water nanofluids

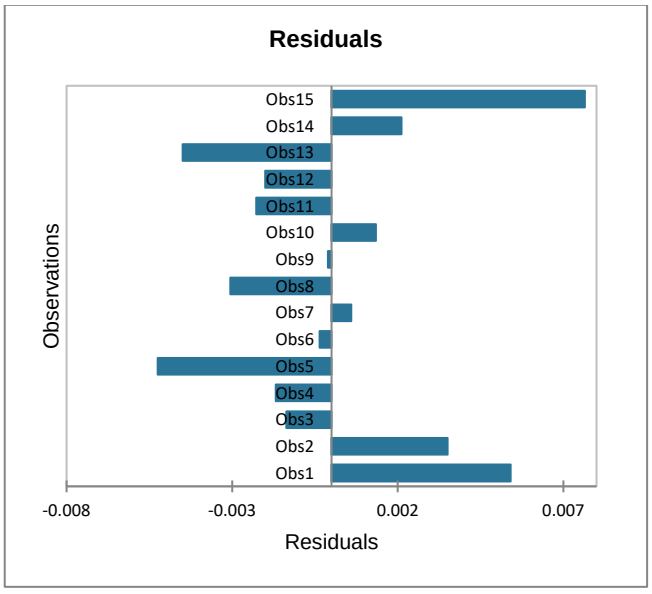

Figure C.46. Residuals of observations for TM 5 concerning CuO/water nanofluids

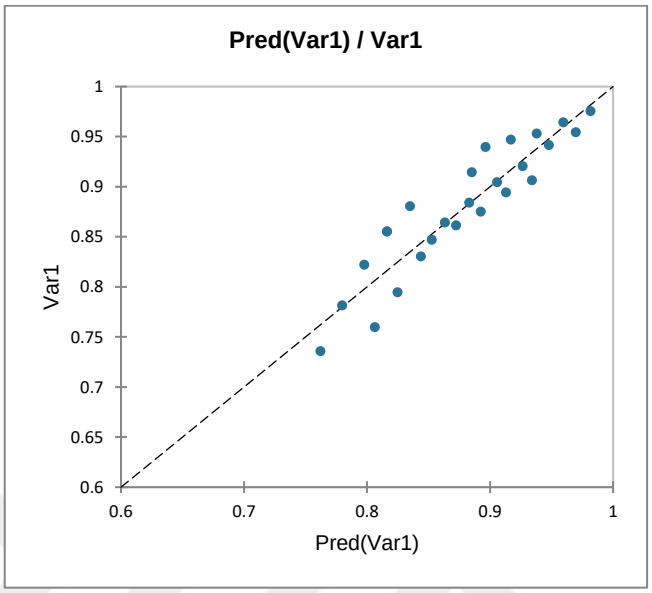

Figure C.47. The compatibility of predicted values with measured values for TM 5 concerning Ag/water nanofluids

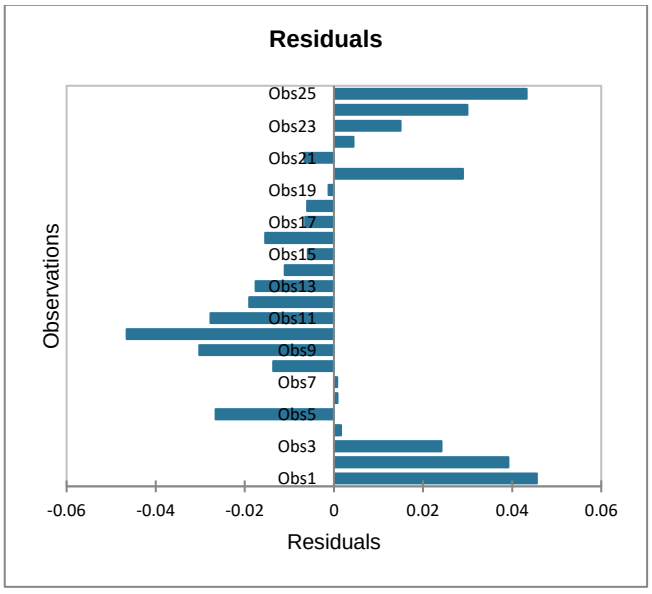

Figure C.48. Residuals of observations for TM 5 concerning Ag/water nanofluids

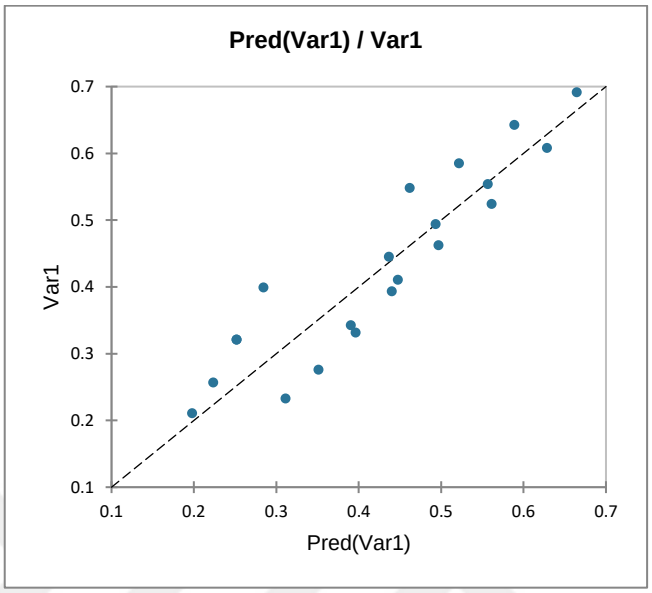

Figure C.49. The compatibility of predicted values with measured values for TM 5 concerning citric acid coated superparamagnetic Fe_3O_4/water nanofluids

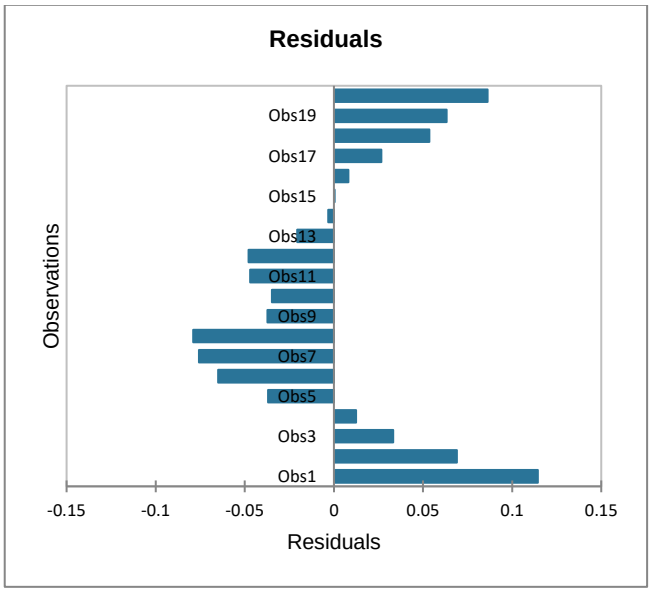

Figure C.50. Residuals of observations for TM 5 concerning citric acid coated superparamagnetic Fe_3O_4/water nanofluids

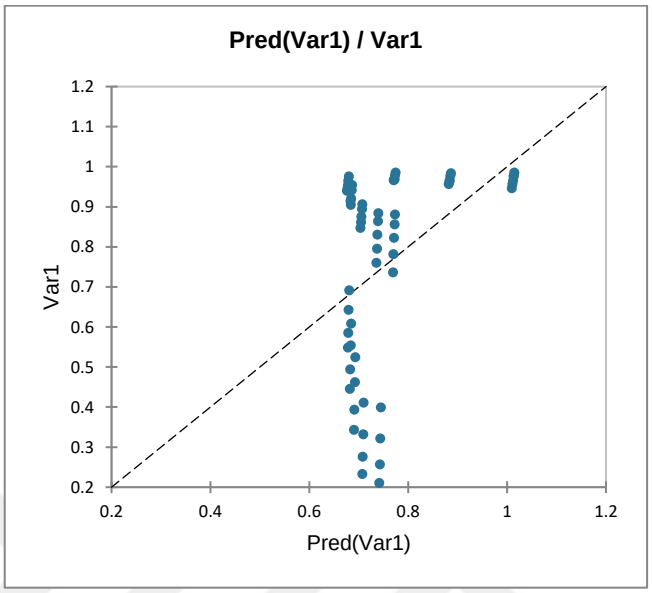

Figure C.51. The compatibility of predicted values with measured values for TM 5 concerning water-based Ag. Fe_3O_4 and CuO nanofluids together

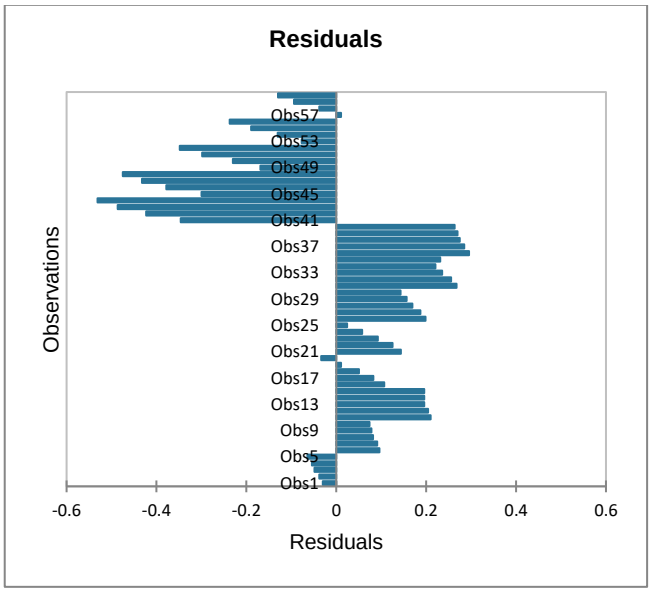

Figure C.52. Residuals of observations for TM 5 concerning water-based Ag. Fe_3O_4 and CuO nanofluids together

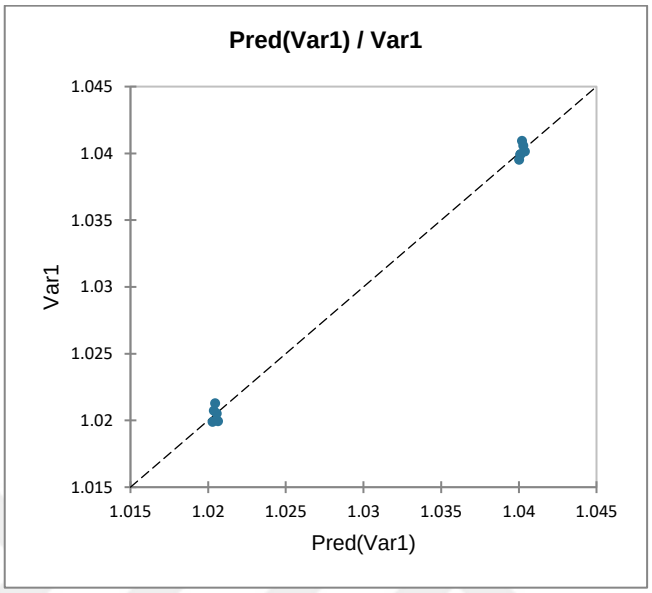

Figure C.53. The compatibility of predicted values with measured values for TM 5 concerning CuO/ethylene glycol nanofluids

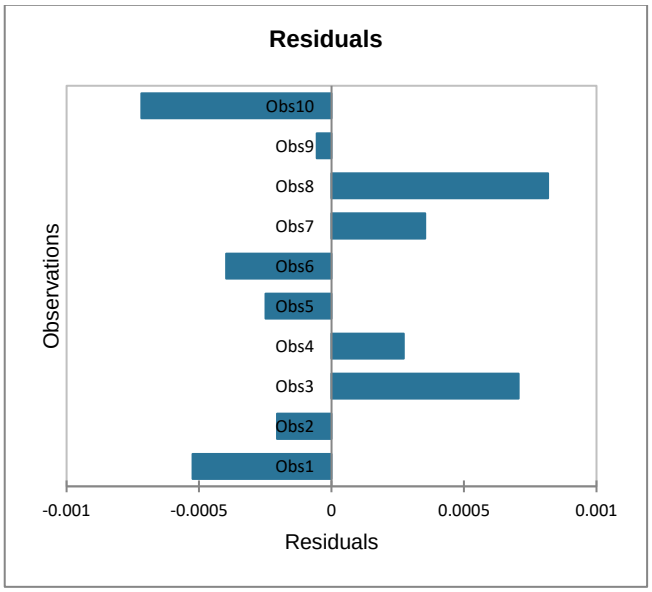

Figure C.54. Residuals of observations for TM 5 concerning CuO/ethylene glycol nanofluids

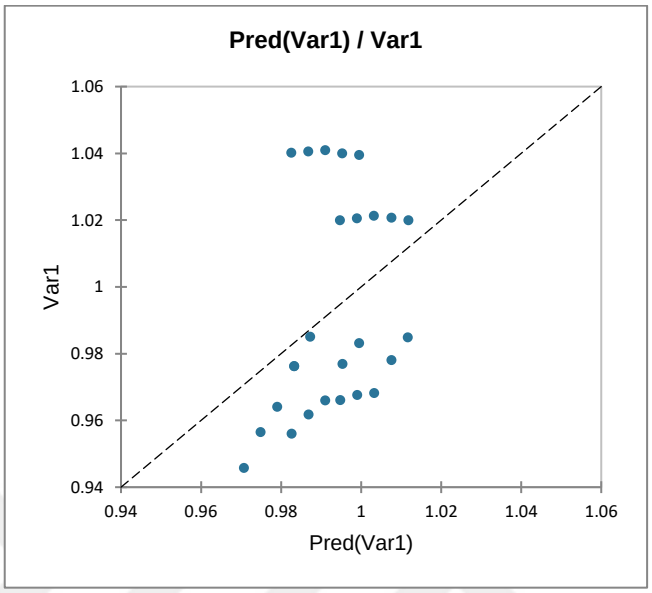

Figure C.55. The compatibility of predicted values with measured values for TM 5 concerning all CuO nanofluids

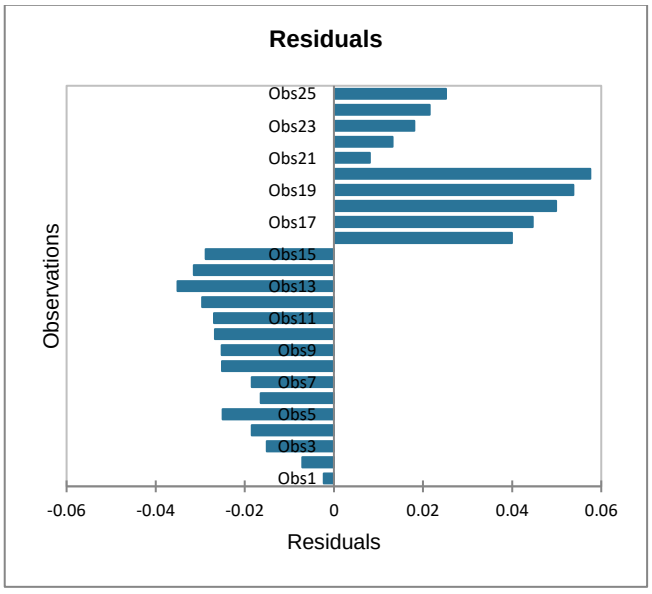

Figure C.56. Residuals of observations for TM 5 concerning all CuO nanofluids

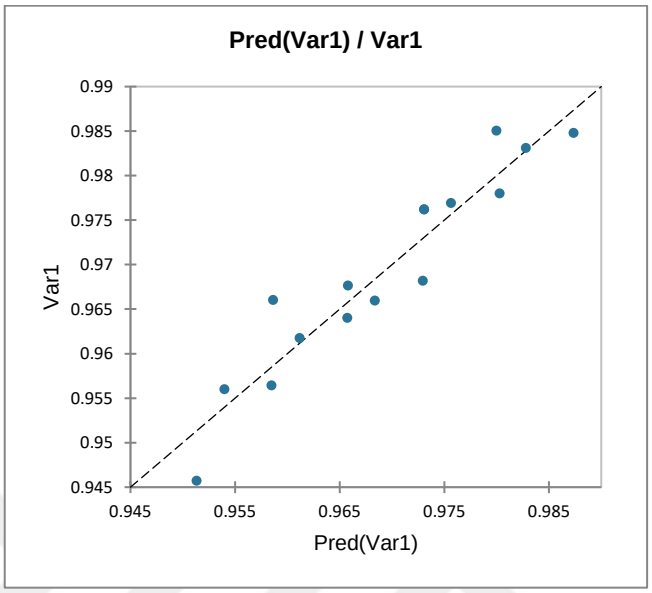

Figure C.57. The compatibility of predicted values with measured values for TM 6 concerning CuO/water nanofluids

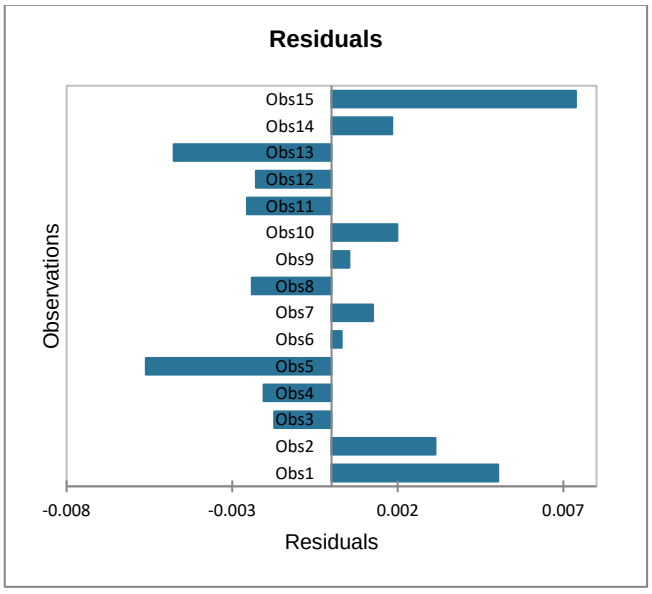

Figure C.58. Residuals of observations for TM 6 concerning CuO/water nanofluids

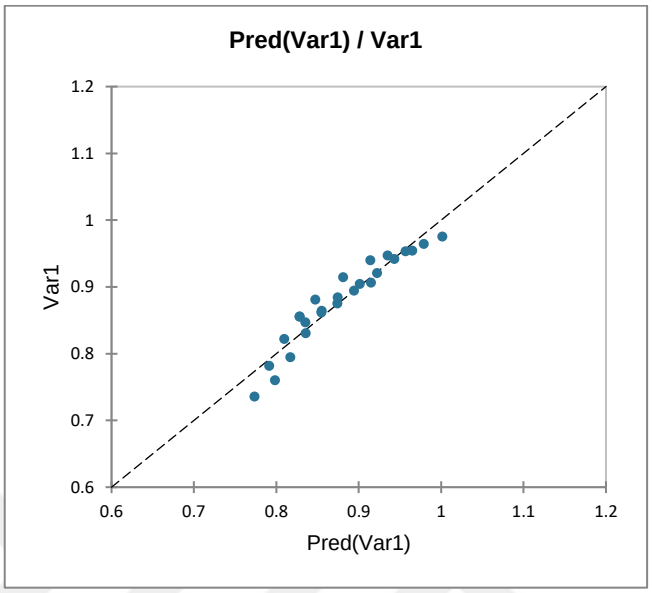

Figure C.59. The compatibility of predicted values with measured values for TM 6 concerning Ag/water nanofluids

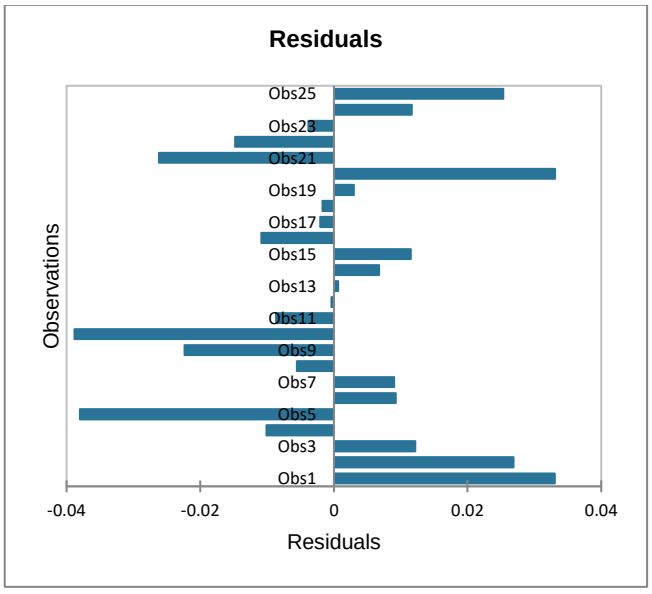

Figure C.60. Residuals of observations for TM 6 concerning Ag/water nanofluids

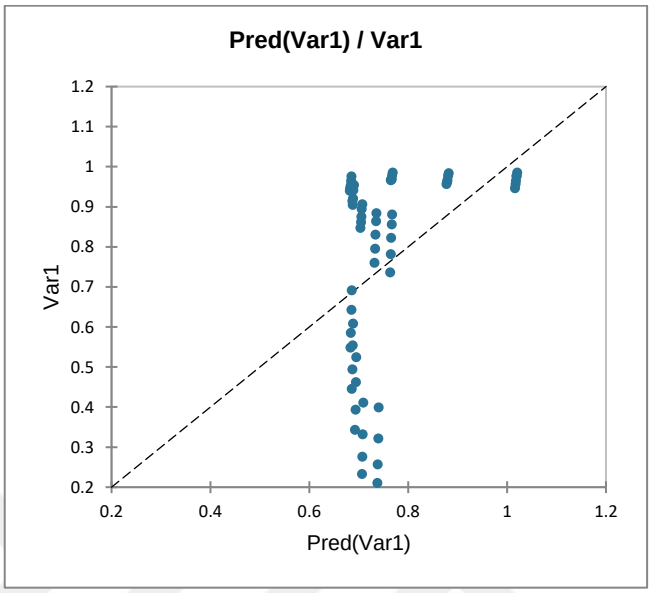

Figure C.61. The compatibility of predicted values with measured values for TM 6 concerning water-based Ag. Fe_3O_4 and CuO nanofluids together

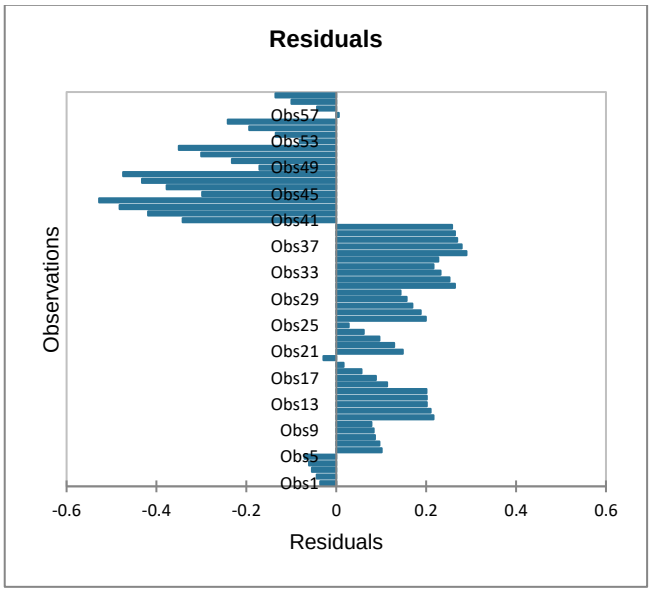

Figure C.62. Residuals of observations for TM 6 concerning water-based Ag. Fe_3O_4 and CuO nanofluids together

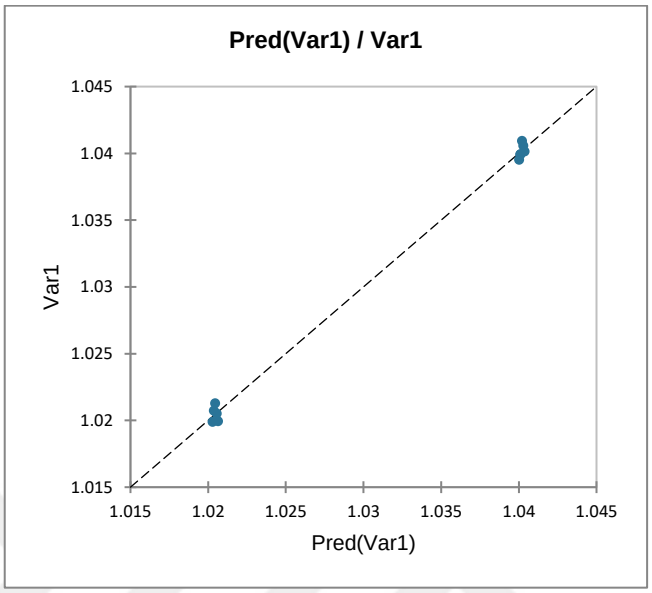

Figure C.63. The compatibility of predicted values with measured values for TM 6 concerning CuO/ethylene glycol nanofluids

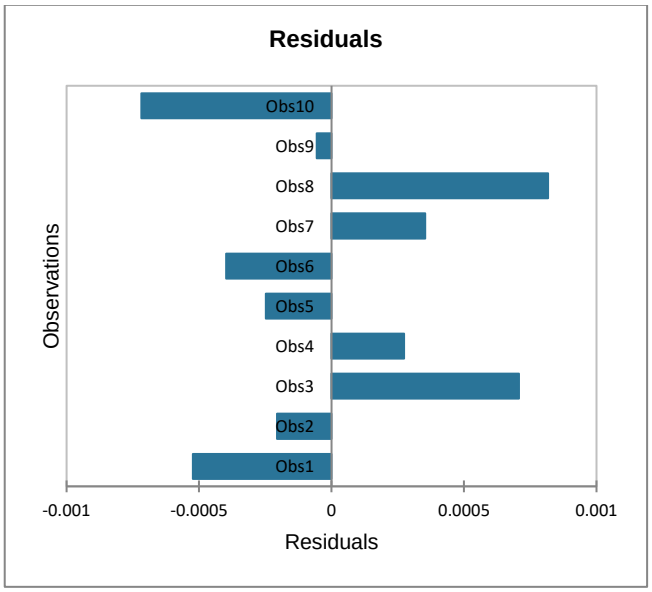

Figure C.64. Residuals of observations for TM 6 concerning CuO/ethylene glycol nanofluids

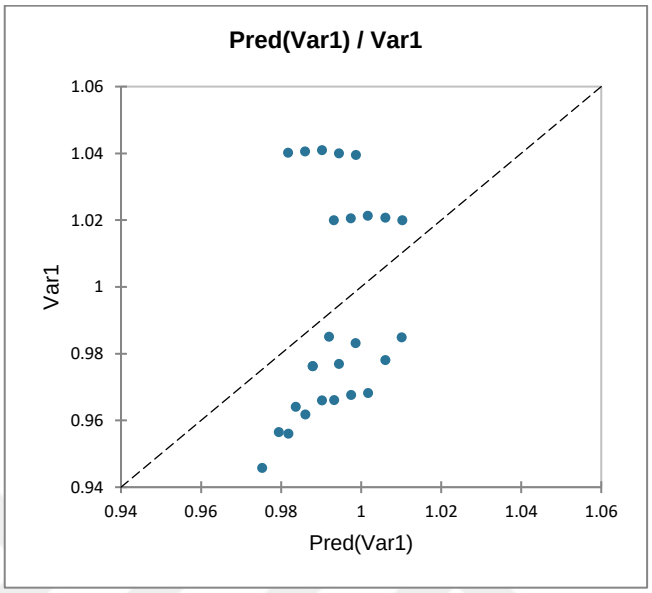

Figure C.65. The compatibility of predicted values with measured values for TM 6 concerning all CuO nanofluids

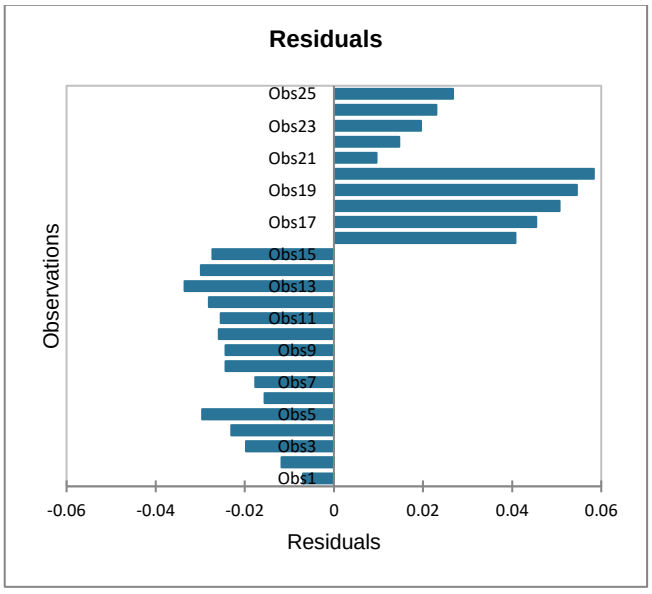

Figure C.66. Residuals of observations for TM 6 concerning all CuO nanofluids